Aberrant transcriptional pathways in t(12;21) Acute Lymphoblastic Leukaemia

Aishwarya Sundaresh

Developmental Biology and Cancer Section

Institute of Child Health

University College London

A thesis submitted for the Degree of Doctor of Philosophy

2016

DECLARATION

I, Aishwarya Sundaresh, confirm that the work presented in this thesis is my own. Where information has been derived from other sources, I confirm that this has been indicated in the thesis.

Signature…..……..……..…

ABSTRACT

The single most frequent chromosomal translocation associated with childhood Acute Lymphoblastic Leukaemia is the t(12;21) rearrangement, that creates a fusion gene between *TEL* (*ETV6*) and *AML1* (*RUNX1*). Although TEL-AML1$^+$ patients have a very good prognosis, relapses occur in up to 20% of cases and many patients face long-term side effects of chemotherapy. Our laboratory has previously shown that TEL-AML1 regulates Signal Transducer and Activator of Transcription 3 (STAT3) activation, which is critical for survival of the leukaemic cells. In this study, inhibition of STAT3 in TEL-AML1$^+$ cells results in decreased *SMAD7* gene expression. SMAD7 is an antagonist of TGF-β signalling, functioning through a negative feedback mechanism, but is also known to function in other biological pathways. In order to investigate the role of SMAD7 in TEL-AML1$^+$ leukaemia, lentiviral mediated *SMAD7* knockdown was performed in human TEL-AML1$^+$ cell lines. *SMAD7* silencing inhibited proliferation of TEL-AML1$^+$ cell lines, eventually leading to growth arrest and apoptosis. Furthermore, our data showed that this effect is not mediated through TGF-β signalling, indicating that SMAD7 was functioning through an alternative pathway. We also observed growth arrest following *SMAD7* knockdown in other ALL and AML subtypes. Furthermore, silencing of *SMAD7* in TEL-AML1$^+$ ALL cells transplanted into immunodeficient mice impaired disease progression *in vivo*, resulting in prolonged disease latency. To investigate the essential pathways regulated by SMAD7 in these leukaemic cells, we performed RNA-sequencing analysis on TEL-AML1$^+$ cells following *SMAD7* knockdown. Global gene expression analysis revealed SMAD7 to be a regulator of cholesterol biosynthesis, a pathway critical for leukaemia cell survival. Our

experiments establish a novel transcriptional pathway operating specifically in t(21;21) ALL, but regulating downstream pathways essential for ALL in general. This study highlights new therapeutic opportunities for ALL.

TABLE OF CONTENTS

LIST OF FIGURES

LIST OF TABLES

ABBREVIATIONS

2-ME	2-mercaptoethanol
aa	Amino acids
ACAT	Acetyl-CoA Acetyltransferase
AGM	Aorta-gonad-mesonephros
AID	Activation-induced cytidine deaminase
ALL	Acute Lymphoblastic Leukaemia
AML	Acute Myeloid Leukaemia
AML1	Acute Myeloid Leukaemia 1 protein
APC	Allophycocyanin
APOBEC	Apoliprotein B mRNA editing enzyme, catalytic polypeptide-like
APS	Ammonium persulphate
ATM	Ataxia telangiectasia mutated
BCL	B-cell lymphoma
BCR	Breakpoint cluster region
BFU-E	Burst-forming unit-erythroid
BMP	Bone morphogenetic protein
BSA	Bovine serum albumin
BTG1	B-cell translocation gene 1
CBF	Core binding factor
CDKN	Cyclin-dependent kinase inhibitor
CFU	Colony-forming unit
CFU-GEMM	Colony-forming unit-granulocyte, erythrocyte, macrophage, megakaryocyte

CFU-GM	Colony-forming unit-granulocyte, macrophage
CFU-M	Colony-forming unit-macrophage
ChIP	Chromatin immunoprecipitation
CLP	Common lymphoid progenitors
CMP	Common myeloid progenitors
CMRP	Common myeloid cells with long-term repopulating activity
CMV	Cytomegalovirus
c-MYC	avian Myelocytomatosis viral oncogene homolog
cPPT	Central polypurine tract
CSF	Colony stimulating factor
$CuSO_4$	Copper (II) sulphate
CYLD	Cyclindromatosis
DAPI	4',6-diamidino-2-phenylindole
DHCR	Dehydrocholesterol reductase
DMEM	Dulbecco's modified eagle's medium
DMSO	Dimethyl sulphoxide
DOX	Doxycycline
DTT	Dithiothreitol
EBF-1	Early B-cell factor 1
EDTA	Ethylenediaminetetraacetic acid
EdU	5-ethynyl-2'-deoxyuridine
EGF	Epidermal growth factor
eGFP	Enhanced green fluorescent protein
EGTA	Ethylene glycol tetraacetic acid
EMT	Epithelial to mesenchymal transition

ENU	*N*-ethyl-*N*-nitrosourea
ETS	E-twenty six
ETV6	ETS-translocation variant 6
FCS	Foetal calf serum
FDPS	Farnesyl diphosphate synthase
Flt3	Fms-like tyrosine kinase 3
FTI	Farnesyltransferase inhibitor
G-CSF	Granulocyte-colony stimulating factor
GLI1	Growth factor independence 1
GMP	Granulocyte-monocyte restricted progenitors
HAT	Histone acetyltransferase
HDAC	Histone deacetylases
HLH	Helix-loop-helix
HMG-CoA	3-hydroxy-3-methylglutaryl-coenzyme A
HMGCR	3-hydroxy-3-methylglutaryl-coenzyme A reductase
hp	Hairpin
HPC	Haematopoietic progenitor cells
HRP	Horseradish peroxide
HSC	Haematopoietic stem cells
IFN-γ	Interferon- γ
Ig	Immunoglobulin
IKZF1	Ikaros family zinc finger 1
IL	Interleukin
IL-7Rα	Interleukin-7 Receptor α chain
IMDM	Iscove's modified dulbecco's medium

INT	2-2-(P-iodophenyl)-3-(p-nitrophenyl)-5-phenyl tetrazolium chloride
IPA	Ingenuity pathway analysis
IPP	Isopentenyl pyrophosphate
IRF1	Interferon regulatory factor 1
I-SMAD	Inhibitory SMAD
JAK	Janus Kinase
JNK	c-Jun N-terminal kinase
LBR	Lamin B receptor
LC	Light chain
LDL	Low density lipoprotein
LDLR	Low density lipoprotein receptor
Lin	lineage-associated surface marker
LMO2	Lim domain only 2
LMPP	Lymphoid-primed multipotent progenitors
LPS	Lipopolysaccharaide
LSK	$Lin^{-}Sca1^{+}c\text{-}kit^{hi}$
LSS	Lanosterol Synthase (2,3-Oxidosqualene-Lanosterol Cyclase)
LT-HSC	Long-term haematopoietic stem cells
LTR	Long terminal repeat
mAb	Monoclonal antibody
MACS	Magnetic activated cell sorting
MAPK	Mitogen-activated protein kinase
MCL-1	Myeloid cell leukaemia sequence 1
MDS	Myelodysplastic syndromes
MEP	Megakaryocyte-erythroid restricted progenitors

MERP	Megakaryocyte-erythroid with long-term repopulating activity
MHC	Major histocompatibility complex
MkRP	Megakaryocytes with long-term repopulating activity
MLL	Mixed-lineage leukaemia
MPP	Multipotent progenitors
MSMO1	Methylsterol Monooxygenase 1
mTOR	Mammalian target of rapamycin
MyRP	Myeloid-restricted progenitors with long-term repopulating activity
NaCl	Sodium chloride
NES	Nuclear export signal
NF-kB	Nuclear factor kappa B
NK	Natural killer
NSG	NOD.Cg-*Prkdc*^{scid}Il2rg^{tm1Wjl}/SzJ
OSCC	Oral squamous cell carcinoma
PAX	Paired box
PBS	Phosphate buffered saline
PCR	Polymerase chain reaction
PD	Pointed domain
PDGF	Platelet-derived growth factor
PE	Phycoerythrin
PFA	Paraformaldehyde
PGK	Phosphoglycerate kinase promoter
PI	Propidium iodide
PI3K	Phosphatidylinositol 3-Kinase
PIAS3	Protein inhibitor of activated STAT3

PU.1	Haematopoietic transcription factor PU.1
PURO	Puromycin
PVDF	Polyvinylidenefluoride
qRT-PCR	Real-time quantitative polymerase chain reaction
R-SMAD	Regulatory-SMAD
RAC	Ras-Related C3 Botulinum Toxin Substrate 1
RAG	Recombination activating gene
RAS	Rat sarcoma
RIPA	Radio-Immunoprecipitation Assay
rpm	Revolutions per minute
RPMI	Roswell Park Memorial Institute
RRE	Rev response element
RSS	Recombination signal sequences
RUNX1	Runt-related transcription factor
S1P	Site-1 protease
S2P	Site-2 protease
SAD	SMAD4 activation domain
SB	Sleeping Beauty
SBE	SMAD-binding element
Sca1	Stem cell antigen 1
SCAP	SREBP cleavage-activating protein
SCF	Stem cell factor
SCID	Severe Combined Immunodeficiency
SCL	Stem cell leukaemia
SDS	Sodium dodecyl sulphate

SDS-PAGE	SDS- polyacrylamide gel electrophoresis
SFEM II	Serum-Free Expansion Medium II
SFFV	Spleen focus-forming virus
SH2	Src Homology 2
shRNA	Small hairpin ribonucleic acid
SID	mSin3 interaction domain
SILAC	Stable isotope labelled by amino acids in cell culture
SIN	Self-inactivating
siRNA	Small interfering ribonucleic acid
SLAM1	Signaling lymphocytic activation molecule 1
SMAD	Mothers against decapentaplegic homolog
SMURF	Smad ubiquitination-related factor
SNP	Single nucleotide polymorphism
SOCS	Suppressor of cytokine signalling
SREBP	Sterol regulatory element binding protein
ST-HSC	Short-term haematopoietic stem cells
STAT	Signal transducer and activator of transcription
SUMO	Small ubiquitin-like modifier
TBL1XR1	Transducin (Beta)-Like 1 X-Linked Receptor 1
TdT	Terminal deoxynucleotidyl transferase
TEL	Translocation-Ets-leukaemia
TEMED	Tetramethylethylenediamine
TGF-β	Transforming growth factor receptor
TGFβR	Transforming growth factor beta receptor
TNF-α	Tumour necrosis factor-α

Tris-HCL	Tris(hydroxymethyl)aminomethane
v-SRC	Sarcoma viral oncogene homolog tyrosine kinase
WNT	Wingless-type
WPRE	Woodchuck Hepatitis Virus post-transcriptional regulatory element
Ψ	viral packaging signal

ACKNOWLEDGEMENTS

First of all, I would like to thank my principal supervisor, Dr. Owen Williams for his tremendous supervision throughout my PhD. He has always encouraged and supported me with incredible patience and dedication. His advice and guidance have been invaluable at every stage of my PhD and for that I am extremely grateful.

I would like to thank all my colleagues and friends in the Cancer Section for their support and friendship during my PhD. I am especially thankful to Dr. Jasper de Boer for helping with experimental problems and his scientific advice, Dr. Luca Gasparoli and Sandra Cantilena for their help and friendship and Kedison Mutswakatira for organising everything in the laboratory. I would also like to thank Dr. Mike Hubank, Tony Brooks and Kerra Pearce at UCL Genomics for running the RNA-sequencing experiment and their help in analysing the data.

I am thankful to all my friends, especially Olivia, Fiona and Emine for their friendship and encouragement during the last four years. I am also deeply grateful to Maurizio, firstly for teaching me practical laboratory skills and for numerous scientific discussions, but more so for his love, kindness and invaluable support at all times – I cannot thank you enough.

Finally, I would like to thank my family- my sister Akshya, for being my best friend and my parents, for their love and encouragement, with a special mention to my mother for her constant support and unwavering belief in me.

This thesis is dedicated to my family.

CHAPTER I. INTRODUCTION

1.1 Haematopoiesis

Haematopoiesis is the formation and development of blood cells. Blood is one of the most regenerative tissues, with approximately one trillion cells generated daily in human adult bone marrow. It is a well-studied process in mouse using functional repopulation assays, providing insight for the human model of haematopoiesis (Doulatov et al., 2012). Establishment of the haematopoietic system begins in the early stages in the embryo in vertebrates, functioning throughout embryonic and adult life. The first haematopoietic cells are produced in the embryonic yolk sac, a process known as primitive haematopoiesis (Orkin, 2000). This is followed by progression to the allantois and placenta. Following this, the production of blood cells enters an intra-embryonic site known as the aorta-gonad-mesonephros (AGM) before migrating to the foetal liver, which is the major site of blood cell expansion. The haematopoietic process in the embryo is known as definitive haematopoiesis (Orkin, 2000). Shortly after, the blood cells migrate to the spleen and then at the time of birth, they seed the bone marrow, which becomes the main site of haematopoiesis activity after birth. Interestingly, transient populations of blood cells have been observed in the early stages of embryo. Primitive erythrocytes, macrophages and megakaryocytes are found to be present in the extraembryonic sac but disappear as the embryo develops further (Chen et al., 2011).

The haematopoietic process occurs in a hierarchical manner with haematopoietic stem cells (HSCs) at the apex, exhibiting two main characteristics:

the capacity to self-renew and to differentiate into various haematopoietic progenitor cells (HPCs). These HPCs become increasingly restricted in their lineage potential, generating lineage specific precursors that eventually differentiate into mature blood cell types (Till and McCulloch, 1980). Different lineage markers identify the populations of cells generated. Although there are many similarities in the haematopoietic system between mice and humans, cells from the two species express different markers. Murine HSCs express the markers Sca1 and the signalling lymphocyte activation molecule family member 1 (SLAM1/CD150), whilst human HSCs do not express them (Larochelle et al., 2011). In mouse, HSCs are present in a small fraction of $Lin^{-}Sca1^{+}c\text{-}Kit^{hi}$ (LSK) bone marrow cells. Within the LSK fraction, long-term self-renewing HSC (LT-HSC) reside in the $CD34^{-}CD38^{+}$ fraction, whereas short-term HSCs (ST-HSCs), which have short-term self-renewal capacity, are found in the CD34+CD38- compartment (Matsuoka et al., 2001) (Tajima et al., 2001). Human HSCs are found to be present in the $CD34^{+}CD38^{-}$ fraction of cells and are found within the $Lin^{-}CD34^{+}CD45RA^{-}CD90^{+}Rhodamine123^{low}CD49f^{+}$ population (Notta et al., 2011). However, recent studies have shown a population of $CD34^{-}$ cells expressing HSC-like features in the human bone marrow. Furthermore, this population of cells are shown to be present above $CD34^{+}$ cells in the haematopoietic hierarchy, suggesting significantly greater similarity between mouse and human haematopoiesis than previously appreciated (Anjos-Afonso et al., 2013).

In the classical model of haematopoiesis, ST-HSCs in the LSK population, expressing fms-related tyrosine kinase 3 (Flt3), give rise to multipotent progenitors (MPPs) that have lost self-renewal capability (Fig. 1). These MPPs in turn differentiate into common lymphoid progenitors (CLPs) and common myeloid progenitors (CMPs). The CLPs are lymphoid cell lineage restricted progenitors,

whilst the CMPs are myeloid cell restricted progenitors. The CLPs generate natural killer (NK) cells, B cell progenitors (Pro-B) and T-cell progenitors (Pro-T) which in turn give rise to the three main lymphoid cell types: T cells, B cells and NK cells. CLPs express low levels of c-Kit but express high levels of interleukin-7 receptor α-chain (IL-7Rα) and Flt3. The CMPs generate megakaryocyte-erythrocyte restricted progenitors (MEPs) and granulocyte-macrophage-restricted progenitors (GMPs) which in turn give rise to the mature myeloid lineage cells: erythrocytes, megakaryocytes, granulocytes and monocytes (Bhandoola and Sambandam, 2006). The CMPs, unlike CLPs, do not express IL-7Rα but do express c-Kit, therefore residing in the $Lin^{-}Sca1^{-}c\text{-}Kit^{+}$ population. To further distinguish the myeloid progenitors, the Fcγ receptorII/III (FcγRII/III) and CD34 are used. MEPs have the phenotype $Fc\gamma RII/III^{lo}CD34^{-}$ whilst GMPs are $Fc\gamma RII/III^{hi}CD34^{-}$ (Akashi et al., 2000).

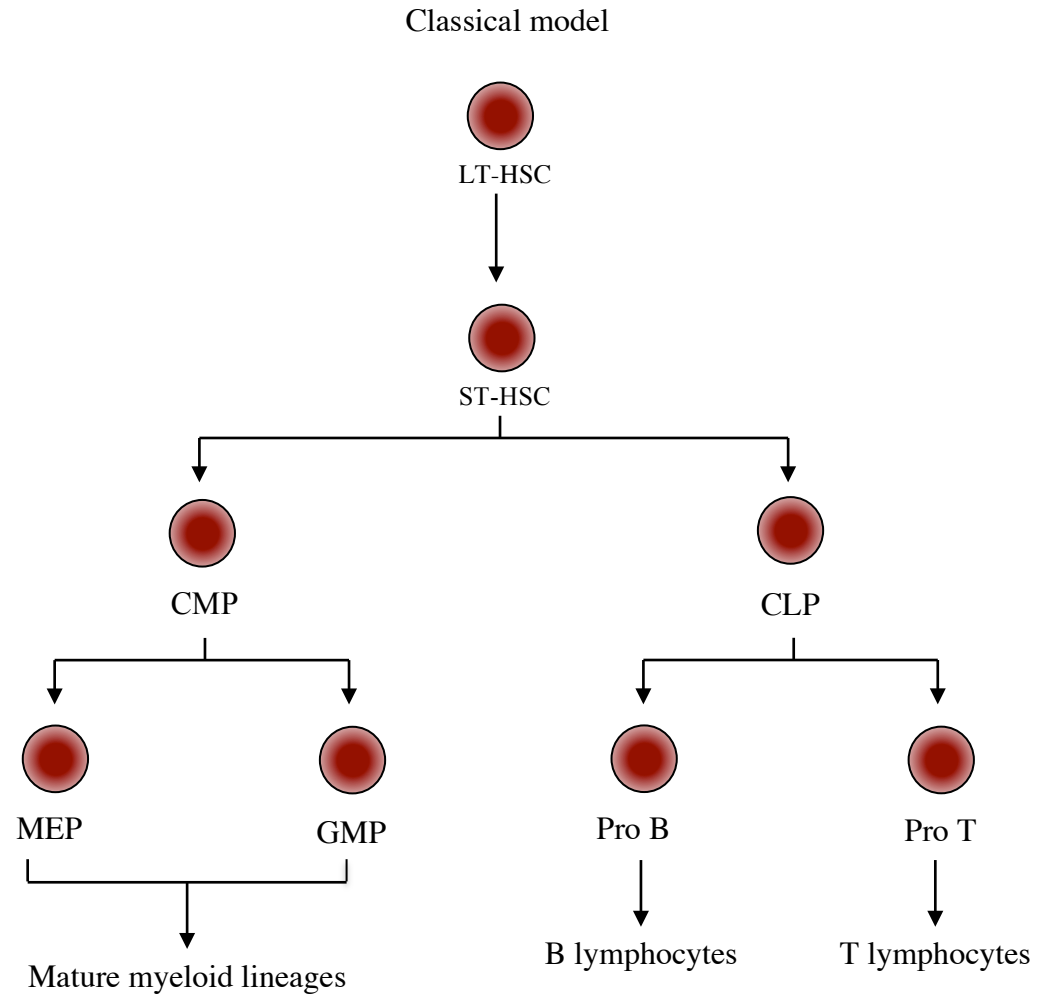

Figure 1 - Classical model of haematopoiesis

Long-term haematopoietic stem cells (LT-HSCs) have the potential to self-renew and give rise to short term haematopoietic stem cells (ST-HSCs) that have limited self-renewal capacity. The ST-HSCs then differentiate into common myeloid progenitors (CMPs) or common lymphoid progenitors (CLPs). CLPs give rise to NK cells, B cell progenitors (Pro-B) and T-cell progenitors (Pro-T), which then give rise to mature B lymphocytes and T lymphocytes, the mature lymphoid lineage cell types. The CMPs give rise to megakaryocyte-erythrocyte restricted progenitors (MEPs) and granulocyte-macrophage restricted progenitors (GMPs), which give rise to mature myeloid lineage cell types. Adapted from (Iwasaki and Akashi, 2007)

However, beside the classical model, two other models have been proposed for haematopoietic development. The second model, known as the alternative model, does not support a strict division into CLPs and CMPs, as it identifies a population of cells with combined lympho-myeloid differentiation potential but unable to differentiate into erythroid and megakaryocyte lineages (Adolfsson et al., 2005) (Fig. 2A). Using Flt3 as a marker, it was proposed that this LSK $Flt3^+$ population of cells had the potential to differentiate into granulocytes, macrophages, B cell and T cell lineages. This population of cells was labelled as lymphoid-primed multipotent progenitors (LMPP), since although this population preferentially differentiates into lymphoid progenitors it was capable of differentiating into GMPs. The alternative model, therefore, has an asymmetric hierarchy where the ST-HSC can generate MEPs and LMPPPs, and excludes the existence of CMPs (Adolfsson et al., 2005).

A third model known as the composite model, combines the alternative and classical models of haematopoiesis (Fig. 2B). The composite model takes into account the existence of CMPs in the $LinSca1^-Kit^+IL^-7R\alpha^-Fc\gamma RII/III^oCD34^+$ compartment, suggesting that ST-HSCs give rise to CMPs and LMPPs. Both CMPs and LMPPs have the potential to produce granulocyte-macrophage lineage cells, whilst CMPs can also give rise to megakaryocyte-erythrocyte lineage cells and LMPPs to B- and T-cell lineages (Adolfsson et al., 2005; Iwasaki and Akashi, 2007).

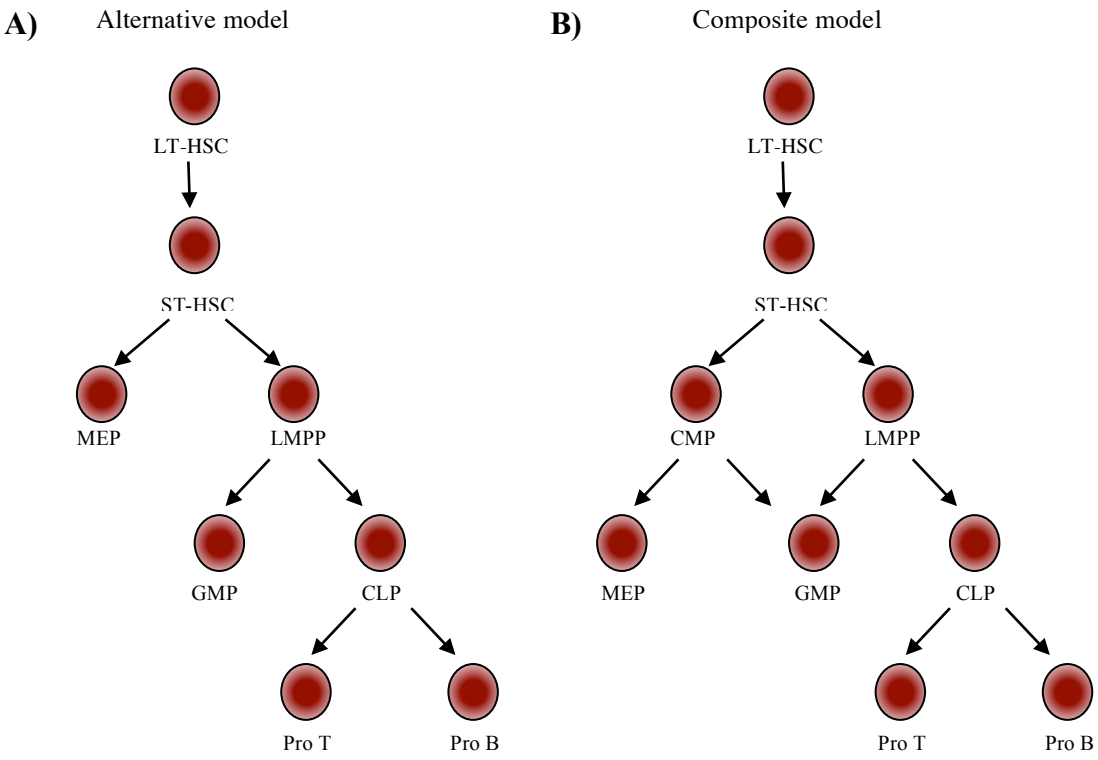

Figure 2 - Alternative and Composite models of haematopoiesis.

The alternative and composite models of haematopoiesis show an asymmetric lineage restriction in haematopoietic cells. The alternative model (A) shows a less lineage-restricted haematopoiesis development by introducing a lymphoid-primed multipotent progenitor (LMPP) population. The composite model (B) shows the co-existence of the common myeloid progenitor (CMP) and LMPP populations, both capable of generating GMPs. Adapted from (Iwasaki and Akashi, 2007)

However, a recent study has challenged the stepwise manner of lineage commitment in haematopoietic development. This work proposes that while HSCs retain self-renewal capacity and multipotency, they can directly generate myeloid-

restricted progenitors with long-term repopulating ability and differentiation potential. This model suggests HSCs preferentially produce particular myeloid progenitors, such as common myeloid repopulation progenitors (CMRPs), megakaryocyte-erythroid repopulating progenitors (MERPs) and megakaryocyte repopulating progenitors (MkRPs), but not lymphoid-restricted progenitors (Yamamoto et al., 2013). Lymphoid priming was only observed in MPPs and LMPPs as previously noted. Furthermore, gene expression patterns between HSCs and megakaryocyte lineage cells have previously been shown to be similar, compatible with the current findings that MkRPs, MERPs and CMRPs are close to HSCs in the haematopoietic hierarchy. Therefore, it is possible that the most primitive HSCs can directly give rise to cells restricted to the myeloid lineage compartment, upstream of the MPP stage (Yamamoto et al., 2013).

1.2 Molecular control of haematopoiesis

Regulation of HSCs is achieved by internal and external regulatory factors, which are fundamental in controlling the different stages of haematopoiesis, including stem cell maintenance, lineage commitment and differentiation. Transcription factors that regulate gene expression are important in maintaining the self-renewal capacity and cell survival of HSCs and determining cell fate in the haematopoietic system. Haematopoietic transcription factors include MLL, TEL (ETV6), AML1 (RUNX1), c-MYC, PU.1, SCL and LMO2 (Orkin and Zon, 2002). Some important transcription factors were originally identified through studying their roles in haematological malignancies, using loss-of-function or overexpression studies in mice. Studies in knock-out mice have shown crucial roles of several

transcription factors in early haematopoietic commitment steps and lineage outcomes (Sive and Gottgens, 2014). For example, mixed lineage leukaemia (MLL) was identified as a critical transcription factor when *Mll*-deficient mice were generated by homologous recombination in embryonic stem cells. This resulted in an embryonic lethal phenotype (Yagi et al., 1998). Furthermore the HPCs isolated from the yolk sac and foetal liver from these mice showed impaired clonogenic capacity *in vitro* (Hess et al., 1997; Yagi et al., 1998). Although *Mll* loss affected early haematopoiesis, it did not affect later stages of differentiation. It was also shown to be important in self-renewal and promoting proliferation in progenitors. Two *Mll* conditional knock out models also showed its importance in stem cell self-renewal and promotion of proliferation of progenitors, although important differences were noted in the severity of the haematopoietic phenotype between these models (Jude et al., 2007; McMahon et al., 2007).

Knockout studies have shown the importance of Homeobox A9 (*Hoxa9*) in self-renewal of cells, as *Hoxa9*$^{-/-}$ mice were unable to reconstitute the haematopoietic system of transplanted recipient mice (Lawrence et al., 2005). This is also the case for growth factor independence (*Gli1*) ablated mice, most likely due to the role of GLI1 as a repressor of p53 activity, which is essential for the quiescent status of HSCs (Liu et al., 2009; Zeng et al., 2004). Other effector molecules in the cell cycle such as *p21* are also involved in maintaining HSCs in a quiescent state (Cheng et al., 2000). The main pathways controlling regulation of self-renewal in HSCs are the wingless-type MMTV integrate site family (WNT) and the Janus kinase (JAK)-signal transducer and activator of transcription (STAT) pathways. Exposure to WNT proteins leads to increased self-renewal activity *in vitro* and haematopoietic reconstitution ability *in vivo* (Reya and Clevers, 2005). To achieve a balance between

self-renewal and differentiation, c-myc avian myelocytomatosis viral oncogene homolog (c-MYC) has been shown to control the interactions between HSCs and their niche by regulating the expression of N-cadherin and integrins (Wilson et al., 2004).

PU.1 and GATA-1 are two transcription factors that have been shown to be important in lineage commitment. PU.1 expression in the erythroid-myeloid lineage results in monocytic differentiation while GATA-1 expression results in erythroid and megakaryocytic differentiation (Arinobu et al., 2007). Transcription factors have been shown to often inhibit each other, while co-expressed in multipotent cells, leading to one gaining dominance over the other and therefore, regulating the differentiation process. In this case, GATA-1 has been shown to inhibit PU.1 expression and activity (Nerlov et al., 2000). A study using mathematical modelling has shown that the mutual inhibition and repression of opposing downstream targets of the two transcription factors leads to antagonistic interaction in lineage commitment (Wontakal et al., 2012).

Many haematopoietic growth factors also play key roles in regulating HSCs. Stem cell factor (SCF) and its receptor, c-Kit, are expressed on HSCs and are involved in promoting survival of primitive progenitors. They also act with other growth factors such as IL-3 and IL-6 to induce proliferation of HSCs (Larsson and Karlsson, 2005). The colony stimulating factor (CSF) family are the main group of cytokines responsible for myeloid lineage commitment. The multi-CSF (IL-3) stimulates a broad range of haematopoietic cell colony types (Metcalf, 2010). One of the main cytokines responsible for lymphoid commitment in mice is IL-7. *Il-7*$^{-/-}$ mice exhibit severely impaired B and T lymphopoiesis, since the CLP compartment is

dramatically reduced in these mice (Peschon et al., 1994; Puel et al., 1998; Tsapogas et al., 2011). However, in contrast to mice, the dependence of IL-7 for human B cell development is controversial. While some studies show a role for IL-7 in Pro-B cell development, other studies consistently show that B cells can develop independent of IL-7 (Prieyl and LeBien, 1996). Furthermore, cytokines have been shown to be able to redirect lineage specification in cells already committed to a particular lineage. For example, expression of the IL-2 receptor in CLPs can change their cell fate specification towards the myeloid lineage (Kondo et al., 2000).

The maintenance of HSCs is believed to be controlled by a balance between positive and negative factors. Although transcription factors and growth factors that positively regulate haematopoiesis have been well established, less is known about the negative regulators of haematopoiesis (Larsson and Karlsson, 2005). Tumour necrosis factor-α (TNF-α) has been shown to activate Fas, which inhibits self-renewal of murine LT-HSCs, highlighting two important negative regulators of HSCs (Bryder et al., 2001). Furthermore, the immune modulators transforming growth factor-β (TGF-β) and interferon-γ (IFN-γ) have been associated with negative regulation of haematopoietic progenitors (Larsson and Karlsson, 2005).

1.3 B-cell development

The process of B-lymphocyte development is best understood in mice. B-lymphocytes are generated from HSCs in the foetal liver during mid to late foetal development and then the bone marrow following birth. B cell development in bone marrow is continuous throughout life. B cell development begins with lymphoid-primed multipotent progenitors (LMPPs) that continue through the common

lymphoid progenitor stage (CLP) and are $CD34^{+}CD10^{+}CD19^{-}$ (Li et al., 1996; Nunez et al., 1996; Rumfelt et al., 2006). Cell specification is initiated at this stage, with progenitors that have an increase in CD19 and a decrease in CD10 expression maturing into the pro-B stage (Gounari et al., 2002; Li et al., 1996). At the pro-B cell stage, immunoglobulin heavy chain rearrangements begin with rearrangement of the D and J segments followed by a second rearrangement joining an upstream V region to the DJ segment. Following this rearrangement, cells progress into the pre-B stage where they express an immunoglobulin μ chain with a surrogate light chain (LC) to form a pre-B-cell receptor (pre-BCR) (Melchers, 2015; Pieper et al., 2013). This stimulates pre-B cell proliferation. Finally, these cells undergo immunoglobulin light chain rearrangement to become surface BCR-expressing immature B cells. Immature B cells then develop into $CD34^{-}CD10^{-}CD19^{+}$ mature B cells (Blom and Spits, 2006).

B cell development is a highly regulated process and requires hierarchical expression of a multitude of transcription factors. As the process of development progresses, gene expression associated with multipotency and stemness give way to expression of genes associated with B cell fate. The transcription factors IKAROS (IKZF1) (Yoshida et al., 2006), SPI1 (PU.1) (Arinobu et al., 2007) and E2A (Dias et al., 2008) are involved in the first stages of transition from HSCs into lymphoid progenitors and reduced myeloid lineage potential (Somasundaram et al., 2015). IKZF1 plays a fundamental role in lymphoid commitment and specification as *Ikzf*-/- mice are completely deficient in NK, B and T cells. Regarding B cells, they lack the pre-pro-B cell transitional population (Georgopoulos et al., 1994; Wang et al., 1996). The main function of IKZF1 is to reduce myeloid potential and induce expression of lymphoid specific genes. In addition to this transcription factor, studies have also

shown that loss of PU.1, E2A and MYB reduce the expression of *Flt3* and other lymphoid lineage genes (Somasundaram et al., 2015).

Multipotent progenitors expressing high levels of PU.1 are primed towards myelolymphoid development. Absence of PU.1 results in disruption in the formation of granulocyte/monocyte progenitors, as well as lymphoid progenitors. Subsequent differentiation towards B-lymphoid cells is accompanied by the loss of myeloid potential, which involves the interplay between IKZF1 and PU.1 (Somasundaram et al., 2015). Although high expression of PU.1 can result in myeloid cell specification, intermediate expression stimulates B-lineage cells (DeKoter and Singh, 2000). The zinc-finger transcriptional repressor, GFI1, plays a crucial role in reducing the transcriptional activity of PU.1 and disrupting its autoregulatory loop driving PU.1 expression. Its importance in B-lineage cell development has been shown in *Gfi1*$^{-/-}$ mice, where pre-pro-B and pro-B cell generation is impaired (Moroy and Khandanpour, 2011).

E2A is essential for promoting B-lineage specification and differentiation. It belongs to the E protein (class I) family of helix-loop-helix transcription factors (Dias et al., 2008) and its reduced function as a result of mono-allelic inactivation of the *E2a* gene results in a loss of pro-B cells (Zhuang et al., 1994). E2A is also known to regulate expression of the gene encoding the IL-7 receptor (IL-7R) (Dias et al., 2008). This is necessary for complete commitment to the B cell lineage as deficiency in *Il-7R* or *Il-7* itself leads to an early block in B cell development at the pro-B cell stage (Peschon et al., 1994) due to impaired *Vh* gene rearrangement, regulated by STAT proteins (Goetz et al., 2004). E2A also regulates the transcription factor, early B-cell Factor 1 (EBF1) essential for B-lineage commitment (Reynaud et al., 2008;

Smith et al., 2002), which in turn regulates Paired box 5 (PAX5). EBF1 can rescue the aberrant B lymphoid phenotype in *Ikzf1*$^{-/-}$ mice and *E2a* deficient cells. EBF1 is crucial in B cell development as *Ebf1*$^{-/-}$ mice show a block in differentiation at the pre-pro-B cell stage (Lin and Grosschedl, 1995). The main function of EBF1 is to induce PAX5 expression, which is initiated at the pro-B cell stage (Fuxa and Busslinger, 2007). It has a critical role in maintaining B lineage restriction as inactivation of *Pax5* allowed generation of multiple haematopoietic cell types from cells that would normally be restricted to B lineage commitment (Barberis et al., 1990; Nutt et al., 1999). Studies using *Pax5* knockout mice have suggested that it has a different role in B cell development in the bone marrow in comparison to foetal liver (Nutt et al., 1997). Whilst *Pax5*-deficient cells proceeded to the progenitor cell stage with normal immunoglobulin gene rearrangement in the bone marrow, B lymphoid cells were undetectable in the foetal liver. This suggested a critical role for PAX5 during foetal haematopoiesis (Nutt et al., 1997). However, the bone marrow cells were not committed to the B lineage, as *in vitro* culture of these cells in the presence of specific lineage cytokines resulted in differentiation into a variety of haematopoietic cell types (Nutt et al., 1999).

PAX5 is also known to target genes that encode important components of pre-BCR signalling in B cell development, therefore it has a fundamental role in signal transduction of pre-BCR and BCR, which result in differentiation into immature B cells that are ready to leave the bone marrow (Cobaleda et al., 2007). Following successful generation of immature B cells, some newly generated immature B cells expressing high-affinity autoreactive BCRs are eliminated, in order to positively select for B cells with functional surface BCR expression whilst maintaining immunological self-tolerance (Sandel and Monroe, 1999). Following

this, B cells enter the peripheral mature B cells pool, where they recognise foreign antigens. The response of the B cell to the foreign antigen drives B cell proliferation, hypermutation to generate a better fit for the antigen and longevity of the fully developed, foreign-antigen specific memory B cell (Melchers, 2015).

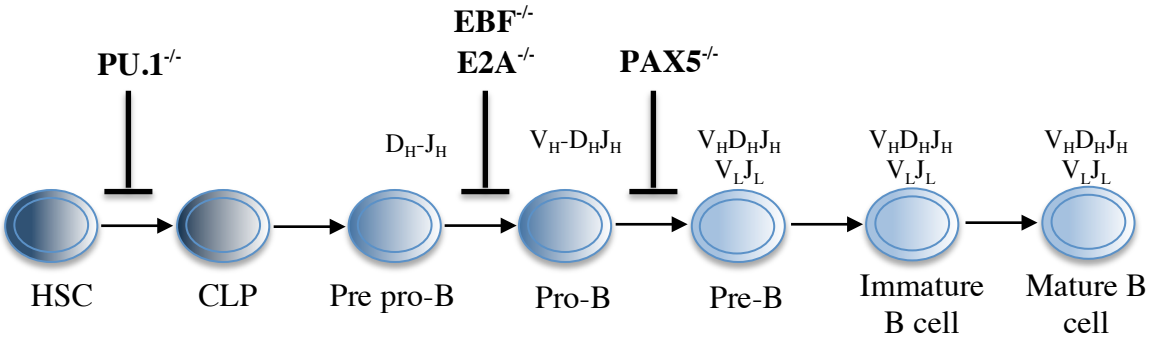

Figure 3 - B-cell development

The different stages of B-lymphopoiesis are indicated below the figure. The status of V(D)J recombination in the heavy and light immunoglobulin chains are indicated above the respective stages. The point of block in B cell development as a result of mice deficient in the transcription factors PU.1, E2A, EBF and PAX5 are also shown.

1.4 Disruption of transcription factor genes

B-lymphocyte development is controlled by specific transcription factor networks, which ensure activation of B-lymphoid lineage cells and silencing of alternate cell fates. However, these same regulatory networks can undergo genetic alterations contributing to malignant transformation (Somasundaram et al., 2015). Mutations, deletions or translocation of many of the genes encoding transcription factors essential for B cell lineage commitment and development, such as *IKZF1*, *E2A*, *EBF1*, *PAX5* and *RUNX1* have been associated with leukaemia. Such mutations

can cause a differentiation block at an early stage of development, which is a common feature of most leukaemias. For example, analysis of a large set of childhood leukaemias found frequent heterozygous deletions of *EBF1* and *PAX5*. This may result in a partial block in B cell development, contributing to malignant transformation (Mullighan et al., 2007). Furthermore, a block in expression of the pre-BCR complex and bypassing pre-BCR checkpoints can cause leukaemic cells to evade normal clonal selection (Eswaran et al., 2015). Therefore, appropriate expression of genes during B-cell development and differentiation is crucial, and disruption of these mechanisms may lead to cellular transformation, contributing to leukaemogenesis.

1.5 Acute Lymphoblastic Leukaemia

The term 'blast' refers to the morphology of a subpopulation of progenitors that are the earliest, most immature cells committed to the myeloid or lymphoid lineages, before the appearance of the definitive characteristics of the cell (Encylopedia, 2016). Morphologically, blasts usually form around 5% of cells in a normal healthy bone marrow. When blasts represent more than 20% of the cells of a specific lineage, it is considered to be a pathological status known as leukaemia (Harris et al., 1999). Leukaemia is further divided into subgroups. The first division separates acute and chronic forms of leukaemia followed by a subdivision based on the type of blood progenitor cells affected. This results in either lymphoblastic or myeloid leukaemia (Harris et al., 1999).

Acute lymphoblastic leukaemia (ALL) is the most commonly occurring paediatric cancer and accounts for 80% of all childhood leukaemia. ALL is a

heterogeneous disorder affecting both adults and children, with a peak prevalence in children of between the ages of 2 and 5 years (Pui et al., 2008). It is characterised by the malignant proliferation and clonal expansion of lymphoid progenitor cells arrested at an immature stage of differentiation in the T and B cell lineages. Although remarkable progress has been made in the treatment of ALL, with 5-year event free survival rate exceeding 90%, it still remains one of the main causes of cancer deaths in children (Pui et al., 2011). Furthermore, in developed countries the incidence of ALL has increased consistently by 1% a year over the past two decades (Linabery and Ross, 2008). The genetic events underlying the induction of ALL include aberrant expression of proto-oncogenes, chromosomal translocations and hyperdiploidy and hypodiploidy (Chen et al., 2010). These genetic alterations in blood progenitor cells committed to T or B cell differentiation promote leukaemic transformation by altering crucial cellular functions. For example, they maintain or enhance unlimited self-renewal capacity of these committed progenitors, subvert their normal proliferation controls, block differentiation at specific stages and promote resistance to apoptosis (Pui et al., 2004). A few cases (<5%) of ALL are associated with inherited, predisposing genetic syndromes, such as Down's syndrome, Bloom's syndrome and ataxia-telangiectasia. The majority of ALLs are represented by a pre-B cell phenotype, displaying cell surface marker expression associated with normal pre-B cells. The leukaemic cells are blocked at this particular stage of the differentiation process and accumulate in the body (Inaba et al., 2013).

Chromosomal translocations affecting specific genes are a defining characteristic of acute lymphoblastic leukaemia, in particular. These translocations sometimes result in the erroneous joining of two chromosome breaks, generating a fusion gene whose function is dissimilar to its wild type counterpart. ALL associated

fusion genes mainly encode active kinases or altered transcription factors (Pui et al., 2008). Many of these altered transcription factors control cell differentiation and frequently encode proteins at the apex of crucial transcriptional pathways. These oncogenic transcription factors are expressed aberrantly in leukaemic cells and can exist as one gene product or as a fusion protein combining two different transcription factors that play critical roles in normal haematopoiesis. Studies that examined gene-expression patterns in different leukaemias demonstrate that specific chromosomal translocations define unique disease subtypes (Fig. 4) (Pui et al., 2008).

1.6 'Delayed infection' hypothesis

One model to explain the induction of frank leukaemia in ALL suggests that an abnormal immune response to common pathogens can result in malignant transformation. Based on this idea, two different possible hypotheses were suggested (Greaves, 2006b). One mechanism, the Kinlen 'population mixing' hypothesis, was generated when in the early 1980s clusters of childhood leukaemia were observed in specific areas of England and Scotland (Kinlen, 1988). The 'population mixing' hypothesis stated that increased incidence of childhood leukaemia might have infectious origins due to unusual population mixing that occurred when isolated communities in Seascale and Thurso accommodated a sudden influx of migrant professional workers. People in isolated places may escape exposure to common infections in the usual age groups, and therefore are relatively 'non-immune' to these infections. Therefore, it was suggested that some childhood leukaemia clusters were an unusual outcome of common infections in these non-immune individuals, following contact or 'population mixing' with newcomers who are carriers of infections (Greaves, 2006b; Kinlen, 1988). Kinlen made a parallel comparison

between the communities of Seascale and Thurso to a 'rural' new town of Glenrothes with no migrant influx, to note a threefold transient increase in the incidence rate of childhood leukaemia, as measured by mortality statistics (Kinlen, 1988). Although in Kinlen's studies most patients had ALL, the data supporting this hypothesis could be interpreted to show that all childhood and infant leukaemia could share a common aetiology.

The second hypothesis was proposed in 1988 and is known as the 'delayed infection' hypothesis (Greaves, 1988). This model sought to explain the peak age prevalence of leukaemia between 2 and 5 years and at the time suggested a 'two-hit' model, which has now gathered substantial evidence. The 'two-hit' model proposed that the chromosomal translocation (first hit) was insufficient to induce overt leukaemia but rather acts as an initiating event resulting in pre-leukaemic cells that persist for years before onset of leukaemia, resulting from further acquisition of secondary genetic mutations (second hit). The 'delayed infection' hypothesis proposed that in affluent societies, many children have reduced exposure to common infectious agents during infancy. This predisposes the immune systems of such children to aberrant or atypical immune responses following 'delayed' infectious exposure to these common infections. These aberrant immune responses can provide a microenvironment that promotes secondary mutations, which then act as a trigger for progression of pre-leukaemic clones into overt leukaemia. Although there is substantial epidemiological evidence supporting this hypothesis, there is limited experimental data to support the reasons behind higher ALL incidence upon infection in young children (Greaves, 2006b).

1.7 t(12;21) ALL

The most frequent single chromosomal translocation associated with paediatric ALL is the t(12;21)(p13;q22) rearrangement (Fig. 4). This translocation results in the fusion of *the ETS transcription variant 6 (ETV6),* also known as *translocation-Ets-leukaemia (TEL)* gene, that maps on chromosome 12, and *Runt-related transcription factor 1 (RUNX1),* also known as *Acute myeloid leukaemia 1 (AML1)* gene, that maps on chromosome 21 (Romana et al., 1995). This gives rise to the *ETV6-RUNX1 (TEL-AML1)* fusion gene, which is exclusively associated with pre-B ALL, present in up to 25% of cases (Golub et al., 1995). *TEL* and *AML1* genes both encode transcription factors that play important roles in haematopoiesis. Both genes have been shown to be essential in establishing haematopoiesis of all lineages in the bone marrow and constitutive loss of either gene results in embryonic lethality (Okuda et al., 1996; Wang et al., 1997; Wang et al., 1996). The TEL transcription factor is required for HSC survival in the adult and is an essential regulator of post-natal HSCs. HSCs require TEL in order to migrate to the bone marrow from the foetal liver and for subsequent survival within the bone marrow microenvironment (Hock et al., 2004; Wang et al., 1997; Wang et al., 1998). In contrast, although AML1 is required for haematopoiesis at the embryonic stage, unlike TEL, loss of AML1 in the adult does not result in complete loss of haematopoiesis. Studies using conditional knock out mice have shown that AML1 is required for maturation of megakaryocytes and differentiation of T and B cell lineages, but not for maintenance of HSCs during adult haematopoiesis (Ichikawa et al., 2004). Furthermore, germline variants and somatic mutations in both genes have been linked to predisposition to leukaemia (Osato et al., 1999; Topka et al., 2015;

Zhang et al., 2015). *TEL* and *AML1* are also frequently disrupted by numerous different translocations in lymphoblastic and myeloid leukaemias.

The *AML1* gene belongs to the Runt-related transcription factor (RUNX) family of genes, also known as core binding factor (CBF) genes. The highly conserved RUNT domain of AML1 mediates DNA binding and heterodimerisation with CBFβ (Roudaia et al., 2009). Although the protein alone is capable of regulating expression of various different genes, binding to the CBFβ subunit enhances the affinity of the RUNT domain to DNA by 7- to 10- fold. Furthermore, it can inhibit RUNX1 degradation mediated by the ubiquitin proteasome pathway. It has been shown that TEL-AML1 fusion relies on CBFβ for its activity in experimental models, by participating in the formation of protein complexes necessary for its function (Roudaia et al., 2009).

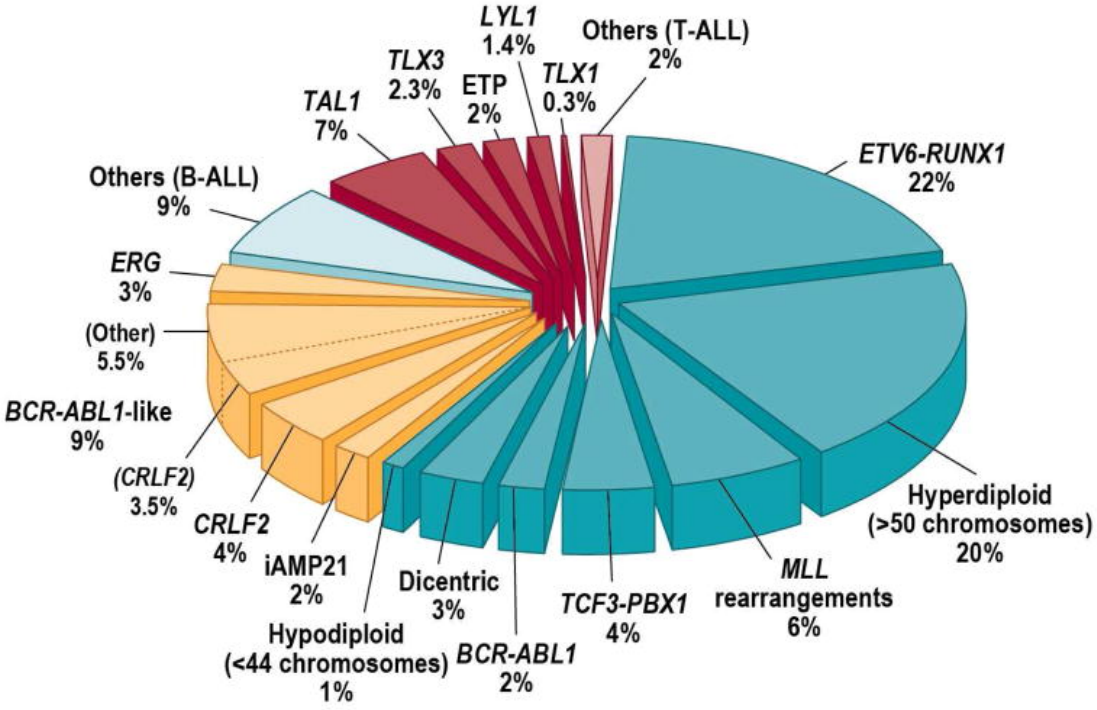

Figure 4 - Cytogenetic and molecular genetic abnormalities in childhood ALL

The frequencies of the different cytogenetic and molecular genetic abnormalities present in childhood ALL. The TEL-AML1 fusion gene represents the most frequent abnormality. Adapted from (Mullighan, 2012)

The TEL transcription factor comprises three important domains: The N-terminal pointed domain (PD) required for mediating protein-protein interactions, including TEL oligomerisation; C-terminal DNA-binding domain; and a central repressor domain, which is mainly involved in recruitment of repression complexes. The resulting translocation between the *TEL* and *AML1* genes creates a fusion transcript between the 5' of the TEL region, excluding the region encoding the DNA-

binding domain, to almost the entire coding region of *AML1* (Poirel et al., 1997; Zelent et al., 2004) (Fig. 5).

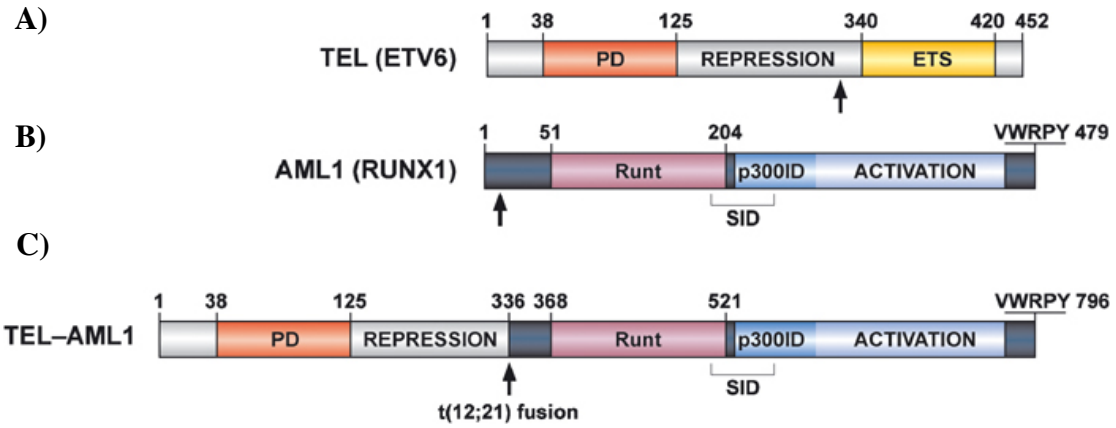

Figure 5 - Schematic representation of TEL, AML1 and the TEL-AML1 fusion protein

The figure shows the functional domains present in (A) TEL, (B) AML1 and the (C) TEL-AML1 fusion. TEL has three main domains: the Pointed Domain (PD) is necessary for oligomerisation and protein-protein interactions, the central repression domain (Repression) for binding with transcriptional repressors and the ETS DNA binding domain. AML1 has the RUNT DNA binding domain (RUNT), the mSin3A interaction domain (SID, bracket), the p300 HAT interacting domain (p300 ID) and the transcriptional activation domain (ACTIVATION). The carboxy-terminal VWRPY is a motif that binds Groucho-related co-repressors. The t(12;21) translocation results in the TEL-AML1 fusion with the arrow indicating the fusion points between TEL and AML1. The TEL-AML1 fusion has lost the TEL ETS domain. Adapted from (Zelent et al., 2004)

In patients the translocation is detected during B cell differentiation prior to the onset of immunoglobulin gene rearrangement, giving rise to leukaemic blasts that appear to be blocked at the pre-B cell stage (Panzer-Grumayer et al., 2005; Romana

et al., 1995). The most immature TEL-AML1 population is in fact identified by the aberrant $CD34^{+}CD38^{-}CD19^{+}$ phenotype, that has been associated with a very early stage of lineage commitment (Castor et al., 2005; Hong et al., 2008). The presence of the fusion gene, most likely occurring *in utero*, is largely detectable years before the clinical onset of the disease (Zelent et al., 2004). However, despite the prevalence of TEL-AML1 in childhood pre-B ALL it is unlikely that the presence of the fusion alone is sufficient for the resulting leukaemia. This is consistent with the variable and protracted latency in the onset of leukaemia in identical twins with concordant TEL-AML1 ALL (Wiemels et al., 1999). Furthermore, analysis of *TEL-AML1* frequency in unselected normal cord blood cells, showed that 1% of blood samples had detectable *TEL-AML1* transcripts. This was 100 times more frequent than the incidence of disease (Mori et al., 2002). Furthermore, estimation of the frequency of $TEL\text{-}AML1^{+}$ cells in these cord blood samples suggested that acquisition of the fusion was associated with clonal expansion of progenitor cells (Mori et al., 2002). In contrast, another model has shown that the presence of the fusion is as rare as the incidence of disease, suggesting that a high proportion of babies born with the *TEL-AML1* fusion go on to develop leukaemia (Lausten-Thomsen et al., 2011). Although the frequency of the fusion is still a matter of debate, whatever the frequency in the normal population, experimental models also indicate that TEL-AML1 alone is insufficient to induce overt leukaemia. Rather, in agreement with the 'two-hit' model, it is thought that TEL-AML1 acts as an initiating event resulting in the generation and expansion of pre-leukaemic cells that persist for years before onset of leukaemia, upon acquisition of secondary genetic mutations (Greaves, 1999; Greaves and Wiemels, 2003) (Fig. 6).

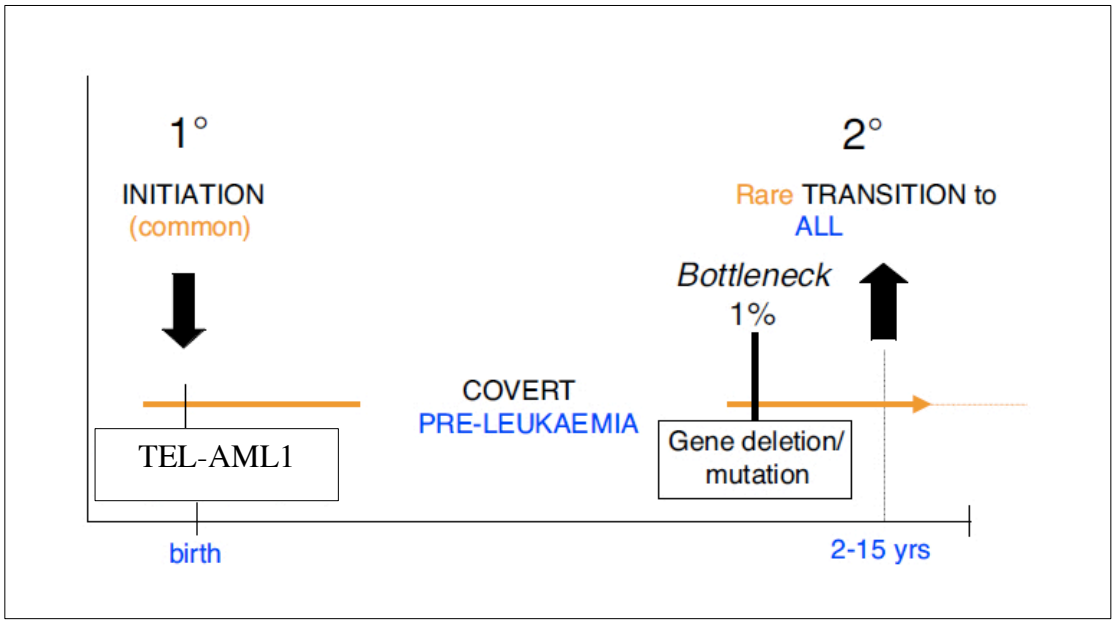

Figure 6 - 'Two-step' model for the pathogenesis of TEL-AML1 leukaemia

The fusion gene, TEL-AML1, although insufficient to cause overt leukaemia, occurs *in utero* and acts as an initiating event. The TEL-AML1 pre-leukaemic cells generated are susceptible to further acquisition of mutations that trigger development of overt leukaemia. Adapted from (Greaves, 2006a)

1.8 Experimental models of t(12;21) ALL

Modeling of TEL-AML1 ALL with *in vitro* and *in vivo* experiments has provided substantial insight into leukaemia induction. Andreasson et al. cloned the *TEL-AML1* fusion gene into a retroviral vector and used it to transduce growth factor dependent murine haematopoietic cell lines. Although expression of the fusion transcript was observed, none of the cell lines expressing TEL-AML1 showed factor-independent growth potential. Furthermore, to test the role of TEL-AML1 *in vivo*, transgenic mice were generated in which the expression of the fusion gene was directed to lymphoid cells under the control of a B cell-specific immunoglobulin

heavy chain enhancer. Although TEL-AML1 expression was confirmed in the mice, none of the transgenic mice developed any malignant disorder or abnormality (Andreasson et al., 2001). In line with this finding, transduction of adult bone marrow cells with a retroviral vector expressing TEL-AML1, followed by transplantation into syngeneic mice resulted in a low incidence of leukaemia after a long latency. However, expression of TEL-AML1 in mice deficient for $p16^{INK4a}p19^{ARF}$ resulted in a significantly high frequency of leukaemia induction. This provided the first evidence that co-operating secondary genetic aberrations may play a critical role in TEL-AML1 leukaemia (Bernardin et al., 2002).

As the fusion gene is thought to occur *in utero*, previous work in our laboratory examined the effect of TEL-AML1 expression on the function of foetal liver haematopoietic progenitor cells (HPC). In this model, TEL-AML1 enhanced the self-renewal capacity of B cell precursors *in vitro*, and hematopoietic reconstitution by transduced foetal liver HPC *in vivo*, with no block in B cell development (Morrow et al., 2004). Two additional studies used retroviral transduction, but in adult bone marrow derived HPC, to examine the effect of TEL-AML1 expression on haematopoiesis *in vivo*. Both studies noted TEL-AML1 caused a block in B cell development *in vivo*, resulting in a reduced number of TEL-AML1$^+$ mature B cells (Tsuzuki et al., 2004) (Fischer et al., 2005). However, all three studies provided evidence that TEL-AML1 perturbs normal haematopoiesis. The differences between these models may be a result of the nature of HPC targeted or differences in levels of TEL-AML1 protein expressed by the retroviral constructs used in each study. In the case of the latter explanation, the possibility was recently tested using two different retroviral vectors expressing high and low levels of TEL-AML1 (Tsuzuki and Seto, 2013). This showed that high levels of TEL-AML1 expression in mouse foetal liver

HPC or pro-B cells resulted in compromised B cell development *in vitro*. This was in contrast to low-level expression of TEL-AML1, which promoted B progenitor self-renewal. However, this was not evident in low-level expression of TEL-AML1 in pro-B cells derived from adult bone marrow. Following transplantation, low level TEL-AML1 expression in foetal liver derived pro-B cells resulted in a B cell differentiation block, but this block was incomplete and mature TEL-AML1 B cells did eventually emerge (Tsuzuki and Seto, 2013).

Two other recent studies created knock-in mouse models where *TEL-AML1* expression was driven from the endogenous *Tel* promoter. Although expression of the fusion gene alone did not cause disease in either study, both models showed that it predisposed to leukaemia and lymphoma under chemical mutagenesis or transposon-mediated mutagenesis (Schindler et al., 2009; van der Weyden et al., 2011). Schindler et al, showed that induction of T-cell leukaemia following treatment with the *N* ethyl-N-nitrosourea (ENU) mutagen was faster and more penetrant in knock-in mice compared to controls. Van der Weyden and colleagues used a sleeping beauty transposase to obtain B-ALL in almost 20% of the mice (Schindler et al., 2009; van der Weyden et al., 2011). Similarly, expression of a *TEL-AML1* transgene in mice heterozygous for *Cdkn2a* was found to predispose to radiation-induced B-cell malignancies (Li et al., 2013). In exploring how TEL-AML1 alters normal haematopoiesis, Schindler et al, noted that expression of TEL-AML1 in adult bone marrow resulted in increased numbers of quiescent HSCs and a loss of lymphoid committed progenitors. Furthermore, transplantation of TEL-AML1^{+} foetal liver cells into adult mice failed to reconstitute even the most immature B lineage compartment (Schindler et al., 2009). However, the fusion gene did not affect B cell differentiation in the embryo but induced a transient increase in self-renewal capacity

of foetal liver-derived TEL-AML1 B cell progenitor *in vitro*, consistent with the previous study from our laboratory (Morrow et al., 2004). This increase in B cell progenitors by TEL-AML1 may explain the increased frequency of *TEL-AML1*$^{+}$ cells in normal cord blood, in which leukaemia was absent (Mori et al., 2002).

Furthermore, another study where human cord blood HPC were transduced with a lentiviral vector expressing TEL-AML1, generated the aberrant $CD34^{+}CD38^{-}$ $CD19^{+}$ B lineage population associated with TEL-AML1 leukaemia (Castor et al., 2005) in transplanted mice (Hong et al., 2008). Consistent with other murine models, TEL-AML1 expressing human HPCs did not induce leukaemia in transplanted mice, suggesting that this population of cells represent pre-leukaemic B lineage cells. Therefore, taking into account all the experimental models, evidence for TEL-AML1 pathogenesis favours the 'two-hit' model where secondary genetic aberrations are necessary for the transformation of the TEL-AML1 pre-leukaemic cells to overt leukaemia.

1.9 Co-operating secondary genetic lesions

A current lack of murine models that successfully recapitulate human TEL-AML1 ALL could be due to the weak oncogenic activity of the fusion, stressing the importance to identify co-co-operating, secondary genetic alterations in *TEL-AML1* leukaemia. At diagnosis, most cases associated with the *TEL-AML1* fusion have deletions of the normal untranslocated *TEL* allele (Stams et al., 2006). A recent study reported that in 143 TEL-AML1 patient samples analysed for additional genetic lesions, 62% showed complete deletion of the normal *TEL* allele. The frequent occurrence of *TEL* deletions in TEL-AML1 patients suggested a selective advantage

for cells with the secondary mutation. This could be attributed to loss of either the suppressor function of normal TEL (Fenrick et al., 2000) (Rompaey et al., 2000) or its ability to dimerise with TEL-AML1 and reduce its transforming activity (Lopez et al., 1999). However, these deletions were sub-clonal to TEL-AML1 fusions (Romana et al., 1996), different between identical twins with concordant leukaemia (Maia et al., 2001) and distinct in late-relapse versus diagnostic samples (Ford et al., 2001). This suggested that these secondary mutations were associated with leukaemic progression rather than leukaemic transformation.

To identify co-operating secondary events in ALL in general, Mullighan et al. performed a genome-wide analysis of leukaemic cells from 242 paediatric ALL cases using high-resolution, single-nucleotide polymorphism (SNP) arrays and genomic DNA sequencing (Mullighan et al., 2007). This study established that a high proportion of lesions such as deletions, point mutations and amplifications in ALL occurred in genes involved in B cell development and differentiation. *PAX5* was found to be the most frequently altered gene in ALL. Deletions of other genes encoding transcription factors directly involved in B lineage development and differentiation pathways, such as *EBF1*, *IKZF1* (*IKAROS*), *E2A* and *IKZF3*, were also noted. In *TEL-AML1*$^{+}$ ALL deletions were most frequent, occurring at a rate from 6 deletions per case. More interestingly, 28% of cases contained mono-allelic *PAX5* deletions without mutations in the second allele. In an independent study, focal deletions in *PAX5* were detected in 20% of TEL-AML1^{+} cases (Lilljebjorn et al., 2010). The significance of the mutations in *PAX5* was recently highlighted by a study where chemical and viral mutagenesis was performed on mice heterozygous for a loss-of-function *PAX5* allele. This showed a higher incidence of pre-B ALL,

suggesting that loss of one *PAX5* allele may co-operate with TEL-AML1 to induce leukaemia (Dang et al., 2015).

Multiple studies have demonstrated that many of the deletions and translocations commonly found in lymphoid malignancies are a result of recognition of recombination signal sequences (RSS), close to the breakpoints of affected loci, by the RAG complex, which results in illegitimate recombination events (Marculescu et al., 2002; Mullighan et al., 2008a; Zhang and Swanson, 2008). The RAG recombinase is encoded by *recombination activating genes 1 and 2* (*RAG1* and *RAG2*) and is involved in V(D)J rearrangement during B and T cell development. Although RAG1 and RAG2 expression is tightly controlled, most pre-B ALL express both genes constitutively (Bories et al., 1991). Furthermore, high expression of *RAG1* gene is associated with TEL-AML1^{+} ALL (Haferlach et al., 2010). A recent study used whole genome and exome sequencing to examine the association between RSS and the genomic breakpoints of structural variations found in t(12;21) ALL (Papaemmanuil et al., 2014). Truncated RSS motifs were found at 40% and terminal deoxynucleotidyl transferase (TdT) activity at 70% of breakpoints. Most of these variants were present at promoter regions of genes known to be mutated in pre-B ALL such as *ETV6*, *BTG1*, *TBL1XR1*, *RAG2* and *CDKN2A-CDKN2B*. This suggested that the secondary events leading to leukaemic transformation in the presence of *TEL-AML1* are mainly driven by genomic rearrangement mediated by aberrant RAG activity (Papaemmanuil et al., 2014). Another enzyme, activation-induced cytidine deaminase (AID), normally involved in immunoglobulin class switching and somatic hypermutation in B cells, has also been associated with leukaemia. Aberrant AID activity has been observed in B-ALL, generating AID-dependent chromosomal translocations (Tsai et al., 2008). Further analysis showed

that AID co-operates with the RAG complex to generate these chromosomal translocations. A more recent study has shown that many of the genes recurrently mutated in pre-B ALL are potential targets of AID. Therefore, continuous illegitimate RAG- and AID-mediated recombination appears to be a major driver of diverse secondary mutations in TEL-AML1 leukaemia (Swaminathan et al., 2015).

1.10 Heterogeneity in ALL

Genome-wide expression analysis of acquired copy number alterations in paired diagnostic and relapse ALL samples showed that in some cases, the relapse clones did not contain lesions present in the diagnostic clone, suggesting that both clones were derived from an ancestral clone present at diagnosis (Mullighan et al., 2008b). An independent study comparing profiles of genome wide copy number alterations at diagnosis and relapse of 21 TEL-AML1 patients, reported that irrespective of the time of relapse, the relapse clone was derived from a major or minor sub-clone, present at diagnosis (van Delft et al., 2011). Furthermore, backtracking analysis by fluorescence *in situ* hybridization (FISH) identified a minor sub-clone at diagnosis that matched the genotype of a clone present at relapse 10 years later. This suggests sub-clonal diversity at diagnosis in TEL-AML1 patients, from which intraclonal origins of relapse are generated (van Delft et al., 2011).

Anderson et al, recently used multiplexed FISH to analyse copy number alterations in single cells from 30 paediatric TEL-AML1^{+} ALL cases. They reported significant heterogeneity in the sub-clones present at diagnosis and relapse, suggesting a dynamic and evolving clonal architecture in ALL (Anderson et al., 2011) (Fig. 7). More recently, Gawad et al, also used single-cell genomics to

examine the genomic heterogeneity of mutations in 1479 single cells from six different ALL patients. They reported significant subclonal heterogeneity in point mutations as well as structural lesions. Furthermore, they found that structural variants were acquired prior to point mutations, which occurred at later stages of clonal evolution and had hallmarks of apoliproprotein B mRNA editing enzyme, catalytic polypeptide-like (APOBEC) mutagenesis (Gawad et al., 2014). APOBEC, like AID, is a cytidine deaminase that has key roles in inducing genomic damage in multiple cancers due to its DNA deaminating activity. While AID acts in antigen-driven antibody diversification processes, APOBEC function in the innate immune system against viruses. Therefore, this report highlighting APOBEC mutagenesis was consistent with studies showing continuous AID- and RAG- mediated mutagenesis acting as a driver of sub-clonal diversity in ALL (Papaemmanuil et al., 2014; Swaminathan et al., 2015).

These studies suggest that significant heterogeneity is present in ALL, although the order in which mutations are acquired and the precise clonal structure at diagnosis is still largely unknown. It is possible that minor sub-clones can escape therapies targeting pathways deregulated by additional lesions, and pre-leukaemic cells that are not targeted can remain post-treatment to give rise to disease relapse. Therefore, it is important to identify therapies that target the one indispensable abnormality common to pre-leukaemic cells and all leukaemia sub-clones, the TEL-AML1 fusion protein.

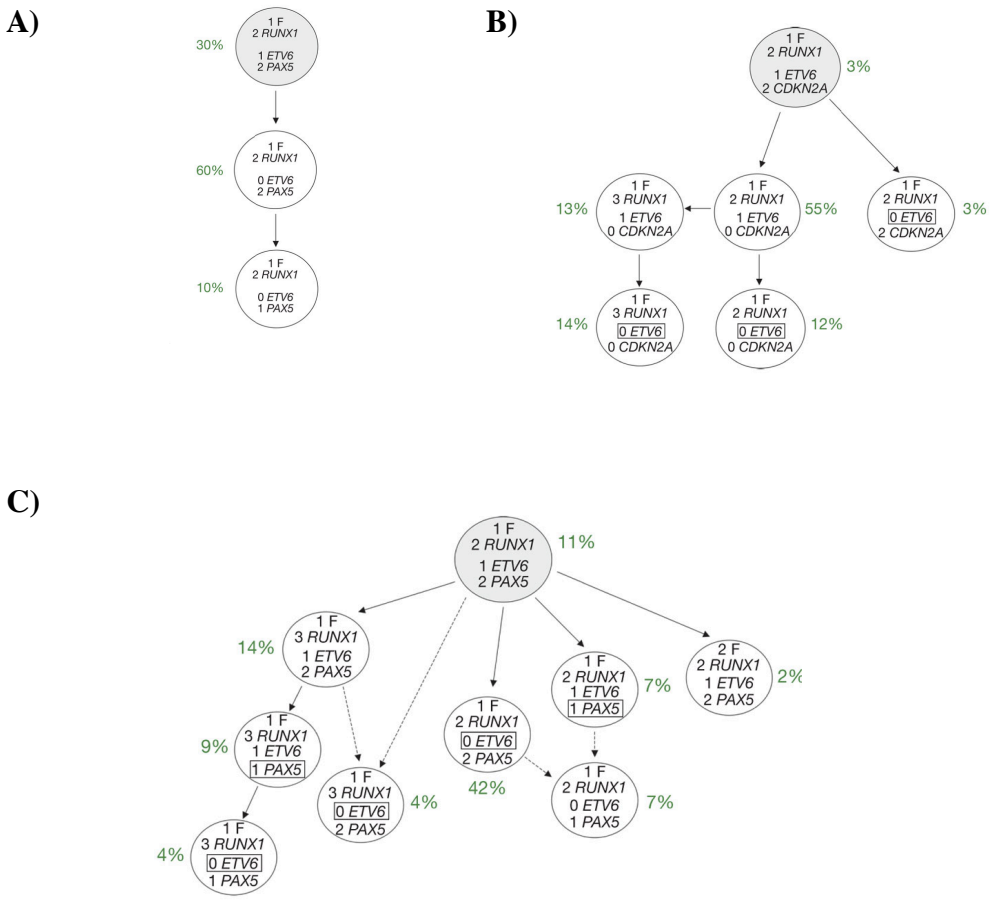

Figure 7 - Clonal architecture in TEL-AML1^{+} ALL

(A) The figure shows a linear architecture with three different clones. A moderately complex architecture with five subclones is seen in (B), with loss of the untranslocated *TEL* allele occurring independently in three separate subclones. (c) This figure shows a complex architecture with eight subclones, where *PAX5* deletions occur independently in two separate subclones. Although this shows that the clonal architecture can range from very simple to complex, in all cases, all subclones contain the fusion gene shown with F. Adapted from (Anderson et al., 2011)

1.11 Mechanism of TEL-AML1 function

Since the AML1 moiety in the fusion still retains its RUNT domain, TEL-AML1 can bind to AML1 transcriptional target genes. Indeed, the RUNT DNA binding domain has been shown to be crucial for TEL-AML1 function (Morrow et al., 2007). AML1 can act as a DNA-binding transcriptional activator, involved in expression of genes such as *PU.1* (Okada et al., 1998) and *IL-3* (Uchida et al., 1997), but can also act as a transcriptional repressor when associated with mSin3A or other co-repressors, through recruitment of Histone deactylases (HDACs) (Fears et al., 1997; Fenrick et al., 2000; Hiebert et al., 1996). Therefore, the effect of AML1 on target gene transcription may depend on the balance between its association with positive and negative cofactor complexes (Brettingham-Moore et al., 2015). The most frequently postulated mechanism for TEL-AML1 function is that the fusion protein acts as an antagonist of endogenous RUNX1 transcriptional activity (Fears et al., 1997; Hiebert et al., 1996; Uchida et al., 1999). TEL-AML1 repression activity depends on its ability to recruit co-repressor/HDAC complexes to the TEL moiety through its pointed domain, forming stable repressor complexes (Petrie et al., 2003). This results in deregulation of AML1 target genes. Although the AML1 moiety may still have the ability to associate with p300, its HAT activity may be suppressed in the context of the other bound cofactors (Zelent et al., 2004).

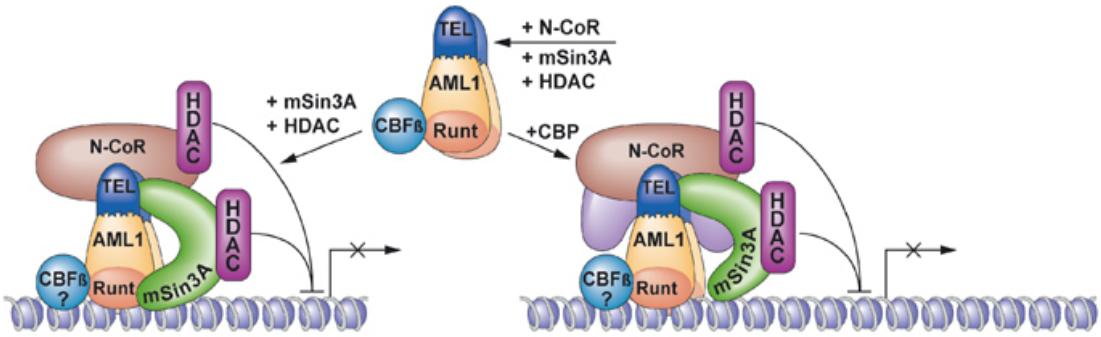

Figure 8 - Hypothetical model of TEL-AML1 function

This diagram shows a hypothetic model for the molecular function of TEL-AML1. In this model the TEL-AML1 fusion uses its TEL moiety to bind to co-repressors such as N-CoR and mSin3A to form a stable repressor complex. The fusion retains its ability to bind to DNA using the RUNT domain of AML1, so it may function as a HDAC-dependent repressor causing deregulation of AML1 target genes. Although p300 may still bind to the AML1 moiety of TEL-AML1, its HAT activity may not function correctly. Adapted from (Zelent et al., 2004)

A recent study examined gene expression and protein changes in TEL-AML1 expressing BaF3 cells using global gene expression analysis and stable isotope labeling by amino acids in cell culture (SILAC) (Linka et al., 2013). Using a novel anti-TEL-AML1 antibody, followed by chromatin immunoprecipitation (ChIP), they identified direct targets of the fusion protein. Although the bound promoters were found to be enriched in consensus AML1 binding motifs, most of the genes were not bound by TEL or AML1 in these cells. Therefore, this indicates that although TEL-AML1 functions by binding DNA at AML1 binding sequences to regulate

transcription, many of the genes it regulates are distinct to those regulated by wild-type TEL or AML1 (Linka et al., 2013).

Although experimental models and studies have demonstrated that TEL-AML1 alone is insufficient to cause leukaemia, data from recent studies have established its importance in leukaemia maintenance. One study used short hairpin RNA (shRNA) directed against *TEL-AML1* fusion to silence the fusion gene expression in REH cells (Fuka et al., 2011). Global gene expression analysis revealed that the fusion protein was involved in regulating various essential pathways such as cell survival, stem-cell self-renewal pathways. In particular the PI3K/AKT/mTOR signalling pathway was highly enriched in the list of down-regulated genes. This study also showed induction of apoptosis in TEL-AML1 cell lines following shRNA gene silencing. Furthermore, silencing of *TEL-AML1* resulted in impaired leukaemia engraftment and disease progression in immunodeficient recipient mice (Fuka et al., 2012).

1.12 STAT3 signalling in cancer

1.12.1 Structure and signalling of STAT3

Signal transducer activator of transcription 3 (STAT3) is a member of the signal transducers and activators of transcription (STAT) family. The STAT proteins are involved in various signal transduction pathways that control apoptosis, cell cycle progression and cell migration. It is the most ubiquitous of the STAT proteins and can be activated by a variety of cytokines, growth factors and oncogenes, including interleukin 6 (IL-6), epidermal growth factor (EGF) and platelet-derived growth

factor (PDGF) (Levy and Lee, 2002; Wake and Watson, 2015). However, its activation is primarily through IL-6 cytokine receptor-associated Janus Kinases (JAK), which phosphorylate STAT3 on a conserved tyrosine residue. The structure of STAT3 is similar to other members of the STAT family, consisting of a C-terminal transactivation domain, an N-terminal coiled-coil domain, a DNA-binding domain, a linker domain and a Src homology (SH2) domain. The N-terminal coiled-coil domain is necessary for dimer-dimer interactions during STAT3-driven transcriptional activation of genes (Fig. 9). The SH2 domain has three sub-pockets that stabilise homo and hetero-dimerisation with other STAT3 molecules or other members of the STAT family, and also plays a role in STAT3-receptor interactions. The DNA binding domain is responsible for DNA binding, enabling activated STAT3 dimers to bind specific DNA sequences and initiate transcription of target genes (Caldenhoven et al., 1996; Wake and Watson, 2015). An alternative splice variant of STAT3, STAT3β lacks the C-terminal transactivation domain, and was originally thought to have a dominant negative role, until it was shown to be a functional transcription factor regulating expression of several distinct target genes (Caldenhoven et al., 1996; Maritano et al., 2004; Yoo et al., 2002). It is phosphorylated on tyrosine 705 and can therefore form dimers that have been shown to possess DNA-binding activity (Maritano et al., 2004).

STAT3 activation requires phosphorylation of specific tyrosine residues (Tyr705) in the C-terminal region by receptor or intracellular tyrosine kinases (Fig. 9). Once phosphorylated, STAT3 homodimerises through reciprocal SH2 domain-Y705 interactions and dimers translocate to the nucleus (Yu and Jove, 2004). These can then bind distinct canonical palindromic sequences in promoter regions of genes

to generate important cellular responses (Kang et al., 2013). STAT3 is also capable of forming heterodimers with STAT1 due to their sequence similarity, and other STAT proteins, to control transcription of a larger set of target genes (Ho and Ivashkiv, 2006; Schroder et al., 2004). The serine residue, Ser727 is phosphorylated to promote full STAT3 activation and is important in prolonging nuclear retention. However, it is only found to be present in the STAT3α isoform (Wake and Watson, 2015).

STAT3 expression is tightly regulated in cells by various endogenously expressed proteins that are capable of inhibiting STAT3 signalling. Suppressors of cytokine signalling (SOCS) can bind activated JAKs or receptor domains to block STAT phosphorylation and effectively inhibit JAK/STAT signalling. SOCS3 is a transcriptional target of STAT3, which specifically inhibits STAT3 signalling in a negative feedback mechanism (Starr et al., 1997). Likewise, protein inhibitor of activated STAT3 (PIAS3) is a member of a family of small ubiquitin-like modified (SUMO) E3 ligases, and directly inhibits STAT3 by blocking its DNA-binding activity (Chung et al., 1997).

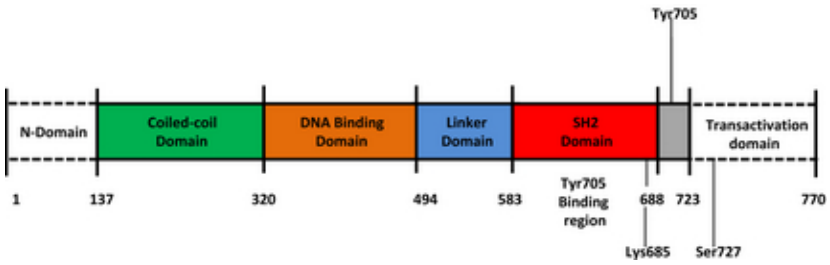

Figure 9 - STAT3 functional domains

The diagram depicts the functional domains of STAT3 and the respective amino acid boundaries between each domain. The N-terminal domain, coiled-coil domain, DNA-binding domain, linker domain, SH2 domain and transactivation domain are shown. The phosphorylation sites Tyr705 and ser727 are shown along with the acetylation site Lys685. Adapted from (Wake and Watson, 2015).

1.12.2 STAT3 in cancer

Abnormal STAT3 activity is found in multiple haematological and solid cancers and was first observed to be constitutively active in breast cancers. It is directly associated with oncogenic transformation mediated by different oncoproteins, such as sarcoma viral oncogene homolog tyrosine kinase (v-SRC). For example, constitutively active STAT3 in AML patients correlated with significantly shorter disease-free survival (Benekli et al., 2009). Furthermore, constitutive activation of STAT3 affects the function of many oncogenic mediators known to be deregulated in cancers. For example, STAT3 up-regulates cell cycle-regulators such as *c-MYC* and *cyclins D1* and *D3* (Amin et al., 2004) and can also inhibit *TP53* expression (Niu et al., 2005). These main target genes of STAT3 alter cell cycle progression and prevent apoptosis. Therefore, STAT3 inhibition impedes tumour progression and can induce cell death (Wake and Watson, 2015). In contrast to most oncogenes, *STAT3* mutations are not common in tumours but recently activating *STAT3* mutations have been discovered in 40% of T-cell large granular lymphocytic leukaemia (Koskela et al., 2012).

STAT3 inhibition and knockdown have been shown to increase cell death and reduce cancer cell growth *in vivo* and *in vitro*. For example, STAT3 inhibition in malignant glioma xenograft models, inhibited c-MYC, BCL-X_L and MCL-1 expression measured by western blot analysis and induced apoptosis (Iwamaru et al., 2007), and *STAT3* siRNA-mediated knockdown in laryngeal tumours down-regulated BCL-2, survivin and cyclin D1 protein levels and stimulated apoptosis (Gao et al., 2006). Therefore, targeting the STAT3 pathway may be effective at

inhibiting cancer progression. In addition, identification of STAT3 regulated genes may provide additional targets for therapy.

1.12.3 Role of STAT3 in TEL-AML1$^+$ leukaemia

Recent work from our laboratory used shRNA to establish a direct role for TEL-AML1 in aberrant signalling pathways that promote leukaemia (Mangolini et al., 2013). A *TEL*-specific shRNA was used to silence *TEL-AML1* expression in REH cells, which lack the untranslocated wild type *TEL* allele. *TEL-AML1* silencing resulted in growth inhibition and reduced colony formation. This study reported that TEL-AML1 leukaemia cells are dependent on aberrant activity of STAT3 for survival and *in vivo* progression. STAT3 activation is mediated through TEL-AML1 induced RAC1 activation in these cells (Fig. 10). Furthermore, TEL-AML1$^+$ primary ALL cells were also susceptible to pharmacological STAT3 inhibition. These findings suggest that the fusion protein has an active role in up-regulating expression of genes fundamental to the activity of oncogenic pathways, in addition to functioning as an atagonist to wild-type AML1.

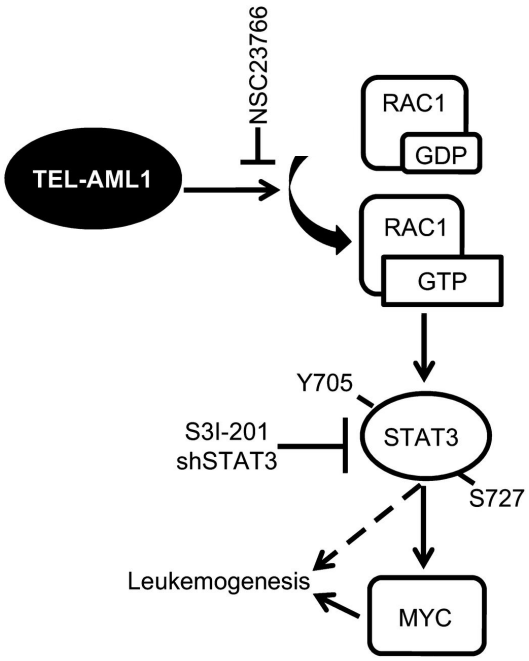

Figure 10 - Model of TEL-AML1-induced leukaemogenesis

This figure shows TEL-AML1 induces RAC1 activation, which in turn promotes STAT3 phosphorylation at specific residues. This results in *c-MYC* transcriptional induction leading to leukaemogenesis. Adapted from (Mangolini et al., 2013)

The significant degree of clonal heterogeneity in ALL suggests that minor clones may escape therapies targeting pathways deregulated by secondary lesions. Therapies that spare pre-leukaemic cells are also likely to give rise to higher relapse rates. Therefore, one possible solution would be to identify therapies targeting the common abnormality in pre-leukaemic cells and leukaemic clones, in this case the TEL-AML1 fusion protein itself. Moreover, since TEL-AML1 is thought to induce aberrant *RAG* gene expression, which contributes to secondary genetic events,

targeting the fusion may also impair acquisition of these lesions (Papaemmanuil et al., 2014). Therefore, significant focus has been placed on identifying transcriptional and signalling pathways regulated by TEL-AML1. Studies showing TEL-AML1$^+$ cells to be particularly susceptible to PI3K/AKT/mTOR (Fuka et al., 2012) and STAT3 inhibition (Mangolini et al., 2013) suggest promising therapeutic approaches by targeting these pathways.

1.13 Role of infection in TEL-AML1$^+$ leukaemia

As previously mentioned, although there is limited experimental evidence for the role of delayed infection and abnormal immune signalling in leukaemia, recent studies have explored the role of immune modulators in TEL-AML1$^+$ leukaemia. The study by Swaminathan et al, suggested a role for inflammatory factors in leukaemia pathogenesis (Swaminathan et al., 2015). In normal pre-B cell development, AID expression increases at the developmental stage associated with pre-BCR signaling-mediated IL7R downregulation, concomitant with increased RAG expression. However, stimulation of pre-B cells with the inflammatory lipopolysaccharide (LPS) in the absence of IL7 further increased AID expression. Since TEL-AML1 is known to induce expression of the RAG complex, this study demonstrated that strong inflammatory stimuli can co-operate with TEL-AML1 to induce RAG- and AID-dependent mutagenesis in t(12;21) leukaemia (Swaminathan et al., 2015).

As well as indirectly promoting secondary mutagenesis, evidence suggests that TEL-AML1 may also contribute to leukaemogenesis through a different mechanism. Thus, the fusion was found to confer resistance to TGF-β in mouse

BAF3 cells and human cord blood cells (Ford et al., 2009). The authors suggest that this may reveal the underlying mechanism responsible for the association of leukaemogenesis and delayed infection. According to the hypothesis, TEL-AML1-expressing pre-leukaemic cells would expand at the expense of normal progenitors in the face of abnormal systemic TGF-β exposure, favouring their progression to overt leukaemia (Fig. 11). Indeed, it is possible that expansion of the pre-leukaemic subpopulation would have the effect of increasing the likelihood that RAG- and AID- dependent mutagenesis would generate leukaemia promoting lesions. The precise mechanism by which TEL-AML1 inhibits TGF-β signalling remains unclear, although the study suggested it may be due to sequestration of SMAD3 by TEL-AML1 (Ford et al., 2009).

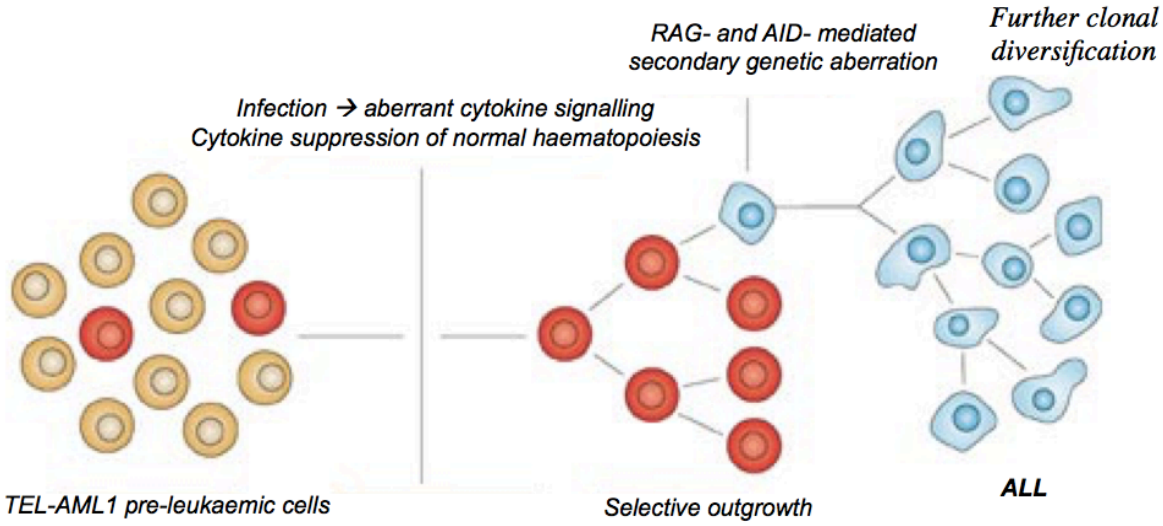

Figure 11 - Speculative model of the role of infection in leukaemia induction.

Abnormal cytokine and immune modulators' signalling can result in the suppression of normal haematopoietic cells and select for the outgrowth of TEL-AML1 pre-leukaemic cells. This results in proliferation of pre-leukaemic cells, increasing the pool of cells available to undergo RAG- and AID-

mediated secondary genetic aberrations, resulting in ALL. Further clonal diversification may be present at later stages of clonal evolution, for example hallmarks of APOBEC mutagenesis have been detected. Adapted from (Greaves, 2006b)

1.14 TGF-β signalling

1.14.1 TGF-β canonical signalling pathway

TGF-β belongs to the transforming growth factor superfamily, along with other family members such as nodals, activins and bone morphogenetic proteins (BMPs). TGF-β exists in three different isoforms: TGF-β1, TGF-β2 and TGF-β3. The three isoforms have high sequence homology but *in vivo* the gene knockouts of the isoforms result in very different phenotypes. About half of *TGF-β1* null mice die after birth as a result of uncontrolled inflammation (Clark and Coker, 1998). *TGF-β2* knockout mice exhibit perinatal mortality and instead have multiple developmental defects that are not found in *TGF-β1/3* knockout phenotypes (Sanford et al., 1997). *TGF-β3* null mice die within 20 hours of birth and have a unique phenotype of delayed pulmonary development and defective palatogenesis (Kaartinen et al., 1995). TGF-β1 is the most abundant isoform present in tissues (Vaidya and Kale, 2015). TGF-β has a wide range of activities, controlling different developmental pathways in a tissue-dependent manner. The complexity of TGF-β activity was discovered in the 1980s, when it was found that effects of TGF-β were different depending on the cell type examined and the conditions analysed (Massague, 2012). TGF-β regulates gene expression of numerous different target genes, both positively and negatively,

depending on the target gene and the cellular context. The complexity behind how TGF-β transcriptional responses result in activation or repression of hundreds of target genes, under tightly controlled conditions, has been an on-going area of research and involves understanding canonical TGF-β signalling (Massague, 2012)

TGF-β signalling is mediated by receptor activation of SMAD transcription factors (Fig. 12). Eight SMAD proteins are encoded in the human genome, with only five acting as substrates for TGF-β family of receptors, known as receptor-regulated SMADs (R-SMADs) (Massague, 1998). SMAD2 and SMAD3 are two R-SMADs specific to activin, nodal and TGF-β signalling, while SMAD1/5/8 act as substrates to BMP signalling. SMAD4 is known as co-SMAD and acts as a common SMAD for all TGF-β family members. SMAD7 is an inhibitory SMAD (I-SMAD) of TGF-β, acting negatively to disrupt R-SMAD interactions and activation in TGF-β signalling (Massague and Chen, 2000). TGF-β functions as a homodimeric ligand but is secreted in a latent form, bound to its propeptide, or is trapped by binding occluding factors. Once released from its inactive complexes, the ligand binds to a pair of membrane receptor serine/threonine kinases, the TGF-β receptors, generating a hetero-tetrameric receptor complex. This results in the phosphorylation of SMAD2 and SMAD3 (Fig. 12). SMAD2 and SMAD3 can exist as homodimers or heterodimers, which then bind to the co-SMAD, SMAD4. In the basal state, the R-SMADs and SMAD4 undergo constant nucleocytoplasmic shuffling (Massague et al., 2005; Whitman, 1998). Following activation, the SMAD complex translocates to the nucleus, and incorporates different DNA-binding cofactors that specify target gene selectivity, influencing binding to different transcriptional co-activators and co-repressors. Hundreds of genes are then transcriptionally regulated by TGF-β,

including *SMAD7*, the product of which subsequently inhibits signalling in a negative feedback mechanism (Massague et al., 2005). Although SMADs are critical mediators of TGF-β signalling, TGF-β can function via SMAD-independent pathways, involving mediators such as mitogen-activated protein kinases (MAPK), c-Jun N-terminal kinases (JNK) and Nuclear factor kappa-light-chain-enhancer of activated B cells (NF-κB) (Vaidya and Kale, 2015).

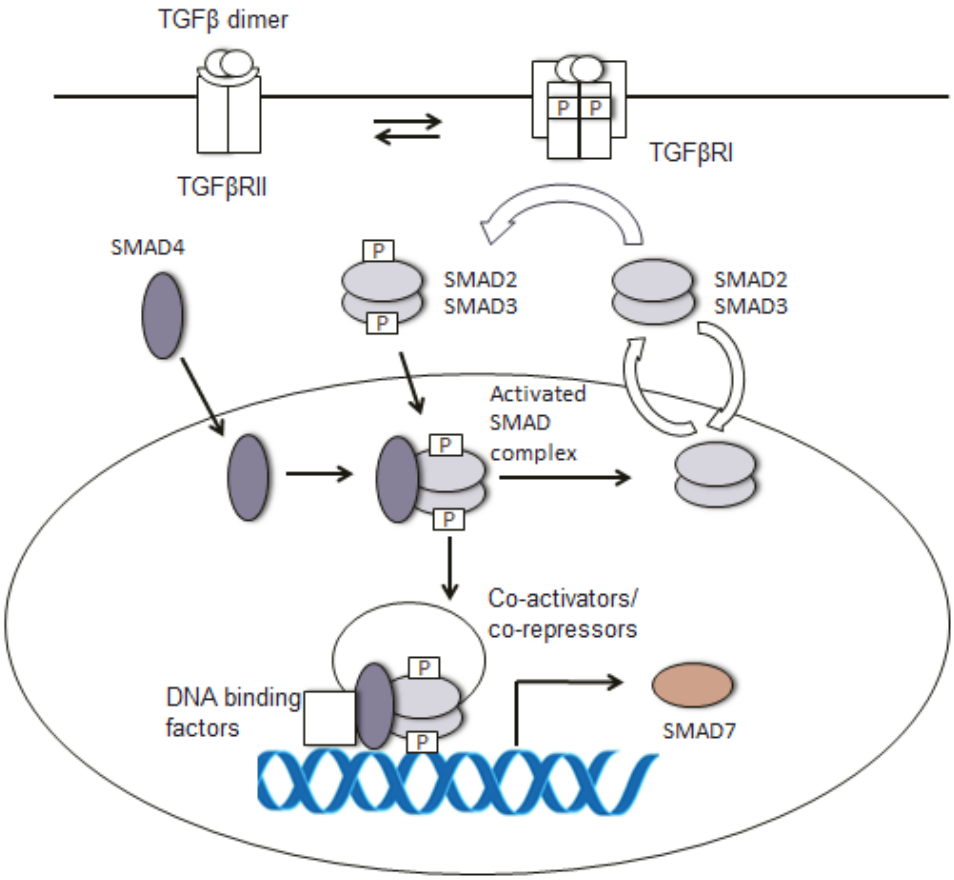

Figure 12 - TGF-β canonical signalling

The TGF-β ligand binds to a pair of TGFβR-II serine/threonine kinases which results in phosphorylation of the GS domain on a pair of TGFβR-I kinases. This creates a repeated pS-X-S motif which serves as a docking site for the R-SMADs. In the basal state, R-SMADs and SMAD4 undergo constant nucleocytoplasmic shuffling. Anchor proteins present the R-SMADs to the receptor resulting in the phosphorylation of R-SMADs at the C terminus, which permits R-SMADs to enter the nucleus and to be recognised by a basic pocket in SMAD4. This SMAD complex then binds to different DNA-binding co-factors and recruits transcriptional co-activators and repressors to regulate several different genes, including *SMAD7*, the I-SMAD.

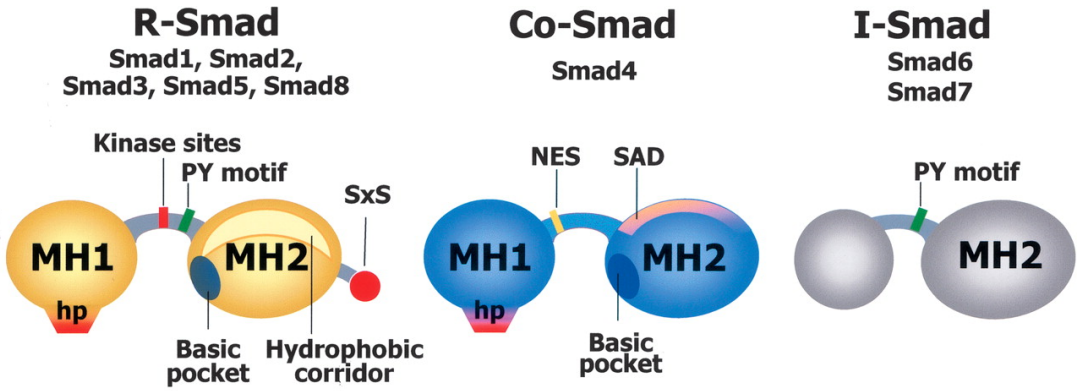

Figure 13 - Structure of SMAD proteins

This figure illustrates the structural domains of SMAD proteins. SMAD proteins have two globular domains, MH1 and MH2. R-SMADs and SMAD4 use the MH1 domain to bind to DNA using a β-hairpin structure (hp). I-SMADs lack the MH1 domain. The linker region of R-SMADs and I-SMADs contains a PY motif for recognition by Smurf ubiquitin ligases, involved in the deactivation of SMAD signalling. R-SMADs also have kinase sites in their linker region for interactions with protein kinases such as MAPKs and CDKs. The MH2 domain of R-SMADs and SMAD4 contains a basic pocket for interaction with activated type I receptors. The SxS motif of R-SMADs is the site phosphorylated by the activated receptor. The hydrophobic corridor is a site for multiple interactions. The linker region of SMAD4 contains a nuclear export signal (NES) for nuclear translocation. The Smad4 activation domain (SAD) mediates interactions with transcriptional activators and repressors. Adapted from (Massague et al., 2005)

TGF-β plays an important role in regulating the immune system. It is produced by every leukocyte lineage, including lymphocytes, macrophages and

dendritic cells but can also be produced by many non-immune cells (Letterio and Roberts, 1998; Travis and Sheppard, 2014). It has an effect on adaptive immunity, mainly in the regulation of effector and regulatory $CD4^+$ T cell responses, and plays a fundamental role in regulating differentiation of T cells into effector and regulatory cells, in a context specific manner. For example, TGF-β acts as a suppressor of Th1 effector T-cell differentiation, however under certain *in vitro* conditions it can enhance Th1 cell differentiation in the presence of IFN-γ (Travis and Sheppard, 2014). It is also involved in initiation and resolution of inflammatory responses (Wrzesinski et al., 2007), driving either pro- or anti-inflammatory responses depending on the amount of TGF-β present in the cells and other factors present at the time of TGF-β exposure (Travis and Sheppard, 2014).

1.14.2 The role of TGF-β in haematopoiesis

The role of TGF-β in regulation of HSCs and progenitor cells has been studied from the late 1980s (Kulkarni et al., 1993; Larsson et al., 2001; Oshima et al., 1996). Studies in both human and mouse models have shown inhibitory functions of TGF-β on early haematopoietic stem cells and primitive progenitors *in vitro*. Studies showed that TGF-β inhibited the growth of early MPPs, whilst more mature progenitors remained unaffected (Larsson and Karlsson, 2005). Although the exact mechanism of how TGF-β acts on HPCs is not fully understood, some studies suggest that these effects are largely due to its regulation of cytokine receptors such as receptors for IL3, SCF and granulocyte-colony stimulating factor (G-CSF) (Larsson and Karlsson, 2005). One study reported that TGF-β induces cell cycle arrest in primary human haematopoietic cells by down-regulating c-MYC and

upregulating a cyclin-dependent kinase inhibitor, p57 (Scandura et al., 2004). These studies complement data showing that the growth inhibitory effect of TGF-β can be reversed, by expressing a dominant negative TβRII to block autocrine TGF-β signalling, resulting in enhanced proliferation and survival of human HSCs *in vitro*. This suggests that the main effect of TGF-β on HSCs is the inhibition of proliferation, rather than induction of apoptosis. In contrast, some other studies suggest TGF-β may be pro-apoptotic, for example by inhibiting stem cell factor and other cytokines that promote viability of primitive murine haematopoietic cells (Jacobsen et al., 1995). However, it is also thought to have an anti-apoptotic role by inhibiting Fas-induced growth suppression and apoptosis of murine progenitor cells (Dybedal et al., 1997). These data collectively suggest that TGF-β may regulate HSCs via both cell cycle control and apoptotic mechanisms (Soderberg et al., 2009) (Vaidya and Kale, 2015).

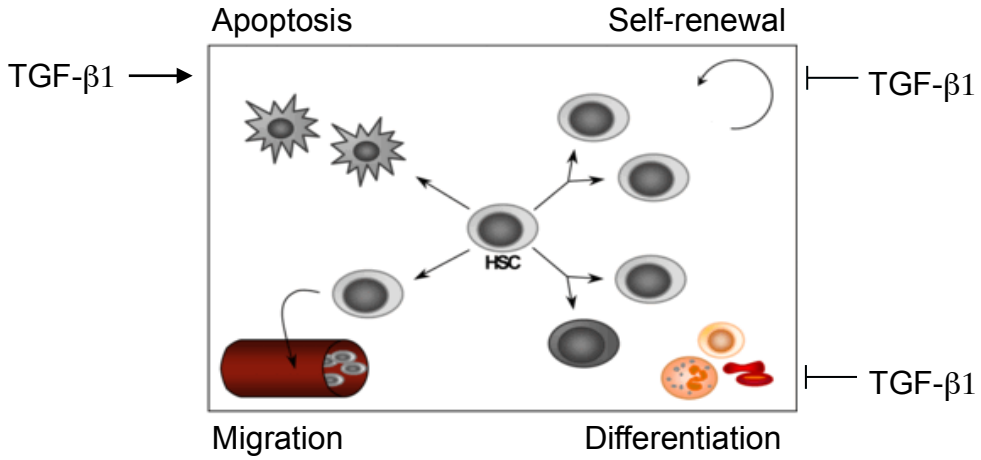

Figure 14 - Role of TGF-β1 in the different cell fates of HSCs

HSCs can self-renew to maintain the stem cell pool, differentiate into different haematopoietic cell lineages, migrate out into the blood steam or undergo apoptosis. TGF-β1 inhibits self-renewal and differentiation of HSCs, as well as promoting apoptosis. Therefore, it has a prominent role in HSC development, with positive and negative effects on the different stages of development.

To examine the role of SMAD transcription factors in haematopoiesis, one study blocked SMAD signalling in HSCs (Soderberg et al., 2009). This was achieved by either expressing SMAD7, which inhibits phosphorylation of all R-SMADs, or conditional deletion of *Smad4*, which is critical for nuclear transduction of SMAD signalling (Soderberg et al., 2009). Forced expression of SMAD7 in HSCs resulted in disrupted SMAD signalling and TGF-β responsiveness *in vitro*. Furthermore, bone marrow (BM) transplantation assays showed that SMAD7 overexpressing HSCs had significantly greater capacity to engraft secondary recipients compared to control cells. As SMAD7 overexpression blocks R-SMAD signalling this suggests that when R-SMAD signalling is blocked, self-renewal is promoted *in vivo,* whereas in control animals the HSC pool becomes exhausted (Blank et al., 2006; Blank and Karlsson, 2011). Since differentiation appeared to be unperturbed, this suggests that self-

renewal and differentiation are modulated independently by SMAD signalling. However, experiments with *Smad4* deficient cells did not support these findings, since deletion of *Smad4* resulted in impaired self-renewal and maintenance of the HSC pool. The apparent contradiction in these findings can be explained by the role of SMAD4 in balancing the negative effects of the SMAD pathway and the positive regulation of HSCs in cross-talk with Notch and Wnt signalling pathways, involved in haematopoiesis regulation (Soderberg et al., 2009). Therefore, abolishing SMAD4 expression in HSCs may result in impaired interactions between SMAD4 and other positive regulatory pathways, leading to impaired self-renewal, explaining why cells behave differently to cells overexpressing SMAD7.

TGF-β is involved in lymphopoiesis and affects B cells at all stages of development. Primarily, TGF-β has a role in the generation of B cells from lymphoid precursors. TGF-β down-regulates IL-7 production by stromal cells which can inhibit IL-7 dependent B cell proliferation. (Lebman and Edmiston, 1999). Furthermore, TGF-β also inhibits the pre-B to B cell transition by inhibiting light chain rearrangement at the pre-B cell stage. (Lebman and Edmiston, 1999). TGF-β can also induce apoptosis, although this appears to be independent to proliferation inhibition, since one study found that TGF-β induced apoptosis of human B-cell lymphoma occurred prior to cell cycle arrest (Lebman and Edmiston, 1999). TGF-β has further roles in B cell maturation, such as regulating expression of cell surface molecules, including inhibition of IgM, IgD, and IgA, and induction of MHC class II expression on both pre-B and mature B cells (Letterio and Roberts, 1998). It is also known to induce class switch recombination to IgA in humans, but the specific events leading to this class switching are yet to be elucidated. In mature B cells,

TGF-β does not inhibit proliferation, unlike in B cell progenitors. Therefore, TGF-β is important for normal B cell development but differentially affects B cells according to their stage of differentiation (Letterio and Roberts, 1998).

1.14.3 TGF-β and cancer

Since TGF-β has multiple functions, perturbations in its signalling pathway are linked to many clinical disorders, including cancer. It has a complex role in cancer as it can act as both a tumour suppressor and promoter, at different stages of tumourigenesis (Roberts and Wakefield, 2003) (Drabsch and ten Dijke, 2012). At early stages, it can act as a tumour suppressor due to its ability to induce apoptosis. At later stages, tumour cells can become resistant to the anti-proliferative effects of TGF-β, but remain responsive to TGF-β signalling, frequently secreting TGF-β, in cases such as pancreatic cancer. In this context, the pro-oncogenic activities of TGF-β may be revealed, such as induction of epithelial to mesenchymal transition (EMT), and increasing motility, invasiveness and metastasis (Nicolas and Hill, 2003). Mutations in genes encoding mediators of the TGF-β pathway are frequent in cancer, with alterations mainly affecting genes encoding TGF-β receptors, R-SMADs and SMAD4. These mutations have been recorded in almost all pancreatic and colon cancers. Aberrations affecting *SMAD2* and *SMAD4* take the form of deletions, frameshift mutations and loss of entire chromosomal regions (Lebrun, 2012). Reduced expression of SMAD2 is associated with enhanced tumourigenicity in breast cancer cell lines (Kretzschmar, 2000) and *SMAD4* mutations are found in the germ line of a subset of juvenile polyposis families (JNP) (Howe et al., 1998). In leukaemia, TGF-β has recently been implicated in the natural killer (NK) cell

mechanism of immune evasion in childhood B-ALL (Rouce et al., 2015). A study showed that ALL-derived TGF-β was an important mediator of NK cell dysfunction, which was abrogated by blocking TGF-β. The data indicated that by regulating the TGF-β/SMAD pathway, ALL blasts induced changes in NK cells to circumvent innate immune surveillance (Rouce et al., 2015).

As TEL-AML1 has been shown to have a direct role in regulating TGF-β signalling, this suggests that the fusion gene has an active role in not only functioning as an antagonist of wild-type AML1, but dysregulates important signalling pathways in leukaemia. Due to the significant heterogeneity of the disease, it is important to target the transcriptional networks and oncogenic pathways directly deregulated by the TEL-AML1 fusion itself to gain a better understanding of how it promotes childhood ALL and to generate better therapies.

PROJECT AIM

A popular hypothesis to explain childhood leukaemia aetiology is that aberrant signalling responses of pre-leukaemic clones to cytokines and immune modulators trigger progression to overt leukaemia. Since TGF-β has previously been implicated in promoting outgrowth of pre-leukaemic cells, one aim of this project was to examine the role of TGF-β signalling in TEL-AML1$^+$ leukaemia. Recent data from our laboratory established the importance of STAT3 signalling in TEL-AML1$^+$ leukaemia. Since STAT3 and TGF-β signalling pathways are known to be subject to cross-talk in many different systems, we also aimed to investigate the importance of such interactions in leukaemia progression. Therefore the objectives of my project were to:

1. Examine the impact of TEL-AML1 on TGF-β sensitivity in ALL and pre-leukaemia cells
2. Determine the role played by SMAD7 in regulating TGF-β responses and leukaemia progression

CHAPTER II. Materials and Methods

2.1 Molecular Biology

2.1.1 Transformation of bacteria

Sub-cloning efficiency DH5α™, library efficiency DH5α™ and One Shot® *Stbl3*™ chemically competent cells (ThermoFisher Scientific, Loughborough, UK) were used for transforming bacteria. The competent cells were thawed on ice and incubated with 1µg of DNA in polypropylene tubes (BD Bioscience, Oxford, UK). The mixture was incubated for 20 minutes on ice, followed by 30 seconds of heat shock in 37°C water bath. Following this, the mixture was incubated for a further 2 minutes on ice. 300µl pre-warmed SOC outgrowth medium (New England BioLabs, Ipswich, UK) was then added to the mixture and shaken at 37°C for 1 hour at 225rpm. The mixture was then plated onto plates containing: LB agar (1.5g bacto Agar [BD Bioscience] per 100 ml LB broth (1% w/v Bacto Tryptone [BD Bioscience], 0.5% w/v bacto Yeast Extract [BD Bioscience], 1% w/v Sodium Chloride [NaCl], [pH 7.0]) and 100µg/ml Ampicillin (Sigma-Aldrich, Dorset, UK) and shaken at 37°C overnight.

2.1.2 Isolation of plasmids

Individual bacterial colonies were inoculated into 3ml LB broth containing 100µg/ml Ampicillin for selection and incubated at 37°C overnight at 225 rpm. The bacterial cultures were then used to extract DNA using the PureYield™ Plasmid

Miniprep System (Promega, Southampton, UK) according to the manufacturer's instructions. 600µl of bacterial cell culture was mixed with 100µl of lysis buffer. The mixture was inverted several times and 350µl of cold neutralisation buffer added. The mixture was centrifuged at 15,000x*g* for 3 minutes. The supernatant was then transferred to a column and centrifuged at 15,000x*g* for 15 seconds and the flow-through discarded. 450µl of endotoxin removal buffer was used to wash the column, followed by a second wash with 200µl wash solution containing ethanol. The plasmid DNA was eluted with 30µl of distilled water. The extracted plasmid DNA concentration was measured using a spectrophotometer at an absorbance of 260/280nm (NanoDrop.ND-1000, Lebtech International, East Sussex, UK).

In order to obtain large quantities of plasmid DNA, individual bacterial colonies were inoculated into 3ml LB broth with 100µg/ml ampicillin and incubated in a shaker at 37°C for 6 hours at 225rpm. This starter culture was then added to 300ml LB broth containing 100µg/ml ampicillin and shaken at 225rpm at 37°C overnight. The Genopure Plasmid Maxi Kit (Roche, Burgess Hill, UK) was used to isolate the plasmid DNA according to manufacturer's guidelines. The bacterial culture was centrifuged for 20 minutes at 15,000x*g* at 4°C. The pellet was re-suspended in 12ml or 24ml chilled resuspension buffer for lentiviral vector DNA and normal plasmid, respectively. The same volume of lysis buffer was added and incubated for 2-3 minutes at room temperature. Following incubation, the same volume of chilled neutralisation buffer was added to the mixture and the tubes inverted 10 times and incubated on ice for 5 minutes. The lysate was cleared by filtration and the supernatant added to a pre-equilibrated column. The column was washed 3 times with 16ml wash buffer followed by 15ml pre-warmed elution buffer to elute the DNA. The eluted plasmid DNA was precipitated with 11ml isopropanol

and centrifuged at 15,000x*g* for 30 minutes at 4°C. The supernatant was carefully discarded and the plasmid DNA was washed with 4ml chilled 70% ethanol and centrifuged again for 10 minutes at 15,000x*g* in 4°C. The DNA pellet was air-dried and dissolved in distilled water. The concentration of the plasmid DNA was determined using the Nanodrop and the purity was assessed by the absorbance at 260/280nm.

2.1.3 Plasmid sub-cloning

Restriction enzyme digest

Digestion of plasmid DNA using restriction enzymes was performed according to manufacturer's instructions. In general, 5µg plasmid DNA was digested with 1µl of 10U/µl restriction enzyme, 20µl of 10x restriction enzyme buffer, 2µl of 10µg/µl BSA in a final volume of 200µl, made up with H_2O. The DNA was digested for 1-4 hours depending on the restriction enzymes used. The digested products, depending on the size of the fragment, were subjected to electrophoresis on 0.7-2% w/v agarose gels [Agarose (Invitrogen, Paisley, UK), 1x TAE buffer (National diagnostics, Hessle, UK), 0.5% Ethidium Bromide (Sigma)] in order to be visualised (UV1doc HD/26M, Cambridge, UK) and isolated.

To generate blunt end fragments required for some cloning procedures, T4 DNA polymerase (Promega) was used to fill dNTPs to linearised DNA with a 5' overhang, according to manufacturer's protocol. In general, 2µg of fragmented DNA was filled in with 10 units of T4 DNA polymerase (Promega), 100µM of each dNTP, 10µl of 10x reaction buffer [250mM Tris-Acetate (pH 7.7), 1M potassium acetate, 100mM magnesium acetate and 10mM DTT] and H_2O was added to make the final

volume of 100µl. The mixture was incubated for 30 minutes at 37°C and 4µl of 0.5M Ethylenediamineetetraacetic acid (EDTA) was added to stop the reaction. The blunt end product was purified using the QIAquick Nucleotide removal kit (Qiagen, Manchester, UK) according to manufacturer's instructions.

Gel Extraction

The isolated digested DNA products were purified from the agarose gel using QIAquick Gel Extraction Kit (Qiagen) according to manufacturer's guidelines. The DNA fragment was excised from the agarose gel and weighed. Buffer QG was added to the excised DNA fragment at a volume corresponding to 3x the weight of the fragment. The mixture was incubated at 50°C for 10 minutes, or until the gel was completely dissolved. 1x the gel volume of isopropanol was added to the mixture and transferred into a QIAquick spin column and centrifuged at maximum speed for 1 minute. The column was washed with 0.75ml of Buffer PE to remove any traces of salt contamination at maximum speed for 1 minute. The column was emptied and centrifuged for an additional 1 minute to remove ethanol contamination from Buffer PE. DNA was then eluted by centrifuging the QIAquick spin column, with 30µl of elution buffer [10mM Tris-Cl (pH8.5)].

Ligation

Following gel extraction, the DNA fragment and vector were ligated to generate plasmid DNA. The concentrations of the DNA fragment and vector were measured using the Nanodrop and depending on the cloning, the molar ratio between the fragment and the vector varied from 1:1 to 10:1 for the ligation. The following formula was used to determine the mass of insert required for each ratio. For example, for 3:1 ratio (vector: DNA) ligation:

Xng insert required = [(100ng vector x kb insert)/ kb vector] x 3

100ng vector and the required amount of insert DNA were ligated with 5µl of 2x Rapid Ligation Buffer (Promega) and 1 Weiss unit of T4 DNA ligase (Promega), with nuclease-free H_2O to make up the final volume of the reaction to 10µl. The mixture was incubated at room temperature for 30 minutes for ligation, prior to transformation (Section 2.1).

2.1.4 DNA constructs

Schematic diagram of the lentiviral expression constructs is shown in Fig. 15. The pHR-SIN-CSGW was a kind gift from Y.Ikeda (Mayo Clinic, Rochester, MN). This vector was generated by removing one NotI site from the SIN-CSGW vector. The vector was subsequently modified to replace the eGFP sequence with a PGK-PURO-IRES-eGFP from a pMSCV-PGK-PURO-IRES-eGFP vector.

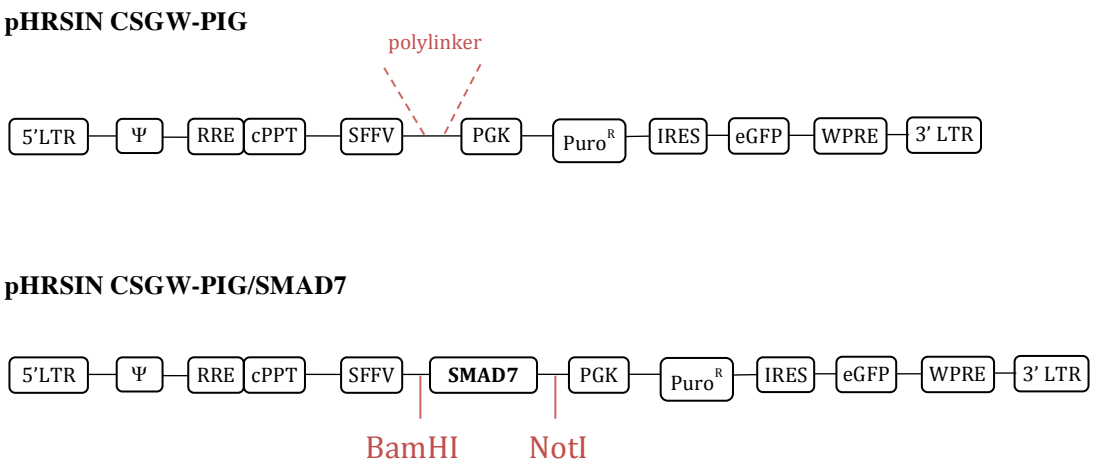

Figure 15 – Lentiviral expression vectors used in this study

LTR, long terminal repeat; Ψ, viral packaging signal; RRE, rev response element; cPPT, central polypurine tract; SFFV, spleen focus-forming virus LTR; PGK, phosphoglycerate kinase eukaryotic promoter; Puro^{R}, puromycin resistance gene; IRES, internal ribosomal entry site; eGFP, green fluorescent protein; WPRE, woodchuck hepatitis posttranscriptional regulatory element.

Small hairpin RNA (shRNA) vector

The following shRNA vectors used in this study were purchased from Sigma-Aldrich (Table 1). Lentiviral MISSION shRNA constructs targeting *STAT3*, *SMAD7*, *SREBP-1* were used to silence relevant gene expression. A non-targeting shRNA was used as a negative control that activates the RISC and RNAi pathway but without targeting any human or mouse genes (referred to as control [scramble] in this thesis). Therefore it is a useful reference for the interpretation of knockdown.

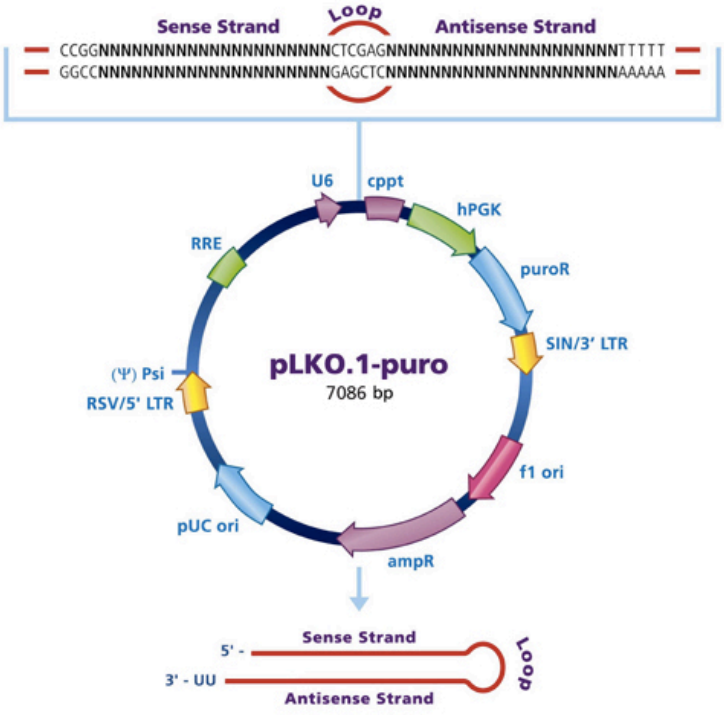

Figure 16 - Graphic representation of the pLKO shRNA vector used in this study

The human U6 promoter (a pol III promoter) is used to drive the expression of the shRNA hairpin. The human phosphoglycerate kinase eukaryotic (hPGK) promoter drives the expression of the

puromycin resistance gene for mammalian selection (puroR); ccpt, central polypurine tract; SIN/LTR, 3' self-inactivating long terminal repeat; f1 ori, f1 origin of replication; amp^R, ampicillin resistance gene; pUC ori, pUC origin of replication; 5' LTR, 5' long terminal repeat; Ψ, viral packaging signal; RRE, Rev response element. Adapted from (http://www.sigmaaldrich.com/life-science/functional-genomics-and-rnai/shrna/library-information/vector-map.html)

GENE (Accession no)	**Sequence (5'-3') (sense-loop-antisense)**
Non-mammalian shRNA control	CCGG CAACAAGATGAAGAGCACCAA CTCGAG TTGGTGCTCTTCATCTTGTTG TTTTT
SMAD7_1 (86) (NM_005904)	CCGG CGTGCAGATCAGCTTTGTGAA CTCGAG TTCACAAAGCTGATCTGCACG TTTTT
SMAD7_2 (44) (NM_005904)	CCGG CTTAGCCGACTCTGCGAACTA CTCGAG TAGTTCGCAGAGTCGGCTAAG TTTTTTGAAT
SMAD7_3 (72) (NM_005904)	CCGG ACTACTTTGCTGCTAATATTT CTCGAG AAATATTAGCAGCAAAGTAGT TTTTTTGAAT
STAT3_1 (42) (NM_003150)	CCGG GCACAATCTACGAAGAATCAA CTCGAG TTGATTCTTCGTAGATTGTGC TTTTT
SREBP1_1 (05) (NM_004176)	CCGGGCCATCGACTACATTCGCTTTCTCGAGAAA GCGAATGTAGTCGATGGC TTTTT
SREBP1_2 (07) (NM_004176)	CCGGCCAGAAACTCAAGCAGGAGAACTCGAGTTC TCCTGCTTGAGTTTCTGG TTTTT

Table 1 – pLKO driven shRNA sequences used in this study

2.1.5 Preparation of total protein lysate for western blot analysis

Cells were harvested and washed with Phosphate Buffer Saline (PBS) by centrifugation at 300x*g* for 5 minutes at 4°C. The cells were lysed using 60µl 1x Radio-Immunoprecipitation Assay (RIPA) buffer (Cell Signaling) [20mM Tris-HCl (pH 7.5), 150mM NaCl, 1mM Na_2EDTA, 1mM EGTA, 1% NP-40, 1% sodium deoxycholate, 2.5mM sodium pyrophosphate, 1mM beta-glycerophosphate, 1mM Na_3VO_4, 1µg/ml leupeptin], 1X HALT Protease Inhibitor Cocktail (ThermoFisher Scientific) and 1X Phosphatase Inhibitor Cocktail Set V (Merck, Nottingham, UK) per $1x10^6$ cells. The mixture was incubated on ice for 30 minutes, vortexed for 10 seconds and centrifuged at 16,000x*g* for 20 minutes at 4°C. The supernatant was collected and total cell lysate was stored at -80°C. For time-course experiments involving treatments of less than an hour, cells were harvested by centrifugation for 30 seconds at 16,000x*g* at 4°C, lysed in RIPA buffer and immediately incubated on dry ice for 5 minutes before storing in -80°C. Alternatively, cell pellets were lysed using 60µl 2x Reducing Sample Buffer [100mM Dithiothreitol (DTT), 4% w/v sodium dodecyl sulphate (SDS), 20% v/v Glycerol, 0.1% w/v Bromophenol blue, 125mM Tris-HCl (pH 6.8)] per $1x10^6$ cells. The lysate was boiled for five minutes at 100°C in a heating block followed by vortexing for 10 seconds. The lysate was then centrifuged at 16,000x*g* for 10 minutes at 4°C. The supernatant was collected and stored at -80°C. In order to denature proteins before loading, samples were boiled for five minutes in a 100°C heating block and kept on ice until loading.

For nuclear and cytoplasmic extracts, the Nuclear Extract kit (Activ Motif) was used according to the manufacturer's instructions. At least $3x10^6$ cells were harvested and washed with PBS by centrifugation at 300g for 5 minutes at 4°C. Cell

pellets were lysed using 250µl of 1x Hypotonic Buffer and incubated on ice for 15 minutes. 12.5µl of detergent was added to the nuclear pellet and vortexed at highest setting for 10 seconds. The suspension was centrifuged for 30 seconds at 14,000x*g* at 4°C. The supernatant (Cytoplasmic fraction) was stored at -80°C. The nuclear pellet was then suspended in 25µl of Complete Lysis Buffer and vortexed at the highest setting for 10 seconds. The suspension was incubated on ice for 30 minutes. Following the incubation, the nuclear lysate was vortexed for 30 seconds and centrifuged for 10 minutes at 14,000x*g* at 4°C. The supernatant (nuclear fraction) was stored at -80°C. Protein concentration was measured using the Bradford reagent (BioRad), by measuring the absorbance at a wavelength of 595nm using the Ultrospec 2100 pro (Amersham Pharmacia Biotech) spectrophotometer.

2.1.6 Western blot analysis

Protein gel electrophoresis was performed using Bio-Rad Mini-PROTEAN® Tetra handcast system. Protein samples were resolved on 10% SDS-Polyacrylamide gels (Table 2) and stacked in 4% Sodium Dodecyl Sulphate (SDS)-polyacrylamide gels (Table 3). Protein samples and PageRuler Protein Ladder plus molecular weight marker (ThermoFisher Scientific) were subjected to electrophoresis at 140V at room temperature for 1.5 hours.

Components of a 10% Resolving gel

Reagent	Required volume
30% w/v Acrylamide/Bis-acrylamide solution (37.5:1) (Geneflow)	3ml
Buffer [1.25M BisTris (pH 6.8)]	2.7ml
H_2O	3.2ml
10% w/v Ammonium Persulfate (APS, BioRad)	50µl
Temed (BioRad)	6µl

Table 2 - Components of a 10% resolving gel used for western blot analysis

Components of a 4% Stacking gel

Reagent	Required volume
30% w/v Acrylamide/Bis-acrylamide solution (37.5:1) (Geneflow)	0.7ml
Buffer [1.25M BisTris (pH 6.8)]	1.1ml
H_2O	2.4 ml
10% w/v Ammonium Persulfate (APS, BioRad)	50µl
Temed (BioRad)	6µl

Table 3 - Components of a 4% stacking gel used for western blot analysis

20x Running Buffer (Tris, MOPS, 0.5M EDTA, 20% SDS) was diluted with distilled water to generate 1x Running buffer, which was used to perform SDS-PAGE. The samples were subsequently transferred onto a polyvinylidenefluoride

(PVDF) membrane (Millipore, Hertfordshire, UK) for 3 hours at 4°C at 400mA using Transfer Buffer [25mM Tris (Sigma-Aldrich), 192mM glycine (Sigma-Aldrich), 20% methanol)].

Following transfer, membranes were blocked in PBS with 5% non-fat milk and 0.2% v/v Tween-20 (Sigma-Aldrich) and stained with one of the primary antibodies listed. The antibodies were diluted in PBS with 5% non-fat milk and 0.2% v/v Tween-20. In the case of phospho-proteins, membranes were blocked in PBS with 5% Bovine Serum Albumin (BSA) (Sigma Aldrich) and 0.2% v/v Tween-20. The antibodies were diluted in PBS with 5% BSA and 0.2% v/v Tween-20. Excess antibody was removed by washing with PBS with 0.2% v/v Tween-20 3 times for 10 minutes each. Proteins were detected using the listed secondary antibodies conjugated with horseradish peroxidise listed and a chemiluminescent substrate (ECL, Amersham Biosciences) or SuperSignal West Pico Chemiluminescent Substrate (ThermoFisher Scientific), according to manufacturer's instructions. Hypofilms ECL (Amersham) were exposed to membranes for different exposure times and developed using a Xograph CompactX4 (BioRad) developer. Exposed films were scanned using a calibrated densitometer (GS-800, BioRad) and individual bands were quantified using QuantityOne software (BioRad). The relative protein expression was calculated by dividing the value of the protein of interest by the value of the loading control. Membranes were stripped using Restore™ Western Blot Stripping Buffer (ThermoFisher Scientific) for some experiments for 10 minutes at room temperature followed by re-probing with different primary and secondary antibodies.

Antibody	Supplier	Dilution
Phospho-SMAD2 (Ser465/467)	Cell Signaling Technology	1:1000
Phospho-SMAD3 (Ser 423/425)	Cell Signaling Technology	1:1000
SMAD2/3 (D27F4)	Cell Signaling Technology	1:1000
SMAD7 (IMG-531A)	Imgenex	1:500
SREBP-1 (C-20) (SC-366)	Santa Cruz Biotechnology	1:1000
Human influenza hemagglutinin (HA) (3F10)	Roche	1:1000
TATA Binding Protein (AB51841)	Abcam	1:1000
GAPDH (SC-32233)	Santa Cruz Biotechnology	1:1000
HSP90 (SC-13119)	Santa Cruz Biotechnology	1:3000
Tubulin (SC-53029)	Santa Cruz Biotechnology	1:3000

Table 4 - Primary antibodies used for western blot analyses in this study

Antibody	Supplier	Dilution
Anti-mouse IgG HPR-linked whole antibody	GE Healthcare	1:3000
Anti-rat IgG HPR-linked whole antibody	GE Healthcare	1:3000
Anti-rabbit IgG HPR-linked whole antibody	GE Healthcare	1:5000
Anti-goat IgG HPR-linked whole antibody	Santa Cruz Biotechnology	1:5000

Table 5 - Secondary antibodies used for western blot analyses in this study

2.1.7 RNA isolation, cDNA preparation and quantitative real-time PCR

Total RNA was isolated from cells using the RNeasy Mini Kit (Qiagen) according to manufacturer's instructions. The cells were disrupted by adding Lysis buffer RLT, containing 2-mercaptoethanol, followed by vortexing at the highest setting for 30 seconds to ensure homogenization of the samples. One volume of 70% ethanol was added to the samples and the mixture transferred to a RNeasy spin column. After centrifugation for 15 seconds at 14,000x*g*, the flow-through was discarded. 700µl of RWI wash buffer was added to the spin column followed by centrifugation. The sample was subsequently washed twice with 500µl of RPE wash buffer. RNA was then eluted using 30µl of RNase free water and the concentration determined using a spectrophotometer (NanoDrop ND-1000, Lebtech International). The purity of the extracted RNA was determined by measuring the ratio of the absorbance at 260nm and 280nm. A ratio of ~2.0 was considered as pure RNA (NanoDrop user's manual).

RNA was converted into cDNA using the High Capacity RNA-to-cDNA kit (Applied Biosystems) according to manufacturer's guidelines. 1µg of RNA or 500ng of RNA was converted using 1µl of 20X Enzyme mix and 10µl of 2X RT Buffer Mix in a total volume of 10µl. Samples were treated with DNase (Invitrogen) prior the reverse transcription.

Quantitative RT-PCR (qRT-PCR) was performed on isolated mRNA using Taqman probe based chemistry and an ABI Prism 7900HT fast Sequence Detection System (Life Technologies). All probes used were inventoried probes from Applied Biosystems, Life Technologies.

2.2 Cell Biology

2.2.1 Cell culture and cell lines

The 293FT (Invitrogen) packaging cell line was cultured in 10cm culture dishes (NUNC) in Dulbecco's Modified Eagle's medium (DMEM, Sigma-Aldrich), supplemented with 10% heat-inactivated Foetal Calf Serum (FCS) (Sigma-Aldrich), 100U/ml Penicillin (Sigma-Aldrich), 100μg/ml Streptomycin (Sigma-Aldrich) and 2mM L-glutamine (Sigma-Aldrich) (complete DMEM). 293FT were maintained in 500μg/ml Geneticin selection antibiotic (G418 Sulfate) (ThermoFisher Scientific). To replate the cells, the cells were washed with 5ml PBS (Gibco) followed by trypsinisation using 1ml of 1xTrypsin/EDTA (Gibco) for 5 minutes, at 37^0C. Cells were then diluted in complete DMEM in order for the FCS to inactivate trypsin and centrifuged at 300x*g* for 5 minutes at room temperature and seeded at a density of approximately 0.35 x 10^6/ml for 3 to 4 days in the presence of Geneticin.

Human leukaemic cells lines REH, 697, TOM-1 and SUP-B15 were obtained from the German Collection of Microorganisms and Cell Cultures (DSMZ, Brunswick, Germany). BEl-1 and SEMK-2 were kind gifts from R. Stam (Erasmus MC, Rotterdam, Netherlands) and AT-2 a kind gift from R.Panzer-Grümayer (Children's Cancer Research Institute, Vienna, Austria). For RNA-sequencing, REH cells that were a kind gift from R.Stam (Erasmus MC, Rotterdam, Netherlands) were used (Table 4). The identities of the human leukaemic cell lines used were confirmed by STR profiling in the GOSH Haematology department. All human leukaemic cell lines with the exception of AT-2 cells, were cultured in Roswell Park Memorial Institute (RPMI) medium (Sigma-Aldrich) supplemented with 10% heat-inactivated

Fetal Calf Serum (FCS) (Sigma Aldrich, Dorset), 100U/ml Penicillin (Sigma-Aldrich), 100µg/ml Streptomycin (Sigma-Aldrich) and 2mM L-glutamine (Sigma-Aldrich) (complete RMPI). AT-2 cells were cultured in Iscove's Modified Eagle's medium (IMDM, Sigma-Aldrich), supplemented with 10% heat-inactivated Fetal Calf Serum (FCS) (Sigma Aldrich), 100U/ml Penicillin (Sigma-Aldrich), 100µg/ml Streptomycin (Sigma-Aldrich) and 2mM L-glutamine (Sigma-Aldrich) (complete IMDM). Each cell line was sub-cultured every 3-4 days and plated between 0.25-0.8x10^6 cells/ml according to supplier's instructions (DSMZ).

Cell Line	Translocation	Fusion gene
REH	t (12;21)	*TEL-AML1*
AT-2	t (12;21)	*TEL-AML1*
BEL-1	t (4;11)	*MLL-AF4*
SEMK-2	t (4;11)	*MLL-AF4*
SUP-B15	t (9;22)	*BCR-ABL*
TOM-1	t (9;22)	*BCR-ABL*
697	t (1;19)	*E2A-PBX1*

Table 6 - ALL cell lines used in this study

2.2.2 Lentiviral packaging cell line transfection

To transfect the 293FT lentiviral packaging cell line, the cells were seeded at a density of 0.75 x 10^6 per 10 cm culture dish three days prior to transfection,

without geneticin. To transfect the cells, 5μg of expression vector, 3.75μg of pCMV-PAX2 (kindly supplied by Professor D. Trono, Lausanne, Switzerland) and 1.5μg of pVSV-G were added in 1ml of Optimem (GIBCO) medium. 30μl of MegaTran transfection reagent (OriGene) was added to the mixture followed by immediate vortexing at the highest setting for 10 seconds. The DNA-megatran complexes were then incubated for 10 minutes at room temperature and added to the cells. MegaTran containing medium was then replaced with 8ml of complete DMEM medium the following day.

2.2.3 Lentiviral transduction of human leukaemic cell lines

To transduce REH, AT-2, SEMK-2, REH-LUC-CD2 and THP-1, an MLL-AF9^{+} AML cell line, 293FT supernatant was cleared using Ministart 0.45μm filters (Sartorius Stedim Biotech). In order to concentrate lentivirus for the purpose of some experiments, ultracentrifugation was performed using Sorvall 12ml centrifuge tubes (ThermoFisher Scientific). The tubes were sterilised with 70% ethanol followed by 2 washes with PBS prior to use. The tubes were filled with 11ml of virus each and concentrated using an ultracentrifuge (ThermoFisher Scientific, Discovery 100) at 17,000x*g* for 2 hours at 4°C. The supernatant was discarded and the pellet was re-suspended in 1.1ml of complete RPMI medium. $0.65x10^{6}$ cells supplemented with 5μg/ml polybrene in 24 well plates were transduced by spinoculation at 700x*g* for 45 minutes at 25°C. 24 hours following transduction, 1ml of complete RPMI or complete IMDM was added to the cells. 48 hours following transduction, cells were harvested and plated in complete RPMI or complete IMDM supplemented with 1μg/ml puromycin.

2.2.4 Flow cytometry

Cells were washed with wash buffer (PBS supplemented with 0.05% w/v sodium azide). Cells were stained with anti-human CD2-PE (Tonbo Biosciences) antibody diluted 1:20 in stain buffer (PBS supplemented with 0.05% w/v sodium azide and 1% w/v BSA) for 15 minutes on ice. The cells were then washed with wash buffer and re-suspended in 200µl stain buffer prior to analysis. All flow cytometry was performed on an LSRII analyser (BD Biosciences) and the data was analysed with or FlowJo v8.6 (Tree Star, Ashland, Oregon) software.

2.2.5 Apoptosis

Apoptosis was detected using the Annexin V Apoptosis Detection Kit APC (eBioscience). Cells were washed with PBS followed by a second wash with 1X Annexin V Binding Buffer. Following centrifugation, the pellet was re-suspended in 95µl of 1X Binding buffer and 5ul of Annexin V-APC and incubated for 15 minutes at room temperature in the dark. The mixture was washed with 1X Binding buffer and re-suspended in 195µl of 1X Binding buffer and 5µl of 500ug/ml 4',6-diamidino-2-phenylindole (DAPI) or Propidium Iodide (PI). Cells were analysed by flow cytometry.

2.2.6 Cell cycle assays

Cell cycle analysis was performed using the Click-iT EdU Alexa Fluor 647 Flow Cytometry Assay Kit (Invitrogen). Cells were cultured with 10µM Click-iT®

EdU for 1 hour. The cells were harvested and fixed with 100µl 4% paraformaldehyde (PFA) for 15 minutes at room temperature. Following one wash with PBS supplemented with 0.01% w/v sodium azide and 1% w/v BSA, the cells were permeabilised with Saponin-based buffer (PBS with 1% BSA, 0.1% Saponin and 0.1% sodium azide). 500µl Click-it® reaction cocktail [Copper (II) sulphate (CuSO4); 1:10 Reaction Buffer Additive (1M ascorbic acid); Fluorescent dye; TBS up to 500µl] was added to the cells and incubated for 30 minutes at room temperature in the dark. Following incubation, the cells were washed in Saponin-buffer and re-suspended in 500µl of Saponin buffer containing 0.5µl of 1µg/ml Ribonuclease A (Qiagen) and 500µg/ml DAPI (Roche) or 1mg/ml PI. Cells were then analysed by flow cytometry.

2.2.7 Dead cell removal

Apoptosis, cell cycle analysis and injection of shRNA transduced cells into mice was performed following dead cell removal using the Dead Cell Removal Kit (Miltenyi Biotec, Woking, UK) to obtain equivalent numbers of viable cells. Cells were centrifuged at 300g for 5 minutes, re-suspended in 100µl of Dead Cell Removal microbeads and incubated at room temperature for 15 minutes. MS columns were prepared by washing with 1X binding buffer and placed in a magnetic field of a MACS® Separator. 500µl of 1X binding buffer was added to the cells and the mixture was loaded to the column. The effluent collected contained the live cell fraction. The column was then washed 4 times with 500µl of 1X binding buffer, which was collected and added to the live cell fraction. This was then centrifuged at 300g for 5 minutes and re-suspended in appropriate medium.

2.2.8 Mouse cell-depletion

To enrich for human cells following xenotransplantation of patient samples and a transduced human leukaemia cell line in mice, mouse cell depletion was performed using the Mouse Cell Depletion Kit (Miltenyi Biotec). Cells were centrifuged at 300g for 10 minutes and re-suspended in 80µL of MACS buffer and 20µL of Mouse Cell Depletion cocktail per $2x10^6$ tumour cells or 10^7 total cells. The mixture was incubated for 15 minutes in 4°C. The volume of the mixture was adjusted to 500µl per $2x10^6$ tumour cells or 10^7 total cells. A 40µm pre-separation filter was placed above an LS type column in the magnetic field of a MACS separator. The filter and column were prepared by rinsing with 3mL of MACS buffer. The mixture was then added and the effluent collected contained the enriched human tumour cells. The column was washed with 1ml buffer twice and the effluent was centrifuged at 300g for 5 minutes. The cells were then re-suspended in the appropriate medium.

2.2.9 Proliferation assays

Cells were cultured at a density of $7x10^4$ cells per well in flat bottomed 96-multiwell plates (TPP, Trasadingen, Switzerland) in the presence of dimethyl sulphoxide (DMSO) vehicle control, specific drugs or following shRNA mediated knockdown. 10µl of CellTiter 96® Aqueous One Solution Reagent (Promega) was added to 100µl of assay volume in each well according to the manufacturer's instructions. Following 2 hours of incubation at 37°C, proliferation was determined by measuring the absorbance at 490nm using a Infinite® 200 PRO plate reader (Tecan, Reading, UK).

2.2.10 Colony forming assays

For $CD34^+$ human cord blood cells (purchased from Zen-bio), $1.5x10^3$ cells were re-suspended in 300µl of StemSpan™ Serum-Free Expanison medium II (SFEM II) (Stemcell Technologies, Cambridge, UK). The cells were added to 3ml of methylcellulose (HSC005 R&D Systems). DMSO or different concentrations of Fatostatin were then added to the 3.3ml aliquot containing methylcellulose and cells. The mixture was then vortexed briefly and allowed to sit at room temperature for 10 minutes. 1.1ml of this mixture was added using a blunt end needle into a 35mm plate, in duplicate (non-TC treated, Greiner Bio One, Stonehouse, UK). Following 14 days in culture, the cells were then counted manually and scored according to their morphology. 800µl of 10mg/ml 2-2-(P-iodophenyl)-3-(p-nitrophenyl)-5-phenyl tetrazolium chloride (INT) in 75% ethanol, diluted 1:20 with PBS, was added to each plate and cultured for an additional day. An image of the cultures was then acquired using a calibrated densitometer (GS-800, BioRad).

For human cell lines transduced with shRNA vectors, cells were re-suspended in 600µl medium and added to 2.7 ml of human methylcellulose (HSC002 R&D systems). 600µl of this mixture was plated into 24 multi-well plates (Non-TC treated, Greiner Bio One) using blunt end needles. In the case of cell lines treated with DMSO or 20µM Fatostatin, this was added to the methylcellulose aliquot containing cells and the mixture was then vortexed and plated into 24 multi-well plates as previously mentioned. The cells were cultured for 14 days before being cultured for an additional two days in the presence of 180µl of 10mg/ml INT in 75% ethanol, diluted 1:20 with PBS. An image of the cultures was then acquired using a

calibrated densitometer (GS-800, BioRad) and the colonies quantified using OpenCFU software (http://opencfu.sourceforge.net).

For serum-free colony forming assays, human cell lines were cultured in AIM V® Serum Free Medium (ThermoFisher Scientific) for 1 day. Following this, the cells were re-suspended in 600µl of serum-free medium with different concentrations of TGF-β. The mixture was then added to 2.7ml of human serum-free methylcellulose (HSC002SF, R&D Systems) and 600µl of this mixture was plated into 24 multi-well plates using blunt needles. The cells were cultured for 14 days before being cultured for an additional two days in the presence of 180µl of 10mg/ml INT in 75% ethanol, diluted 1:20 with PBS. An image of the cultures was then acquired using a calibrated densitometer (GS-800, BioRad) and the colonies quantified using OpenCFU software.

2.2.11 Cholesterol assays

Total cholesterol was measured using the Amplex® Red Cholesterol Assay Kit (ThermoFisher Scientific) according to manufacturer's instructions. This assay is based on an enzyme-coupled reaction that detects both free cholesterol and cholesteryl esters. Following hydrolysation of cholesteryl esters by cholesterol esterase, the cholesterol is oxidised by cholesterol oxidase. The hydrogen peroxide (H_2O_2) that is produced in addition to the ketone product upon oxidisation is detected by the 10-acetyl-3,7-dihydroxyphenoxazine (Amplex Red reagent), when it is in the presence of Horseradish peroxidase (HRP). A cholesterol standard curve was performed by diluting 2mg/ml (5.17mM) cholesterol reference standard into 1X Reaction Buffer to produce cholesterol concentrations of 0 to 8µg/ml (0-20µM). To

perform the assay, $1x10^5$ cells were diluted in 50µl of 1X Reaction buffer and plated in triplicate in a 96 multi-well plate. A solution of 300µM Amplex Red Reagent, 2U/ml HRP, 2U/ml cholesterol oxidase and 0.2U/ml cholesterol esterase was prepared and 50µl was added to the cells and in addition, to the cholesterol reference standard to generate a standard curve. The reaction was incubated for 60 minutes at 37°C, protected from light and the fluorescence measured using the Infinite® 200 PRO plate reader (Tecan) using excitation detection at 550nm and emission detection at 590nm wavelength. The amount of total cholesterol was calculated using the standard curve.

2.2.12 Luciferase assays

To measure luciferase signal expressed by cells, the Luciferase Assay System (Promega) was used according to manufacturer's instructions. Briefly, $1x10^3$ cells were plated in a white 96-multiwell plate (Non-TC treated, Greiner Bio One) and washed with PBS. Following centrifugation, cells were re-suspended in 20µl 1X Lysis reagent and incubated on a shaker in the dark for 15 minutes. Following this, 100µl of Luciferase assay reagent was injected into each well by the injector in the Infinite® 200 PRO plate reader (Tecan) and the level of luciferase signal in each well measured.

2.3 Animal work

2.3.1 NSG mice

All mice were maintained in the animal facilities of UCL Institute of Child Health. Experiments were performed according to the United Kingdom Home Office regulations. Dr. Owen Williams and Dr. Luca Gasparoli performed xenotransplantations in this study on 5-12 week old NOD.Cg-*Prkdc*^{scid}Il2rg^{tm1Wjl}/SzJ (NSG) mice. These mice lack mature T cells, B cells and natural killer (NK) cells and are deficient in multiple cytokine signalling pathways. Furthermore, they have multiple defects in innate immunity. NSG mice have features of the NOD/ShiltJ background, the combined immune deficiency mutation (scid) and IL-2 receptor γ chain deficiency. They have been shown to support high levels of human haematopoietic stem cell engraftment (McDermott et al., 2010). The NSG mice used in this study were recipients for transplantation of luciferase-expressing REH cells that were transduced with lentiviral vectors expressing scramble shRNA (referred to as control scramble in this thesis) or shRNA targeting *SMAD7* or *SREBP1*. Mice were injected intravenously in the lateral tail vein with 1 x 10^5 transduced cells. Mice were sacrificed when they developed clinical signs of disease and the spleen and bone marrow were harvested for analysis.

2.3.2 Primary patient samples

Informed consent was given by parents and/or guardians to use excess leukaemic cell material remaining following diagnostic procedures, for research purposes as approved by an NHS Health Research Authority sub-committee ethical

review panel. NSG mice were transplanted with excess diagnostic material. Following primary engraftment, the primograft cells were stored in cryovials in -80°C. Prior to experiment, cells were defrosted, purified, mouse cell depleted and cultured in SFEM II for 24 hours in the presence of 100ng/ml Flt3, 50ng/ml IL-7 and 10ng/ml IL-3. Dead cell removal was then performed and cells were treated in the same culture conditions but with added DMSO or 20μM Fatostatin for 72 hours. An apoptosis viability assay was then performed on the cells.

2.4 RNA-sequencing

Total cellular RNA was extracted using the RNeasy Plus Mini Kit (Qiagen) according to manufacturer's instructions. 250ng of RNA for each sample was analysed using Bioanalyzer 2100 (Agilent Technologies, Santa Clara, CA) to verify RNA integrity prior to amplification. The samples were submitted to UCL Genomics for RNA-seq and processed using an Illumina TruSeq RNA sample prep kit Version2 (p/n RS-122-2001) according to manufacturer's instructions (Illumina, Cambridge, UK). Briefly, mRNA was selected using paramagnetic dT beads and fragmented by metal hydrolysis to approximately 150bp lengths. Random primed cDNA was generated and adapters compatible with Ilumina sequencing were ligated followed by 14 cycles of PCR. Libraries were quantified, normalised and pooled prior to sequencing on an Illumina NextSeq 500 (Illumina), generating approximately 20-24 million reads for each sample. Sequencing reads were aligned to NCBI build 37.2 of the human genome using TopHat 2.0.10 and deduplicated using a Picard Tools 1.79. As part of the in-house pipeline, Cufflinks 2.1.1 was then used to generate normalised estimates of expression from each gene transcript. Ilumina BaseSpace (Ilumina) and Strand NGS (Strand, San Francisco, CA) software was used to analyse and visualise RNA-seq data. A list of gene transcripts ordered according to differential expression between control cells and *SMAD7* knockdown cells was generated by setting different parameters using both Ilumina BaseSpace and Strand NGS software. Further downstream analysis such as Ingenuity Pathway Analysis (IPA) (Qiagen) was performed on the sets of differentially expressed genes between the two data sets.

CHAPTER III. The role of TGF-β in TEL-AML1$^+$ leukaemia

3.1 Introduction

A growing body of epidemiological studies suggest a role for 'delayed infection' as a trigger of ALL. In affluent societies, many children have reduced exposure to infectious pathogens in early life. This may generate an aberrant or atypical immune response when exposed to these infections at a later stage. In the presence of initiating genetic lesions such as chromosomal translocations, this atypical immune response may select for leukaemic transformation by providing a favourable environment for selective pre-leukaemic clone expansion and acquisition of secondary mutations (Greaves, 2006b). There is evidence showing that inflammatory cytokines might provide this selective pressure for the outgrowth of pre-ALL clones. Moreover, B-cell precursor ALL cells show a gene expression signature that indicates exposure to interferons, similar to breast and ovarian cancer (Einav et al., 2005). Different childhood ALL samples separated on the basis of 'high' and 'low' expression of 30 identified genes of the interferon pathway showed a large clustering of leukaemic subgroups prevalent in early childhood (age at which children are most susceptible to infection) in the 'high' interferon-related gene set signature (Einav et al., 2005).

Recently, a study by Ford et al. tested the hypothesis that selective proliferative advantage of TEL-AML1$^+$ pre-leukaemic cells occurs in the presence of

the immune modulator, TGF-β (Ford et al., 2009). They used mouse and human model systems to demonstrate that TEL-AML1 may block the inhibitory effect of TGF-β in the ALL cells themselves. A murine B cell progenitor cell line expressing inducible TEL-AML1, although proliferating at a slower rate, showed resistance to proliferation suppression by TGF-β. In mice with pre-pro-B cells expressing the *TEL-AML1* transgene, reduced sensitivity to TGF-β mediated inhibition of proliferation was observed. Importantly, human cord blood $CD34^+$ cells transduced with a TEL-AML1-expressing lentiviral vector were enriched, relative to cells not expressing the oncogene, in MS-5 stromal co-cultures exposed to TGF-β. This was not seen in the absence of TGF-β (Ford et al., 2009). These experiments suggest that TEL-AML1 may confer a survival and growth advantage to pre-leukaemia cells in the context of high systemic TGF-β. Although the precise mechanism by which this resistance to TGF-β occurs remains to be established, the data indicate that the inhibition occurs downstream of R-SMAD phosphorylation. As TEL-AML1 has been shown to bind SMAD3, one possibility is that it sequesters SMAD proteins away from their target sites in the nucleus. Alternatively, the TEL-AML1/SMAD3 complex may additionally bind to NcoR and Sin3A co-repressors, disabling SMAD–mediated transcriptional activation. Therefore, in this study we focused on examining the mechanisms behind the interplay between TEL-AML1 and TGF-β signalling, to further understand how TEL-AML1 modulates the anti-neoplastic activity of TGF-β.

3.2 Results

3.2.1 Sensitivity of human ALL cell lines to TGF-β

In order to determine whether TGF-β resistance correlated with TEL-AML1 expression, we decided to study responses to TGF-β stimulation across a panel of human ALL cell lines, including two TEL-AML1 expressing cell lines. Cell lines were subjected to treatment with varying concentrations of TGF-β1, and their proliferation was measured using an MTS proliferation assay, at 48 and 96 hours post treatment. Unexpectedly, this assay showed that whilst TEL-AML1$^+$ REH cells were resistant to TGF-β, AT-2 cells, also TEL-AML1$^+$ were sensitive to suppression by TGF-β1. 697 cells, expressing the *E2A-PBX1* fusion gene, were the most sensitive cells and therefore were used as positive controls for further experiments. Other cell lines expressing a variety of fusion genes showed varying degrees of sensitivity to TGF-β1 (Fig. 17).

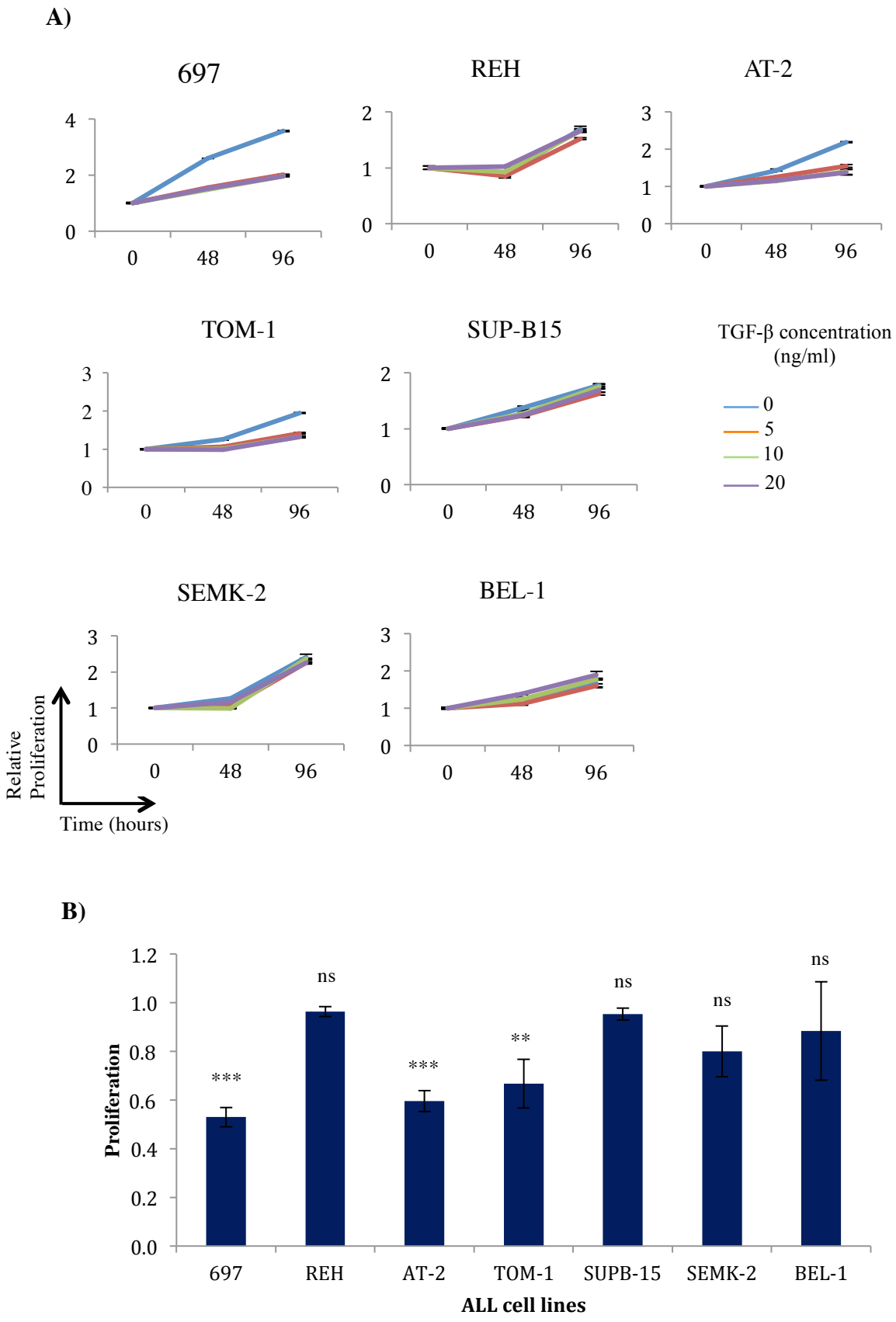

Figure 17 - Effect of TGF-β1 on human ALL cell lines

(A) The graph shows the relative proliferation (relative to day 0) of seven human leukaemic cell lines

by MTS assay at 48 hours and 96 hours when treated with the indicated concentrations of TGF-β1 compared to untreated cells. (B) The bar chart shows the mean decrease in proliferation of all cell lines following 10ng/ml TGF-β1 treatment normalised to untreated cells, measured at 96 hours. All data show mean ± s.d. for three independent experiments. *P < 0.05, **P < 0.01, ***P < 0.005 compared to control (One-sample *t* test).

Due to the unexpected sensitivity of one of the TEL-AML1$^+$ cell lines to TGF-β1, we then further investigated the effect of TGF-β1 on cell cycle in 697 cells and both TEL-AML1$^+$ cells. The cell lines were treated with TGF-β1 for 48 hours and an EdU incorporation cell cycle assay was performed and analysed by flow cytometry. TGF-β1 induced a significant decrease in the percentage of cells in the S-phase of cell cycle in both 697 and AT-2 cells, but had almost no effect on REH cells. This confirmed that while REH cells were resistant to suppression by TGF-β, both 697 and AT-2 cells were sensitive to TGF-β, showing a decrease in the number of actively cycling cells (Fig. 18 and 19).

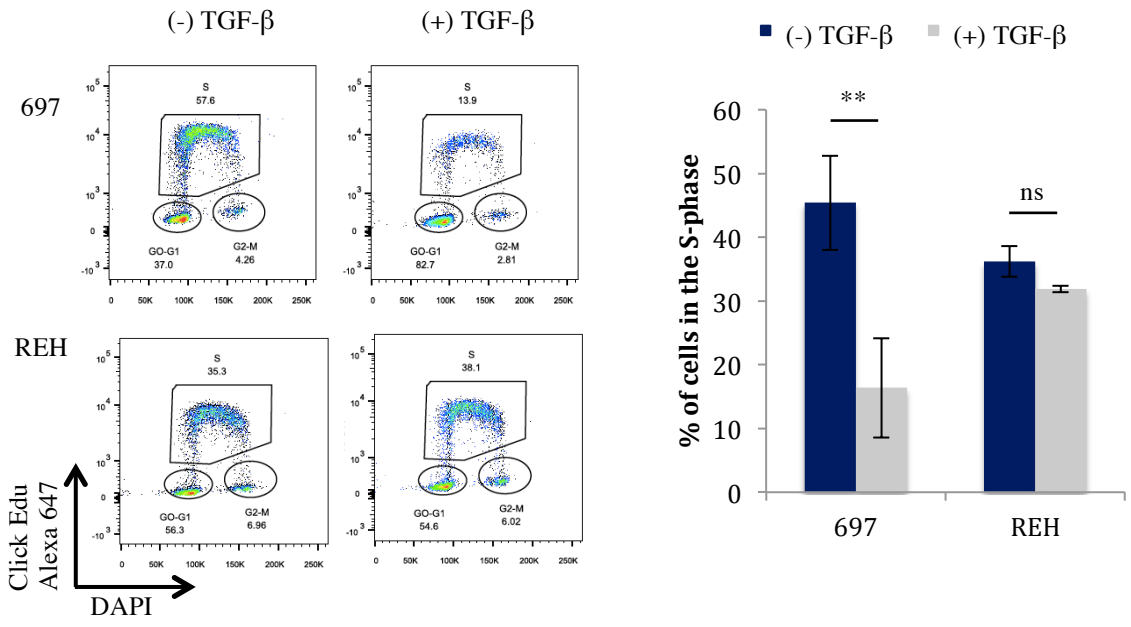

Figure 18 - TGF-β causes cell cycle block in 697 but not REH cells

The flow cytometry plots are examples of the cell cycle profiles of 697 and REH cells following treatment with 10ng/ml TGF-β1 for 48 hours from three different experiments. Cell cycle profile was evaluated after pulsing with 10μM EdU for 1 hour. The percentages of cells in G0/G1, S and G2/M phases of the cell cycle are indicated in the plots. The bar chart represents the mean percentages of cells in the S-phase ± s.d. for three independent experiments. *P < 0.05, **P < 0.01, ***P < 0.005 compared to control (Student's unpaired *t* test).

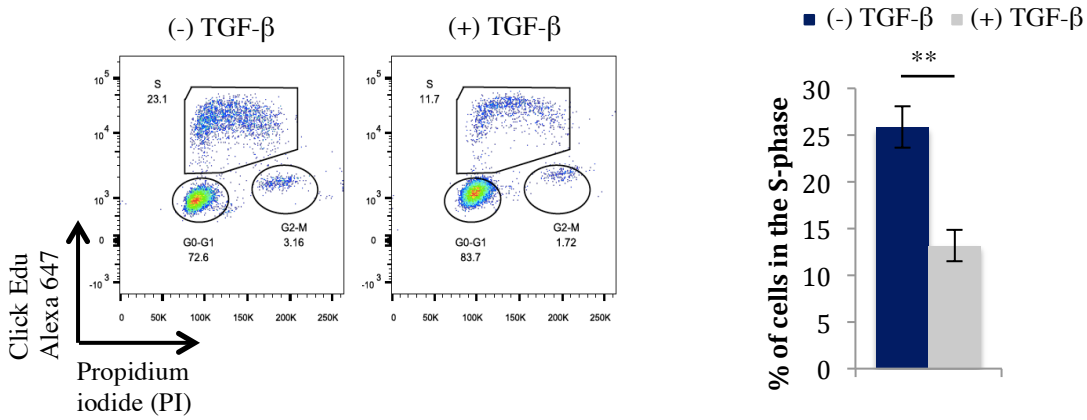

Figure 19 - TGF- β causes cell cycle block in AT-2 cells

The flow cytometry plots are examples of the cell cycle profile of AT-2 cells following treatment with 10ng/ml TGF-β1 for 48 hours from three different experiments. Cell cycle profile was evaluated after pulsing with 10μM EdU for 1 hour. The percentages of cells in G0/G1, S and G2/M phases of the cell cycle are indicated in the plots. The bar chart represents the mean percentages of cells in the S-phase ± s.d. for three independent experiments. *P < 0.05, **P < 0.01, ***P < 0.005 compared to control (Student's unpaired *t* test).

Cell culture medium containing FBS can have low levels of latent TGF-β present (Oida and Weiner, 2010), which can be activated by changes in the medium during cell culture, such as alterations in pH (Lyons et al., 1988). The resulting

'background' stimulation may confound evaluation of TGF-β responsiveness. To eliminate any effect of autocrine TGF-β signalling or any TGF-β present in the culture medium while observing sensitivity of cells to TGF-β1, cell lines were treated with 1D11, an anti-human/mouse TGF-β monoclonal antibody (Affymetrix eBioscience), that blocks all three isoforms of TGF-β. First, we tested to confirm that 1D11 blocks TGF-β in these leukaemic cells. To do this, we cultured 697, with and without 1D11 for 1 hour in the presence of TGF-β and observed phosphorylation of SMAD2 by Western blot analysis (Fig. 20A and B). We hypothesised that if TGF-β signalling was blocked, a decrease in the phosphorylation of SMAD2 would be observed. As expected, we saw a decrease in phospho-SMAD2 levels following 1D11 treatment. REH and AT-2 cells treated with 1D11 alone, showed a decrease in phospho-SMAD2 levels, suggesting that 1D11 blocks TGF-β in culture medium. Once we confirmed that ID11 blocks TGF-β, we treated 697 cells with different concentrations of TGF-β in the presence of 1D11. This showed that 1D11 rescued the TGF-β mediated proliferation suppression in 697 cells. When REH cells were treated with 1D11 alone, no change in proliferation was apparent (Fig. 20C).

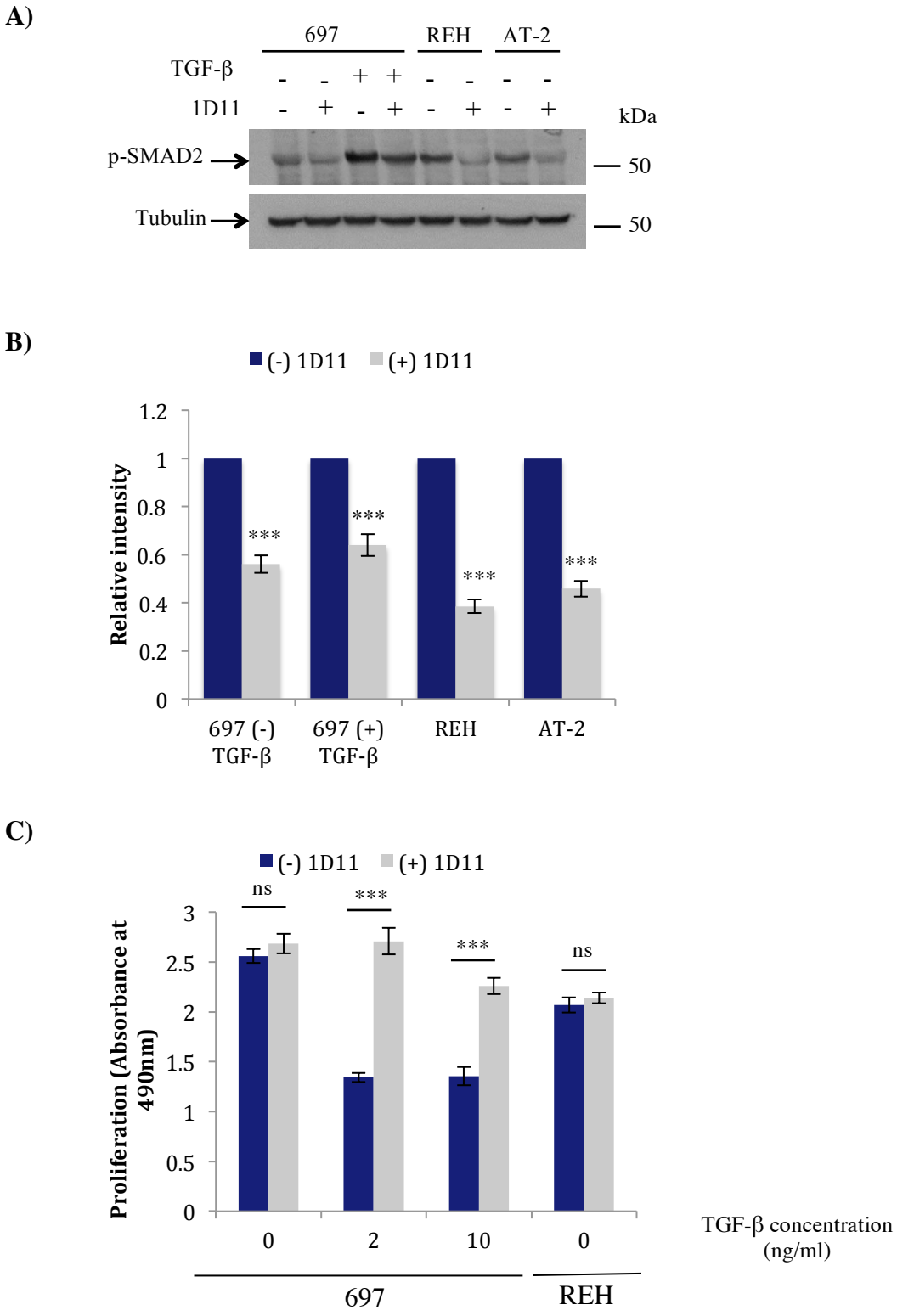

Figure 20 - 1D11 blocks TGF-β mediated SMAD2 phosphorylation

(A) The western blot analysis shows phospho-SMAD2 levels of 697, REH and AT-2 cells following 1D11 treatment at the protein level. Cells were treated for 1 hour with and without 50ug/ml 1D11 and in the case of 697, with and without 10ng/ml TGF-β to make cell lysates. The western blots were

probed with an anti-phospho-SMAD2 antibody. An anti-α-tubulin antibody was used as a control for protein loading. (B) The bar chart represents the mean densitometric quantitation of phospho-SMAD2 levels normalised to α-tubulin ± s.d. for three independent experiments. *P < 0.05, **P < 0.01, ***P < 0.005 compared to control (One-sample *t* test). (C) The bar chart shows the mean cell viability of 697 and REH cells following 1D11 treatment measured by an MTS assay after 72 hours of culture. The data show mean ± s.d. for three independent experiments. *P < 0.05, **P < 0.01, ***P < 0.005 compared to control (Student's unpaired *t* test)

Next, we decided to evaluate colony forming ability of the ALL cell lines in the presence of TGF-β. Cells were grown in a serum-free medium (AIM V® Serum Free Medium, ThermoFisher Scientific, UK) for 24 hours and subsequently plated in serum-free methylcellulose with or without TGF-β1 to examine their colony forming ability (Fig. 21). Unfortunately, AT-2 could not be used in this assay, since they failed to form colonies at the time these experiments were performed. However, two AML cell lines, THP1 and OCI-AML3 were used along with 697 and REH cells. As expected, REH cells were resistant to TGF-β1 and maintained their colony formation in its presence, whereas colony formation by 697, THP-1 and OCI-AML3 cells was severely impaired upon TGF-β1 stimulation. Taken together, these data indicate that ALL cell line resistance to TGF-β does not correlate with expression of TEL-AML1. Furthermore, the concentrations of TGF-β required to inhibit colony formation by sensitive cell lines were roughly equivalent in ALL and AML cells.

However, it is possible that experiments in leukaemia cell lines do not accurately reflect TGF-β responsiveness in original pre-leukaemic cells. For this reason, we decided to examine TGF-β responses in primary haematopoietic cells,

using an experimental mouse model previously described in our laboratory (Mangolini et al., 2013; Morrow et al., 2004; Morrow et al., 2007); (Lyons et al., 2010).

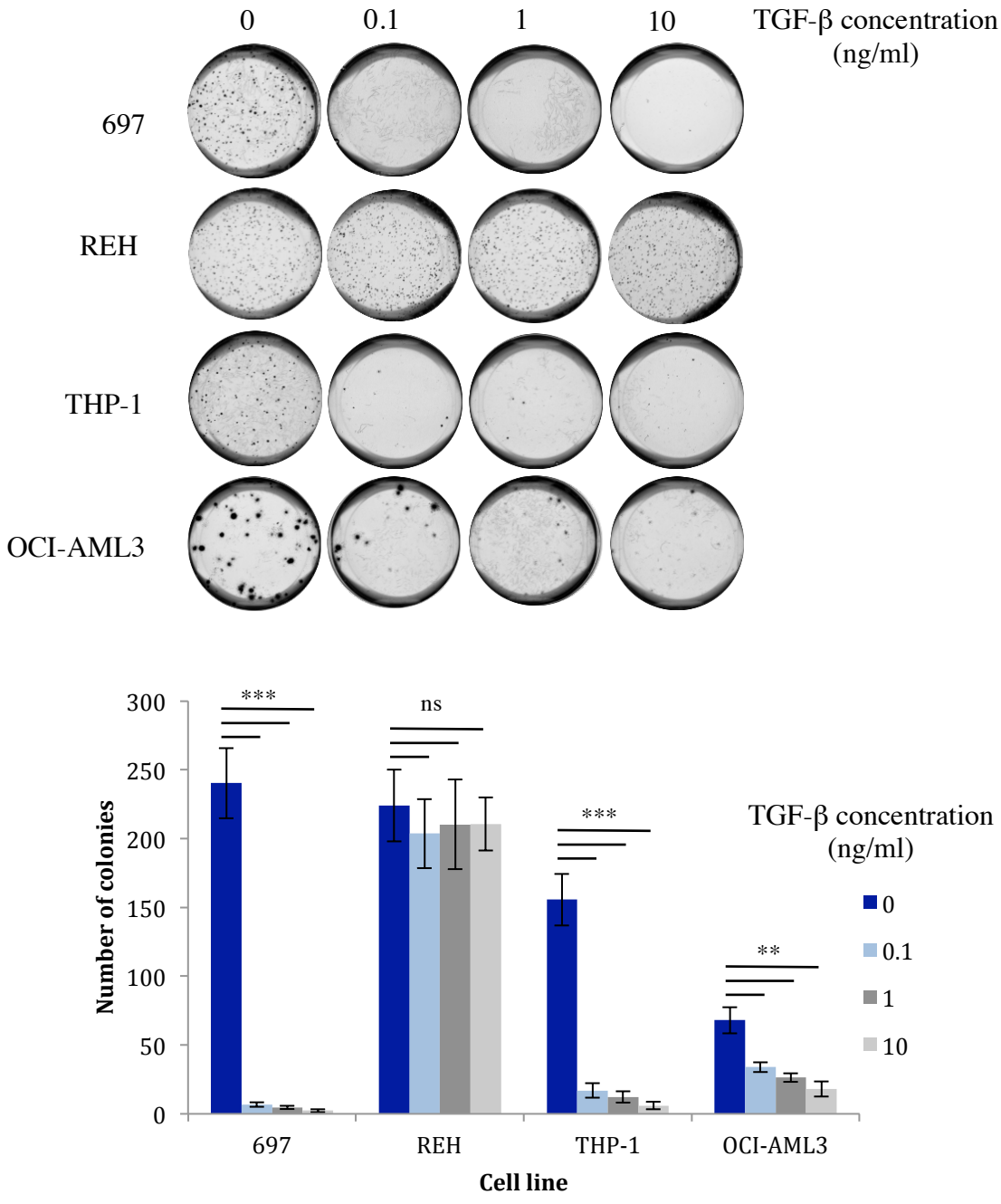

Figure 21 - The effect of TGF-β1 on self-renewal ability of human leukaemic cell lines

The figure shows an example of a colony forming assay of the indicated cell lines plated in methylcellulose in the presence of the indicated TGF-β1 concentrations. $1x10^3$ 697 and REH cells,

$0.3x10^3$ THP-1 cells and $0.15x10^3$ OCI-AML cells were plated in each well. The cells were stained with INT 10-14 days following plating. The bar chart shows the mean number of colonies for each cell line treated with the indicated TGF-β1 concentration ± s.d. for three independent experiments, from quadruplicate wells in each experiment. *P < 0.05, **P < 0.01, ***P < 0.005 compared to control (Student's unpaired *t* test).

3.2.2 TEL-AML1$^+$ immortalised mouse pre-B cells

In order to examine the effect of TEL-AML1 on TGF-β responsiveness in primary cells, we used immortalised mouse pre-B cells derived from Ter119$^-$ckit$^+$ mouse foetal liver cells, conditionally expressing the TEL-AML1 fusion. These cells had been transduced with a conditional Tet-off retroviral expression vector, TEL-AML1 expression being switched off upon exposure of the cells to doxycycline (Lyons et al., 2010). Since the TEL-AML1 protein was fused with an HA-epitope tag, an anti-HA antibody was used to detect its expression. Western blot analysis of $2x10^5$ cells confirmed that TEL-AML1 expression was lost following 48 hours of doxycycline treatment (Fig. 22).

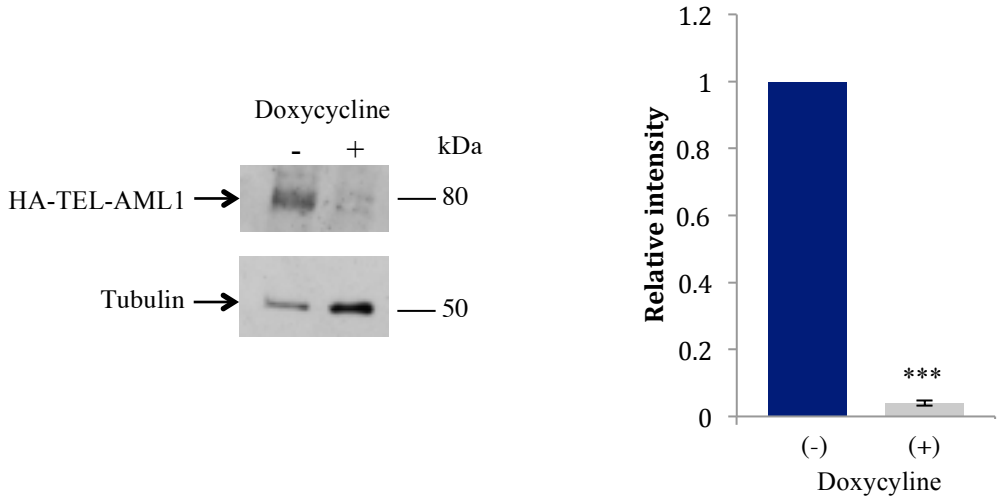

Figure 22 - Doxycycline treatment turns off TEL-AML1 expression

The western blot analysis shows conditional TEL-AML1 pre-B cells following 48 hours culture in normal medium or medium containing 1 mg/ml doxycycline. The western blots were probed with an anti-HA antibody. An anti-α-tubulin antibody was used as a control for protein loading. The bar chart represents the mean densitometric quantitation of HA-TEL-AML1 levels normalised to α-tubulin ± s.d. for three independent experiments. *P < 0.05, **P < 0.01, ***P < 0.005 compared to control (One-sample *t* test).

In this experiment, both untreated and doxycycline treated cells were cultured in mouse methylcellulose in the presence of 20ng/ml IL-7, 20ng/ml Flt-3 and 100ng/ml SCF, and re-plated with and without TGF-β1 to test their colony forming ability (Fig. 23). Upon INT addition it was observed that TGF-β1 stimulation resulted in decreased colony formation in cells not expressing TEL-AML1. However, cells expressing TEL-AML1 also showed an inhibition in their colony forming ability following TGF-β1 stimulation. This showed an inhibition of self-renewal ability upon TGF-β stimulation irrespective of TEL-AML1 expression.

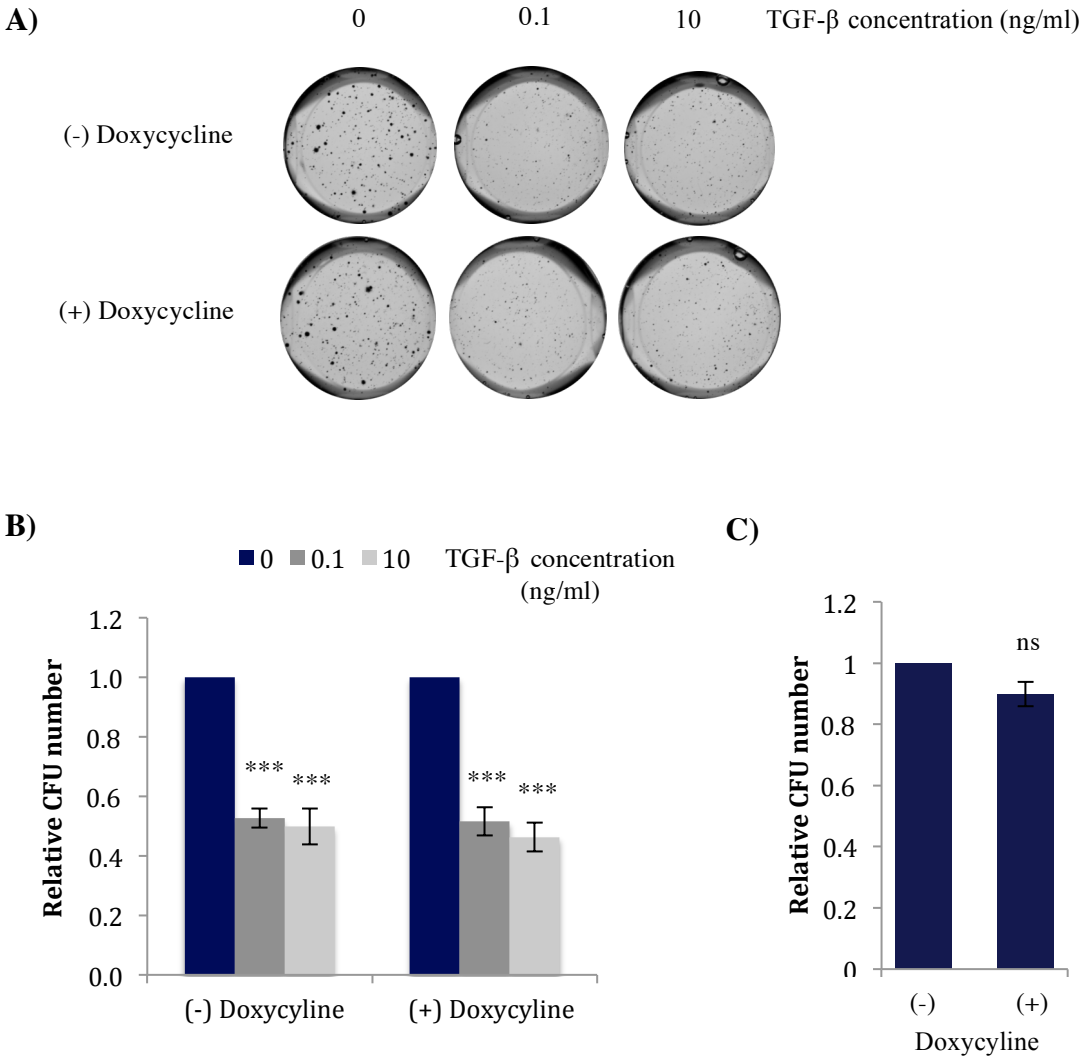

Figure 23 – TGF-β impairs self-renewal ability of mouse progenitor cells conditionally expressing the TEL-AML1 fusion

(A) The figure shows an example of colony forming assays of untreated and doxycycline-treated conditional TEL-AML1 pre-B cells, in the presence of the indicated TGF-β1 concentrations. $5x10^4$ untreated and doxycycline cells were plated in a 3cm dish in methylcellulose in the presence of the indicated TGF-β1 concentrations. Cells were stained with INT 14 days following plating. (B) The bar chart shows the mean fold change ± s.d in colony formation by the conditional TEL-AML1 pre-B cells upon TGF-β stimulation for three independent experiments. (C) The bar chart shows the mean fold change ± s.d in colony formation by pre-B cells constitutively expressing TEL-AML1, for three independent experiments. *P < 0.05, **P < 0.01, ***P < 0.005 compared to control (One-sample *t* test).

Therefore, it appears that TGF-β responsiveness is not affected by TEL-AML1 expression in this model either. To exclude the possibility of a non-specific doxycycline effect on colony formation, cells constitutively expressing TEL-AML1 were used as a control. These cells were plated in methylcellulose in the presence of doxycycline and colony formation was observed. Treatment with doxycycline had no effect on colony forming ability of TEL-AML1 expressing cells. Therefore, these data indicate that doxycycline *per se* did not significantly alter colony formation by the pre-B cells in these experiments.

3.2.3 Characterisation of TGF-β signalling in human ALL cells

In order to determine which point of the TGF-β signalling cascade was blocked in REH cells, we examined SMAD2 phosphorylation by western blot analysis by preparing lysates at various time-points after TGF-β stimulation. If the TGF-β receptors in REH cells were non-functional, this would be reflected in the absence of downstream activation of the TGF-β signalling pathway. An increase in SMAD2 phosphorylation was apparent after 5 minutes of TGF-β1 stimulation, and this continued to increase over the time course, indicating that signals from the receptors were transmitted to SMAD2 upon TGF-β binding (Fig. 24).

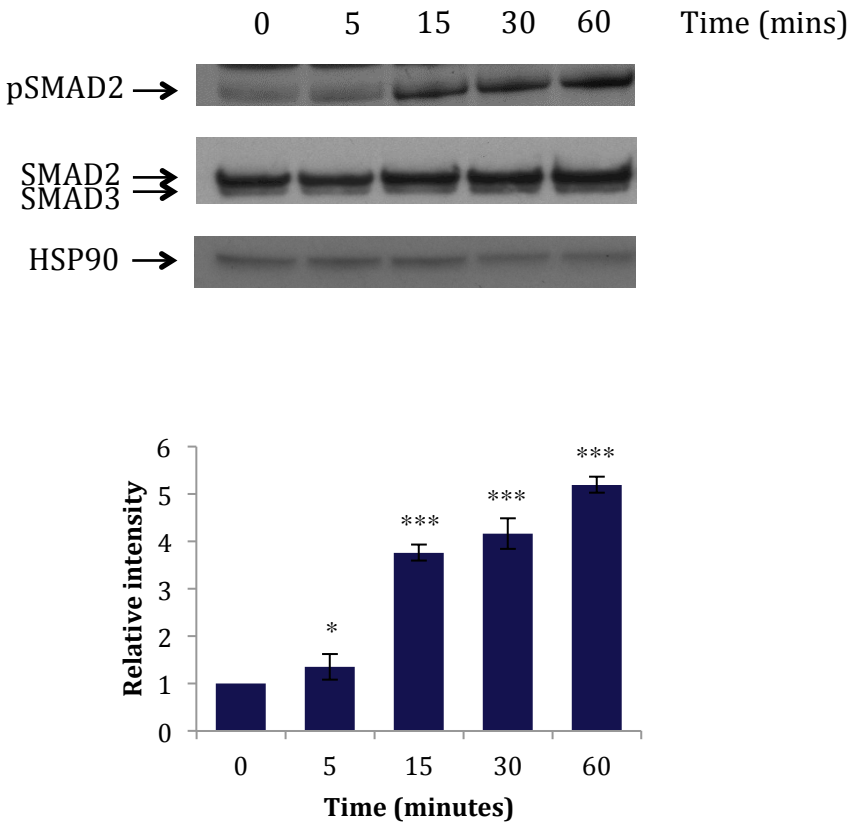

Figure 24 – TGF-β1 exposure results in SMAD2 phosphorylation in REH cells

The western blot analysis shows levels of phosphorylated SMAD2, total SMAD2 and total SMAD3, in REH cells at different time points following 10ng/ml TGF-β1 treatment. The western blot was probed with anti-phospho-SMAD2 and anti-total SMAD2/3 antibodies. An anti-HSP90 antibody was used as a control for protein loading. The bar chart represents the mean densitometric quantitation of phosphorylated SMAD2 bands, normalised to total SMAD2 bands, which are then plotted relative to the loading control, HSP90. The means ± s.d. are shown for three independent experiments. *P < 0.05, **P < 0.01, ***P < 0.005 compared to control (One-sample *t* test).

These data suggest that the TGF-β receptors expressed in REH cells are functional and capable of transmitting TGF-β1 induced signals, and that the resistance of REH cells to TGF-β must occur further downstream in the pathway. Since TGF-β responses are transmitted by nuclear translocation of phosphorylated

SMAD2, we then examined the levels of phosphorylated SMAD2 in the nucleus following TGF-β1 stimulation (Fig. 25 and 26).

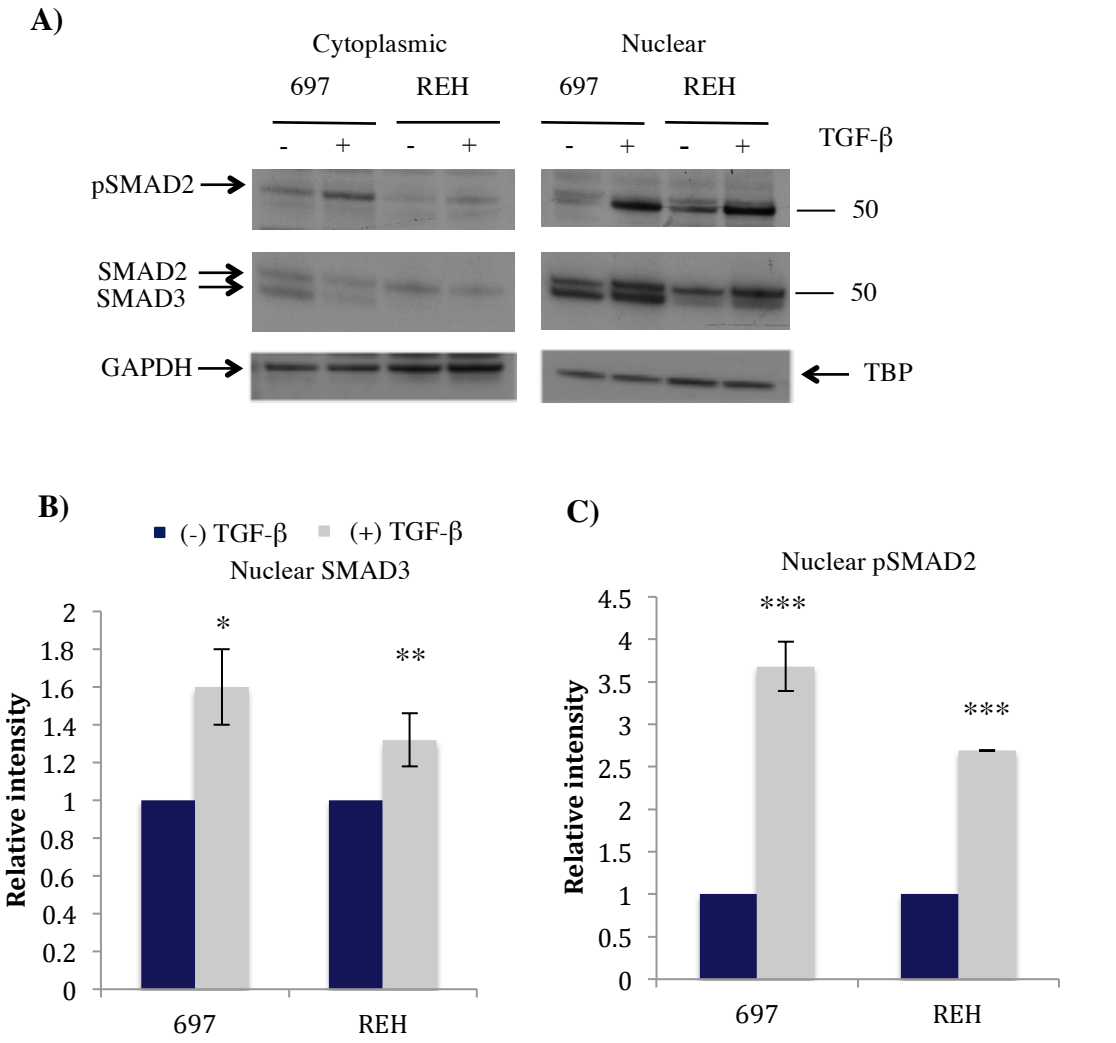

Figure 25 – TGF-β1 treatment of 697 and REH cells results in phosphorylated SMAD2 nuclear translocation

(A) The western blot analysis shows phosphorylated SMAD2, total SMAD2 and total SMAD3 in the cytoplasm and nucleus following 10ng/ml TGF-β1 treatment for 30 minutes, in 697 and REH cells. The western blots were probed with anti-phospho-SMAD2 antibody and anti-Total SMAD2/3 antibody. An anti-GAPDH antibody and an anti-Tata Binding Protein (TBP) antibody were used as controls for protein loading for the cytoplasmic and nuclear extracts, respectively. (B) The bar chart shows the mean densitometric quantitation of total SMAD3 levels in the nucleus relative to the loading control, TBP. (C) The bar chart represents the mean densitometric quantitation of

phosphorylated SMAD2 bands in the nucleus, normalised to total SMAD2 bands, which are then plotted relative to the loading control, TBP. All data show means ± s.d. for three independent experiments. *P < 0.05, **P < 0.01, ***P < 0.005 compared to control (One-sample *t* test).

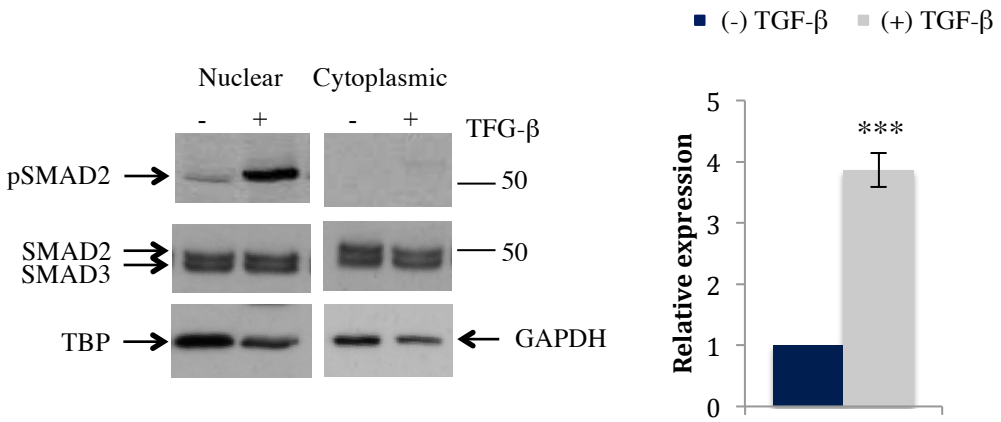

Figure 26 – TGF-β1 treatment of AT-2 cells results in phosphorylated SMAD2 nuclear translocation

The western blot analysis shows phosphorylated SMAD2 levels and total SMAD2 and SMAD3 levels in the nucleus and cytoplasm of AT-2 cells following 10ng/ml TGF-β1 treatment for 30 minutes. The western blots are probed with anti-phospho-SMAD2 antibody and anti-Total SMAD2/3 antibody. An anti-GAPDH and an anti-TBP antibody were used as controls for protein loading for cytoplasmic and nuclear extracts respectively. The bar chart represents the mean densitometric quantitation of phosphorylated SMAD2 bands in the nucleus, normalised to total SMAD2 bands, which are then plotted relative to the loading control, TBP. The means ± s.d. are shown for three independent experiments. *P < 0.05, **P < 0.01, ***P < 0.005 compared to control (One-sample *t* test). Since there was almost no detectable phosphorylated SMAD2 in the cytoplasm, this data could not be quantified.

An increase in the levels of phosphorylated SMAD2 in the nucleus was apparent in the three cell lines, 697, REH and AT-2 cells in response to TGF-β1

stimulation. No differences were observed in the expression of total SMAD2 protein levels between the cell lines. However, unlike 697 and AT-2, REH showed a striking deficit in total SMAD3 protein expression. Therefore, to investigate further we studied the levels of phosphorylated SMAD3 in REH cells, using 697 as controls. Low levels of phosphorylated SMAD3 protein were detected in REH cells, relative to 697 cells. Furthermore, there was almost no increase in SMAD3 phosphorylation following TGF-β exposure in REH cells. As expected, there was a significant deficit in total SMAD3 protein in REH cells.

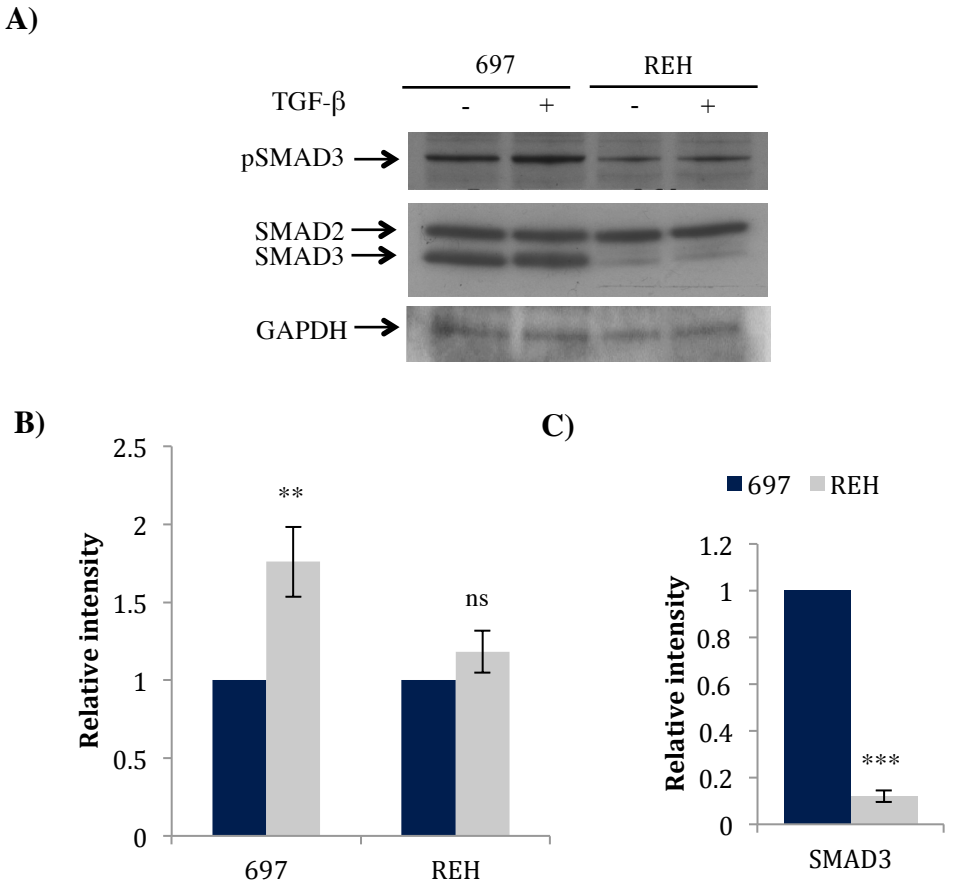

Figure 27 - SMAD3 is deficient in REH cells

(A) The western blot analysis shows phosphorylated SMAD3 following 10ng/ml TGF-β1 treatment for 30 minutes in 697 and REH cells. Total SMAD2 and SMAD3 levels are also shown. The western

blot was probed with anti-phosphorylated SMAD3 antibody and anti-Total SMAD2/3 antibody. An anti-GAPDH antibody was used as a control for protein loading. (B) The bar chart shows the mean densitometric quantitation of phosphorylated SMAD3 levels relative to total SMAD3 levels, which in turn is measured against the control, GAPDH. The means ± s.d. are shown for three independent experiments. (C) The bar chart shows the mean densitometric quantitation of total SMAD3 levels of untreated REH cells relative to untreated 697. The mean ± s.d. are shown for three independent experiments. $*P < 0.05$, $**P < 0.01$, $***P < 0.005$ compared to control (One-sample *t* test).

Next, we examined the total levels of SMAD2 and SMAD3 across our panel of ALL cell lines. BEL-1, an MLL-AF4$^+$ cell line, showed almost no expression of SMAD2 and SMAD3. While SMAD2 levels were mostly similar across the panel, there were significant differences between SMAD3 expression levels between cell lines. Moreover, cell lines with almost no SMAD3 or very low levels of SMAD3 expression were previously shown to be resistant to TGF-β, whereas cell lines expressing SMAD3 were sensitive to the anti-proliferative effects of TGF- β (Fig. 28).

A)

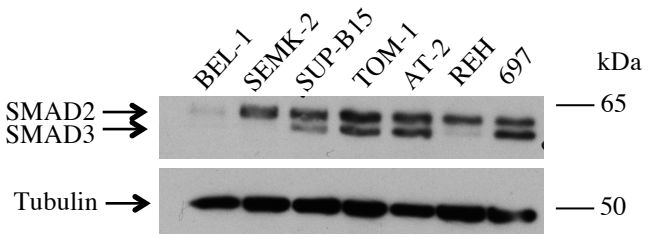

B)

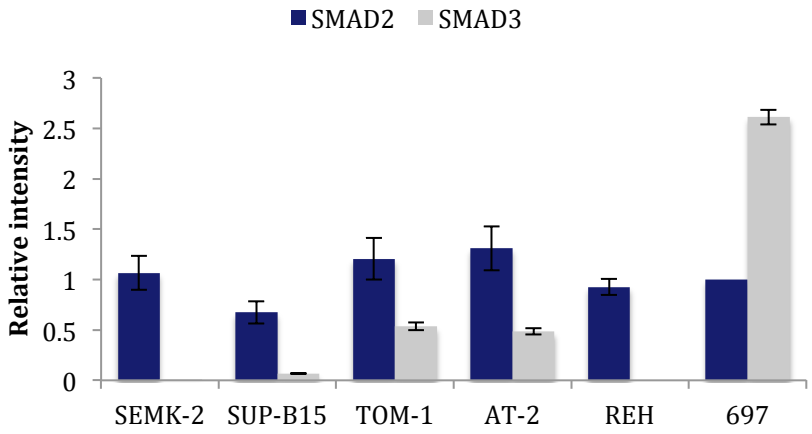

C)

Cell line	SMAD3 signal	Sensitivity to TGF-β
BEL-1	Undetected	-
SEMK-2	Low	-
SUP-B15	Low	-
TOM-1	High	+
AT-2	High	+
REH	Low	-
697	High	+

Figure 28 – SMAD2 and SMAD3 expression in ALL cell lines

(A) The western blot analysis shows total SMAD2 and SMAD3 levels following 10ng/ml TGF-β1 treatment for 30 minutes across a panel of ALL cell lines. The western blot was probed with an anti-Total SMAD2/3 antibody. An anti-tubulin antibody was used as a control for protein loading. (B) The bar chart shows the mean densitometric quantitation of total levels of SMAD2 and SMAD3 in all cell

lines relative to corresponding tubulin expression, followed by relativity to the level of total SMAD2 expression in 697 cells. The means ± s.d. are shown for three independent experiments except in the case of AT-2 cells which was performed once. Expression of SMAD2/3 in BEL-1 was too low to be detected and quantified. (C) The table shows the ratio of SMAD3 expression in all cell lines and its correlation to the sensitivty to TGF-β.

3.3 Discussion

To investigate the putative link between TGF-β responsiveness and leukaemia aetiology hypothesised in a recent publication, we examined TGF-β signalling in a panel of ALL cell lines. We treated this panel of cell lines with TGF-β and showed that while TEL-AML1$^+$ REH cells were resistant to TGF-β growth inhibition, TEL-AML1$^+$ AT-2 cells were sensitive. This was further shown by cell cycle assays, where there was decreased proliferation of AT-2 cells following TGF-β treatment, while such treatment did not cause a change in the percentage of REH cells in the S-phase of the cell cycle. Since the FBS used to culture cells may contain traces of TGF-β, we cultured REH and 697 cells in parallel with two AML cell lines in a serum-free medium and subsequently used serum-free methylcellulose to culture cells with and without TGF-β, to monitor their colony forming ability. These experiments demonstrated that colony formation by REH cells was not affected by TGF-β treatment, whereas colony formation was reduced in the other cell lines, including 697 cells, confirming the MTS and cell cycle assays. Unfortunately, we were not able to perform colony assays with AT-2 assays at this time in the laboratory. Taken together, this data indicated that resistance to TGF-β did not correlate with TEL-AML1 expression in ALL cell lines.

There are several possible explanations for these results. The simplest explanation is that TEL-AML1 does not influence TGF-β responsiveness. However, it is also possible that examining responses to TGF-β in ALL cell lines does not reflect responsiveness in pre-leukaemic cells. Thus, the capacity of cells to respond to TGF-β may change upon acquisition of overt leukaemia characteristics. Ford et al.

used three human and mouse models to show resistance of TEL-AML1 expressing cells to TGF-β induced suppression of proliferation: Inducible TEL-AML1 BaF3 cells, that is a pro-B cell line, murine B progenitor cell lines transduced with retroviral TEL-AML1 constructs and human cord blood cells transduced with lentiviral TEL-AML1 and plated on MS-5 stroma. In this project, we wanted to examine TGF-β responsiveness of TEL-AML1 expressing cells in a model previously developed in our laboratory (Lyons et al., 2010; Mangolini et al., 2013; Morrow et al., 2004; Morrow et al., 2007). To do this, we used mouse cells with conditional TEL-AML1 expression, where the addition of doxycycline repressed expression of the fusion protein. Colony forming assays of these mouse pre-B cells demonstrated that TGF-β stimulation resulted in a similar decrease in colony formation, independent of the presence of doxycycline, and consequent TEL-AML1 expression. Thus, TEL-AML1 expression failed to affect TGF-β responsiveness in this experimental model, consistent with the lack of correlation between its expression and resistance to TGF-β in human ALL cells.

To examine whether TGF-β was capable of initiating signal cascades in resistant REH cells, we monitored phosphorylated SMAD2 levels following stimulation. SMAD2 showed a gradual increase in phosphorylation with time, when treated with TGF-β. Moreover, we observed SMAD protein translocation to the nucleus upon TGF-β exposure. Meanwhile, SMAD3 protein appeared to be underexpressed in REH cells, with little increase in the nucleus upon TGF-β stimulation. However, this was not the case in AT-2 cells, where SMAD3 was observed at similar levels to SMAD2 protein. This may suggest that REH resistance to TGF-β may have been acquired as a result of deficiency in SMAD3 protein, a

crucial transcriptional regulator in the TGF-β pathway. Reduced SMAD3 expression in other ALL cell lines in our panel also correlated with TGF-β resistance. Therefore, it is possible that resistance to TGF-β is acquired as a result of SMAD3 deficit, and not TEL-AML1 expression.

In conclusion, our experiments do not support the hypothesised link between resistance to the anti-proliferative effects of TGF-β and TEL-AML1 expression. However, there are a number of caveats to this conclusion, including the possibility that human ALL cell lines and mouse primary cells do not accurately reflect the biology of pre-leukaemic cells. Thus, it remains possible that this fusion may influence TGF-β responsiveness, but only under very specific conditions.

CHAPTER IV. SMAD7 is crucial for leukaemia survival

4.1 Introduction

4.1.1 STAT3 and SMAD7

Although we established that it is unlikely in our models that TEL-AML1 expression is linked to resistance to TGF-β in ALL cells, we decided to investigate if the negative regulator of TGF-β, SMAD7, can regulate TGF-β responsiveness in ALL cells. SMAD7 can inhibit TGF-β in a negative feedback loop through downregulation of R-SMADs and has previously been suggested to play a role in different cancers (Zhu et al., 2011). Furthermore, studies have also shown a link between STAT3, which is important in TEL-AML1 pathogenesis, and SMAD7 signalling in different cancers (Jenkins et al., 2005). One study noted that STAT3 hyper-activation promoted gastric adenoma growth and desensitised cells to the cytostatic effect of TGF-β (Jenkins et al., 2005). Using luciferase reporter assays and qRT-PCR, this study observed that this desensitisation was achieved through STAT3 transcriptional induction of *SMAD7*. Furthermore, siRNA mediated *SMAD7* silencing blocked the ability of STAT3 to desensitise cells to TGF-β-mediated suppression. This demonstrated the molecular link between the STAT3 and SMAD pathways, specifically identifying SMAD7 as a key mediator in desensitising cells to TGF-β and promote STAT3 induced gastric adenomas (Jenkins et al., 2005). Another more recent study showed that tumour-associated overexpression of EGFR desensitised cells to TGF-β signalling, via STAT3 activation and SMAD7 induction (Luwor et al., 2013). They identified STAT3 as a key mediator, persistently activated by EGFR, in desensitising cells to TGF-β, using shRNA-mediated *STAT3*

knockdown in head and neck and epidermoid tumour cell lines. Furthermore, *STAT3* knockdown xenografts showed decreased SMAD7 expression compared to control xenografts *in vivo*. SMAD7 mRNA and protein expression were also decreased when EGFR activity was blocked and in *STAT3* knockdown tumours (Luwor et al., 2013).

4.1.2 SMAD7: canonical and non-canonical signalling

SMAD7 is transcriptionally induced by TGF-β but acts as an inhibitor of TGF-β signalling, establishing a negative feedback mechanism (Massague et al., 2005). SMAD7 has a conserved C-terminal MH2 domain, but unlike R-SMADs it lacks the N-terminal MH1 domain and the C-terminal amino acid residue phosphorylated by TGF-βRI (Yan et al., 2009) (Fig. 13). SMAD7 localisation differs between cell types, with SMAD7 being predominantly localised in the nucleus in most cell types (Zhang et al., 2007). SMAD7 acts as a negative regulator of TGF-β in many ways. Firstly, it can inhibit signalling by interfering with activation of R-SMADs through blocking TGF-βRI induced phosphorylation of SMAD2 and SMAD3 (Nakao et al., 1997). The association of SMAD7 with TGF-β receptors suggests it competes with R-SMADs for receptor binding, forming a stable complex (Massague and Chen, 2000). Its interaction with TGF-βRI also inhibits association of SMAD2 with SMAD4 and the nuclear accumulation of SMAD2, as shown in HepG2 cells (Hayashi et al., 1997). Additionally, a recent study has shown SMAD7 can also directly inhibit R-SMAD-SMAD4 complex, irrespective of its interaction with TGF-βRI (Yan et al., 2016). Secondly, SMAD7 can recruit the HECT type E3 ubiquitin ligases, SMURF1 and SMURF2. SMAD7 binds to SMURFs in the nucleus and translocates to the cytoplasm in response to TGF-β and recruits the ubiquitin ligases

to the activated type I TGF-β receptor, leading to degradation of the receptor through the proteasomal pathway (Ebisawa et al., 2001; Yan et al., 2009). SMAD7 also acts as an adaptor protein for other E3 ligases such as NEDD4-2- and WWP1- mediated degradation of TGF-β receptors, R-SMADs and SMAD4 (Yan et al., 2016; Yan et al., 2009). SMAD7 can also interact with a range of other proteins to inhibit TGF-β effectively. For example, SMAD7 works synergistically with the serine/threonine kinase receptor associated protein (STRAP), which associates with TGF-β type I and II receptors and SMAD7 to stabilise the complex between TGF-βRI and SMAD7 and thereby inhibit TGF-β signalling (Yan et al., 2009). While SMAD6, another I-SMAD, is a specific inhibitor of the BMP pathway, SMAD7 has been shown to inhibit both the TGF-β and BMP signalling in some cell types. There are more than 20 BMP family members, involved in regulation of cell proliferation, differentiation and apoptosis, with essential roles in embryonic development (Zhang and Li, 2005). BMPs are also involved in induction of haematopoietic tissue during early embryonic development and BMP signalling is known to function in controlling HSC numbers through regulation of the haematopoietic niche. Moreover, BMP signalling has been reported to play a role in promoting acute leukaemia (Crispino and Le Beau, 2012).

Although *SMAD7* is transcriptionally induced by TGF-β and plays a key role in TGF-β canonical signalling, other signalling pathways have also been shown to be involved in the transcriptional regulation of *SMAD7*. The transcription of *SMAD7* can be induced by inflammatory cytokines, such as interleukin 1, IFN-γ and TNF-α (Fig. 29). There is also increasing evidence to support a role for SMAD7 in p38 MAPK, ERK and JNK signalling pathways (Yan et al., 2009). Furthermore, it also

has an inhibitory role in other intracellular pathways such as disrupting the formation of TRAF2-TAK1-TAB2/3 complex and inhibiting TNF-α/NF-κB signalling to promote apoptosis (Yan et al., 2009). It has been shown to antagonise Wnt signalling, by forming complexes with β-catenin and Smurf2, resulting in proteasomal degradation of β-catenin (Han et al., 2006). This can also result in deregulation of transcription factors involved in tumourigenesis, such as c-Myc (Millar, 2006). Therefore, SMAD7 is crucial in mediating cross-talk between TGF-β signalling and other key pathways, and may have important functions that are independent of TGF-β signalling. In haematopoiesis, SMAD7 is also important in the development of primitive human haematopoietic cells. Its role in altering cell fate commitment decisions in HSCs has been observed, by favouring the development of myeloid progenitors over lymphoid progeny (Chadwick et al., 2005). Indeed, overexpression of SMAD7 in HSCs results in enhanced myeloid differentiation and reduced lymphoid development. In addition, as previously mentioned, overexpression of SMAD7 in murine HSCs results in significantly increased self-renewal capacity of HSCs *in vivo*, through relieving its inhibition by R-SMADs (Blank et al., 2006).

Additionally, SMAD7 has important roles through its nuclear function. As a negative regulator of TGF-β, it interrupts functional R-SMAD-DNA complex formation in the nucleus (Zhang et al., 2007). SMAD7 associates with R-SMADs via its MH2 domain, with studies showing that mutations in four specific amino acids in the SMAD7 MH2 domain disrupt its interaction with R-SMADs (Yan et al., 2016). In addition to its inhibitory role in the nucleus, SMAD7 has also been shown to transcriptionally regulate target genes. It can bind to DNA in the nucleus

by binding DNA elements that contain the SMAD-binding element (SBE) CAGA box. Thus, SMAD7 binding of the SBE in PAI-1, a TGF-β target gene, has been shown to inhibit TGF-β signalling (Hanyu et al., 2001; Yan et al., 2016; Zhang et al., 2007). SMAD7 also regulates gene transcription through interactions with HDACs, such as SIRT1, and HATs, such as p300 (Kume et al., 2007; Simonsson et al., 2005). Furthermore, in addition to directly regulating transcription, SMAD7 can act as a transcriptional co-activator, for example, by promoting the interferon regulatory factor 1 (IRF1) transcription factor to eventually induce apoptosis in breast cancer cells (Hong et al., 2013).

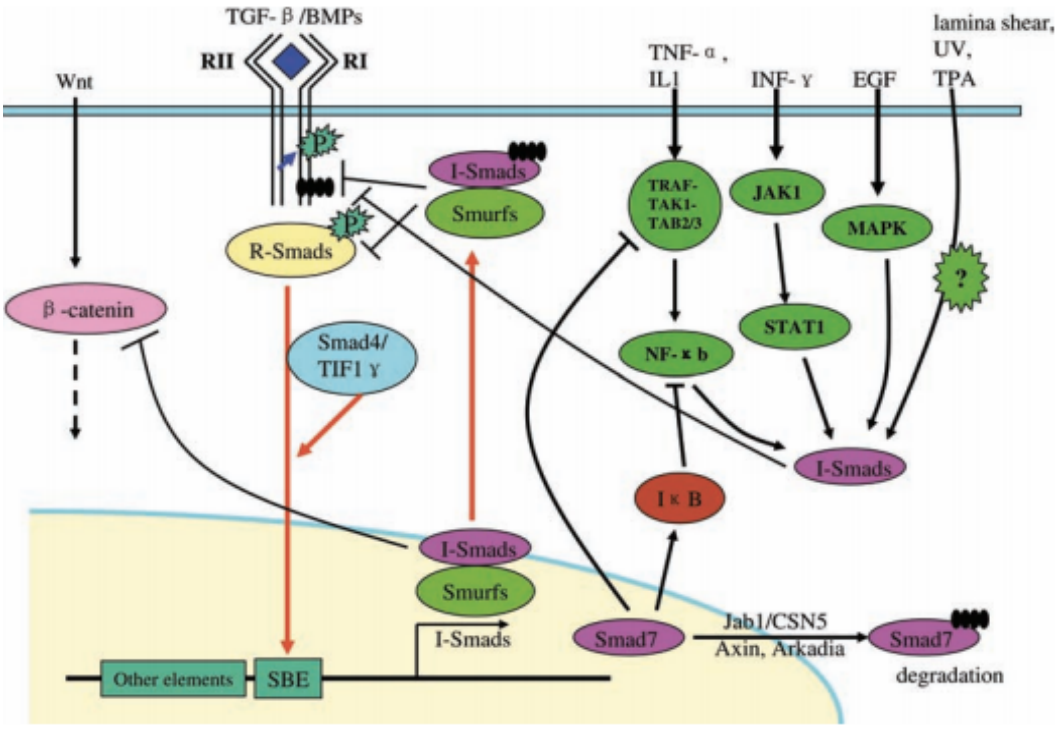

Figure 29 - SMAD7 mediates the cross-talk of TGF-β signalling with other pathways

This diagram shows SMAD7 is transcriptionally induced by TGF-β signalling and inhibits TGF-β signalling via a negative feedback mechanism. SMAD7 is also induced by other indicated cytokines or stimuli such as TNF-α /IL1, INF-γ, EGF, laminar shear stress etc. SMAD7 is also known to enhance transcription of IkB, which is a key inhibitor of NF-κB pathway. SMAD7 can down-regulate

B-catenin protein by recruiting E3ligase SMURF1. Furthermore, SMAD7 itself can also undergo proteasome mediated degradation in both cytoplasm and nucleus. Adapted from (Yan et al., 2009)

4.1.3 SMAD7 and cancer

Due to its functions in various key signalling pathways, SMAD7 affects numerous processes, including modulation of immune responses, embryo cardiac development and function, and skeletal muscle cell differentiation (Stolfi et al., 2013). Deregulated SMAD7 expression has been observed to play a role in many human disorders. For example, SMAD7 is implicated in the progression of fibrosis in different organs such as the pancreas, liver, lung and kidney (Stolfi et al., 2013). Increasing evidence suggests a dual role for SMAD7 in cancers, where it can restrain or enhance cancer cell growth in a cell type dependent manner. In some cancers, stable SMAD7 overexpression has been associated with reduced tumour progression. It has been reported to inhibit formation of osteolytic metastases by human breast cancer and melanoma. On the other hand, high SMAD7 expression levels have been associated with thyroid follicular tumours and hepatocellular carcinomas (Cerutti et al., 2003; Dowdy et al., 2005; Javelaud et al., 2007; Mikula et al., 2006). SMAD7 can also promote tumourigenesis by blocking TGF-β mediated growth inhibition and apoptosis in pancreatic cancer and it has been linked to poor survival rates in oesophageal squamous cell carcinoma (Stolfi et al., 2013). *SMAD7* gene variants have been particularly analysed in colorectal cancers (CRC), showing that patients with *SMAD7* deletion have a favourable clinical outcome compared to patients with *SMAD7* amplification (Stolfi et al., 2014). Silencing of *SMAD7* in CRC cell lines *in*

vitro and *in vivo* after transplantation into immunodeficient mice, results in tumour growth inhibition. Two genome-wide association studies (GWAS) show that further genetic variations of *SMAD7* influence the risk of colorectal carcinogenesis (Broderick et al., 2007; Slattery et al., 2010). SMAD7 has also been linked to adult T-cell leukaemia (ATLL), with constitutively active SMAD7 inhibiting TGF-β mediated growth suppression of cancer cells (Nakahata et al., 2010). This dual role of SMAD7 could be a result of the different functions of the TGF-β pathway in various cancer types. SMAD7 can also switch from tumour-suppressive to tumour-promoting function, which can be caused by the opposite role of TGF-β signalling in early versus advanced tumour stages (Lebrun, 2012). Therefore, further investigation into the mechanisms used by SMAD7 to exert its function in different cancers and different stages of oncogenesis, may reveal new therapeutic strategies.

Since activation of STAT3 has been shown to play a key role in TEL-AML1 pathogenesis and has been shown to regulate SMAD7 in other cancers, we decided to investigate if *SMAD7* was a STAT3 target in TEL-AML1$^+$ leukaemia and further identify its role in regulating TGF-β responsiveness of leukaemic cells.

4.2 Results

4.2.1 STAT3 regulates SMAD7 in TEL-AML1$^+$ cells

In order to establish whether STAT3 regulated SMAD7 in TEL-AML1$^+$ leukaemia, we performed lentiviral transduction of REH cells (Fig. 30A) and AT-2 cells (Fig. 30B) with an shRNA targeting *STAT3*, previously used in our laboratory. Following 72 hours of puromycin selection (five days after transduction), total RNA was extracted and qRT-PCR was performed using a specific probe set to detect *SMAD7* mRNA expression. Following confirmation of *STAT3* knockdown, we observed a decrease in *SMAD7* gene expression as a result of the knockdown in both REH and AT-2 cells (Fig. 30). Therefore, these data indicated that STAT3 did indeed regulate *SMAD7* gene expression in TEL-AML1$^+$ cells.

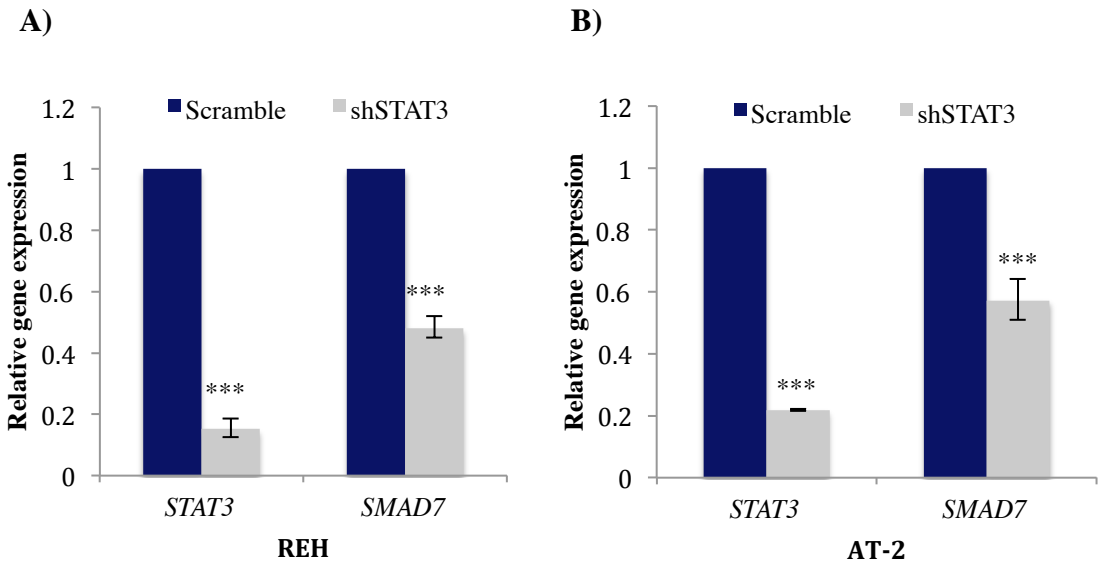

Figure 30 - STAT3 regulates *SMAD7* in TEL-AML1$^+$ cells

The figure shows qPCR analysis of *STAT3* silencing in (A) REH and (B)AT-2 cells transduced with control scramble or *STAT3* shRNA. 2 days after transduction, cells were selected with puromycin for a further 3 days. Dead cell removal was then performed and *STAT3* silencing measured by qPCR (Day

5 post transduction). The gene expression analysis of *SMAD7* following STAT3 knockdown is also shown. The mean ± s.d. is shown for three independent experiments. *$P < 0.05$, **$P < 0.01$, ***$P < 0.005$ compared to control (One sample *t* test).

4.2.2 SMAD7 knockdown in TEL-AML1$^+$ cells results in cell cycle block and apoptosis

Since STAT3 activated *SMAD7* expression, we decided to examine the function of SMAD7 in TEL-AML1$^+$ cells. In particular, we were interested to determine whether STAT3 induced SMAD7 expression played a part in resistance to TGF-β in REH cells. In order to do this, we silenced *SMAD7* in REH cells using shRNA constructs. A set of five different shRNA targeting *SMAD7* were tested, from which we identified two independent hairpins capable of reducing the expression of *SMAD7*. The shRNAs used resulted in silencing of *SMAD7* to different extents, as determined by qRT-PCR analysis (Fig. 31A).

Following *SMAD7* knockdown, we measured the proliferation and survival of leukaemic cells. Cells transduced with control scramble and two different shRNA were cultured with and without TGF-β1 and viability of cells measured by MTS assay, 48 and 96 hours post treatment. These experiments demonstrated that proliferation of REH cells was inhibited by *SMAD7* silencing. It was observed that the greater the knockdown, the greater the inhibition of proliferation (Fig. 31B). Interestingly, TGF-β1 addition had no effect on the degree of proliferation inhibition (Fig. 31C). This suggested that, regardless of TGF-β1, *SMAD7* knockdown resulted

in suppression of leukaemic cell proliferation, implicating a TGF-β independent role for SMAD7 in REH cells.

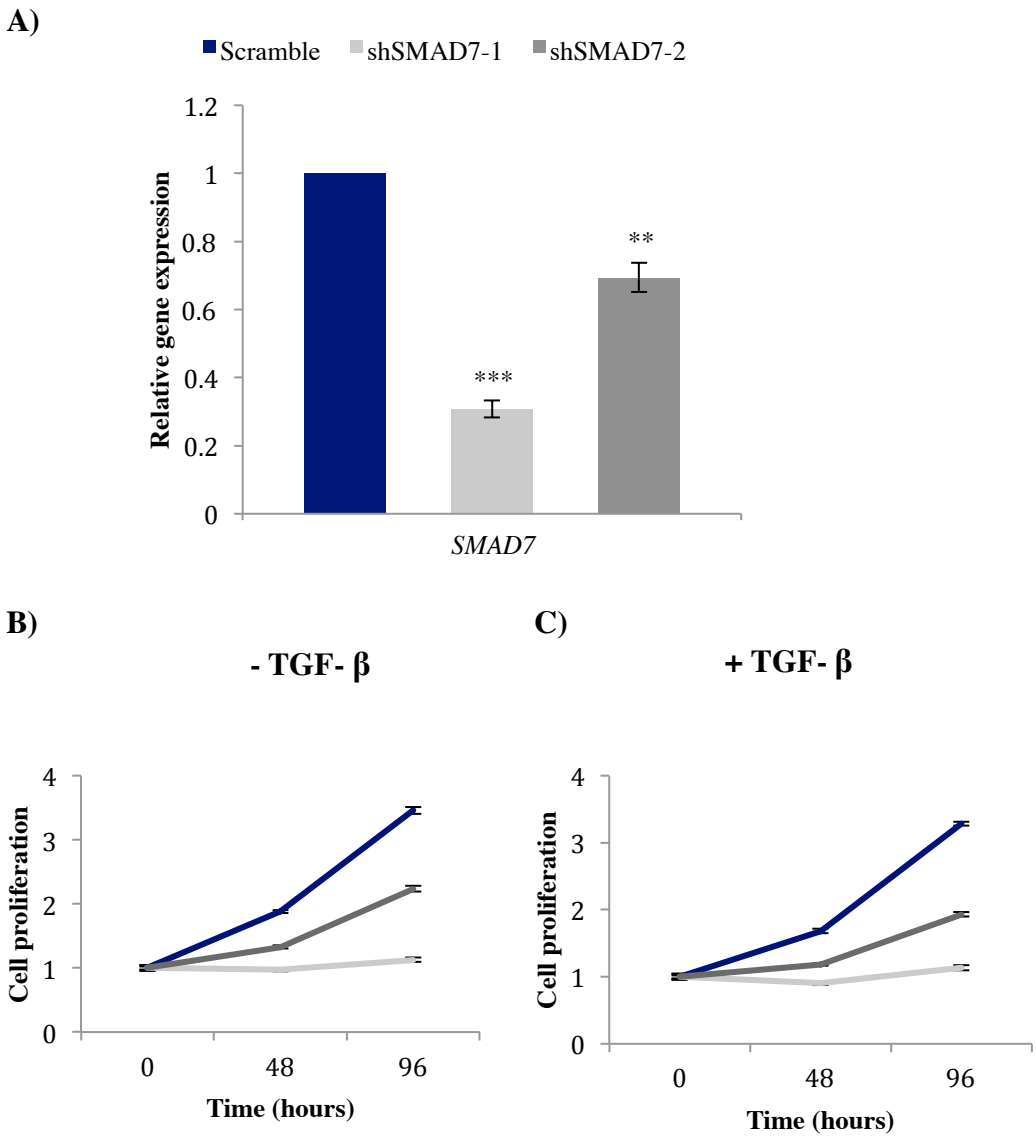

Figure 31 – Inhibition of SMAD7 leads to a specific block in proliferation in REH cells

(A) The figure shows qPCR analysis of *SMAD7* silencing in REH cells transduced with control scramble or two different *SMAD7* shRNAs for three independent experiments. 2 days after transduction, cells were selected with puromycin for a further 3 days. Dead cell removal was then performed *SMAD7* silencing measured by qPCR (Day 5 post transduction). The line charts show mean proliferation of REH cells as measured by MTS 48 and 96 hours following dead cell removal. Cells were either (B) untreated or (C) treated with 10ng/ml TGF-β1. All data show the means ± s.d.

for three independent experiments. *P < 0.05, **P < 0.01, ***P < 0.005 compared to control (One sample *t* test).

Meanwhile we identified a third shRNA targeting *SMAD7* that generated better knockdown of SMAD7 than *shSMAD7-2*. Therefore, for the rest of the experiments, we used this shRNA (*shSMAD7-3*) together with *shSMAD7-1* (Fig. 32A). Although *SMAD7* silenced cells stopped proliferating in the absence of exogenous TGF-β1, it was important to rule out any effect of autocrine TGF-β signalling or by any TGF-β present in the culture medium. Therefore, following *SMDA7* knockdown, REH cells were treated with and without the anti-TGF-β1 mAb 1D11, and we examined whether this would rescue the proliferation suppression upon *SMAD7* silencing. We have previously shown that 1D11 does block TGF-β induced SMAD2 activation and suppression of proliferation in these cells. These experiments showed that despite blocking autocrine TGF-β1 signalling with 1D11 and in the absence of exogenous TGF-β1, *SMAD7* silencing still resulted in proliferation inhibition of REH cells (Fig. 32B). This suggested that SMAD7 function is independent of TGF-β signalling in these cells, suggesting a different mechanism of action.

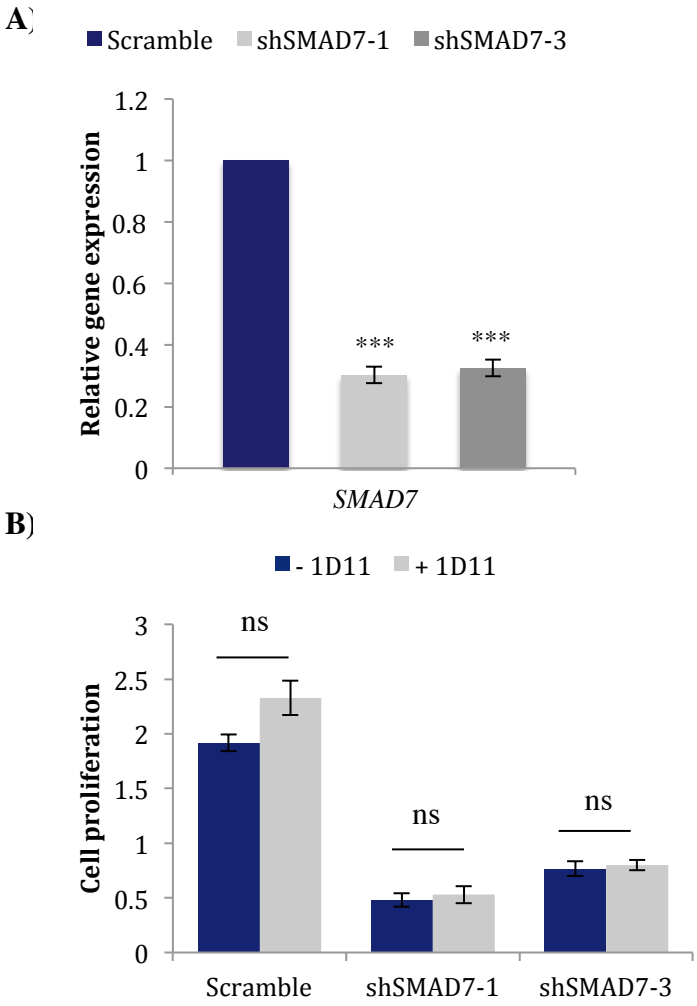

Figure 32 - Treatment of *SMAD7* knockdown cells with 1D11 causes no change in proliferation block

(A) The figure shows qPCR analysis of *SMAD7* knockdown in REH cells transduced with control scramble or two independent *SMAD7* shRNA. 2 days following transduction, cells were selected with puromycin for a further 3 days. Dead cell removal was then performed and *SMAD7* silencing measured by qPCR (Day 5 post transduction). The data show the means ± s.d. for three independent experiments. *P < 0.05, **P < 0.01, ***P < 0.005 compared to control (One sample *t* test). (B) The chart shows proliferation of REH cells transduced with control scramble or the two *SMAD7* shRNA and subjected to 20ng/ml 1D11 treatment on day 5 post transduction. The proliferation is measured by MTS assay at 72 hours following treatment. All data show the means ± s.d. for three independent experiments. *P < 0.05, **P < 0.01, ***P < 0.005 compared to control (Student's unpaired *t* test).

In order to determine whether the sensitivity of REH cells to *SMAD7* knockdown was due to induction of cell cycle block and eventual cell death, we evaluated its effect on cell cycle profile and level of apoptosis in the cells. *SMAD7* knockdown cells resulted in a substantial cell cycle block, in the G_1-S phase transition (Fig. 33) and a significant increase in apoptosis (Fig. 34). This confirmed that knockdown of SMAD7 induced both cell cycle arrest and cell death in REH cells. We then decided to analyse the clonogenic capacity of REH cells following *SMAD7* knockdown using colony-forming assays. Cells were plated out into methylcellulose medium and colony formation assessed after two weeks culture. This showed that the ability of REH cells to form colonies after *SMAD7* silencing was significantly reduced compared to control cells (Fig. 35).

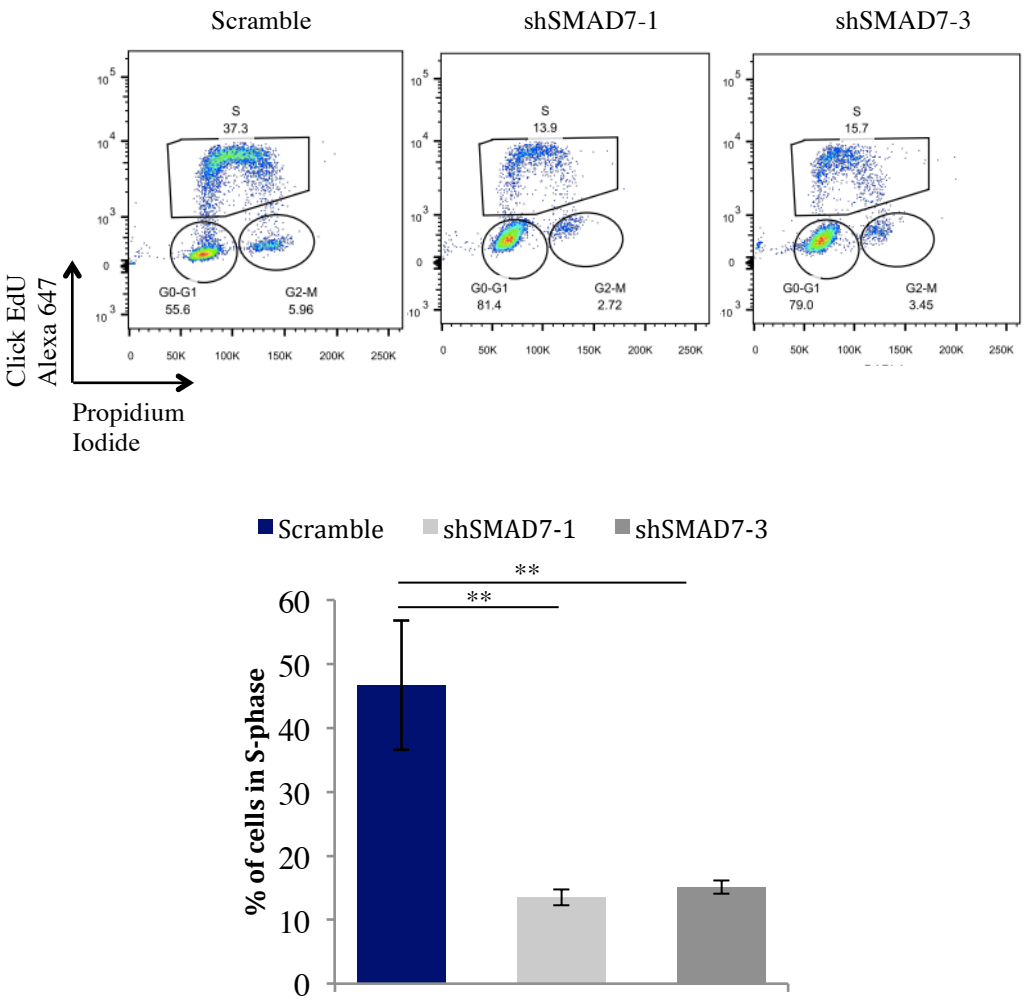

Figure 33 - *SMAD7* knockdown causes cell cycle block in REH cells

The flow cytometry plots are examples of the cell cycle profiles of REH cells transduced with control scramble and two *SMAD7* shRNA. 2 days after transduction, cells were selected with puromycin for 3 days. Dead cell removal was then performed and viable cells were cultured for a further 2 days. Cell cycle profile was then evaluated after pulsing with 10uM EdU for 1 hour (Day 7 post transduction). This figure is representative of three independent experiments. The bar chart represents the mean percentage of cells in the S-phase ± s.d. for three independent experiments. *P < 0.05, **P < 0.01, ***P < 0.005 compared to control (Student's unpaired *t* test).

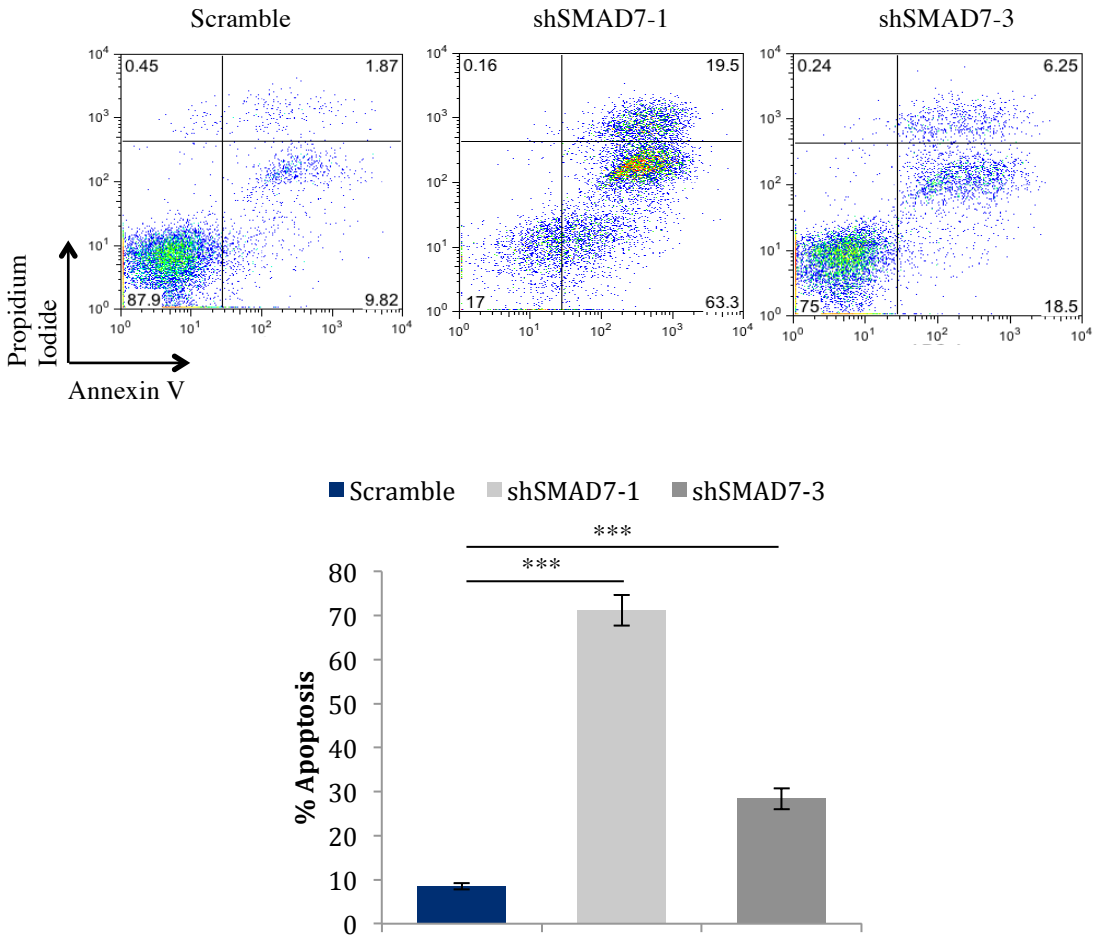

Figure 34 - *SMAD7* knockdown causes apoptosis in REH cells

The flow cytometry plots are examples of the apoptosis profiles of REH cells transduced with control scramble and two *SMAD7* shRNA. 2 days after transduction, cells were selected with puromycin for 3 days. Dead cell removal was then performed and viable cells were cultured for a further 3 days. The cells were then stained with Annexin V and PI (Day 8 post transduction). This figure is representative of three independent experiments. The bar chart represents the mean percentage of apoptotic Annexin V^+PI^- cells ± s.d. for three independent experiments. *P < 0.05, **P < 0.01, ***P < 0.005 compared to control (Student's unpaired *t* test).

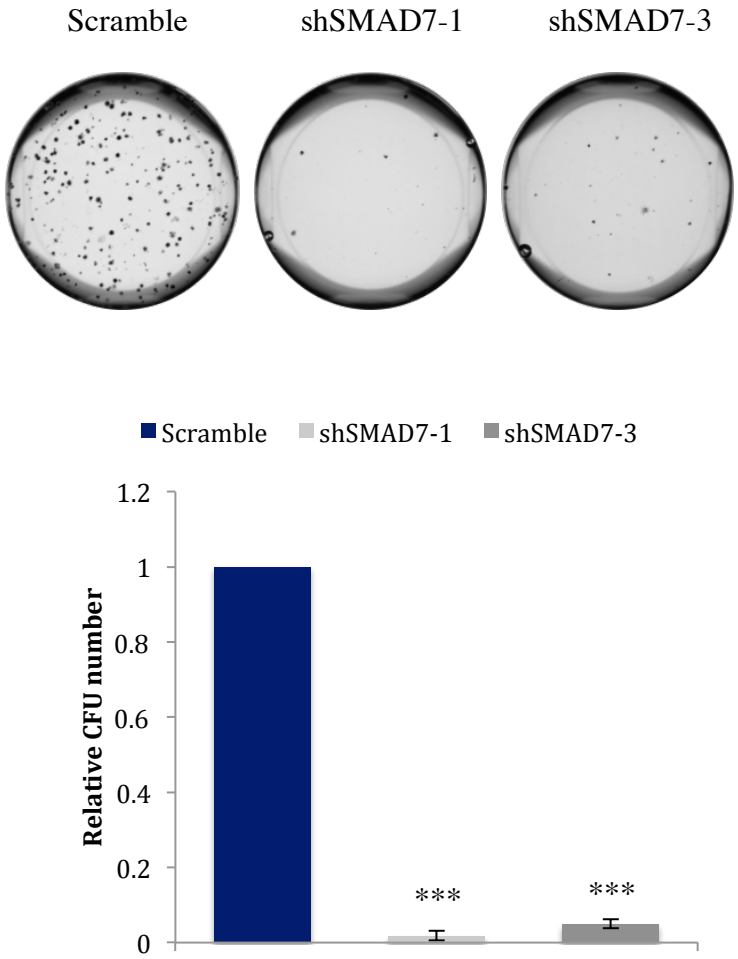

Figure 35 - SMAD7 silencing reduces self-renewal ability of REH cells

The figure shows an example of colony forming assay of REH cells plated in quadruplicate in methylcellulose at $1x10^3$ cells per well after transduction with control scramble and two *SMAD7* shRNA. 2 days after transduction cells were selected with puromycin for a further 3 days. Dead cell removal was then performed and viable cells were plated in methylcellulose (Day 5 post transduction). The cells were stained with INT 14 days following plating. This figure is representative of three independent experiments. The bar chart shows the mean fold change of colonies relative to control scramble ± s.d. for three independent experiments. *P < 0.05, **P < 0.01, ***P < 0.005 compared to control (One sample *t* test).

To examine whether *SMAD7* silencing resulted in a cell cycle block in the second cell line carrying the t(12;21) translocation, AT-2 cells, we performed a cell cycle analysis. This confirmed the data observed in REH cells, showing a similar cell-cycle block in the S-phase of the cycle (Fig. 36). Therefore this data suggests an important role for SMAD7 in TEL-AML1^{+} leukaemia survival *in vitro*.

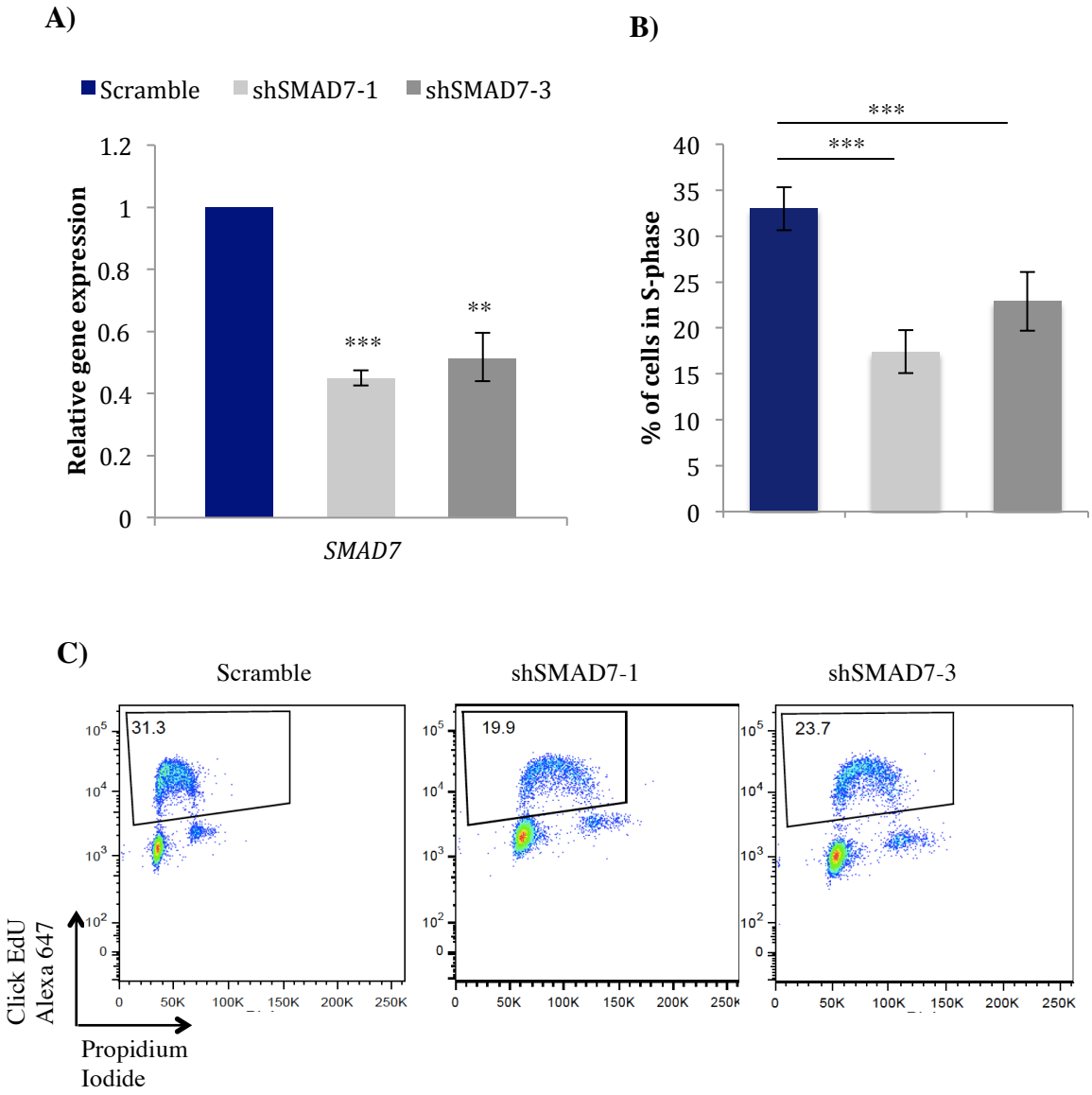

Figure 36 - *SMAD7* silencing causes cell cycle block in AT-2 cells

(A) The figure shows qPCR analysis of SMAD7 silencing in AT-2 cells transduced with control scramble or two different *SMAD7* shRNAs for three independent experiments. 2 days after transduction, cells were selected with puromycin for 3 days. Dead cell removal was then performed

and *SMAD7* silencing measured by qPCR (Day 5 post transduction). The data show means ± s.d. for three independent experiments. *P < 0.05, **P < 0.01, ***P < 0.005 compared to control (One sample *t* test). (B) Viable cells were cultured for a further 2 days and cell cycle profile was then evaluated after pulsing with 10uM EdU for 1 hour (Day 7 post transduction). The bar chart represents the mean percentage of cells in the S-phase ± s.d. for three independent experiments. *P < 0.05, **P < 0.01, ***P < 0.005 compared to control (Student's unpaired *t* test). (C) The flow cytometry plots are examples of the cell cycle profile obtained for three independent experiments.

4.2.3 SMAD7 is necessary for leukaemia progression *in vivo*

In order to address the importance of SMAD7 in leukaemia progression *in vivo*, we next transplanted NSG mice with luciferase expressing REH cells following SMAD7 knockdown. To do this, REH cells were transduced with a lentiviral vector expressing the luciferase gene and a cDNA encoding a tailless human CD2 molecule, lacking most of its cytoplasmic domain (Woodward et al., 2010). Transduced cells were positively selected by magnetic sorting of $CD2^+$ cells (Fig. 37). The sorted cells were then transduced with shSCR or *shSMAD7-1* vectors (Fig. 37B and 37C). Following puromycin selection, viable cells were purified and an equal number of cells were injected into NSG recipient mice.

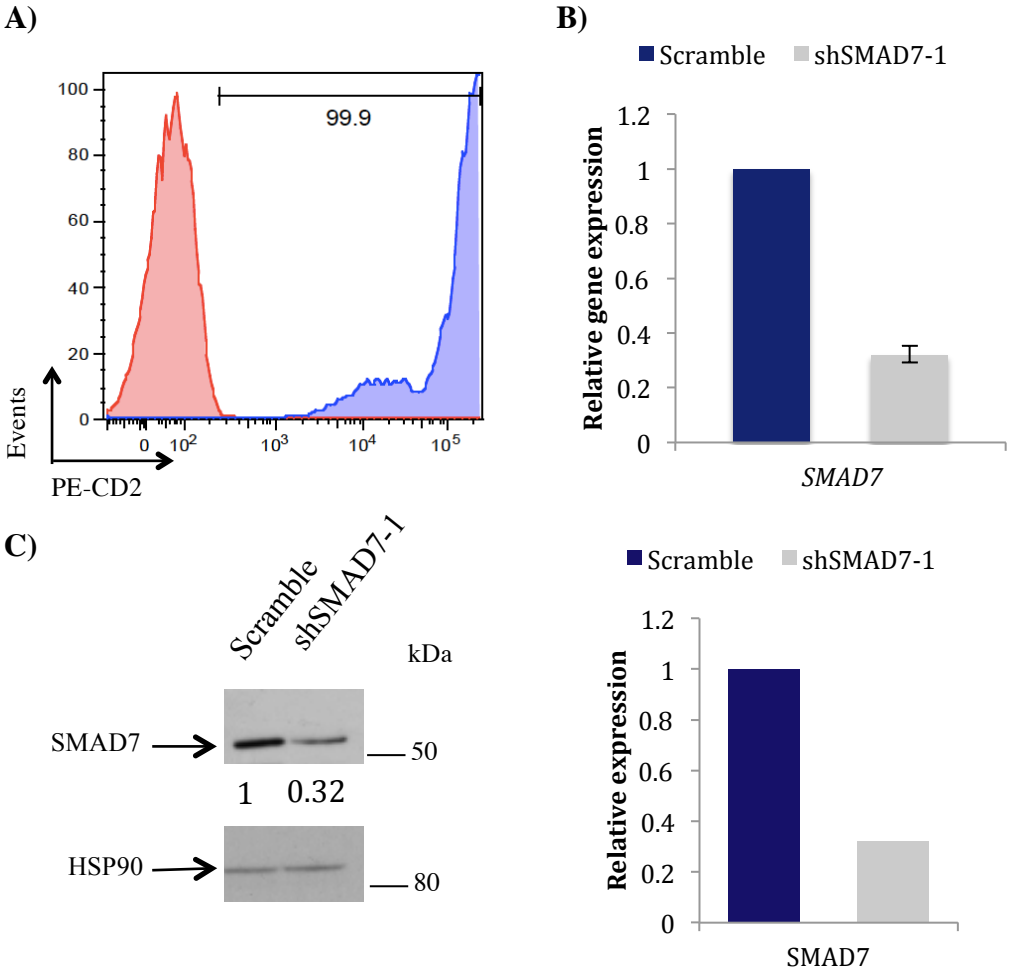

Figure 37 - *SMAD7* silencing in luciferase-CD2 transduced REH cells

The figure shows flow cytometry analysis of REH cells transduced with a vector expressing luciferase and CD2, sorted, and stained using an anti-human CD2-PE antibody (A). Untransduced REH cells (red) were used as control cells. The percentage of luciferase-CD2 transduced cells (blue) is shown. (B) The bar chart shows *SMAD7* silencing of REH-LUC-CD2 cells as measured by qPCR prior to transplantation. 2 days after transduction with control scramble or *shSMAD7-1*, cells were selected with puromycin for 3 days. Dead cell removal was then performed and qPCR and protein levels examined pre-transplantation (pre-transplantation: 5 days post transduction). (C) The western blot analysis shows SMAD7 silencing of REH-LUC-CD2 cells at the protein level, pre-transplantation and the bar chart shows the densitometric quantitation of SMAD7 levels relative to HSP90. All experiments were performed once.

Prior to injection, a luciferase assay was performed to confirm that both groups exhibited similar levels of luciferase activity (Fig. 38A) and the viability of the cells was examined (Fig. 38B) to ensure similar viability of control and knockdown cells. Although most of the mice transplanted with *SMAD7* knockdown cells developed leukaemia, the latency of leukaemia onset was significantly longer than in those transplanted with control scramble cells (Fig. 39). Indeed, one *shSMAD7-1* transplanted mouse survived and was culled at the end of the experiment but showed no signs of clinical disease. Moreover, increased levels of *SMAD7* mRNA expression were detected in the engrafted cells recovered from the first three *shSMAD7-1* mice that were sacrificed, in comparison to levels observed in the cells pre-transplantation, in both cases relative to levels expressed in control scramble cells (Fig. 39D). This demonstrates *in vivo* selection against leukaemic cells with low *SMAD7* expression.

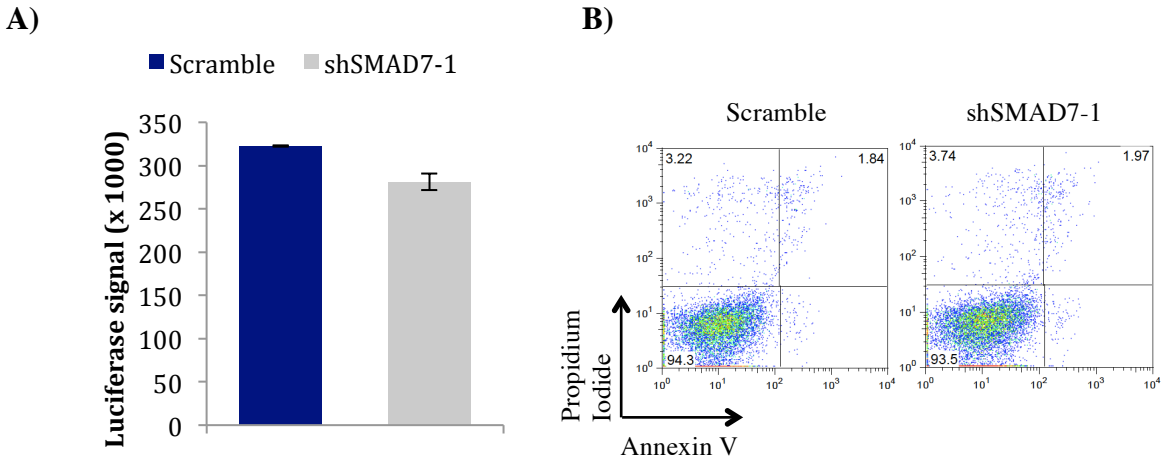

Figure 38 - Testing luciferase levels and viability of REH-LUC-CD2 transduced cells pre-transplantation

(A) The bar chart shows the luciferase signal measured using Promega Luciferase assay kit of REH-LUC-CD2 cells following transduction with control scramble or *shSMAD7-1*. 2 days following transduction, cells were selected with puromycin for 3 days. Dead cell removal was performed and

luciferase signal was then measured on day 5 post transduction. Results were measured in triplicates and the mean ± s.d. shown. (B) The flow cytometry plots show apoptosis analysis of REH-LUC-CD2 cells day 5 post transduction with control scramble or *shSMAD7-1*, prior to transplantation. Apoptosis profiles were evaluated after staining with Annexin V to show equal levels of viability.

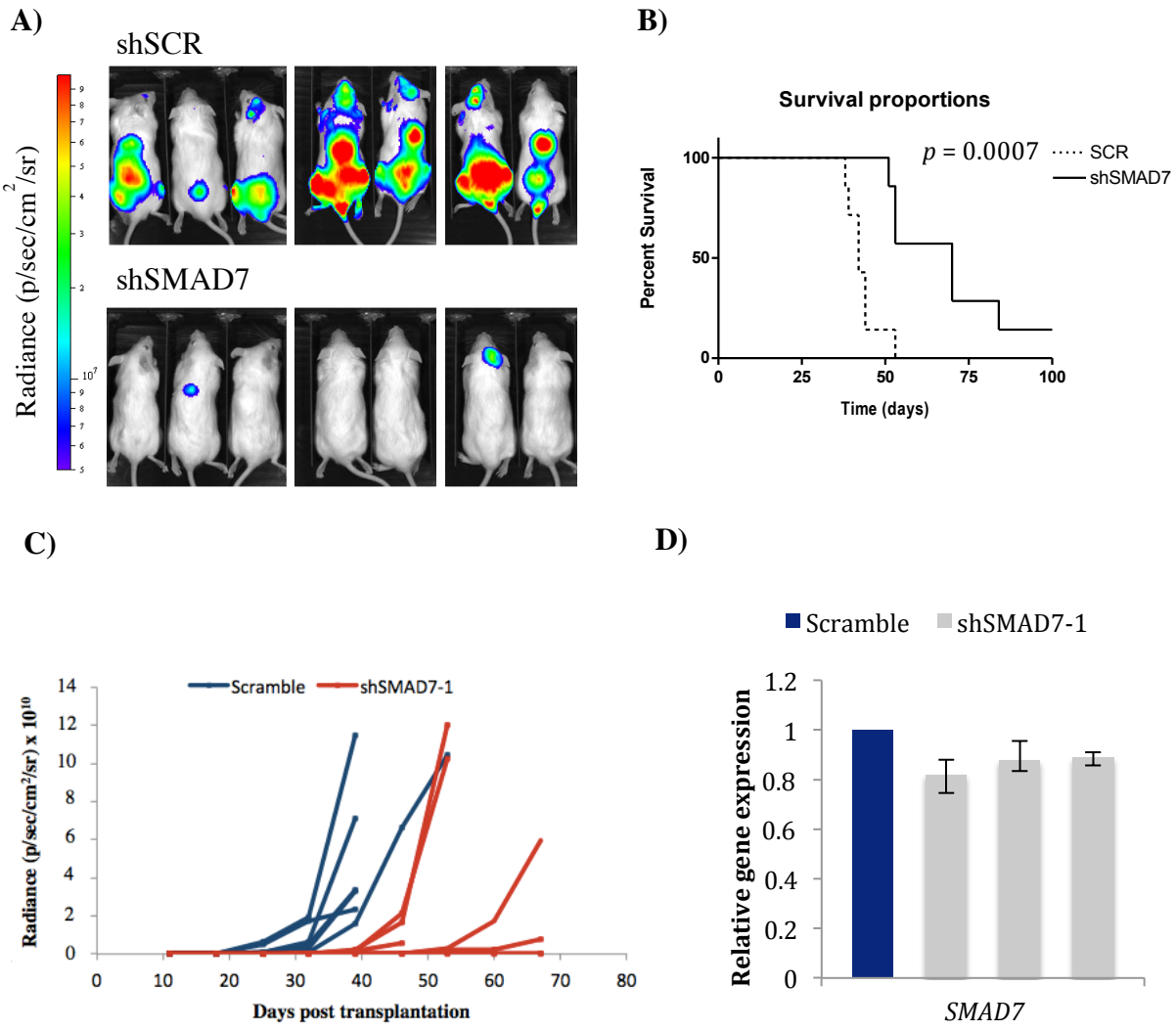

Figure 39 - Leukaemia silencing *in vivo* after SMAD7 silencing

(A) The figure shows a bioluminescent image of NSG mice 32 days after transplantation with $1x10^5$ of control scramble or *shSMAD7-1* luciferase expressing REH cells and (B) the resulting survival curve. (C) The line chart shows the luminescence radiance measured at 7-day intervals starting from day 11 for each mouse transplanted either with control scramble or *shSMAD7-1* luciferase expressing REH cells. (D) *shSMAD7-1* transduced cells isolated from bone marrow of leukaemic mice (post-leukaemia) show loss of knock-down after *in vivo* progression. *SMAD7* expression was normalised to

SMAD7 expression in control scramble shRNA transduced REH-LUC-CD2 cells. qPCR was performed in triplicate wells and mean ± s.d. shown.

4.2.4 SMAD7 is also important in other subtypes of leukaemia

To investigate if SMAD7 was important specifically in TEL-AML1 leukaemia or also required by other subtypes of leukaemia, we used two additional human leukaemic cell lines: MLL-AF4$^+$ SEMK-2 ALL cells and, MLL-AF9$^+$ THP-1 AML cells. Both cells lines were transduced with the two shRNA targeting *SMAD7*. Subsequently, following 72 hours of puromycin, the level of *SMAD7* knockdown was examined by qRT-PCR. Dead cell removal was performed on the cells and after 48 hours cell cycle analysis was performed to determine whether the *shSMAD7*-mediated block in cell cycle observed in TEL-AML1$^+$ cells was also apparent in other leukaemias. Both SEMK-2 and THP-1 exhibited an almost complete block in the S-phase of the cell cycle following *SMAD7* knockdown (Fig. 40 and 41).

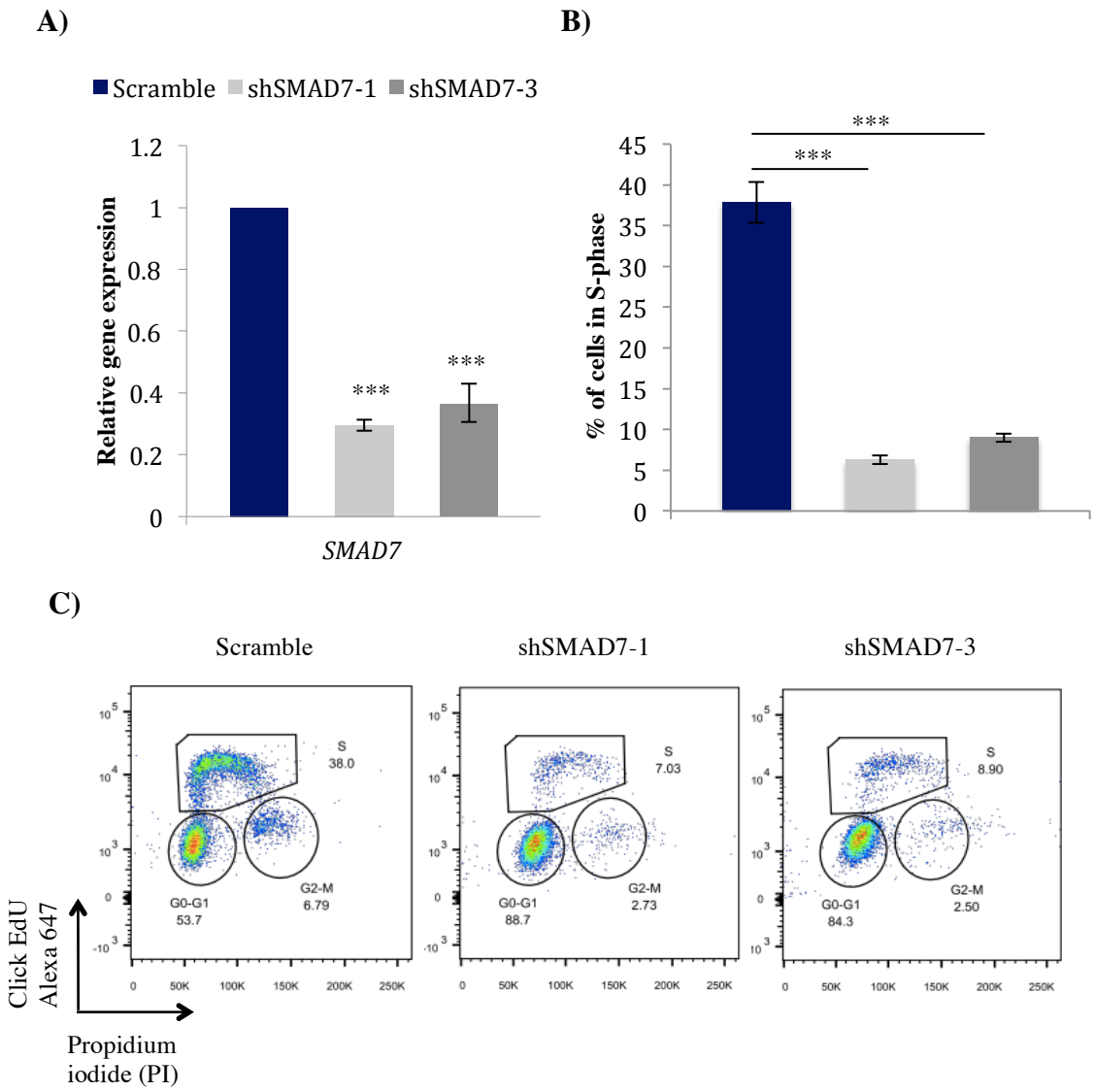

Figure 40 - *SMAD7* silencing causes cell cycle block in MLL-AF4⁺ ALL cells

(A) The bar chart shows qPCR analysis of SMAD7 silencing in SEMK-2 cells transduced with control scramble or two different *SMAD7* shRNAs for three independent experiments. 2 days after transduction, cells were selected with puromycin for 3 days. Dead cell removal was then performed and *SMAD7* silencing measured by qPCR (Day 5 post transduction). The data show means ± s.d. for three independent experiments. *P < 0.05, **P < 0.01, ***P < 0.005 compared to control (One-sample *t* test). (B) Viable cells were cultured for a further 2 days and cell cycle profile was then evaluated after pulsing with 10uM EdU for 1 hour (Day 7 post transduction). The bar chart represents the mean percentage of cells in the S-phase ± s.d. for three independent experiments. *P < 0.05, **P < 0.01, ***P < 0.005 compared to control (Student's unpaired *t* test). (C) The flow cytometry plots are examples of the cell cycle profile obtained for three independent experiments.

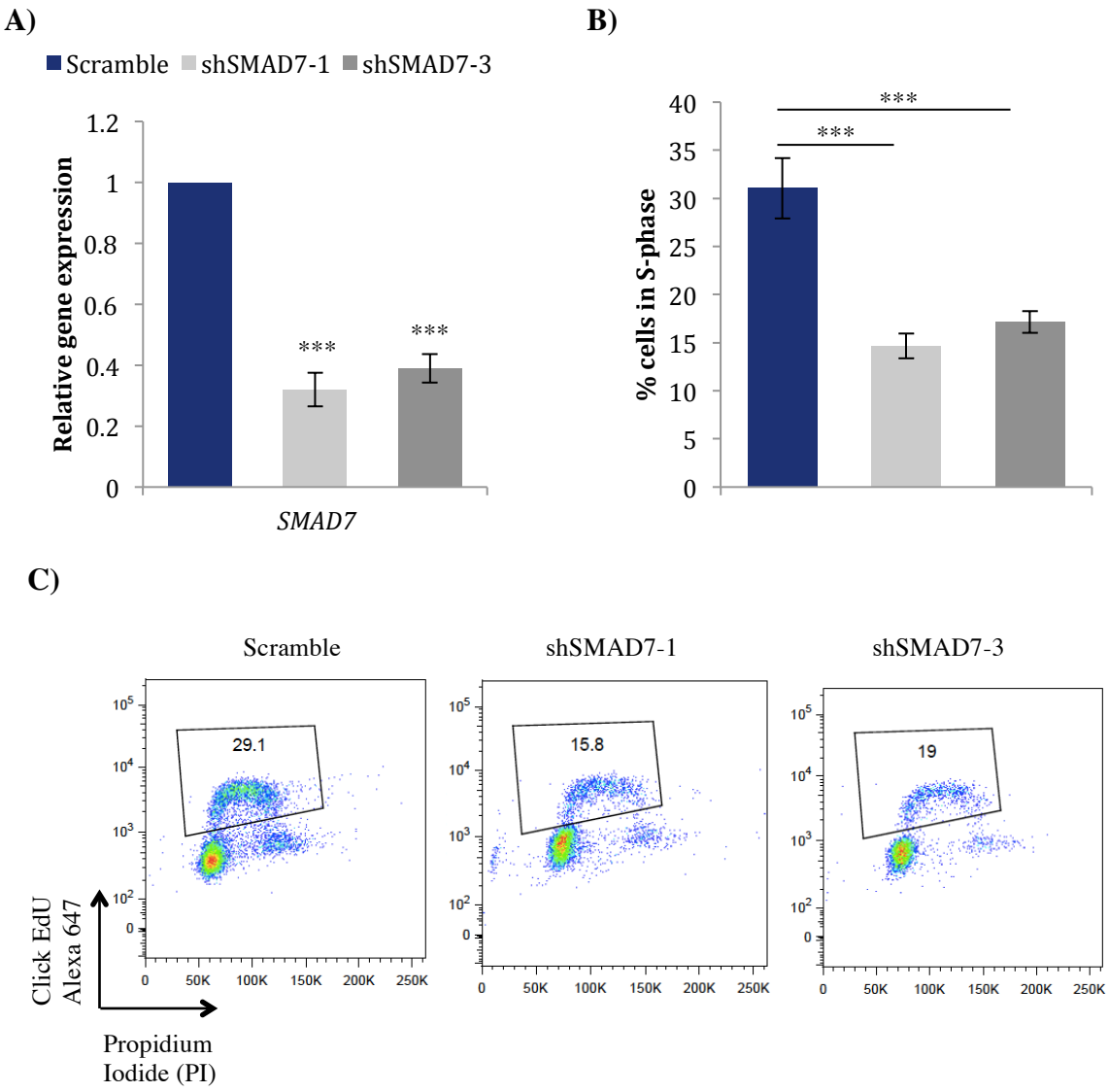

Figure 41 - *SMAD7* silencing results in cell cycle block in MLL-AF9^{+} AML cells

(A) The bar chart shows qPCR analysis of SMAD7 silencing in THP-1 cells transduced with control scramble or two different *SMAD7* shRNAs for three independent experiments. 2 days after transduction, cells were selected with puromycin for 3 days. Dead cell removal was then performed and *SMAD7* silencing measured by qPCR (Day 5 post transduction). The data show means ± s.d. for three independent experiments. *P < 0.05, **P < 0.01, ***P < 0.005 compared to control (One-sample *t* test). (B) Viable cells were cultured for a further 2 days and cell cycle profile was then evaluated after pulsing with 10uM EdU for 1 hour (Day 7 post transduction). The bar chart represents the mean percentage of cells in the S-phase ± s.d. for three independent experiments. *P < 0.05, **P < 0.01, ***P < 0.005 compared to control (Student's unpaired *t* test). (C) The flow cytometry plots are examples of the cell cycle profile obtained for three independent experiments.

4.2.5 Global gene expression analysis in REH cells following *SMAD7* silencing

RNA-seq is a powerful method that uses deep sequencing technology (where the genomic region is sequenced multiple times) to detect and analyse the transcriptome profile of cells. Our data show that SMAD7 expression is required for proliferation and survival of different ALL and AML cell lines, and that it appears to function independently to the TGF-β signalling pathway. In order to establish the mechanisms underpinning the function of SMAD7 in leukaemia, we used this technology to determine global gene expression changes caused by SMAD7 silencing in REH cells. REH cells transduced with control scramble and two different *SMAD7* shRNA were used. When viral supernatant titres for control scramble and the *SMAD7* shRNA were measured, *shSMAD7-3* was found to have a lower titre than *shSMAD7-1*. Despite further rounds of virus supernatant production, using new DNA preparations, *shSMAD7-3* titres were consistently lower than those of *shSMA7-1*. It is important to use equivalent viral titres for control and experimental constructs, such that the gene expression data reflect the loss of the targeted gene rather than the different levels of shRNA expressed in each group. Therefore, we divided the experiment in two, using equivalent control scramble titres to those of each *SMAD7* shRNA (Fig. 42A). In the case of *shSMAD7-3*, this was achieved by diluting the control scramble supernatant (Fig. 42B). 2 days after transduction, cells were selected with puromycin for 3 days. Dead cell removal was then performed and RNA was extracted (Day 5 post transduction). The concentration of RNA was determined using the NanoDrop ND-1000 and the quality using the Agilent 2100 Bioanalyzer. In total 12 samples were submitted to UCL Genomics and RNA-seq was performed by T. Brooks and K. Pearce. The data was analysed using two different software packages, Ilumina BaseSpace and Strand NGS 2.6 (Avadis).

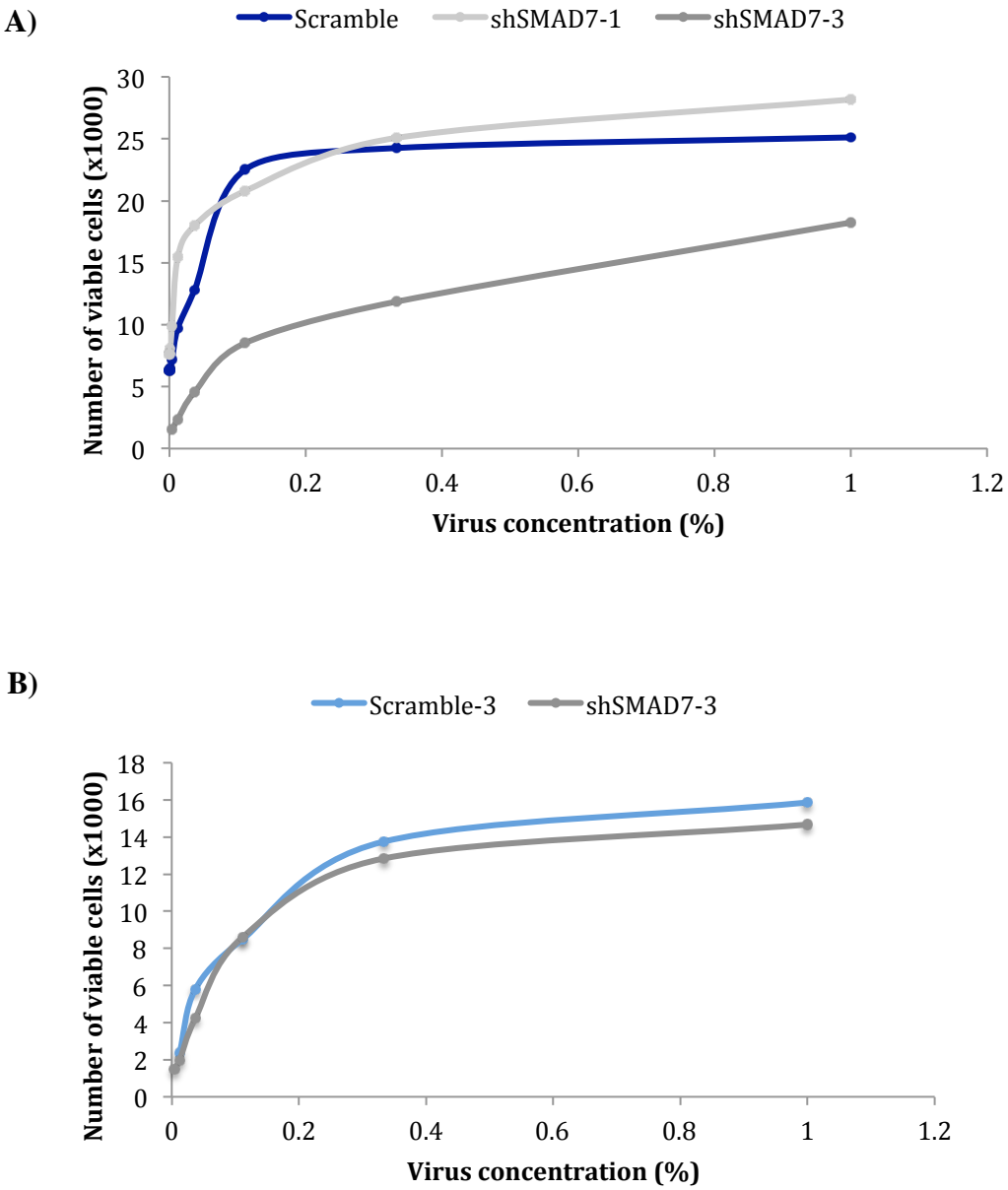

Figure 42 - Measurement of viral titres prior to RNA-sequencing

(A) The chart shows the measured viral titres for REH cells transduced with *scramble* and the two shRNA targeting *SMAD7*. 2 days following transduction in 96 well plates with different virus concentrations, cells were selected with puromycin for a further 3 days. On day 5 post transduction, cells were fixed with 4% PFA for 10 minutes and re-suspended in TO-PRO-3 stain (ThermoFisher Scientific), which was diluted 1:20 in PBS. The viral titres were then measured using flow cytometry. (B) The chart shows viral titres measured as previously for (A) using REH cells transduced with diluted scramble (*Scramble-3*) and *shSMAD7-3* on day 5 post transduction.

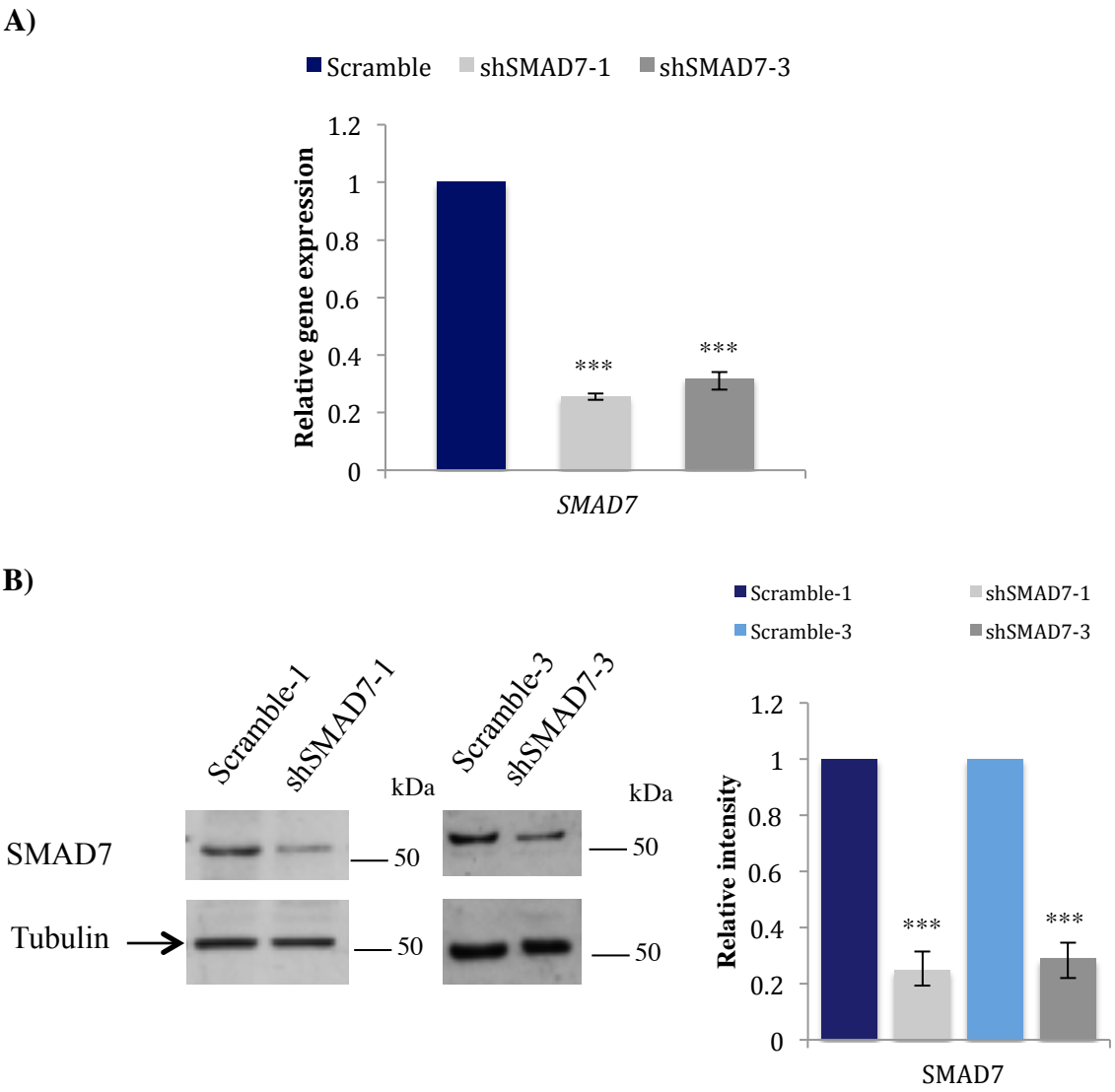

Figure 43 - Detection of SMAD7 knockdown in REH cells for RNA-sequencing

(A) The bar chart shows SMAD7 silencing of REH cells as measured by qPCR after transduction with control Scramble and two different *SMAD7* targeted shRNA. 2 days after transduction, cells were puromycin selected for 3 days. Dead cell removal was then performed and cells were analysed by qPCR (Day 5 post transduction). (B) The western blot analysis is a representative of SMAD7 silencing of REH cells at the protein level (Day 5 post transduction) for three independent experiments. The bar chart shows the mean relative quantity of SMAD7 protein for three independent experiments. All data show mean ± s.d. for three independent experiments. *P < 0.05, **P < 0.01, ***P < 0.005 compared to control (One sample *t* test).

SAMPLES	
Controls	***shSMAD7***
Scramble -1 (x3)	shSMAD7-1 (x3)
Scramble -3 (x3)	shSMAD7-3 (x3)

Table 7 - Samples used for RNA-sequencing

The table shows the RNA samples used for RNA-seq. Three independent experiments were performed using control scramble-1 and *shSMAD7-1* in REH cells and all 6 samples were submitted for RNA-sequencing. Similarly, three independent experiments were performed using a diluted, lower titre control scramble-3 and *shSMAD7-3* in REH cells and all 6 samples submitted for RNA-sequencing.

For the first analysis, we used Ilumina BaseSpace, the RNA-express tool, which aligns the RNA-Seq reads with the STAR aligner and assigns the aligned reads to genes and calculates the differential gene expression with DESeq2 (Ilumina). More than 90% total alignment was observed with all 12 samples. The RNA-express tool then generates the differential gene expression between samples using DESeq2. The sequencing results were normalised using the reads per kilobase per million (RPKM) method and the gene transcripts were assembled using Cufflinks 2.1.1. *Scramble-1* samples were grouped as replicates and *shSMAD7-1* samples were grouped separately as replicates to allow pair-wise comparison. The same grouping was performed for *Scramble-3* and *shSMAD7-3*. Gene transcripts were filtered based on their fold change, keeping only genes with a fold change of 2 or higher. This generated a list of 2,190 genes. With regard to genes differentially expressed between *Scramble-3* and *shSMAD7-3*, when genes were filtered to only show genes with a fold change of 2 or higher this generated a list of 508 genes. We identified 250

out of these 508 gene expression changes present in the list of gene expression changes obtained using *scramble-1* vs *shSMAD7-1* (Fig. 44).

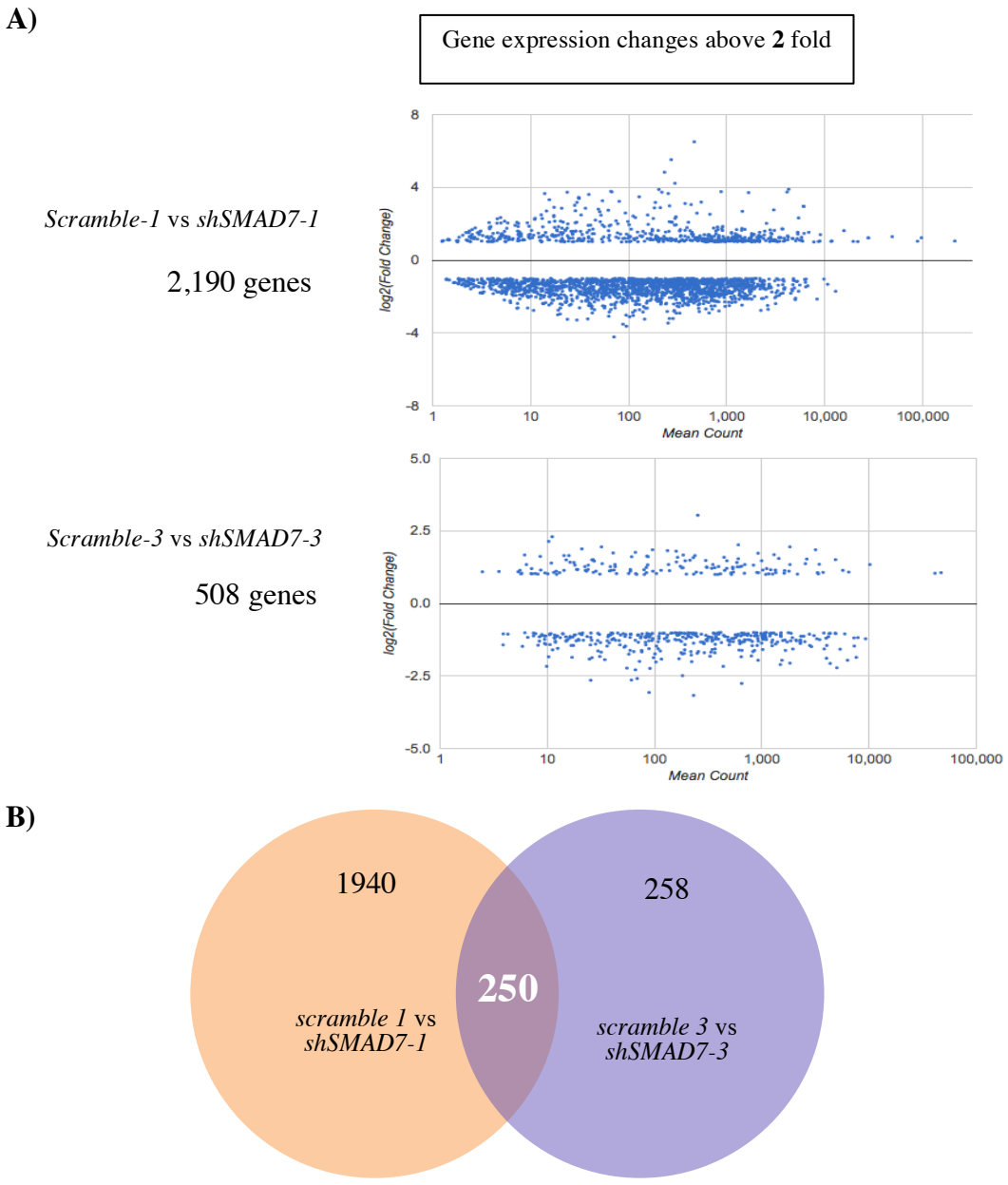

Figure 44 - Analysis of differential gene expression following *SMAD7* silencing using Ilumina BaseSpace software

(A) The scatter plots generated by RNA-express tool in Ilumina BaseSpace show the differentially expressed genes in control scramble vs shSMAD7 for both pairings. The number of genes is reduced when a filter is applied to show genes whose expression changes more than 2-fold. The scatter plots display the log2(fold change) against the mean count of a gene. (B) The venn diagram represents the number of gene changes 2 fold or above, identified using scramble-1 vs shSMAD7-1 (orange) and

scramble-3 vs shSMAD7-3 (purple) and the number of genes common to both gene sets is shown in white.

Next, we used a second approach by analysing the RNA-seq data using the Strand NGS software to gain more confidence in our data sets. We first filtered the data by selecting for genes using a defined p-value cut off at 0.05, whose expression level changed more than 1.5 fold. We then selected for gene expression changes that were detected in at least 2 out of 3 replicates. A p-value is generated for each gene using an unpaired t-test. The p-value cut off at 0.05 allows a 5% chance of error. Therefore, we applied a multiple testing correction procedure, known as the Benjamini-Hochberg method, to control the false positive discovery rate. Multiple testing adjusts the individual p-value for each gene to keep the overall false positive rate to less than or equal to the specified p-value cut-off. We then filtered gene expression changes that were common to both data sets: i.e. *Scramble -1* vs *shSMAD7-1* and *Scramble-3* vs *shSMAD7-3*. Use of a second shRNA, *shSMAD7-3*, allowed filtering out off-target gene expression changes from *shSMAD7-1*. Therefore, we generated a list of genes common to both data sets. Application of these filters generated the final target gene list of 56 upregulated genes and 250 downregulated genes following *SMAD7* silencing (Appendix Tables 10 and 11).

In order to compare the number of these gene expression changes present in the Ilumina BaseSpace analysis, we generated the final downregulated and upregulated gene list common to both shRNA used, setting a 1.5 cut off fold change in Microsoft Excel. This highlighted that 28 out of the 56 upregulated gene

expression changes from NGS Strand analysis was present in the Ilumina BaseSpace list and 196 out of the 250 downregulated gene expression changes from NGS Strand were present in our Ilumina BaseSpace generated analysis (Fig. 45).

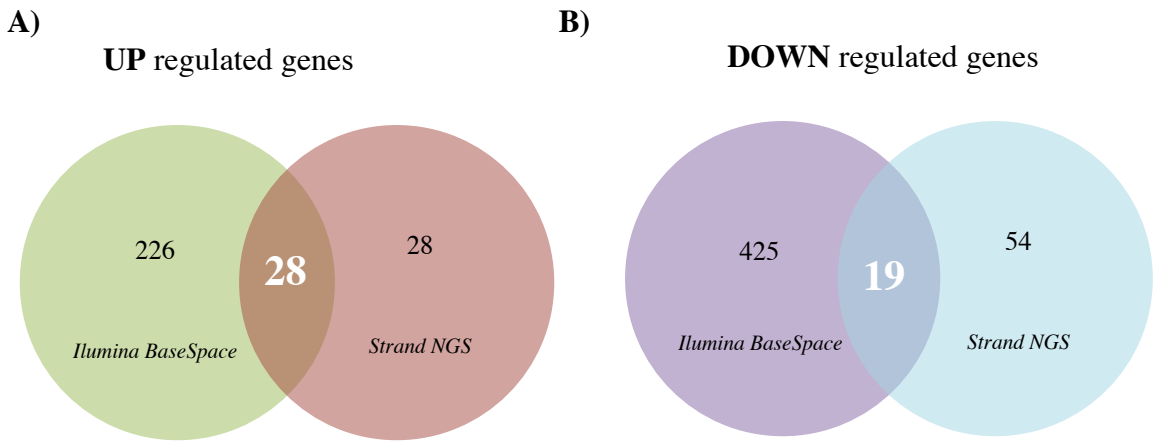

Figure 45 - Comparison of Ilumina BaseSpace vs Strand NGS analysis

(A) The venn diagram represents the number of upregulated gene expression changes 1.5 fold or above, identified using Ilumina BaseSpace (green) and Strand NGS analysis (red). The number of gene expression changes in common to both analyses is displayed in white. (B) The venn diagram represents the number of downregulated gene expression changes, 1.5 fold or above, identified using Ilumina BaseSpace (purple) and Strand NGS analysis (blue). The number of gene expression changes in common to both analyses is displayed in white.

The list of differentially expressed genes following *SMAD7* knockdown obtained using Strand NGS analysis was examined using Ingenuity Pathway Analysis (IPA) (Qiagen) software, which assembles genes with known relationships and identifies relevant pathways using databases of biological pathways pre-loaded

onto the software. This analysis revealed the top canonical pathways generated using our upregulated gene list. This identified pathways related to serine biosynthesis and pathways related to sperm motility and cytokine production. However, only one or two genes in each pathway were present in our list of upregulated genes. We then performed the same analysis using the downregulated gene list. Unexpectedly, this showed that the top four pathways in the analysis were specifically related to cholesterol biosynthesis. The top canonical pathway was found to be the superpathway of cholesterol biosynthesis (Fig. 46). Furthermore, out of 27 well-established genes in this top pathway, 6 of the genes were present in our final list of downregulated genes (22.2%). These six genes also appeared in the next three pathways in the analysis, which consist of intermediates in the cholesterol pathway that contribute to the main superpathway of cholesterol biosynthesis (Table 8). Furthermore, all the gene changes in the cholesterol biosynthesis pathway were also present in our final gene list from Ilumina Basespace analysis. This indicated a significant association between SMAD7 expression and expression of multiple genes in the cholesterol biosynthesis pathway.

A) Analysis of upregulated genes

Top Canonical Pathways		
Name	p-value	Overlap
Serine Biosynthesis	9.38E-03	20.0 % 1/5
Superpathway of Serine and Glycine Biosynthesis I	1.31E-02	14.3 % 1/7
Sperm Motility	1.95E-02	1.8 % 2/114
GADD45 Signaling	3.52E-02	5.3 % 1/19
IL-15 Production	4.97E-02	3.7 % 1/27

B) Analysis of downregulated genes

Top Canonical Pathways		
Name	p-value	Overlap
Superpathway of Cholesterol Biosynthesis	8.02E-07	22.2 % 6/27
Cholesterol Biosynthesis I	1.50E-05	30.8 % 4/13
Cholesterol Biosynthesis II (via 24,25-dihydrolanosterol)	1.50E-05	30.8 % 4/13
Cholesterol Biosynthesis III (via Desmosterol)	1.50E-05	30.8 % 4/13
Mitotic Roles of Polo-Like Kinase	1.27E-04	9.5 % 6/63

Figure 46 - IPA shows the top canonical pathways related to upregulated and downregulated gene sets following *SMAD7* silencing

(A) The top canonical pathways generated by IPL in relation to the final upregulated target gene set. (B) The top canonical pathways generated by IPA in relation to the final downregulated target gene set. 22.2% of genes in the Superpathway of Cholesterol Biosynthesis were present in the target gene set.

Ingenuity Canonical Pathways	-log(p-value)	Molecules
Superpathway of Cholesterol Biosynthesis	**6.10E+00**	**FDPS,DHCR7,ACAT2,MSMO1,LSS,LBR**
Cholesterol Biosynthesis I	4.82E+00	DHCR7,MSMO1,LSS,LBR
Cholesterol Biosynthesis II (via 24,25-dihydrolanosterol)	4.82E+00	DHCR7,MSMO1,LSS,LBR
Cholesterol Biosynthesis III (via Desmosterol)	4.82E+00	DHCR7,MSMO1,LSS,LBR
Mitotic Roles of Polo-Like Kinase	3.90E+00	CDC20, CCNB2, PKMYT1, PLK1, KIF11, SMC1A
Cell Cycle: G2/M DNA Damage Checkpoint Regulation	3.47E+00	TOP2A, CCNB2, PKMYT1, PLK1, SFN
Zymosterol Biosynthesis	2.65E+00	MSMO1,LBR
Role of BRCA1 in DNA Damage Response	2.55E+00	RAD51,BRCA2, PLK1, BRIP1, E2F2
TR/RXR Activation	2.39E+00	RAB3B, CAMK4, SREBF1, NRGN, PCK1
Cell Cycle Control of Chromosomal Replication	2.36E+00	CDT1, CDC6, MCM7
ATM Signaling	2.21E+00	RAD51, SMC2, CCNB2, SMC1A
Oleate Biosynthesis II (Animals)	2.19E+00	FADS2, FADS1
Pyridoxal 5'-phosphate Salvage Pathway	2.11E+00	MAP2K6, PLK1, TTK, NEK2
Asparagine Biosynthesis I	1.91E+00	ASNS
Lanosterol Biosynthesis	1.91E+00	LSS
DNA Double-Strand Break Repair by Homologous Recombination	1.90E+00	RAD51,BRCA2
Superpathway of Geranylgeranyldiphosphate Biosynthesis I (via Mevalonate)	1.79E+00	FDPS,ACAT2

Table 8 - Genes present in the top canonical pathways generated in response to downregulated target gene set

This table shows the list of top canonical pathways highlighted by genes that were downregulated upon *SMAD7* knockdown. The p-value and list of genes associated with each pathway are shown. The top pathway and the six genes related to it from the gene set are highlighted in red.

4.3 Discussion

STAT3 activity has been shown to be necessary for TEL-AML1 leukaemia maintenance (Mangolini et al., 2013). Here, we identify SMAD7, a TGF-β inhibitor, as a transcriptional target of STAT3 in TEL-AML1 leukaemia, and its key role in leukaemia progression.

REH and AT-2, two TEL-AML1$^+$ human cell lines, lentivirally transduced with a shRNA construct targeting *STAT3* showed a decrease in *SMAD7* gene expression. The exact mechanism behind how STAT3 regulates SMAD7 expression in TEL-AML1$^+$ cells is unclear. One possible mechanism is direct regulation via binding of STAT3 to the *SMAD7* gene promoter. Indeed, studies have reported *SMAD7* as a target gene of STAT3 using ChIP analysis and microarray studies (Snyder et al., 2008).

Subsequently, we explored the role of SMAD7 in TEL-AML1$^+$ leukaemia using independent shRNA constructs targeting *SMAD7* in REH cells. Although SMAD7 is known to function through inhibition of TGF-β canonical signalling, cells transduced with *shSMAD7* stopped proliferating even in the absence of exogenous TGF-β1. Moreover, use of the 1D11 mAb, a TGF-β blocking antibody, to exclude autocrine TGF-β signalling or TGF-β1 in the culture medium, did not alter the effect observed following *SMAD7* knockdown. Furthermore, the greater the level of knockdown, the greater the inhibition of proliferation compared to control cells. Therefore, this suggested a role for SMAD7 signalling in inhibiting leukaemia progression through a mechanism independent of TGF-β signalling. While SMAD6

is an inhibitor of the BMP pathway, SMAD7 has been shown to inhibit both the TGF-β and BMP signalling in some cell types. BMP signalling has been reported to play a role in promoting paediatric acute leukaemia through self-renewal of haematopoietic progenitors. Therefore, we thought one possibility was that SMAD7 was involved in regulation of BMP signalling in these cells.

SMAD7 inhibition in REH cells resulted in cell cycle block, apoptosis and impaired colony forming ability. In addition, SMAD7 silencing in AT-2 cells also showed an inhibition of proliferation and a cell cycle block. This indicates an important role for SMAD7 in leukaemic progression in TEL-AML1^{+} leukaemia. Moreover, leukaemic cell lines carrying distinct genetic aberrations, such as SEMK-2 (MLL-AF4) and THP-1 (MLL-AF9), an AML cell line, also showed significant cell cycle arrest upon *SMAD7* knockdown. Therefore, our data indicate that SMAD7 is important not only for TEL-AML1^{+} leukaemia but may play a role in leukaemia cells in general, and more importantly, it functions independent of TGF-β in these cells. Previously, a role for SMAD7 independent of TGF-β signalling, functioning through multiple alternate pathways such as BMP signalling has been established. Therefore, SMAD7 may be a therapeutic target in different subtypes of leukaemia, although exactly how it functions remains unclear.

Similar to the results obtained *in vitro*, when *shSMAD7* transduced REH cells were transplanted into mice, the latency of disease was significantly longer compared to mice transplanted with control scramble cells, indicating that SMAD7 is important for leukaemia progression *in vivo*. These data indicate that SMAD7 has a role in disease maintenance both *in vitro* and *in vivo*.

To determine how SMAD7 functions in leukaemia, we performed RNA-sequencing of REH cells with *SMAD7* silencing using two different shRNAs targeting *SMAD7* and control scramble cells. We expected to identify genes in the BMP family to be regulated by SMAD7, as SMAD7 has been shown to inhibit BMP signalling. However, although genes in the BMP pathway such as *SMAD1*, *SMAD5*, *BMP2* and *BMP3* were differentially expressed, this was not consistent using both shRNA. While some of the genes decreased in expression following knockdown with *shSMAD7-1*, for example, *SMAD1*, other genes had increased expression following knockdown using *shSMAD7-3*. Therefore, we decided to focus on other gene changes between scramble and *SMAD7* knockdown and used IPA software to identify genes that were related and present in the same pathway. This analysis highlighted down regulation of multiple genes in the same metabolic pathway, superpathway of cholesterol biosynthesis, showing 22.2% of genes in this pathway to be present in our final target gene set. These six genes are known to encode various enzyme intermediates in the cholesterol pathway, implicating SMAD7 in the regulation of this metabolic pathway to promote leukaemic progression. There is no previous evidence linking SMAD7 to cholesterol biosynthesis, therefore it is unknown how it may regulate genes in the cholesterol pathway. As SMAD7 is capable of binding DNA and transcriptionally regulating genes it may be possible that it directly regulates some of the highlighted genes in the cholesterol pathway. Another possibility is that SMAD7 may indirectly regulate the genes involved in cholesterol biosynthesis via other target genes.

In conclusion, we observed that STAT3 regulates SMAD7 in TEL-AML1$^+$ cells, where we show SMAD7 has a crucial role in leukaemia survival. Furthermore,

other subtypes of ALL and AML expressing different oncogenes require SMAD7 for survival. RNA sequencing indicates that SMAD7 functions by regulating multiple genes in the cholesterol biosynthesis pathway in TEL-AML1^{+} cells.

CHAPTER V. SMAD7 regulates cholesterol biosynthesis to maintain leukaemia survival

5.1 Introduction

5.1.1 The cholesterol biosynthesis pathway

In humans and animals, cholesterol is a biologically important molecule, with essential physiological functions: it is a major constituent of cell membranes that in turn affects function of membrane proteins such as receptors and transporters, it is a biosynthetic precursor of bile acids and steroid hormones and intermediates of the cholesterol biosynthesis pathway are required to make Vitamin D and for post-translational modification of membrane proteins (J. Thomas, 2012). In addition to cholesterol being obtained from the diet, almost 50% of cholesterol in the body is derived from *de novo* synthesis (Berg JM, 2002). The majority of body cholesterol is synthesised by the liver and secreted as circulating lipoproteins. The process of cholesterol synthesis involves multiple enzymes and stages, but it can be broken down into five major steps (Berg JM, 2002; J. Thomas, 2012):

1. Like most biological lipids cholesterol synthesis begins from acetyl-CoA. In the first step, acetyl-coA is converted to 3-hydroxy-3-methylglutaryl-CoA (HMG-CoA).
2. HMG-CoA is converted to mevalonate
3. Mevalonate is converted to the isoprene-based molecule, isopentenyl pyrophosphate (IPP)
4. IPP is converted to squalene
5. Squalene is converted to cholesterol (Fig. 47)

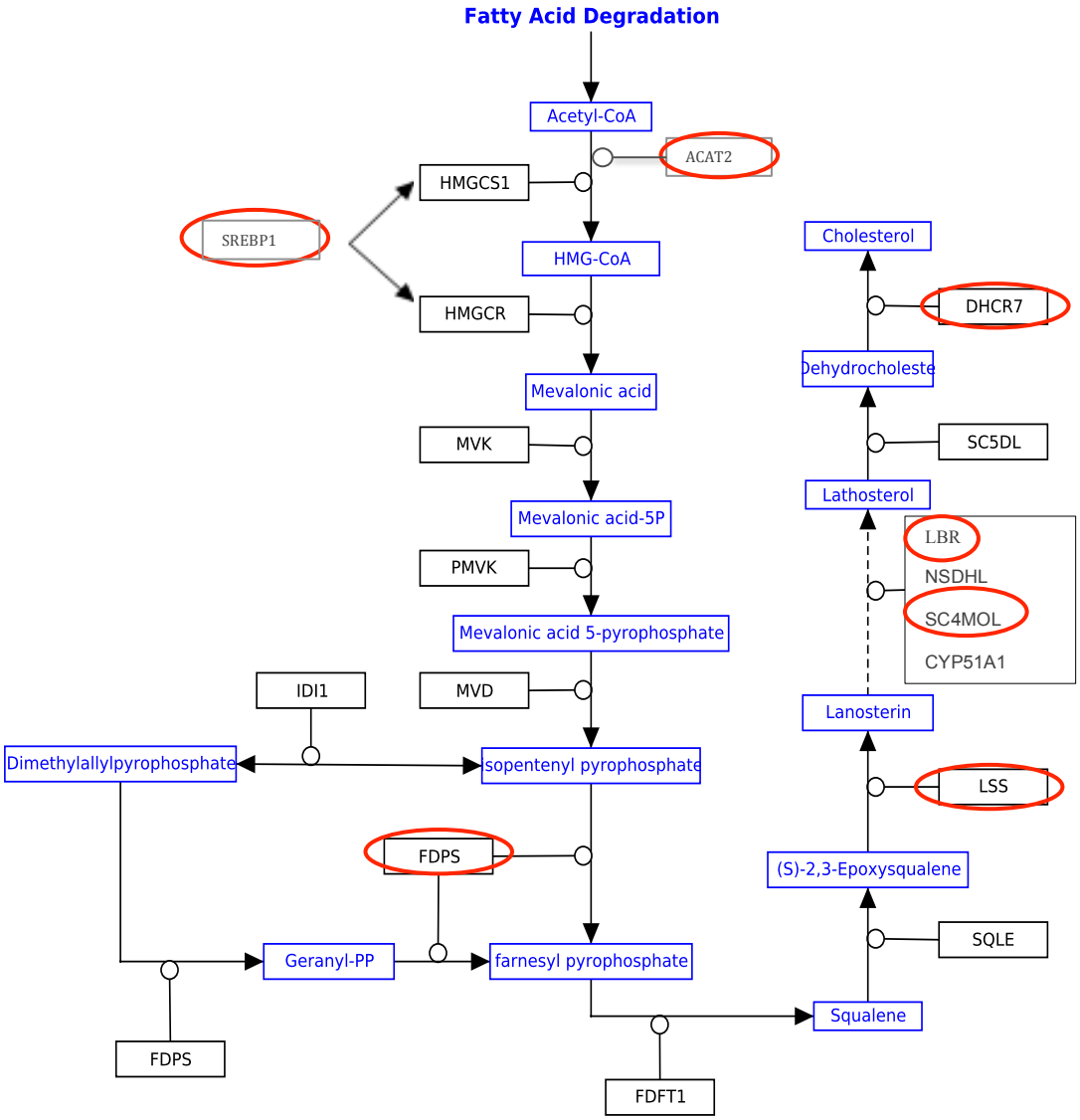

Figure 47 - Cholesterol biosynthesis pathway

This figure shows a simple depiction of the cholesterol biosynthesis pathway. The major intermediates and end products are indicated in blue. Enzymes in the pathway are shown in black. The enzymes circled in red are derived from genes present in the top cholesterol biosynthesis pathways highlighted in the IPA analysis. All genes (except SREBP-1) from our gene list encode enzymes that function to generate different intermediates in the cholesterol pathway, as indicated. SREBP-1 is shown at the beginning of the pathway, where it activates transcription of genes that give rise to substrates for HMG-CoA reductase (HMGCR) and other enzymes.

Although regulation of cholesterol can be controlled by dietary intake it is primarily controlled by the level of *de novo* synthesis. It is important to maintain cholesterol at a steady level to prevent atherosclerosis and heart disease (Dayton. S, 1969). Regulation of HMG-CoA reductase (HMGCR), the enzyme that catalyses the formation of mevalonate is the primary means of controlling cholesterol biosynthesis. This is carried out through controlling different mechanisms: Firstly, sterol regulatory element-binding proteins (SREBPs) enhance transcription of *HMGCR* mRNA. SREBPs are released from the endoplasmic reticulum, migrate to the nucleus and activate transcription. When cholesterol levels rise, SREBP is sequestered in the endoplasmic reticulum and degraded in the nucleus to halt transcription of the genes in the cholesterol biosynthesis pathway including *HMGCR* mRNA (Berg JM, 2002). Secondly, the rate of translation of *HMGCR* mRNA is blocked by non-sterol metabolites derived from cholesterol (Berg JM, 2002). Thirdly, the degradation of HMGCR is a highly controlled process, where oxygenated derivatives of cholesterol such as 24-, 25- and 27-hydroxycholesterol can induce polyubiquitination and degradation via the proteasomal pathway (Berg JM, 2002). Finally, HMGCR is most active in its dephosphorylated state. Therefore, phosphorylation of HMGCR decreases its activity, ceasing cholesterol synthesis. The importance of HMGCR in cholesterol regulation has made it a favourite target for hypercholesterolaemia therapies, specifically using statins, inhibitors of the HMGCR family (Endo, 2010).

5.1.2 SREBPs in cholesterol biosynthesis

SREBPs belong to the helix-loop-helix-leucine zipper family of transcription factors that regulate cholesterol, fatty acid and triglyceride biosynthesis (Brown and Goldstein, 1997; Horton et al., 2002). They directly activate expression of more than 30 genes involved in the synthesis and uptake of cholesterol, fatty acids, triglycerides and phospholipids (Horton et al., 2002). The mammalian genome encodes three SREBP isoforms, SREBP-1a, SREBP-1c and SREBP-2. SREBP-1a and -1c are derived from the same gene but differ through use of alternative transcription start sites that produce alternate forms of exon 1 (Shimano, 2001). In humans, SREBP-1a, is an activator of all SREBP-responsive genes, including genes involved in mediating cholesterol, fatty acids and triglyceride synthesis (Horton et al., 2002). SREBP-1c specifically controls transcription of genes required for fatty acid synthesis while SREBP-2 preferentially regulates cholesterol synthesis-related genes and LDL receptor (LDLR) (Horton et al., 2002). SREBP proteins share a similar structure, which is organised into three main sections: an NH2-terminal transcription factor domain that contains the bHLH-Zip region for DNA binding; a hydrophobic region, containing two hydrophobic transmembrane-spanning segments with a short loop of about 30 amino acids in the middle that projects into the endoplasmic reticulum (ER), and a COOH-terminal regulatory domain (Rawson, 2003).

SREBP precursor protein, which is approximately 120kDa, is anchored in the membranes of the endoplasmic reticulum (ER) using the two transmembrane spanning helices in the protein structure (Rawson, 2003). In order for SREBP to function as a transcription factor, the NH2- terminal domain must be released from the membrane proteolytically. SREBP cleavage-activating protein (SCAP) associated

with SREBPs in the ER, where they are retained by the insulin-induced gene (INSIG) product when cellular sterol levels are sufficient (Horton et al., 2002; Shimano, 2001). When sterol levels drop, SCAP acts as an escort for SREBP from the ER to the Golgi apparatus (Fig. 48). In the Golgi, a specific membrane-bound serine protease, Site-1 protease (S1P), cleaves the SREBP in the loop between the two membrane-spanning regions, splitting the SREBP molecule in half (Horton et al., 2002; Shimano, 2001). Next, the NH2-terminal bHLH-Zip domain is released by a second cleavage, mediated by Site-2 protease (S2P), a membrane-bound zinc protease. Thus, the NH2-terminal domain, known as nuclear SREBP (nSREBP), translocates to the nucleus where it activates transcription by binding to non-palindromic sterol response elements (SREs) in the promoter regions of multiple target genes (Horton et al., 2002). When the cholesterol levels in cells increase, SCAP changes its conformation so that the SCAP-SREBP complex is not incorporated into ER transport vehicles. Therefore SREBPs loses access to S1P and S2P in the Golgi so that the bHLH-Zip domains cannot be cleaved, resulting in a block in transcription of target genes (Horton et al., 2002).

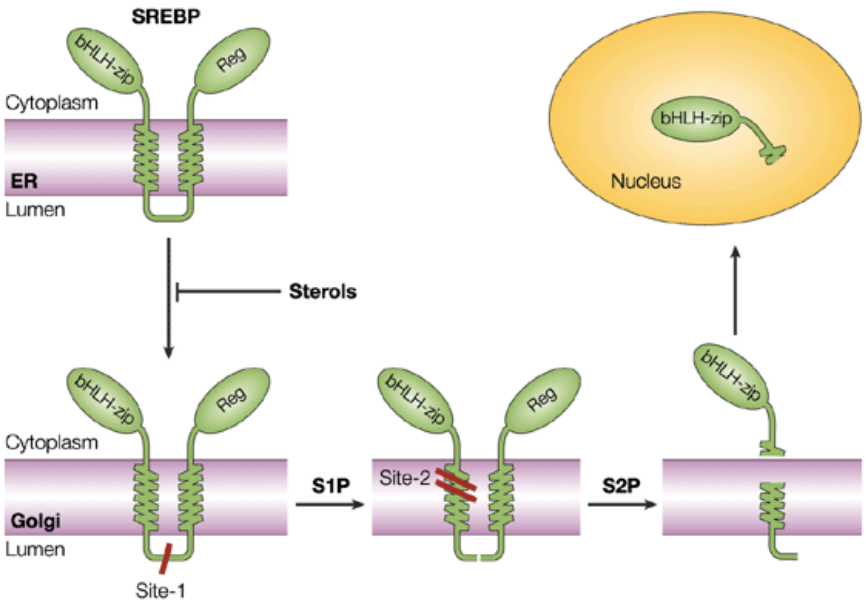

Figure 48 - Two-step processing of SREBPs.

The SREBP precursor is inserted into membranes of the ER. Both the NH2 and COOH terminal domains are in the cytoplasmic compartment. The SREBP precursor protein is transported to the Golgi apparatus where S1P cleaves at Site 1 (red line), giving rise to the intermediate membrane-bound form. Following this, S2P cleaves the intermediate form at Site 2 (red line), releasing the transcription-factor domain from the membrane, allowing for entry into the nucleus to direct transcription of target genes (Rawson, 2003). Adapted from (Rawson, 2003).

Early studies investigating the role of SREBPs were carried out in cultured cells and were then extended *in vivo*, where these were mainly focused on the liver as this tissue has an important role in homeostasis of cholesterol and fatty acids. Cultured cells, including HepG2 hepatocytes and 3T3-L1 mouse pre-adipocytes, show high expression levels of *SREBP-1a* relative to *SREBP1-c* (Shimomura et al., 1997). However, in human and mice livers the *SREBP-1c* transcript is expressed at higher levels than *SREBP-1a*, in contrast to cultured cells, suggesting that the ratio of

expression between the two isoforms differs between *in vivo* and *in vitro* studies. (Shimomura et al., 1997). *Srebp-1* knockout mice have a high incidence of embryonic lethality (Shimano, 2001). Studies overexpressing a constitutively active form of human SREBP1-a in the liver, in which the NH2-terminal region of SREBP-1a terminates between the leucine zipper domain and first transmembrane domain, results in triglyceride- and cholesterol-enriched fatty livers that were enlarged 4-fold above normal (Shimano et al., 1996). Despite this, no feedback repression was triggered and the liver continued fatty acid and cholesterol biosynthesis at 20-fold and 5-fold greater than normal, respectively. Moreover, a 31-fold increase in the mRNAs of genes encoding enzymes such as HMG CoA synthase, HMGCR and squalene synthase and a 6-fold increase in mRNA encoding LDLR, were observed (Shimano et al., 1996). However, over-expression of a similar form of SREBP-1c in the liver showed only a mildly enlarged liver, and a smaller increase in fatty acid synthetic enzymes and fatty acid synthesis, and no change in the mRNAs of cholesterol biosynthesis genes and LDLR (Shimano et al., 1997). Overexpression of the truncated form of SREBP-2 increased the mRNA for cholesterol biosynthetic enzymes, with a dramatic 75-fold increase in HMGCR mRNA. The expression of genes encoding fatty acid synthesis enzymes increased to a lesser extent. These studies highlight specific roles of each SREBP isoform in fatty acid synthesis and cholesterol biosynthesis (Brown and Goldstein, 1997). However, studies show that the SREBP isoforms have significant overlap in lipid biosynthesis regulation, activating either cholesterol or fatty acid synthetic enzymes (Eberle et al., 2004). Moreover, in addition to the role of SREBP-1 in regulating lipogenesis genes and the *LDLR* gene, it can alter regulation of cell cycle and proliferation (Williams et al., 2013). However, whether this is a direct result of SREBP-1 regulated transcription or caused by changes in lipid metabolism is still unclear.

5.1.3 Cholesterol biosynthesis in cancer

Metabolic reprogramming is a hallmark of cancer as oncogenic signalling regulates and accelerates metabolic pathways to meet the extensive needs of rapidly proliferating cancer cells. Increasing evidence suggests that cancer cells carry out *de novo* lipogenesis and become independent of systemic regulation (Gabitova et al., 2014). They require high levels of endogenous cholesterol biosynthesis to build new membranes and maintain active signalling. Moreover, oncogenic proteins such as RAS, PI3K and AKT use the intermediates in the cholesterol pathway such as isoprenoids, farnesyl pyrophosphates and geranylgeranyl pyrophosphates for membrane anchoring (Gabitova et al., 2014). Cancer cells can maintain high intracellular cholesterol through different mechanisms, including accelerating endogenous cholesterol and fatty acid synthesis, regulated by SREBPs, by reducing cholesterol efflux, through ATP-binding cassette class A transporters, or by increasing uptake of LDL (Gabitova et al., 2014). Therefore, interfering with these deregulated pathways would be predicted to compromise cancer cell viability.

Cholesterol has been shown to play an important role in leukaemia. Leukaemia cells have been reported to have increased rates of cholesterol synthesis, with a loss of the negative feedback inhibition of cholesterogenesis, an important feature of malignancy (Madden et al., 1986). Abnormally high cholesterol levels have been observed in AML samples and high HMGCR levels in ALL cell lines (Banker et al., 2004). As HMGCR is a rate-limiting enzyme in the cholesterol pathway, HMGCR inhibitors are used to block cholesterol synthesis. The group of drugs known as statins, used to treat hypercholesterolaemia, work as HMGCR inhibitors. Statins have been used to lower cholesterol concentrations and interfere

with the mevalonate pathway in ALL and AML cells (Sheen et al., 2011; van der Weide et al., 2012). Moreover, AML cells that are resistant to chemotherapy have elevated levels of lipids, resulting from cytoprotective adaptive cholesterol responses (Kornblau et al., 2007; Li et al., 2003). Therefore, treatment with the drugs mevastatin or zaragozic acid reduced cholesterol levels in these leukaemia cells and sensitised them to radiotherapy and chemotherapy (Li et al., 2003). Zaragoic acid blocks cholesterol synthesis at the level of squalene synthase, an enzyme in the final branch of cholesterol synthesis, minimising disruption to the upstream pathway. This is important since statins can have the undesired effect of blocking the production of a mevalonate-derived Ras inhibitor, and thereby relieving an important anti-oncogenic block in some leukaemias. However, this does not occur when targeting the pathway downstream, such as with squalene synthase inhibition, whilst such inhibition does maintain sensitisation to cytotoxic therapy (Li et al., 2003). A recent study also noted that mRNAs encoding *HMGCR* and *LDLR* were both increased by daunorubicin (DNR) and cytarabine (ARA-C) treatment in a large subset of AML samples (Banker et al., 2004). However, in most of these samples, there was no LDL accumulation during drug treatment, implying that cells primarily relied on *de novo* cholesterol biosynthesis as a mechanism for increased cholesterol levels during drug treatment (Banker et al., 2004). This suggests that inhibitors of cholesterol synthesis, such as statins that are toxic to AML, ALL, CLL and other leukaemias, may have a role in suppressing leukaemic progression. Moreover, one study shows that Fluvastatin decreases cardiac fibrosis possibly through regulation of SMAD7 expression (Zhai et al., 2008). As our RNA-sequencing experiment highlighted multiple genes in the cholesterol biosynthesis pathway, we decided to investigate the potential regulation of cholesterol synthesis by SMAD7 in our leukaemic cells and if this can then be targeted for anti-leukaemia therapy.

5.2 Results

5.2.1 Validating RNA-sequencing results

To validate the differentially expressed gene changes in the cholesterol biosynthesis pathway following *SMAD7* knockdown, we transduced REH cells with control scramble and shRNA targeting *SMAD7* as previously and isolated the mRNA to examine gene expression by qRT-PCR. We chose four genes functioning in the superpathway of cholesterol biosynthesis and a fifth gene, *SREBP-1,* which although implicated in the TR/RXR activation pathway in the IPA analysis, is also known to function as a master transcription factor of cholesterol biosynthesis (Table 9). As expected, using both *shSMAD7-1* and *shSMAD7-3*, decreased expression of all six genes was observed in the SMAD7 depleted cells compared to control scramble cells (Fig. 49B), suggesting a novel dependence of cholesterol biosynthesis on SMAD7.

Differentially expressed genes in cholesterol biosynthesis
Sterol Regulatory Elementary Binding Transcription Factor 1 (SREBF-1/ SREBP-1)
Acetyl co-A Acetyltransferase 2 (ACAT2)
7-dehydrocholesterol reductase (DHCR7)
Methylsterol Monooxygenase 1 (MSMO1)
Lamin B receptor (LBR)

Table 9 - List of differentially expressed genes validated using qRT-PCR

A table showing the list of differentially expressed genes in the cholesterol biosynthesis pathway, to be validated using qRT-PCR. Two genes, *Farnesyl Diphosphate Synthase* (*FDPS)* and *Lanosterol*

synthase (*LSS)* that were also present in the gene change list in the cholesterol biosynthesis pathway were not validated, as reliable commercial qRT-PCR taqman probes for these genes were not available.

ACAT2, *DHCR7*, *MSMO1*, *FDPS*, *LSS* and *LBR* all encode proteins that act as enzymes in intermediate stages of cholesterol biosynthesis (Fig. 47) in addition to steroid hormone and vitamin D synthesis. We used the Amplex Red cholesterol assay to examine whether the observed down-regulation of genes in the cholesterol pathway resulting from *SMAD7* knockdown would affect endogenous cholesterol levels. This assay detects both free cholesterol and cholesteryl esters and therefore shows the level of total cholesterol content in the cells. As previously, 2 days following transduction with control scramble and *SMAD7* shRNA, REH cells were puromycin selected for 72 hours. Subsequently dead cell removal was performed (5 days after transduction) and $1x10^5$ cells were plated in each well of a 96 well plate and the assay performed according to manufacturer's instructions. This assay showed a decrease in total cellular cholesterol following *SMAD7* knockdown, indicating a role for SMAD7 in the regulation of cholesterol biosynthesis (Fig. 50).

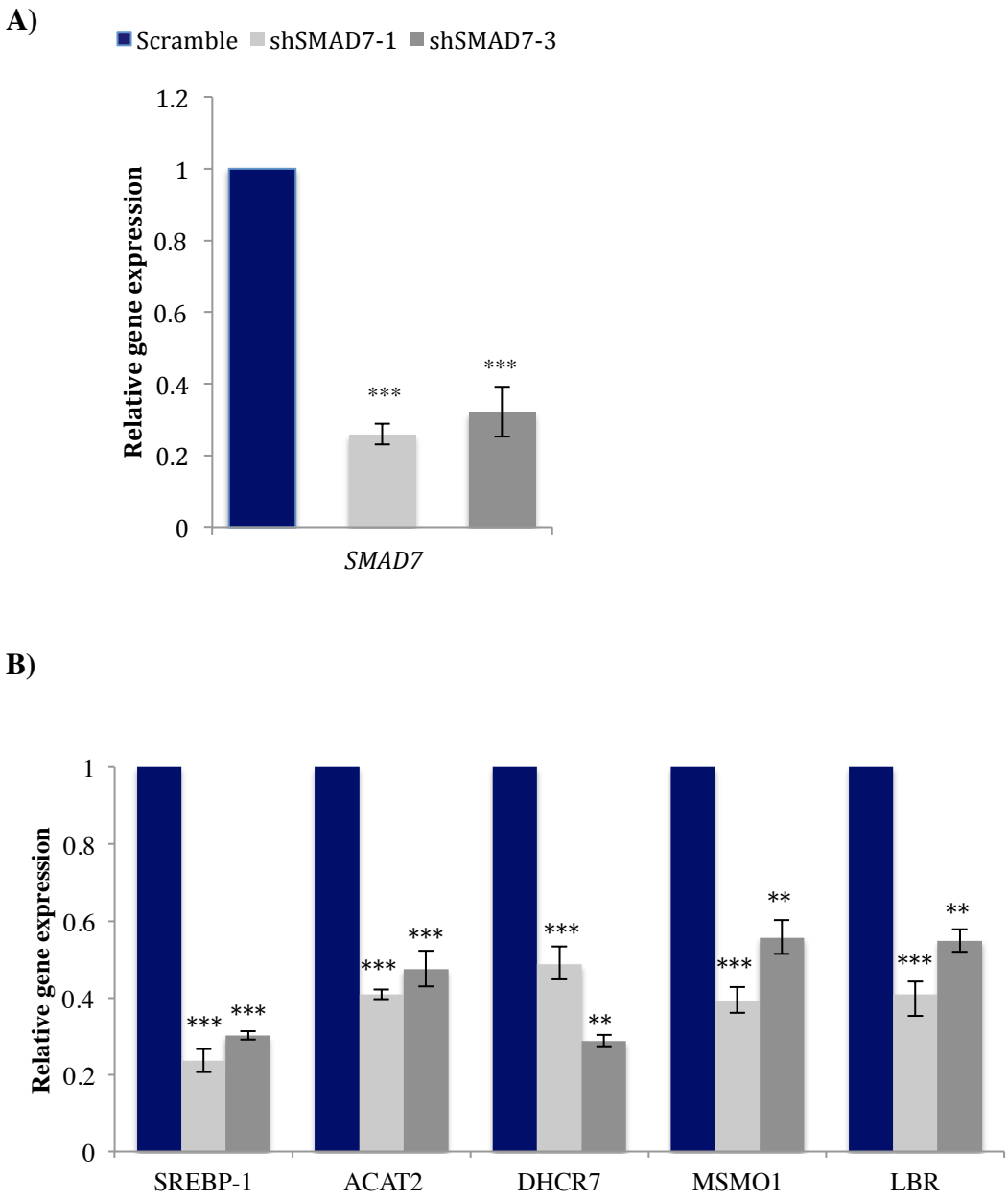

Figure 49 – Validation of SMAD7 regulated gene expression changes

The bar chart shows total cholesterol levels, measured using the Amplex Red Kit per $1x10^5$ cells. Cells were transduced with control scramble or shRNA targeting *SMAD7* for 2 days followed by puromycin selection for a further 3 days. Dead cell removal was performed and total cellular cholesterol levels were measured using the Amplex Red cholesterol assay (Day 5 post transduction). Cells were diluted in reaction buffer, and the Amplex red reagent was added for 60 minutes to the cells prior to measurement. A cholesterol standard curve was generated to calculate total cholesterol levels. The bar charts show mean ± s.d. for three independent experiments. $*P < 0.05$, $**P < 0.01$, $***P < 0.005$ compared to control (Student's unpaired *t* test).

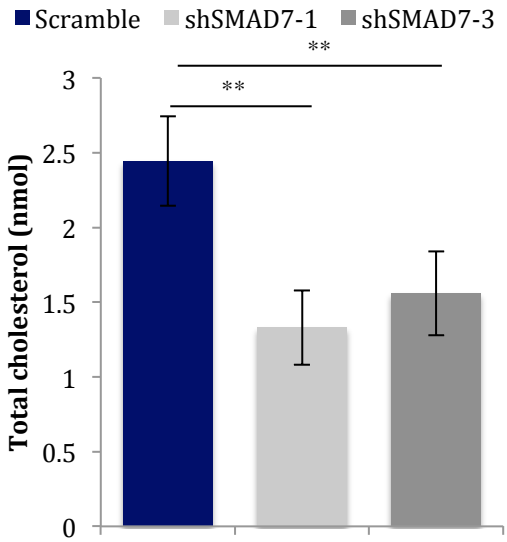

Figure 50 - *SMAD7* knockdown results in a decrease in total cellular cholesterol in REH cells

The bar chart shows total cholesterol levels, measured using the Amplex Red Kit per $1x10^5$ cells. Cells were transduced with control scramble or shRNA targeting *SMAD7* for 2 days followed by puromycin selection for a further 3 days. Dead cell removal was performed and total cellular cholesterol levels were measured using the Amplex Red cholesterol assay (Day 5 post transduction). Cells were diluted in reaction buffer, and the Amplex red reagent was added for 60 minutes to the cells prior to measurement. A cholesterol standard curve was generated to calculate total cholesterol levels. The bar charts show mean ± s.d. for three independent experiments. $*P < 0.05$, $**P < 0.01$, $***P < 0.005$ compared to control (Student's unpaired *t* test).

5.2.2 SMAD7 transcriptionally regulates *SREBP-1* to induce cholesterol synthesis and maintain leukaemia survival

We then questioned how SMAD7 regulates cholesterol synthesis in leukaemic cells. Although all SMAD7-dependent genes in the cholesterol biosynthesis pathway play key roles at different stages of the pathway, *SREBP-1* is

known to be a master transcription factor involved in lipid homeostasis, controlling a range of enzymes required for cholesterol and fatty acid synthesis. For this reason, we decided to focus on SMAD7 regulation of *SREBP-1*. Since *SREBP-1* gene expression levels decreased following *SMAD7* knockdown, we decided to examine its expression following *SMAD7* overexpression. We cloned the *SMAD7* cDNA into the lentiviral CSGW-PIG vector and transduced REH cells. mRNA was extracted 5 days post transduction and gene expression of *SREBP-1* measured by qRT-PCR (Fig. 51). We observed a two-fold increase in *SREBP-1* gene expression following SMAD7 overexpression, compared to empty vector transduced control cells. This complimented the down-regulation of *SREBP-1* following *SMAD7* knockdown and suggested that SMAD7 did indeed regulate *SREBP-1* transcription. SMAD7 overexpression was also found to cause an increase in endogenous cholesterol levels, relative to control cells (Fig. 51B). Therefore, these data indicate that SMAD7 overexpression resulted in elevated *SREBP-1* transcription and increased expression of SREBP-1 in turn promoted increases in cellular cholesterol.

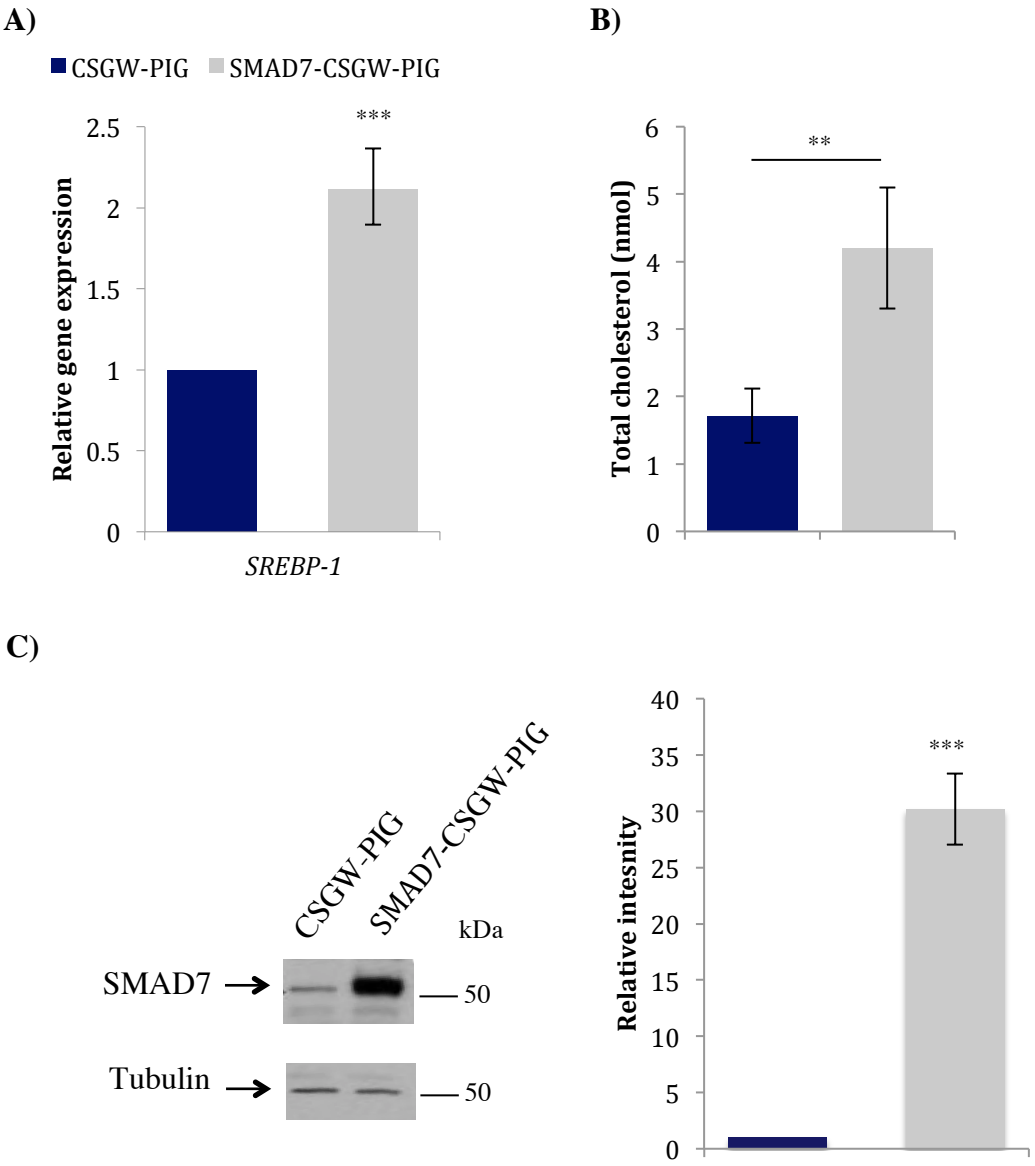

Figure 51 - SMAD7 overexpression in REH cells induces *SREBP-1* gene expression and results in increased cellular cholesterol

A) The bar chart shows *SREBP-1* gene expression levels measured by qRT-PCR in REH cells transduced with control CSGW-PIG empty vector or SMAD7-CSGW-PIG vector. 2 days after transduction, cells were selected with puromycin for a further 3 days. Dead cell removal was then performed and gene expression analysed by qRT-PCR (Day 5 post transduction). The data shows mean values ± s.d. of three independent experiments. *P < 0.05, **P < 0.01, ***P < 0.005 compared to control (One-sample *t* test). (B) The bar chart shows total cholesterol levels measured using the Amplex Red Kit per $1x10^5$ cells at day 5 post transduction following dead cell removal. The data shows mean values ± s.d. of three independent experiments. *P < 0.05, **P < 0.01, ***P < 0.005

compared to control (Student's unpaired *t* test). (C) The western blot analysis is a representative of SMAD7 protein overexpression in REH cells at day 5 post transduction. The western blot was probed with an anti-SMAD7 antibody. An anti-tubulin antibody was used as a control for protein loading. The bar chart represents the mean densitometric quantitation of SMAD7 protein levels relative to tubulin. The data shows mean values ± s.d. of three independent experiments. *P < 0.05, **P < 0.01, ***P < 0.005 compared to control (One-sample *t* test).

5.2.3 SREBP-1 inhibition induces apoptosis and reduces total cellular cholesterol of leukaemic cells

To investigate the role of SREBP-1 in REH cells, we tested five different shRNA constructs targeting *SREBP-1* by qRT-PCR, to identify two independent shRNA that resulted in more than 80% knockdown (Fig. 52A). Following 72-hour puromycin selection, after lentiviral transduction, dead cell removal was performed. *SREBP-1* silencing resulted in a decrease in cholesterol biosynthesis (Fig. 52B) and a significant induction of apoptosis (Fig. 53). Cells were plated out in methylcellulose medium and colony formation assessed after two weeks culture. *SREBP-1* silencing resulted in significant inhibition of colony formation by REH cells (Fig. 54).

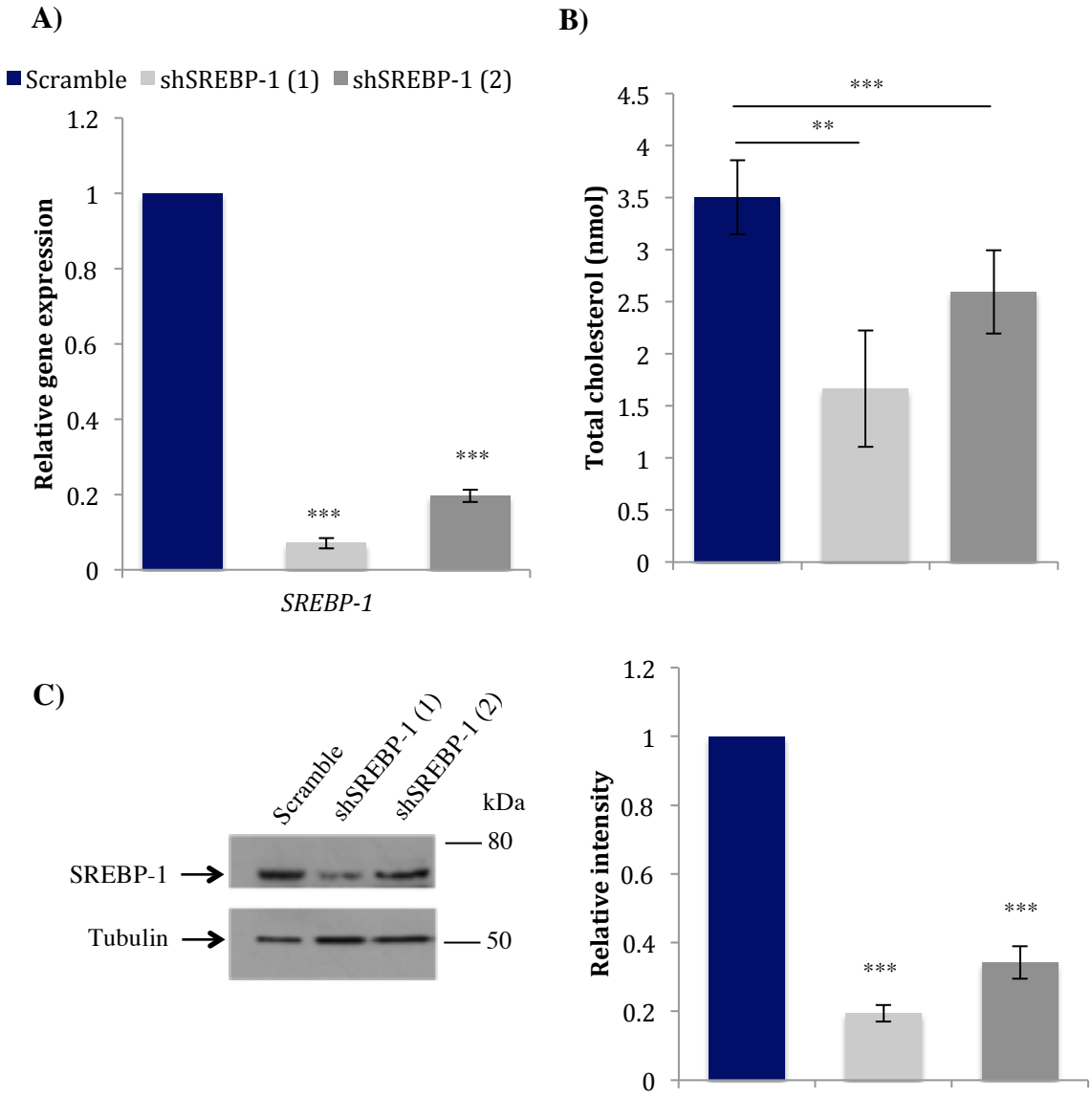

Figure 52 - *SREBP-1* silencing in REH cells decreases level of cholesterol biosynthesis

(A) The bar chart shows *SREBP-1* silencing in REH cells transduced with control scramble and two different *SREBP-1* targeting shRNA. 2 days after transductions, cells were selected with puromycin for a further 3 days. Dead cell removal was then performed and *SREBP-1* silencing measured by qRT-PCR (Day 5 post transduction). The data show mean ± s.d. from three independent experiments. *P < 0.05, **P < 0.01, ***P < 0.005 compared to control (One-sample *t* test). (B) The bar chart shows the cholesterol biosynthesis measured using the Amplex Red Kit per $1x10^5$ at day 5 post transduction. The data show mean ± s.d. from three independent experiments. *P < 0.05, **P < 0.01, ***P < 0.005 compared to control (Student's unpaired *t* test). (C) The western blot analysis shows SREBP-1 silencing of REH cells at the protein level at day 5 post transduction. The western blot was probed

with an anti-SREBP-1 antibody. An anti-Tubulin antibody was used as control for protein loading. The bar chart shows the densitometric quantitation of SREBP-1 levels relative to tubulin. The data show mean ± s.d. from three independent experiments. *P < 0.05, **P < 0.01, ***P < 0.005 compared to control (One-sample *t* test).

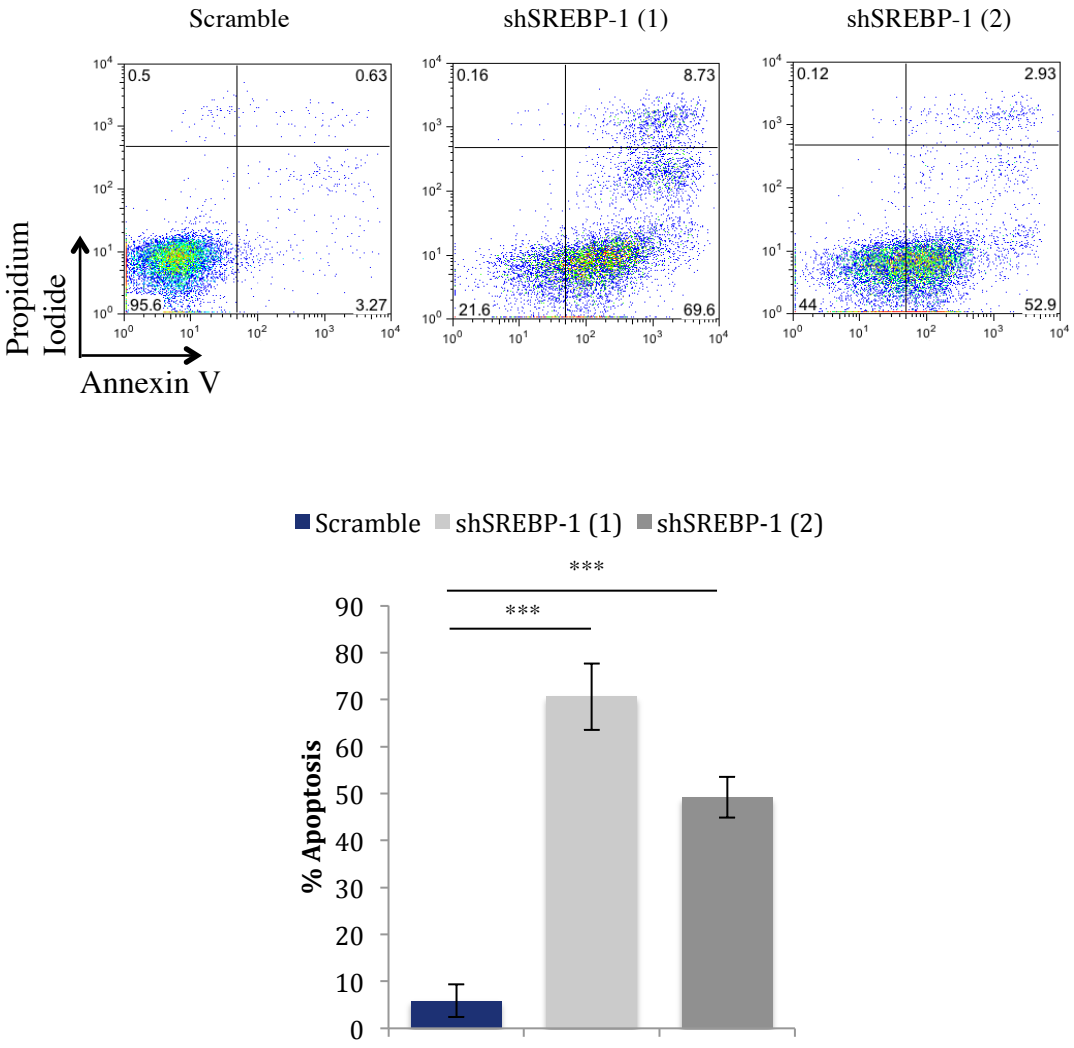

Figure 53 - *SREBP-1* silencing in REH cells induces apoptosis

The flow cytometry plots are examples of the apoptosis profile of REH cells. REH cells were transduced with control scramble or two *SREBP-1* shRNA for 2 days followed by 3 days of puromycin selection. Dead cell removal was then performed on cells and after 24 hours an apoptosis profile was evaluated after staining with Annexin V (day 6 post transduction). The bar chart

represents the mean percentage of apoptotic Annexin V^+PI^- cells ± s.d. for three independent experiments. *P < 0.05, **P < 0.01, ***P < 0.005 compared to control (Student's unpaired *t* test).

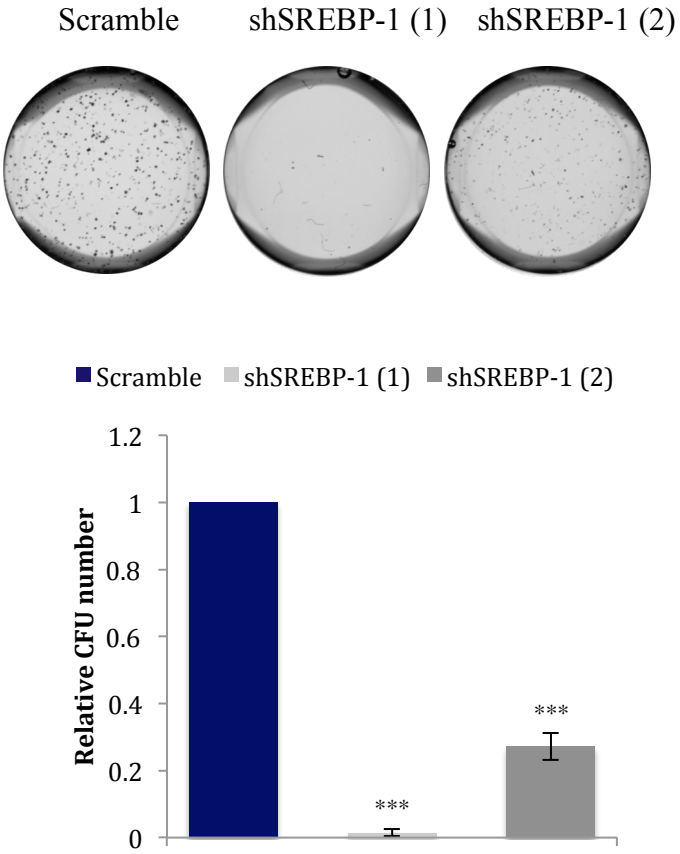

Figure 54 - *SREBP-1* silencing reduces self-renewal ability of REH cells

The figure shows an example of colony forming assays of REH cells plated in quadruplicate in methylcellulose at $1x10^4$ cells per well. REH cells were transduced with control scramble or two *SREBP-1* shRNA for 2 days followed by 3 days of puromycin selection. Dead cell removal was then performed and cells plated in methylcellulose in 24 well-plates. Cells were stained with INT 14 days following plating. The bar chart shows the mean fold change of colonies relative to control scramble ± s.d. for three independent experiments. *P < 0.05, **P < 0.01, ***P < 0.005 compared to control (One-sample *t* test).

To evaluate whether SREBP-1 was important specifically in TEL-AML1^{+} leukaemia or also required by other leukaemia subtypes, we silenced *SREBP-1* in MLL-AF4^{+} SEMK-2 ALL cells. Cells were transduced for 2 days followed by 3 days of puromycin selection. *SREBP-1* expression was then examined by qRT-PCR (Fig. 55A). Dead cell removal was then performed on the cells and after 24 hours they were stained with Annexin V and PI. *SREBP-1* knockdown resulted in significant induction of apoptosis, as observed with REH cells (Fig. 55B and 55C). Taken together, these results show that the requirement for SREBP1 is not limited to TEL-AML1 expressing leukaemia cells.

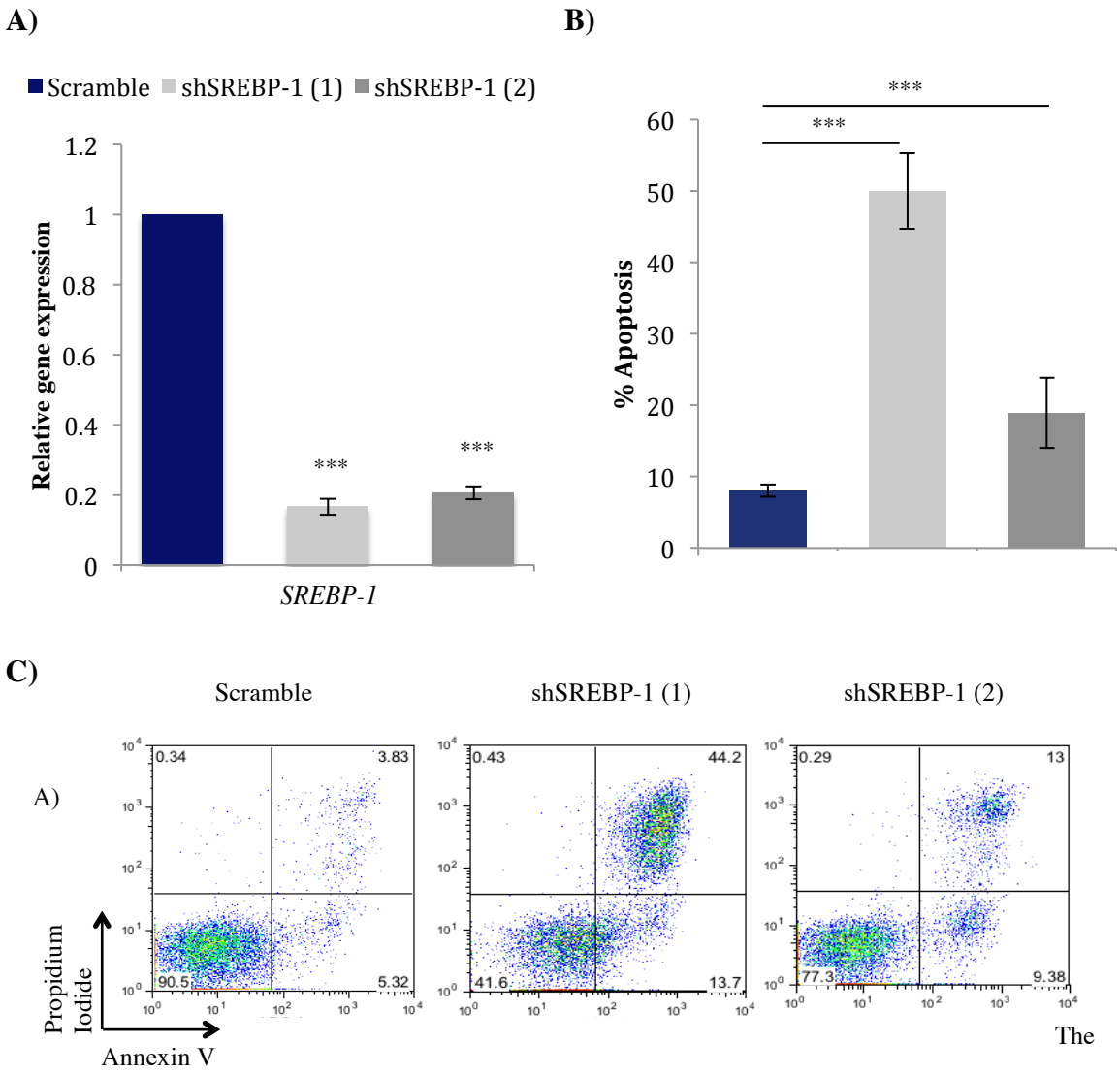

Figure 55 - *SREBP-1* silencing induces apoptosis in SEMK-2 cells

The bar chart shows qRT-PCR analysis of *SREBP-1* silencing in SEMK-2 transduced with control scramble or two different *SREBP-1* shRNAs. 2 days after transduction, cells were selected with puromycin for a further 3 days. Dead cell removal was then performed and *SREBP-1* silencing analysed by qRT-PCR (Day 5 post transduction). The data show mean ± s.d. for three independent experiments. *P < 0.05, **P < 0.01, ***P < 0.005 compared to control (One-sample *t* test). (B) The bar chart represents the mean percentage of apoptotic Annexin V^+PI^- cells ± s.d. for three independent. (C) The flow cytometry plots are examples of the apoptosis profiles of SEMK-2 cells transduced with control scramble or two *SREBP-1* shRNA. 24 hours after dead cell removal on day 5 post transduction, cells were stained with Annexin V and PI (Day 6 post transduction). The data show

mean ± s.d. for three independent experiments. *P < 0.05, **P < 0.01, ***P < 0.005 compared to control (Student's unpaired *t* test).

In order to determine whether *SREBP-1* expression was also regulated by SMAD7 in SEMK-2 and THP-1 cells, as shown for REH cells, we then transduced SEMK-2 and THP-1 cells with two independent shRNA targeting *SMAD7* and measured *SREBP-1* expression by qRT-PCR (Fig. 56).

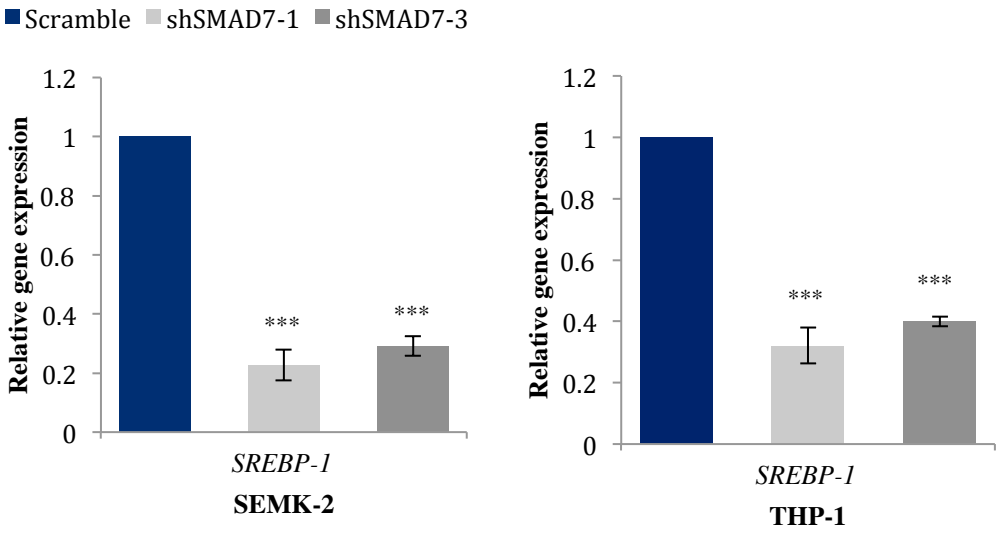

Figure 56 - *SMAD7* knockdown in SEMK-2 and THP-1 cells results in decreased *SREBP-1* gene expression

The bar charts show qRT-PCR analysis of *SREBP-1* expression following *SMAD7* silencing in SEMK-2 and THP-1 cells transduced with control scramble or two different *SMAD7* shRNAs. 2 days after transduction, cells were selected with puromycin for a further 3 days. Dead cell removal was then performed and gene expression analysed by qRT-PCR (Day 5 post transduction). All data show mean ± s.d. from three independent experiments. *P < 0.05, **P < 0.01, ***P < 0.005 compared to control (One-sample *t* test).

5.2.4 SREBP-1 inhibition using the drug Fatostatin induces apoptosis and blocks colony formation

Following *SREBP-1* silencing in leukaemic cell lines, we decided to examine whether leukaemia survival could be compromised by pharmacological inhibition of SREBP-1. We used a small synthetic molecule that has previously been used to block adipogenesis, known as Fatostatin. Fatostatin is a diarylthiazole derivative that impairs the activation process of SREBPs. It is thought to act by blocking ER-Golgi translocation of SREBPs by binding to their escort protein, SCAP (Kamisuki et al., 2009). In order to determine whether Fatostatin could interfere with the leukaemia cell proliferation, REH cells were exposed to different concentrations of the drug for 72 hours and subjected to an MTS assay. This assay demonstrated a dose-dependent inhibition of REH proliferation by Fatostatin (Fig. 57).

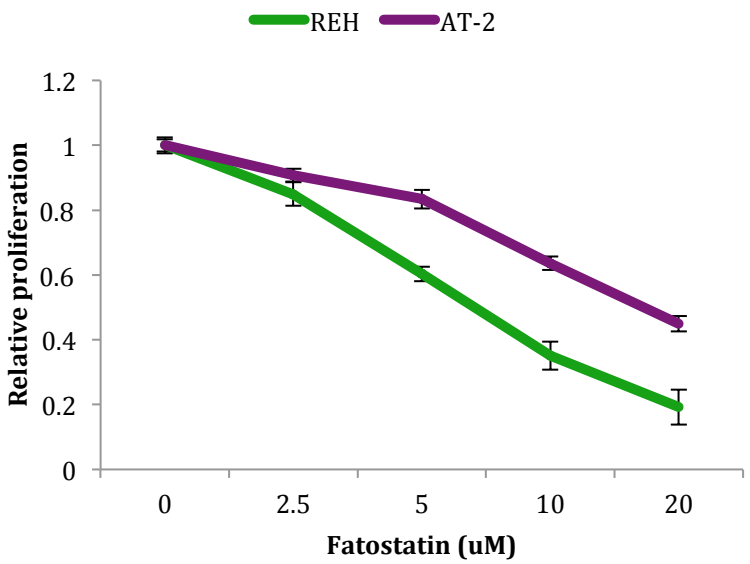

Figure 57 - Fatostatin decreases proliferation of TEL-AML1$^+$ cell lines

The graph above shows the relative proliferation (relative to day 0) of REH and AT-2 cell lines following Fatostatin treatment at the indicated concentrations compared to untreated cells of each cell line. The proliferation of REH cells was measured 3 days and AT-2 cells at 5 days following

treatment using an MTS assay. At each time point, measurements are relative to untreated cells of each cell line. The graph shows mean ± s.d. for three independent experiments.

As we previously observed that *SREBP-1* knockdown results in a block in colony forming ability, we decided to examine whether this could also be achieved with Fatostatin treatment. As previously described, human methylcellulose based colony forming assays were performed using a panel of ALL cell lines. Cells were treated with 20μM Fatostatin or DMSO for 12-14 days (Fig. 58). Colonies were then stained with INT to determine the number of colonies formed. E2A-PBX1$^+$ 697 cells, REH and SEMK-2 cells all showed an almost complete block in colony formation upon treatment with Fatostatin, compared to control cells. This was in agreement with the observed colony formation block after *SREBP-1* silencing in REH cells. MLL-AF4$^+$ BEL-1 and BCR-ABL$^+$ SUP-B15 cells also showed a decrease in colony formation, although to a lesser extent (Fig. 58). These results indicate that targeting SREBP-1 pharmacologically blocks self-renewal and colony forming ability of not only TEL-AML1$^+$ ALL but also other subtypes of ALL. Furthermore, to determine whether SREBP-1 was essential for colony formation in normal haematopoietic progenitor cells, human CD34$^+$ cord blood cells were cultured with a range of Fatostatin concentrations, and their colony forming ability was examined (Fig. 59A). The number of colonies formed and their morphology was determined after 2 weeks culture. (Fig. 59B and 59C). Fatostatin treated cord blood cells showed no block in colony forming ability compared to control cells, even at high concentrations of the drug concentrations. These data suggest a specific requirement for SREBP-1 in leukaemia cell colony formation *in vitro* but not for colony formation by normal haematopoietic progenitors.

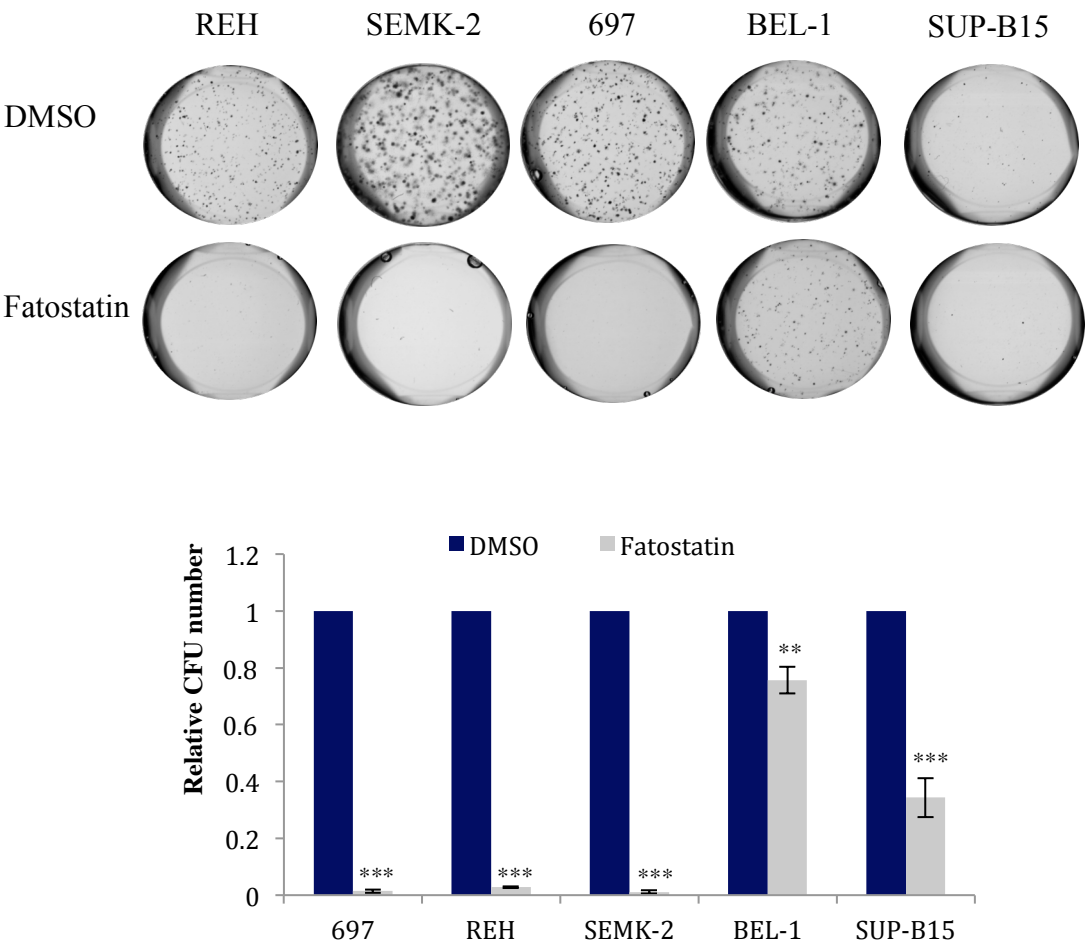

Figure 58 - Fatostatin blocks self-renewal ability of different ALL subtypes

The figure shows an example of colony forming assay of 5 ALL cell lines, REH, SEMK-2, 697, BEL-1, SUP-B15 plated in quadruplicate in methylcellulose with DMSO or 20μM Fatostatin. The cells were stained with INT 12-14 days following plating. The bar chart shows the mean colony formation by Fatostatin treated cells, normalised to DMSO treated control cells ± s.d. for three independent experiments. *P < 0.05, **P < 0.01, ***P < 0.005 compared to control (One-sample *t* test).

A)

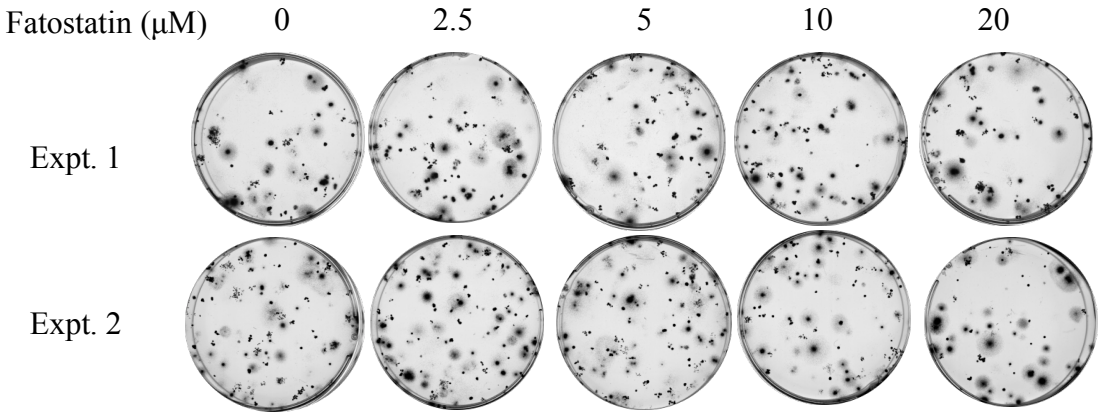

B)

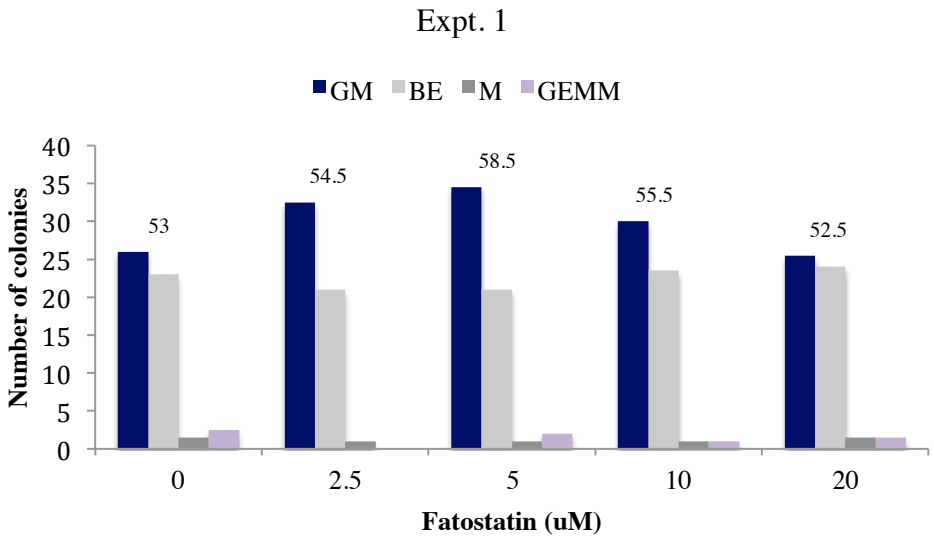

C)

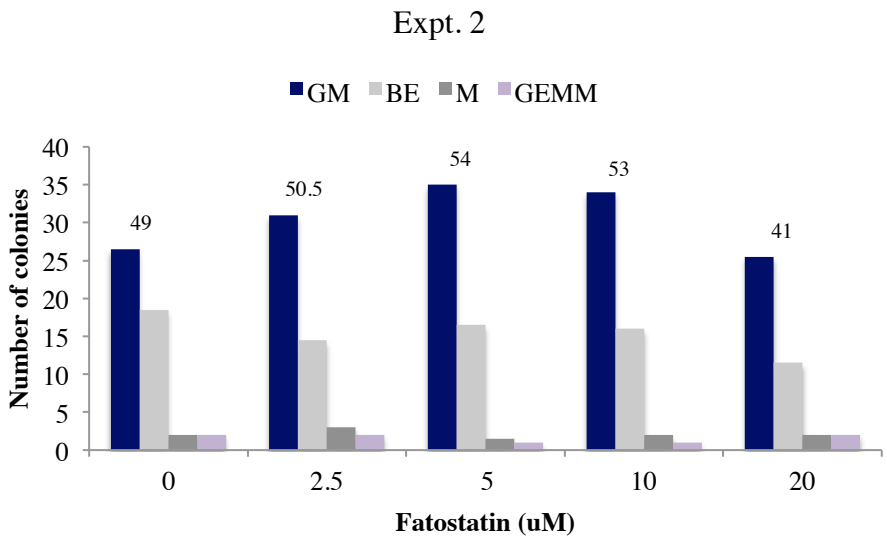

Figure 59 - Fatostatin does not block self-renewal ability of human cord blood cells

(A) The figure shows colony formation of $CD34^+$ human cord blood cells plated in methylcellulose in the presence of Fatostatin. $1x10^3$ cells were plated in duplicate 3 cm dishes and treated with DMSO or

different concentrations of Fatostatin, ranging from 2.5 to 20 μM. The cells were stained with INT 7-10 days following plating. This figure shows two independent experiments. Prior to staining, each colony was counted and its morphology categorised: BFU-E, CFU-GEMM, CFU-GM and CFU-M. The bar chart shows the mean number of colonies counted of each cell type from two technical replicate cultures for (B) experiment 1 and (C) experiment 2. The values above the bars indicate the total number of colonies counted for each concentration of Fatostatin used.

Next, we evaluated if culturing ALL cell lines with Fatostatin would induce apoptosis, as observed by *SREBP-1* knockdown in REH and SEMK-2 cells. Cells were cultured with DMSO or Fatostatin for 72 hours and the apoptosis profile was evaluated. Cells treated with Fatostatin showed significant apoptosis compared to control cells (Fig. 60). Therefore pharmacological inhibition of SREBP-1 resulted in significant cell death, similar to observed apoptosis after shRNA-mediated *SREBP-1* silencing. Furthermore, we evaluated if Fatostatin would induce apoptosis in primograft cells. Five different ALL primograft cells were purified, mouse-cell depleted and cultured in SFEM II for 24 hours in the presence of 100ng/ml Flt3, 50ng/ml IL-7 and 10ng/ml IL-3. Dead cell removal was then performed and cells were treated in the same culture conditions but with added DMSO or 20μM Fatostatin for 72 hours (Fig.61). Although cells treated with DMSO showed some apoptosis to different degrees across the 5 samples, significantly higher cell death was observed in Fatostatin treated cells. Therefore, Fatostatin inhibition of SREBP-1 induced apoptosis in ALL primograft cells.

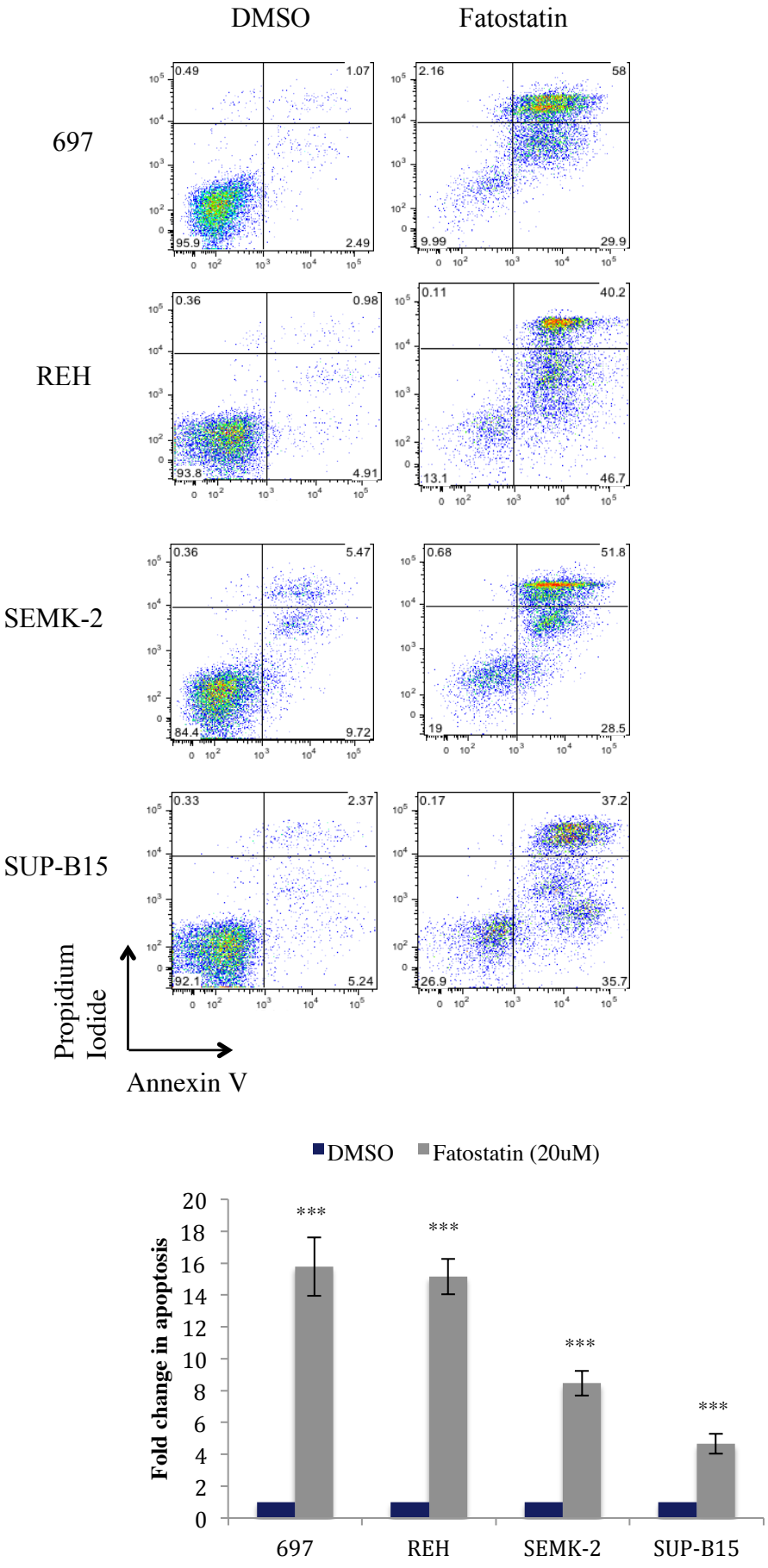

Figure 60 - Fatostatin induces apoptosis in different ALL subtypes

The flow cytometry plots are examples of the apoptosis profiles of 697, REH, SEMK-2, SUP-B15 cells treated with DMSO as control and 20μM Fatostatin for 72 hours. The apoptosis profiles were evaluated after staining with Annexin V and PI. The bar chart represents the mean percentage of apoptotic Annexin V^+PI^- cells ± s.d. for three independent experiments. *P < 0.05, **P < 0.01, ***P < 0.005 compared to control (One-sample *t* test).

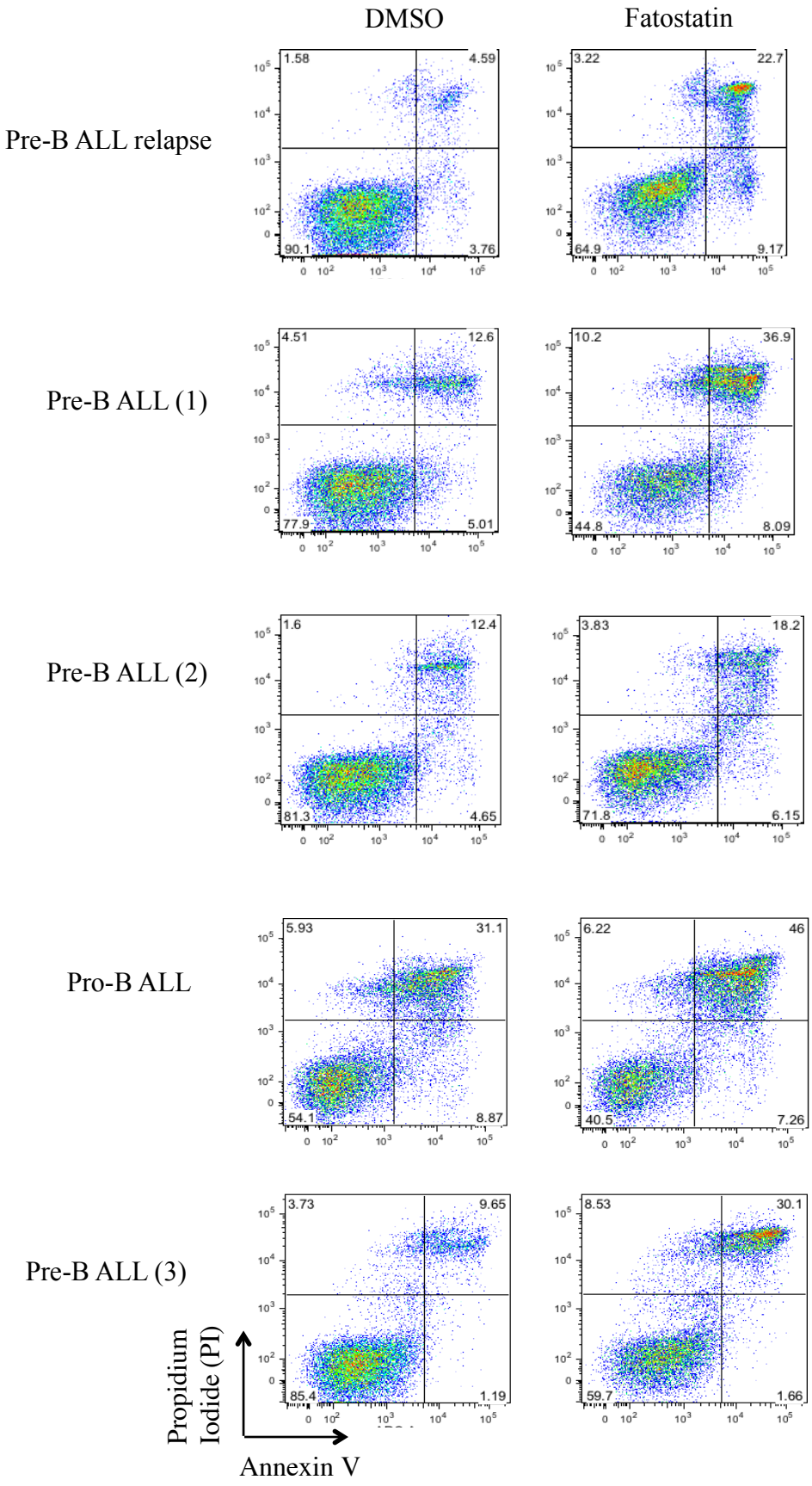
DMSO
Fatostatin
Pre-B ALL relapse
1.58
4.59
90.1
3.76
3.22
22.7
64.9
9.17
Pre-B ALL (1)
4.51
12.6
77.9
5.01
10.2
36.9
44.8
8.09
Pre-B ALL (2)
1.6
12.4
81.3
4.65
3.83
18.2
71.8
6.15
Pro-B ALL
5.93
31.1
54.1
8.87
6.22
46
40.5
7.26
Pre-B ALL (3)
3.73
9.65
85.4
1.19
8.53
30.1
59.7
1.66
Propidium Iodide (PI)
Annexin V

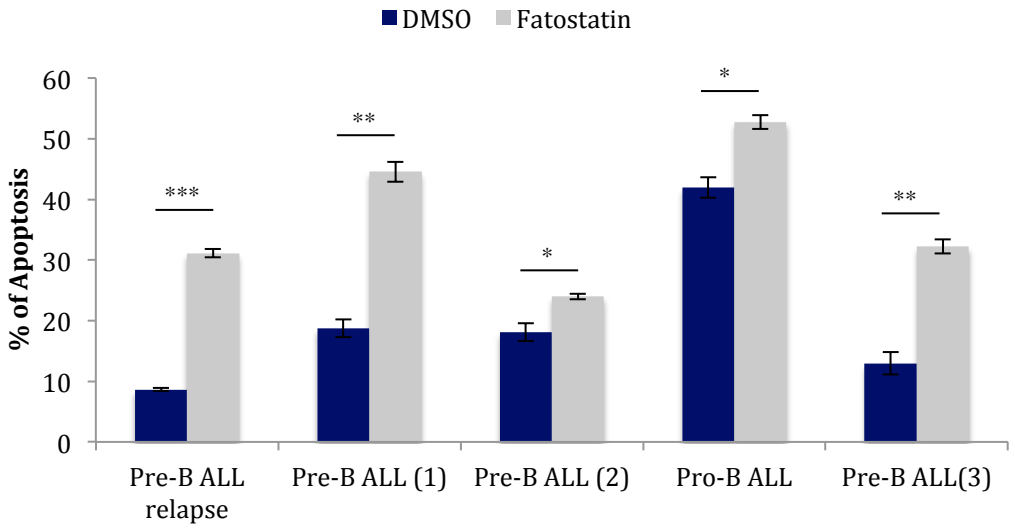

Figure 61 - Fatostatin induces apoptosis in primary ALL samples

The flow cytometry plots are examples of the apoptosis profiles of five different primograft (primary samples from engrafted mice) cells, cultured in SFEMII (supplemented with 100ng/ml human Flt3, 50ng/ml human IL-7 and human 10ng/ml IL-3) and treated with DMSO as control and 20μM Fatostatin for 72 hours following dead cell removal. The apoptosis profile was evaluated after staining with Annexin V and PI. The bar chart represents the mean percentage of apoptotic Annexin V^+PI^- cells ± s.d. for triplicate measurements. *P < 0.05, **P < 0.01, ***P < 0.005 compared to control (Student's unpaired *t* test).

5.2.5 SREBP-1 is essential for leukaemia progression *in vivo*

Since SREBP-1-silencing or pharmacological inhibition resulted in a block in proliferation, loss of colony forming ability and apoptosis, this suggested SREBP-1 may also be required for leukaemia progression *in vivo*. In order to examine this possibility, as previously demonstrated using *shSMAD7*, we transduced luciferase expressing REH cells with control scramble or *SREBP-1* (1) shRNA expressing

vectors (Fig. 62). Following puromycin selection for 3 days, we performed dead cell removal and equivalent numbers of viable cells were transplanted into recipient NSG mice. As previously, we performed a luciferase assay to confirm that both groups exhibited similar levels of luciferase activity (Fig. 63). As predicted, although all mice eventually developed leukaemia, *SREBP-1* silencing resulted in a prolonged latency of disease development *in vivo*. This indicated that SREBP-1 was indeed essential for leukaemia survival and progression *in vivo* as well as *in vitro* (Fig. 64). Moreover, increased levels of *SREBP-1* mRNA expression were detected in the engrafted cells recovered from the first three *shSREBP-1* (1) mice that were sacrificed, in comparison to levels observed in the cells pre-transplantation, in both cases relative to levels expressed in shScramble cells (Fig. 64D). This demonstrates *in vivo* selection against leukaemic cells with low *SREBP-1* expression.

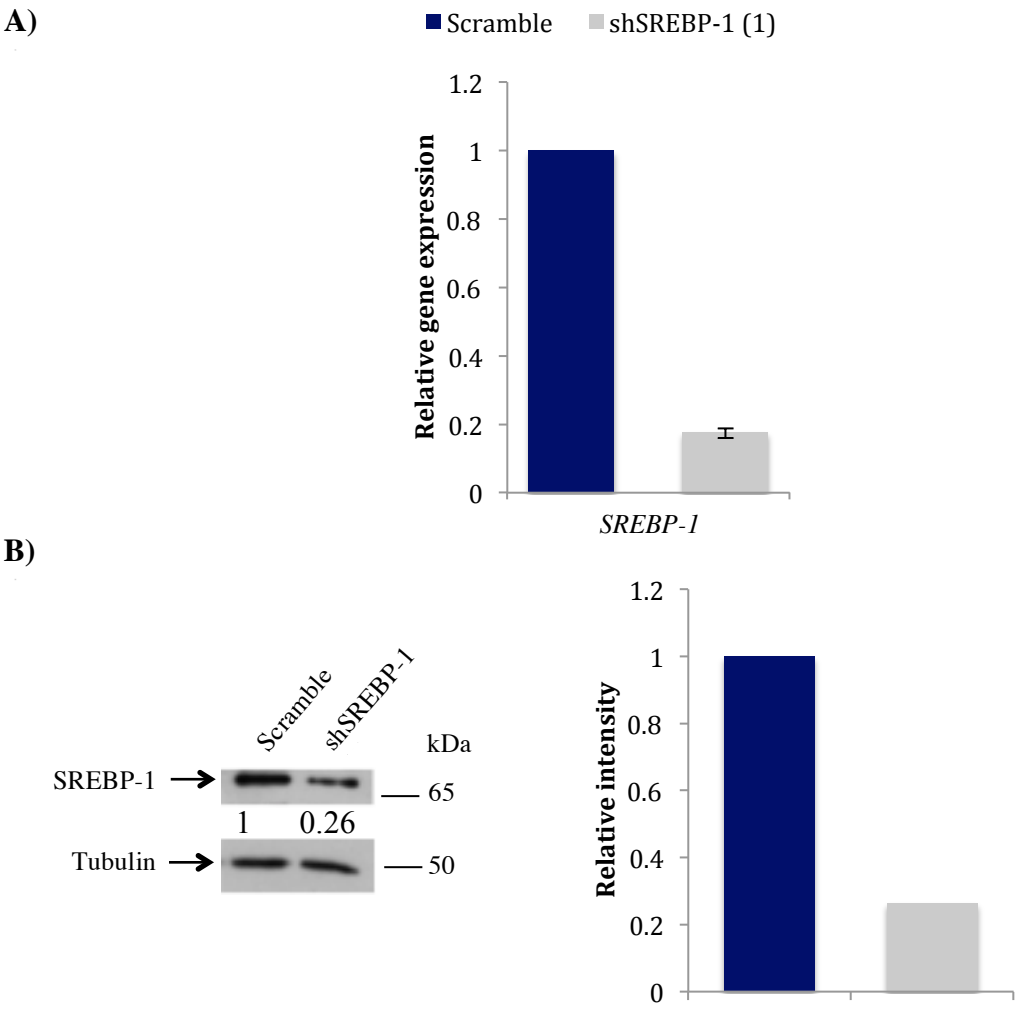

Figure 62 - *SREBP-1* silencing in luciferase-CD2 transduced REH cells

(A) The bar chart shows *SREBP-1* silencing of REH-LUC-CD2 cells transduced with control scramble or *shSREBP-1 (1)*. 2 days after transduction, cells were selected with puromycin for a further 3 days. Dead cell removal was then performed and *SREBP-1* silencing measured by qRT-PCR prior to transplantation (pre-transplantation: Day 5 post transduction). (B) The western blot analysis shows *SREBP-1* silencing of REH-LUC-CD2 cells at the protein level, pre-transplantation and the bar chart shows the densitometric quantitation of SREBP-1 levels relative to Tubulin. All experiments were performed once.

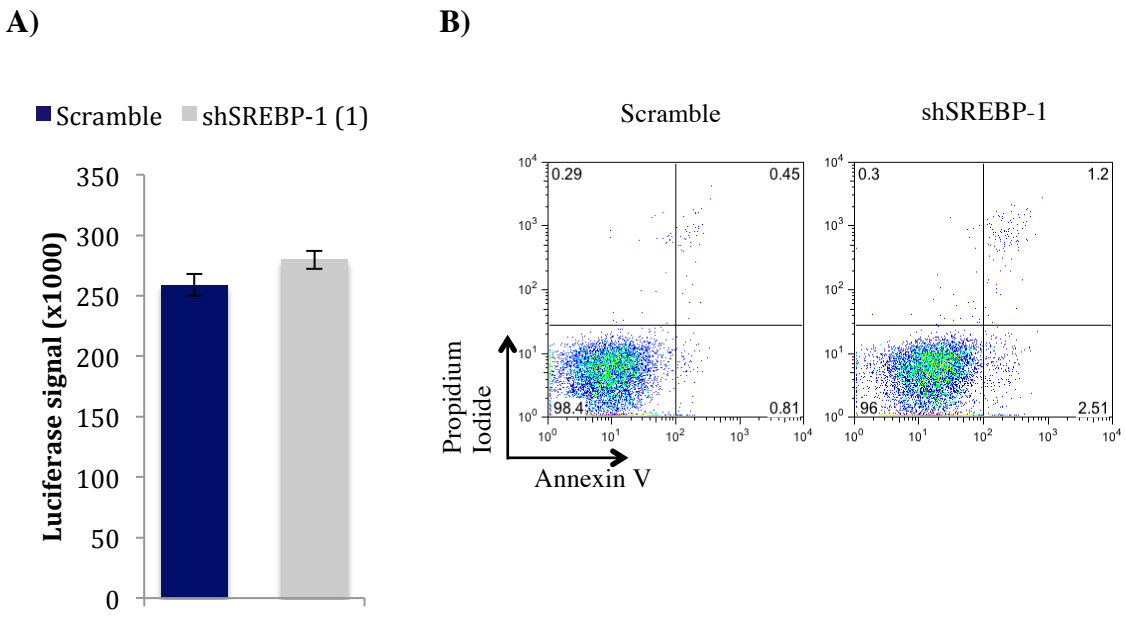

Figure 63 - Luciferase activity and viability of REH-LUC-CD2 transduced cells pre-transplantation

The bar chart shows the luciferase activity measured using the Promega Luciferase Assay System of REH-LUC-CD2 cells 2 days after transduction with control scramble or *shSREBP-1* followed by 3 days of puromycin selection and dead cell removal (A). Results were measured in triplicates and the mean ± s.d. shown. The flow cytometry plots show apoptosis analysis of REH-LUC-CD2 cells 5 days following transduction with control scramble or *shSREBP-1*, after dead cell removal and prior to transplantation. Apoptosis profiles were evaluated after staining with Annexin V and PI. All experiments were performed once.

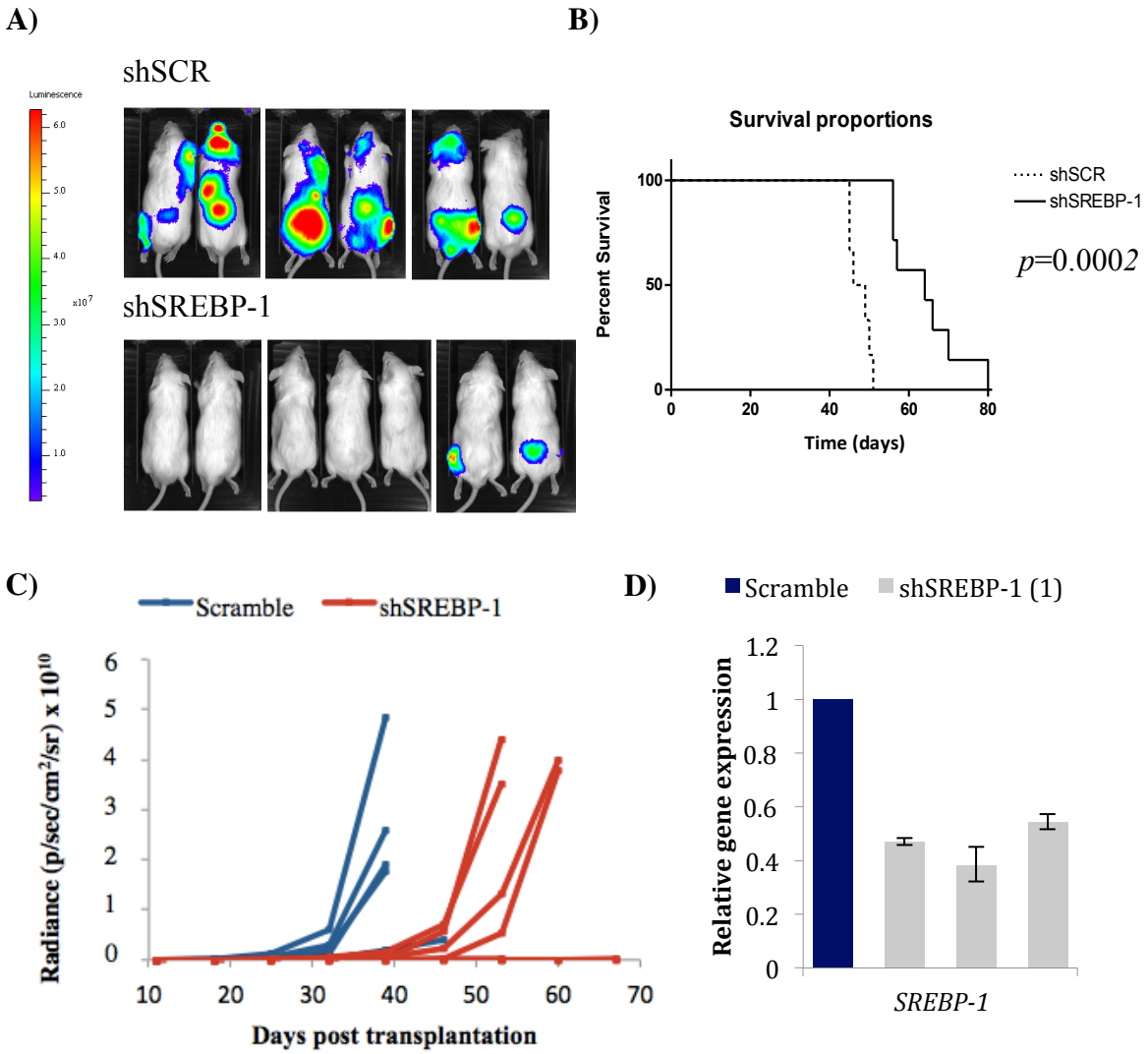

Figure 64 - *SREBP-1* knockdown *in vivo* impairs leukaemia progression

The figure shows a bioluminescent image of NSG mice 25 days after transplantation with $1x10^5$ control scramble or *shSREBP-1 (1)* transduced luciferase expressing REH cells (A) and the resulting survival curve (B). The line chart shows the luminescence radiance measured at 7 day intervals starting from day 11 for each mouse (C). *shSREBP-1 (1)* transduced cells isolated from the bone marrow of leukaemic mice (post-leukaemia) show loss of knock-down after *in vivo* progression (D). *SREBP-1* expression was normalised to *SREBP-1* expression in control scramble shRNA transduced REH-LUC-CD2 cells. qRT-PCR was performed in triplicates and mean ± s.d. is shown.

5.3 Discussion

As mentioned previously, RNA-sequencing established that *SMAD7* knockdown results in down-regulation of multiple genes involved in the cholesterol biosynthesis pathway. Here, we have validated these gene expression changes to show that SMAD7 does indeed up-regulate genes in the cholesterol biosynthesis pathway at the transcriptional level in TEL-AML1$^+$ cells. One of the regulated genes, *SREBP-1* is a known master transcription factor of cholesterol biosynthesis and is downregulated upon *SMAD7* knockdown not only in TEL-AML1$^+$ cells but other subtypes of leukaemia, specifically MLL-AF4$^+$ ALL and MLL-AF9$^+$ AML cells. Using an assay to detect cholesterol synthesis in cells, we demonstrated that SMAD7 knockdown causes a decrease in cholesterol synthesis in leukaemia cells. Additionally, when SMAD7 was overexpressed, an increase in *SREBP-1* gene expression levels was observed, suggesting that SMAD7 is the crucial rate-limiting factor in *SREBP-1* expression. In addition to an increase in *SREBP-1*, SMAD7 overexpression also results in an increase in cholesterol synthesis, implying that SMAD7 induction of *SREBP-1* stimulates cholesterol biosynthesis in these leukaemic cells. It remains unclear how SMAD7 regulates *SREBP-1*. One possibility is that SMAD7 could regulate *SREBP-1* by directly binding to *SREBP-1* promoter sequences. SMAD7 may also require association with complexes involving other co-activators for induction of *SREBP-1* expression. For example, SMAD7 has been shown to interact with p38 and ataxia telangiectasia mutated (ATM) in a complex in order to induce p53-mediated apoptosis in prostate cancer cells (Zhang et al., 2006). Secondly, SMAD7 may function via deregulation of other transcriptional regulators. For example, SMAD7 is known to interfere with TGF-β signalling by blocking SMAD2/3 transcriptional activation or repression of target genes (Yan et al., 2009;

Zhang et al., 2007) (Han et al., 2013). Therefore, it is possible that SMAD7 may be acting indirectly by interfering with SMAD2/3 mediated *SREBP-1* regulation. Thirdly, SMAD7 may act as a transcriptional co-activator for specific transcription factors to trigger transcription of their target genes. SMAD7 has previously been shown to act as a transcriptional co-activator for IRF1 to induce transcription of Caspase 8 and restore TRAIL-mediated apoptosis in breast cancer cells (Hong et al., 2013). It is also a possibility that other factors may control SMAD7 regulation of target genes. For example, the deubiquitinating enzyme, cylindromatosis (CYLD), previously shown to reverse multidrug resistance in leukaemia, has been reported to regulate SMAD7 in oral squamous cell carcinoma (OSCC) (Ge et al., 2016). CYLD overexpression inhibited SMAD7-mediated cell invasion in OSCC cell lines. Therefore, due to the multiple possibilities of how SMAD7 regulates *SREBP-1* in leukaemia, further experiments are required to clarify the mechanisms underlying SREBP-1 activation in these cells.

Metabolic signalling in cancer cells is tightly regulated by SREBPs, which have been found to be highly active in different cancers (Ettinger et al., 2004; Guo et al., 2009). SREBP has a key role in connecting oncogenic signalling-regulated metabolism to *de novo* lipogenesis (DeBerardinis et al., 2008a; Deberardinis et al., 2008b). In leukaemia cells, we show that silencing of *SREBP-1* results in a loss of self-renewal ability, a decrease in cholesterol biosynthesis and induction of apoptosis. Furthermore, *in vivo* transplantation of *SREBP-1* silenced cells results in a longer latency of disease compared to control cells, establishing the importance of SREBP-1 regulated *de novo* cholesterol synthesis for leukaemia progression. However, as with previous studies, it is unclear how *SREBP-1* silencing induces apoptosis. Firstly, apoptosis could occur as a result of *SREBP-1* mediated decrease in

total cholesterol levels. Alternately, the intermediate steps in the cholesterol pathway produce isoprenoids, farnesyl pyrophosphate and geranylgeranyl pyrophosphate. These intermediates are critical for membrane anchoring of multiple oncogenic proteins such as RAS, PI3K and AKT. Metabolic arrest in any of these steps in the cholesterol pathway would therefore result in deregulated signalling of these proteins (Gabitova et al., 2014). Prenylation of Ras, RhoB and other proteins is mediated by farnesyltransferase and geranylgeranyltransferase for farnesylation and geranylgeranylation, respectively. Previously, farnesyltransferase inhibitors (FTI) have been used alone or in combination with chemotherapy in AML, myelodsyplastic syndrome (MDS), head and neck squamous cell carcinoma and breast cancer studies to block RAS activation (Baines et al., 2011; Brunner et al., 2003). FTI treatment of osteosarcoma to block farnesylation of N-Ras and K-Ras resulted in geranylgeranylation of N-Ras and K-Ras (Geryk-Hall et al., 2010). This alters their downstream signalling, resulting in decreased cell survival. Therefore, it is possible that a decrease in isoprenylation of oncogenic signalling molecules could also result in apoptosis.

Fatostatin, an inhibitor of SREBP-1 activity, has been used in a recent study where SREBP-1 has been shown to promote prostate cancer growth and castration resistance progression through induction of lipogenesis and androgen receptor activity (Huang et al., 2012). In this study, Fatostatin was shown to suppress the proliferation and colony formation of two prostate cancer cell lines (Li et al., 2014). In our data, treating different ALL subtypes with Fatostatin resulted in a significant loss of colony formation in methylcellulose assays and induction of apoptosis in four different subtypes of ALL including TEL-AML1$^+$ and BCR-ABL$^+$ ALL cells. Moreover, treatment of human CD34$^+$ cord blood cells did not show a block in

colony formation or change in the morphology of the colonies formed. Therefore, our data provide evidence for the existence of a therapeutic window in SREBP-1 targeting by Fatostatin.

Studies dating back to 1970s show that leukaemia cells become dependent on cholesterol biosynthesis for their continued survival and metabolism. Mononuclear cells from AML patients show increased rates of receptor-mediated uptake and degradation of LDL, which is associated with a high rate of cholesterol synthesis in these cells, compared to cells from healthy subjects (Vitols et al., 1985). This high uptake and degradation of LDL by malignant cells was taken advantage of through the use of LDL-bound chemotherapeutic agents to target leukaemic cells. However, this has had complications and few applications in cancer therapy (Harisa and Alanazi, 2014). Statin targeting of HMG-CoA reductase activity in AML and ALL cells was shown to result in growth inhibition and cell killing (Vilimanovich et al., 2015) (Li et al., 2003; Sheen et al., 2011). However, there is a large discrepancy between statin concentrations used in such *in vitro* experiments and those therapeutically achievable in human plasma. While effects of statins are detected at concentrations of 1-50umol L^{-1}, the mean concentration of statins in human serum at therapeutic doses is only 1-15 nmol L^{-1} (Bjorkhem-Bergman et al., 2011). In addition, a recent study showed that effective simvastatin concentrations used *in vitro* in leukaemia treatment are not clinically achievable, suggesting that statins cannot be used as monotherapies in anti-cancer treatment (Ahmed, 2013). To use higher effective therapeutic doses of statins, toxicity in patients would have to be assessed. Moreover, not all statins have the same outcomes, as leukaemia cells use compensatory mechanisms to overcome the effects of statins by cholesterol importation via LDLR (Guo et al., 2011) and increased expression of genes in the

biosynthesis pathway via SREBPs (Clendening et al., 2010). Our findings highlight an alternate way to target the mevalonate pathway and subsequently block cholesterol synthesis, by inhibiting SREBP-1. Inhibiting SREBP-1 would also block its upregulation of LDL and LDLR expression, which are highly expressed in cancer cells. For example, SREBP-1 has been shown to be highly expressed in cancers such as glioblastoma, where it mediates up-regulation of LDLR to increase cholesterol levels, as a result of EGFR/PI3K/AKT oncogenic signalling (Guo et al., 2014). Uptake of LDL is crucial for cancer cells to maintain their supply of cholesterol to rapidly form new membranes. It is unclear precisely how cancer cells maintain their cholesterol levels, whether it is through uptake or *de novo* synthesis (Guo et al., 2011). In glioblastoma, cells prefer to uptake LDL from exogenous medium to maintain their cholesterol levels. Rather, they use *de novo* biosynthesis as a compensatory mechanism when exogenous cholesterol is not available (Guo et al., 2011). Therefore, targeting SREBP-1 could result in decreased LDL and LDLR mediated cholesterol uptake in addition to *de novo* biosynthesis to inhibit total cholesterol levels. It is also possible that SREBP-1 targeting can synergise with statin-induced HMGCR inhibition, and that combination therapies would require lower concentrations of each inhibitor. Such combination therapies may yet represent effective approaches to treating certain leukaemias.

We have shown that SMAD7 is essential in regulating *SREBP-1* expression and therefore controlling cholesterol biosynthesis and promoting leukaemia cell survival. However, it remains unclear whether SREBP-1 controls the transcriptional activation of all the other genes identified through RNA-sequencing (ACAT2, DHCR7, MSMO1, LBR, LSS) in leukaemic cells. It may be possible that SMAD7 regulation of *SREBP-1* results in the activation of other genes, or alternatively, that

SMAD7 may directly induce the expression of other genes in the cholesterol pathway, therefore inducing cholesterol synthesis via alternate mechanisms in leukaemia cells. Although at present, no pharmacological inhibitor of SMAD7 is available, this possibility may make SMAD7 itself a promising therapeutic target, its inhibition resulting in a block in cholesterol biosynthesis at multiple points in leukaemia cells.

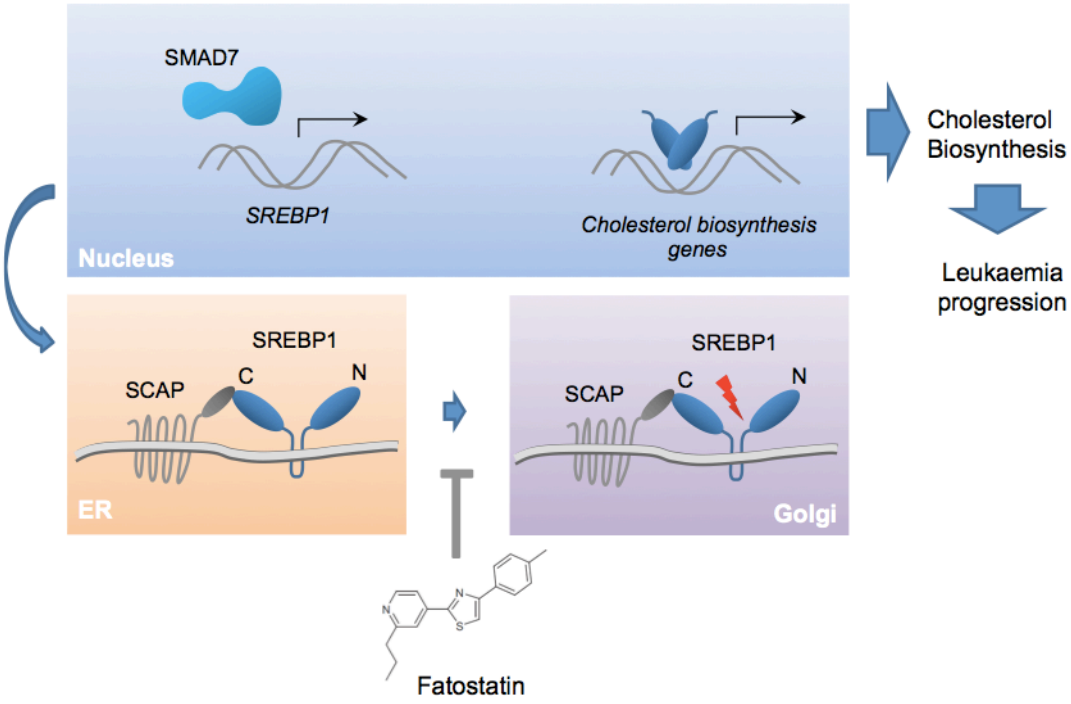

Figure 65 - SMAD7 induces SREBP-1 and cholesterol biosynthesis in leukaemia

In our model, we have established a novel signalling pathway where SMAD7 regulates transcription of *SREBP-1* and other genes involved in the cholesterol biosynthesis pathway, which is essential for leukaemia survival. We used an inhibitor of SREBP-1, Fatostatin, that targets SREBP-1 by blocking its transport from the ER to the Golgi apparatus and consequently its cleavage and nuclear translocation, to induce apoptosis of human leukaemic cell lines and primograft cells.

CHAPTER VI. CONCLUSIONS

This project was based on the hypothesis that aberrant signalling responses of pre-leukaemic clones to cytokines and immune modulators underlie the association between childhood exposure to pathogens and leukaemia progression. In accordance with this hypothesis, in 2009 a study implicated the immune modulator, TGF-β, as promoting outgrowth of pre-leukaemic cells. The oncogene, *TEL-AML1,* was found to dysregulate the TGF-β pathway, reducing sensitivity of pre-leukaemic cells to the anti-proliferative effects of TGF-β (Ford et al., 2009). Therefore, in this project we first aimed to examine the impact of TEL-AML1 upon TGF-β sensitivity across a panel of human ALL cell lines and using a previously established model of immortalized mouse pre-B cells, with conditional TEL-AML1 expression (Lyons et al., 2010). Surprisingly, in our models we discovered that the resistance of human leukaemia cells to the anti-proliferative effects of TGF-β was not linked to TEL-AML1 expression. Furthermore, TGF-β induced equivalent inhibition of self-renewal in mouse pre-B cells, irrespective of TEL-AML1 expression. Moreover, our data showed that leukaemic cell lines that were resistant to TGF-β appeared to have reduced levels of SMAD3 expression, in comparison to SMAD2. In contrast, cell lines that were sensitive to the anti-proliferative effects of TGF-β, expressed higher levels of SMAD3, roughly equivalent to those of SMAD2.

Subsequently, we investigated whether SMAD7, a target gene of TGF-β signalling, could regulate the responses of leukaemia cells to TGF-β. SMAD7 has been shown to inhibit TGF-β signalling through a negative feedback loop, blocking

SMAD2/3 phosphorylation and their consequent activation (Yan et al., 2009). Additionally, recent data from our laboratory established the importance of STAT3 activation in TEL-AML1$^+$ and BCR-ABL$^+$ leukaemia (Mangolini et al., 2013), and previous literature has demonstrated cross-talk between STAT3 and TGF-β signalling via SMAD7 (Jenkins et al., 2005; Luwor et al., 2013). Therefore we questioned whether STAT3 was involved in mediating aberrant TGF-β responsiveness via SMAD7 in some ALL cells. Using shRNA silencing we found that STAT3 was responsible for transcriptional regulation of *SMAD7* gene expression. This suggested a mechanism whereby STAT3 signalling could enforce resistance to TGF-β stimulation. To investigate this possibility, we silenced *SMAD7* gene expression in TEL-AML1$^+$ REH cells and examined their response to TGF-β. Unexpectedly our data showed that loss of SMAD7 compromised REH cell proliferation, independent of TGF-β stimulation. *SMAD7* knockdown resulted in apoptosis and significantly reduced colony-forming ability. The block in cell proliferation following *SMAD7* knockdown was also observed in an MLL-AF4$^+$ ALL cell line and an MLL-AF9$^+$ AML cell line. This showed that *SMAD7* knockdown in ALL and AML cells can lead to a block in leukaemia proliferation. Furthermore, using *SMAD7* knockdown *in vivo* we have demonstrated that mice injected with shSMAD7 knockdown cells exhibited a slower disease progression compared to controls, verifying that SMAD7 has a key role in leukaemia progression *in vivo*.

However, as the role of SMAD7 appeared to be independent of TGF-β signalling, to identify the downstream pathways regulated by SMAD7 in leukaemia, we performed gene expression analysis by RNA-sequencing of REH cells following *SMAD7* knockdown. Following analyses using Ilumina BaseSpace, Strand NGS and

Ingenuity Pathway analysis, we identified that SMAD7 regulates the expression of a number of genes encoding transcription factors and enzymes involved in the cholesterol biosynthesis pathway. Following validation of these gene changes by qRT-PCR, we confirmed that SMAD7 loss resulted in decreased total cholesterol levels in leukaemia cells. We focused on one gene identified by our RNA-seq analysis, *SREBP-1*, encoding a master transcription factor involved in controlling fatty acid and cholesterol synthesis and metabolism (Eberle et al., 2004). Upon SMAD7 overexpression, we observed an increase in *SREBP-1* gene expression and an increase in total cholesterol in leukaemia cells. This appeared to suggest SMAD7 may directly regulate *SREBP-1* expression. However, further studies will be required to examine whether SMAD7 is involved in transactivation of the *SREBP-1* promoter, or whether it acts indirectly, for example by sequestering repressive co-factors.

We have shown that SMAD7 regulation of *SREBP-1* expression is critical to leukaemia survival, since *SREBP-1* knockdown resulted in significant apoptosis, inhibition of colony forming ability and decreased total cholesterol levels in REH cells. In addition, we observed significant apoptosis following loss of *SREBP-1* in MLL-AF4$^+$ ALL cells. Pharmacological inhibition of SREBP-1 using the drug Fatostatin, resulted in inhibition of colony formation by a number of different ALL cell lines. We observed that treatment of CD34$^+$ human cord blood cells with Fatostatin did not affect colony formation, indicating a specific requirement for SREBP-1 expression in leukaemia cells for self-renewal. We have also reported significant apoptosis following Fatostatin treatment of a number of ALL cell lines and primary patient samples harbouring different molecular abnormalities. We also established the role of SREBP-1 in leukaemia survival *in vivo*, as previously with SMAD7, by transplanting *SREBP-1* silenced REH cells into mice. Mice transplanted

with *SREBP-1* knockdown cells exhibited a longer disease latency compared to control mice, confirming that loss of SREBP-1 impairs leukaemia progression *in vivo*.

Although studies have previously indicated that SMAD7 expression is critical in various cancers (Zhu et al., 2011), in this project we have discovered novel aspects of SMAD7 function in different subtypes of ALL and AML cells. Furthermore, we have established, for the first time, a role for SMAD7 in upregulating *SREBP-1* gene expression, ensuring enhanced cholesterol biosynthesis in leukaemia cells. Previous work has shown that leukaemia dependency upon cholesterol biosynthesis can be exploited by targeting HMG-CoA reductase, using inhibitors such as statins (Ahmed, 2013; Crosbie et al., 2013; Vilimanovich et al., 2015). However, the use of statins has proved challenging (Bjorkhem-Bergman et al., 2011). Here, we have identified an alternate target in the cholesterol biosynthesis pathway, SREBP-1 that is critical for leukaemia survival both *in vitro* and *in vivo* and can be successfully targeted by drugs. Therefore, by investigating TEL-AML1-specific transcriptional networks and their relationship with TGF-β signalling pathways, we have discovered a novel pathway present in a broad range of leukaemias and susceptible to pharmacological inhibition. Manipulating this pathway can have new therapeutic implications for the treatment of a range of leukaemia subtypes.

CHAPTER VII. REFERENCES

Adolfsson, J., Mansson, R., Buza-Vidas, N., Hultquist, A., Liuba, K., Jensen, C.T., Bryder, D., Yang, L., Borge, O.J., Thoren, L.A., *et al*. (2005). Identification of Flt3+ lympho-myeloid stem cells lacking erythro-megakaryocytic potential a revised road map for adult blood lineage commitment. Cell *121*, 295-306.

Ahmed, T. (2013). High dose simvastatin as a potential anticancer therapy in leukemia patients (University of Kentucky).

Akashi, K., Traver, D., Miyamoto, T., and Weissman, I.L. (2000). A clonogenic common myeloid progenitor that gives rise to all myeloid lineages. Nature *404*, 193-197.

Amin, H.M., McDonnell, T.J., Ma, Y., Lin, Q., Fujio, Y., Kunisada, K., Leventaki, V., Das, P., Rassidakis, G.Z., Cutler, C., *et al*. (2004). Selective inhibition of STAT3 induces apoptosis and G(1) cell cycle arrest in ALK-positive anaplastic large cell lymphoma. Oncogene *23*, 5426-5434.

Anderson, K., Lutz, C., van Delft, F.W., Bateman, C.M., Guo, Y., Colman, S.M., Kempski, H., Moorman, A.V., Titley, I., Swansbury, J., *et al*. (2011). Genetic variegation of clonal architecture and propagating cells in leukaemia. Nature *469*, 356-361.

Andreasson, P., Schwaller, J., Anastasiadou, E., Aster, J., and Gilliland, D.G. (2001). The expression of ETV6/CBFA2 (TEL/AML1) is not sufficient for the transformation of hematopoietic cell lines in vitro or the induction of hematologic disease in vivo. Cancer Genet Cytogenet *130*, 93-104.

Anjos-Afonso, F., Currie, E., Palmer, H.G., Foster, K.E., Taussig, D.C., and Bonnet, D. (2013). CD34(-) cells at the apex of the human hematopoietic stem cell hierarchy have distinctive cellular and molecular signatures. Cell Stem Cell *13*, 161-174.

Arinobu, Y., Mizuno, S., Chong, Y., Shigematsu, H., Iino, T., Iwasaki, H., Graf, T., Mayfield, R., Chan, S., Kastner, P., *et al*. (2007). Reciprocal activation of GATA-1 and PU.1 marks initial specification of hematopoietic stem cells into myeloerythroid and myelolymphoid lineages. Cell Stem Cell *1*, 416-427.

Baines, A.T., Xu, D., and Der, C.J. (2011). Inhibition of Ras for cancer treatment: the search continues. Future Med Chem *3*, 1787-1808.

Banker, D.E., Mayer, S.J., Li, H.Y., Willman, C.L., Appelbaum, F.R., and Zager, R.A. (2004). Cholesterol synthesis and import contribute to protective cholesterol increments in acute myeloid leukemia cells. Blood *104*, 1816-1824.

Barberis, A., Widenhorn, K., Vitelli, L., and Busslinger, M. (1990). A novel B-cell lineage-specific transcription factor present at early but not late stages of differentiation. Genes Dev *4*, 849-859.

Benekli, M., Baumann, H., and Wetzler, M. (2009). Targeting signal transducer and activator of transcription signaling pathway in leukemias. J Clin Oncol *27*, 4422-4432.

Berg JM, T.J., Stryer L. (2002). Biochemistry, 5th edn (New York: W.H.Freeman).

Bernardin, F., Yang, Y., Cleaves, R., Zahurak, M., Cheng, L., Civin, C.I., and Friedman, A.D. (2002). TEL-AML1, expressed from t(12;21) in human acute lymphocytic leukemia, induces acute leukemia in mice. Cancer Res *62*, 3904-3908.

Bhandoola, A., and Sambandam, A. (2006). From stem cell to T cell: one route or many? Nat Rev Immunol *6*, 117-126.

Bjorkhem-Bergman, L., Lindh, J.D., and Bergman, P. (2011). What is a relevant statin concentration in cell experiments claiming pleiotropic effects? Br J Clin Pharmacol *72*, 164-165.

Blank, U., Karlsson, G., Moody, J.L., Utsugisawa, T., Magnusson, M., Singbrant, S., Larsson, J., and Karlsson, S. (2006). Smad7 promotes self-renewal of hematopoietic stem cells. Blood *108*, 4246-4254.

Blank, U., and Karlsson, S. (2011). The role of Smad signaling in hematopoiesis and translational hematology. Leukemia *25*, 1379-1388.

Blom, B., and Spits, H. (2006). Development of human lymphoid cells. Annu Rev Immunol *24*, 287-320.

Bories, J.C., Cayuela, J.M., Loiseau, P., and Sigaux, F. (1991). Expression of human recombination activating genes (RAG1 and RAG2) in neoplastic lymphoid cells: correlation with cell differentiation and antigen receptor expression. Blood *78*, 2053-2061.

Brettingham-Moore, K.H., Taberlay, P.C., and Holloway, A.F. (2015). Interplay between Transcription Factors and the Epigenome: Insight from the Role of RUNX1 in Leukemia. Front Immunol *6*, 499.

Broderick, P., Carvajal-Carmona, L., Pittman, A.M., Webb, E., Howarth, K., Rowan, A., Lubbe, S., Spain, S., Sullivan, K., Fielding, S., *et al*. (2007). A genome-wide association study shows that common alleles of SMAD7 influence colorectal cancer risk. Nat Genet *39*, 1315-1317.

Brown, M.S., and Goldstein, J.L. (1997). The SREBP pathway: regulation of cholesterol metabolism by proteolysis of a membrane-bound transcription factor. Cell *89*, 331-340.

Brunner, T.B., Hahn, S.M., Gupta, A.K., Muschel, R.J., McKenna, W.G., and Bernhard, E.J. (2003). Farnesyltransferase inhibitors: an overview of the results of preclinical and clinical investigations. Cancer Res *63*, 5656-5668.

Bryder, D., Ramsfjell, V., Dybedal, I., Theilgaard-Monch, K., Hogerkorp, C.M., Adolfsson, J., Borge, O.J., and Jacobsen, S.E. (2001). Self-renewal of multipotent long-term repopulating hematopoietic stem cells is negatively regulated by Fas and tumor necrosis factor receptor activation. J Exp Med *194*, 941-952.

Caldenhoven, E., van Dijk, T.B., Solari, R., Armstrong, J., Raaijmakers, J.A., Lammers, J.W., Koenderman, L., and de Groot, R.P. (1996). STAT3beta, a splice variant of transcription factor STAT3, is a dominant negative regulator of transcription. J Biol Chem *271*, 13221-13227.

Castor, A., Nilsson, L., Astrand-Grundstrom, I., Buitenhuis, M., Ramirez, C., Anderson, K., Strombeck, B., Garwicz, S., Bekassy, A.N., Schmiegelow, K., *et al*. (2005). Distinct patterns of hematopoietic stem cell involvement in acute lymphoblastic leukemia. Nat Med *11*, 630-637.

Cerutti, J.M., Ebina, K.N., Matsuo, S.E., Martins, L., Maciel, R.M., and Kimura, E.T. (2003). Expression of Smad4 and Smad7 in human thyroid follicular carcinoma cell lines. J Endocrinol Invest *26*, 516-521.

Chadwick, K., Shojaei, F., Gallacher, L., and Bhatia, M. (2005). Smad7 alters cell fate decisions of human hematopoietic repopulating cells. Blood *105*, 1905-1915.

Chen, J., Odenike, O., and Rowley, J.D. (2010). Leukaemogenesis: more than mutant genes. Nat Rev Cancer *10*, 23-36.

Chen, M.J., Li, Y., De Obaldia, M.E., Yang, Q., Yzaguirre, A.D., Yamada-Inagawa, T., Vink, C.S., Bhandoola, A., Dzierzak, E., and Speck, N.A. (2011). Erythroid/myeloid progenitors and hematopoietic stem cells originate from distinct populations of endothelial cells. Cell Stem Cell *9*, 541-552.

Cheng, T., Rodrigues, N., Shen, H., Yang, Y., Dombkowski, D., Sykes, M., and Scadden, D.T. (2000). Hematopoietic stem cell quiescence maintained by p21cip1/waf1. Science *287*, 1804-1808.

Chung, C.D., Liao, J., Liu, B., Rao, X., Jay, P., Berta, P., and Shuai, K. (1997). Specific inhibition of Stat3 signal transduction by PIAS3. Science *278*, 1803-1805.

Clark, D.A., and Coker, R. (1998). Transforming growth factor-beta (TGF-beta). Int J Biochem Cell Biol *30*, 293-298.

Clendening, J.W., Pandyra, A., Boutros, P.C., El Ghamrasni, S., Khosravi, F., Trentin, G.A., Martirosyan, A., Hakem, A., Hakem, R., Jurisica, I., *et al*. (2010). Dysregulation of the mevalonate pathway promotes transformation. Proc Natl Acad Sci U S A *107*, 15051-15056.

Cobaleda, C., Schebesta, A., Delogu, A., and Busslinger, M. (2007). Pax5: the guardian of B cell identity and function. Nat Immunol *8*, 463-470.

Crispino, J.D., and Le Beau, M.M. (2012). BMP meets AML: induction of BMP signaling by a novel fusion gene promotes pediatric acute leukemia. Cancer Cell *22*, 567-568.

Crosbie, J., Magnussen, M., Dornbier, R., Iannone, A., and Steele, T.A. (2013). Statins inhibit proliferation and cytotoxicity of a human leukemic natural killer cell line. Biomark Res *1*, 33.

Dang, J., Wei, L., de Ridder, J., Su, X., Rust, A.G., Roberts, K.G., Payne-Turner, D., Cheng, J., Ma, J., Qu, C., *et al*. (2015). PAX5 is a tumor suppressor in mouse mutagenesis models of acute lymphoblastic leukemia. *125*, 3609-3617.

Dayton. S, P.M., Hashimoto.S, Dixon. W, Tomiyasu.U (1969). A Controlled Clinical Trial of a Diet High in Unsaturated Fat in Preventing Complications of Atherosclerosis. Circulation *40*, 1-63.

DeBerardinis, R.J., Lum, J.J., Hatzivassiliou, G., and Thompson, C.B. (2008a). The biology of cancer: metabolic reprogramming fuels cell growth and proliferation. Cell Metab *7*, 11-20.

Deberardinis, R.J., Sayed, N., Ditsworth, D., and Thompson, C.B. (2008b). Brick by brick: metabolism and tumor cell growth. Curr Opin Genet Dev *18*, 54-61.

DeKoter, R.P., and Singh, H. (2000). Regulation of B lymphocyte and macrophage development by graded expression of PU.1. Science *288*, 1439-1441.

Dias, S., Mansson, R., Gurbuxani, S., Sigvardsson, M., and Kee, B.L. (2008). E2A proteins promote development of lymphoid-primed multipotent progenitors. Immunity *29*, 217-227.

Doulatov, S., Notta, F., Laurenti, E., and Dick, J.E. (2012). Hematopoiesis: a human perspective. Cell Stem Cell *10*, 120-136.

Dowdy, S.C., Mariani, A., Reinholz, M.M., Keeney, G.L., Spelsberg, T.C., Podratz, K.C., and Janknecht, R. (2005). Overexpression of the TGF-beta antagonist Smad7 in endometrial cancer. Gynecol Oncol *96*, 368-373.

Drabsch, Y., and ten Dijke, P. (2012). TGF-beta signalling and its role in cancer progression and metastasis. Cancer Metastasis Rev *31*, 553-568.

Dybedal, I., Guan, F., Borge, O.J., Veiby, O.P., Ramsfjell, V., Nagata, S., and Jacobsen, S.E. (1997). Transforming growth factor-beta1 abrogates Fas-induced growth suppression and apoptosis of murine bone marrow progenitor cells. Blood *90*, 3395-3403.

Eberle, D., Hegarty, B., Bossard, P., Ferre, P., and Foufelle, F. (2004). SREBP transcription factors: master regulators of lipid homeostasis. Biochimie *86*, 839-848.

Ebisawa, T., Fukuchi, M., Murakami, G., Chiba, T., Tanaka, K., Imamura, T., and Miyazono, K. (2001). Smurf1 interacts with transforming growth factor-beta type I

receptor through Smad7 and induces receptor degradation. J Biol Chem *276*, 12477-12480.

Einav, U., Tabach, Y., Getz, G., Yitzhaky, A., Ozbek, U., Amariglio, N., Izraeli, S., Rechavi, G., and Domany, E. (2005). Gene expression analysis reveals a strong signature of an interferon-induced pathway in childhood lymphoblastic leukemia as well as in breast and ovarian cancer. Oncogene *24*, 6367-6375.

Encylopedia, M.-K. (2016). blast. In Miller-Keane Encylopedia and Dictionary of Medicine, Nursing, and Allied Health.

Endo, A. (2010). A historical perspective on the discovery of statins. Proc Jpn Acad Ser B Phys Biol Sci *86*, 484-493.

Eswaran, J., Sinclair, P., Heidenreich, O., Irving, J., Russell, L.J., Hall, A., Calado, D.P., Harrison, C.J., and Vormoor, J. (2015). The pre-B-cell receptor checkpoint in acute lymphoblastic leukaemia. Leukemia *29*, 1623-1631.

Ettinger, S.L., Sobel, R., Whitmore, T.G., Akbari, M., Bradley, D.R., Gleave, M.E., and Nelson, C.C. (2004). Dysregulation of sterol response element-binding proteins and downstream effectors in prostate cancer during progression to androgen independence. Cancer Res *64*, 2212-2221.

Fears, S., Gavin, M., Zhang, D.E., Hetherington, C., Ben-David, Y., Rowley, J.D., and Nucifora, G. (1997). Functional characterization of ETV6 and ETV6/CBFA2 in the regulation of the MCSFR proximal promoter. Proc Natl Acad Sci U S A *94*, 1949-1954.

Fenrick, R., Wang, L., Nip, J., Amann, J.M., Rooney, R.J., Walker-Daniels, J., Crawford, H.C., Hulboy, D.L., Kinch, M.S., Matrisian, L.M., *et al*. (2000). TEL, a putative tumor suppressor, modulates cell growth and cell morphology of ras-transformed cells while repressing the transcription of stromelysin-1. Mol Cell Biol *20*, 5828-5839.

Fischer, M., Schwieger, M., Horn, S., Niebuhr, B., Ford, A., Roscher, S., Bergholz, U., Greaves, M., Lohler, J., and Stocking, C. (2005). Defining the oncogenic function of the TEL/AML1 (ETV6/RUNX1) fusion protein in a mouse model. Oncogene *24*, 7579-7591.

Ford, A.M., Fasching, K., Panzer-Grumayer, E.R., Koenig, M., Haas, O.A., and Greaves, M.F. (2001). Origins of "late" relapse in childhood acute lymphoblastic leukemia with TEL-AML1 fusion genes. Blood *98*, 558-564.

Ford, A.M., Palmi, C., Bueno, C., Hong, D., Cardus, P., Knight, D., Cazzaniga, G., Enver, T., and Greaves, M. (2009). The TEL-AML1 leukemia fusion gene dysregulates the TGF-beta pathway in early B lineage progenitor cells. J Clin Invest *119*, 826-836.

Fuka, G., Kantner, H.P., Grausenburger, R., Inthal, A., Bauer, E., Krapf, G., Kaindl, U., Kauer, M., Dworzak, M.N., Stoiber, D., *et al*. (2012). Silencing of ETV6/RUNX1 abrogates PI3K/AKT/mTOR signaling and impairs reconstitution of leukemia in xenografts. Leukemia *26*, 927-933.

Fuka, G., Kauer, M., Kofler, R., Haas, O.A., and Panzer-Grumayer, R. (2011). The leukemia-specific fusion gene ETV6/RUNX1 perturbs distinct key biological functions primarily by gene repression. PLoS One *6*, e26348.

Fuxa, M., and Busslinger, M. (2007). Reporter gene insertions reveal a strictly B lymphoid-specific expression pattern of Pax5 in support of its B cell identity function. J Immunol *178*, 8222-8228.

Gabitova, L., Gorin, A., and Astsaturov, I. (2014). Molecular pathways: sterols and receptor signaling in cancer. Clin Cancer Res *20*, 28-34.

Gao, L.F., Wen, L.J., Yu, H., Zhang, L., Meng, Y., Shao, Y.T., Xu, D.Q., and Zhao, X.J. (2006). Knockdown of Stat3 expression using RNAi inhibits growth of laryngeal tumors in vivo. Acta Pharmacol Sin *27*, 347-352.

Gawad, C., Koh, W., and Quake, S.R. (2014). Dissecting the clonal origins of childhood acute lymphoblastic leukemia by single-cell genomics. Proc Natl Acad Sci U S A *111*, 17947-17952.

Ge, W.L., Xu, J.F., and Hu, J. (2016). Regulation of Oral Squamous Cell Carcinoma Proliferation Through Crosstalk Between SMAD7 and CYLD. Cell Physiol Biochem *38*, 1209-1217.

Georgopoulos, K., Bigby, M., Wang, J.H., Molnar, A., Wu, P., Winandy, S., and Sharpe, A. (1994). The Ikaros gene is required for the development of all lymphoid lineages. Cell *79*, 143-156.

Geryk-Hall, M., Yang, Y., and Hughes, D.P. (2010). Driven to death: Inhibition of farnesylation increases Ras activity and promotes growth arrest and cell death [corrected]. Mol Cancer Ther *9*, 1111-1119.

Goetz, C.A., Harmon, I.R., O'Neil, J.J., Burchill, M.A., and Farrar, M.A. (2004). STAT5 activation underlies IL7 receptor-dependent B cell development. J Immunol *172*, 4770-4778.

Golub, T.R., Barker, G.F., Bohlander, S.K., Hiebert, S.W., Ward, D.C., Bray-Ward, P., Morgan, E., Raimondi, S.C., Rowley, J.D., and Gilliland, D.G. (1995). Fusion of the TEL gene on 12p13 to the AML1 gene on 21q22 in acute lymphoblastic leukemia. Proc Natl Acad Sci U S A *92*, 4917-4921.

Gounari, F., Aifantis, I., Martin, C., Fehling, H.J., Hoeflinger, S., Leder, P., von Boehmer, H., and Reizis, B. (2002). Tracing lymphopoiesis with the aid of a pTalpha-controlled reporter gene. Nat Immunol *3*, 489-496.

Greaves, M. (1999). Molecular genetics, natural history and the demise of childhood leukaemia. Eur J Cancer *35*, 1941-1953.

Greaves, M. (2006a). The causation of childhood leukemia: a paradox of progress? Discov Med *6*, 24-28.

Greaves, M. (2006b). Infection, immune responses and the aetiology of childhood leukaemia. Nat Rev Cancer *6*, 193-203.

Greaves, M.F. (1988). Speculations on the cause of childhood acute lymphoblastic leukemia. Leukemia *2*, 120-125.

Greaves, M.F., and Wiemels, J. (2003). Origins of chromosome translocations in childhood leukaemia. Nat Rev Cancer *3*, 639-649.

Guo, D., Bell, E.H., Mischel, P., and Chakravarti, A. (2014). Targeting SREBP-1-driven lipid metabolism to treat cancer. Curr Pharm Des *20*, 2619-2626.

Guo, D., Prins, R.M., Dang, J., Kuga, D., Iwanami, A., Soto, H., Lin, K.Y., Huang, T.T., Akhavan, D., Hock, M.B., *et al*. (2009). EGFR signaling through an Akt-SREBP-1-dependent, rapamycin-resistant pathway sensitizes glioblastomas to antilipogenic therapy. Sci Signal *2*, ra82.

Guo, D., Reinitz, F., Youssef, M., Hong, C., Nathanson, D., Akhavan, D., Kuga, D., Amzajerdi, A.N., Soto, H., Zhu, S., *et al*. (2011). An LXR agonist promotes glioblastoma cell death through inhibition of an EGFR/AKT/SREBP-1/LDLR-dependent pathway. Cancer Discov *1*, 442-456.

Haferlach, T., Kohlmann, A., Wieczorek, L., Basso, G., Kronnie, G.T., Bene, M.C., De Vos, J., Hernandez, J.M., Hofmann, W.K., Mills, K.I., *et al*. (2010). Clinical utility of microarray-based gene expression profiling in the diagnosis and subclassification of leukemia: report from the International Microarray Innovations in Leukemia Study Group. J Clin Oncol *28*, 2529-2537.

Han, G., Bian, L., Li, F., Cotrim, A., Wang, D., Lu, J., Deng, Y., Bird, G., Sowers, A., Mitchell, J.B., *et al*. (2013). Preventive and therapeutic effects of Smad7 on radiation-induced oral mucositis. Nat Med *19*, 421-428.

Han, G., Li, A.G., Liang, Y.Y., Owens, P., He, W., Lu, S., Yoshimatsu, Y., Wang, D., Ten Dijke, P., Lin, X., *et al*. (2006). Smad7-induced beta-catenin degradation alters epidermal appendage development. Dev Cell *11*, 301-312.

Hanyu, A., Ishidou, Y., Ebisawa, T., Shimanuki, T., Imamura, T., and Miyazono, K. (2001). The N domain of Smad7 is essential for specific inhibition of transforming growth factor-beta signaling. J Cell Biol *155*, 1017-1027.

Harisa, G.I., and Alanazi, F.K. (2014). Low density lipoprotein bionanoparticles: From cholesterol transport to delivery of anti-cancer drugs. Saudi Pharm J *22*, 504-515.

Harris, N.L., Jaffe, E.S., Diebold, J., Flandrin, G., Muller-Hermelink, H.K., Vardiman, J., Lister, T.A., and Bloomfield, C.D. (1999). The World Health Organization classification of neoplastic diseases of the hematopoietic and lymphoid tissues. Report of the Clinical Advisory Committee meeting, Airlie House, Virginia, November, 1997. Ann Oncol *10*, 1419-1432.

Hayashi, H., Abdollah, S., Qiu, Y., Cai, J., Xu, Y.Y., Grinnell, B.W., Richardson, M.A., Topper, J.N., Gimbrone, M.A., Jr., Wrana, J.L., *et al*. (1997). The MAD-related protein Smad7 associates with the TGFbeta receptor and functions as an antagonist of TGFbeta signaling. Cell *89*, 1165-1173.

Hess, J.L., Yu, B.D., Li, B., Hanson, R., and Korsmeyer, S.J. (1997). Defects in yolk sac hematopoiesis in Mll-null embryos. Blood *90*, 1799-1806.

Hiebert, S.W., Sun, W., Davis, J.N., Golub, T., Shurtleff, S., Buijs, A., Downing, J.R., Grosveld, G., Roussell, M.F., Gilliland, D.G., *et al*. (1996). The t(12;21) translocation converts AML-1B from an activator to a repressor of transcription. Mol Cell Biol *16*, 1349-1355.

Ho, H.H., and Ivashkiv, L.B. (2006). Role of STAT3 in type I interferon responses. Negative regulation of STAT1-dependent inflammatory gene activation. J Biol Chem *281*, 14111-14118.

Hock, H., Meade, E., Medeiros, S., Schindler, J.W., Valk, P.J., Fujiwara, Y., and Orkin, S.H. (2004). Tel/Etv6 is an essential and selective regulator of adult hematopoietic stem cell survival. Genes Dev *18*, 2336-2341.

Hong, D., Gupta, R., Ancliff, P., Atzberger, A., Brown, J., Soneji, S., Green, J., Colman, S., Piacibello, W., Buckle, V., *et al*. (2008). Initiating and cancer-propagating cells in TEL-AML1-associated childhood leukemia. Science *319*, 336-339.

Hong, S., Kim, H.Y., Kim, J., Ha, H.T., Kim, Y.M., Bae, E., Kim, T.H., Lee, K.C., and Kim, S.J. (2013). Smad7 protein induces interferon regulatory factor 1-dependent transcriptional activation of caspase 8 to restore tumor necrosis factor-related apoptosis-inducing ligand (TRAIL)-mediated apoptosis. J Biol Chem *288*, 3560-3570.

Horton, J.D., Goldstein, J.L., and Brown, M.S. (2002). SREBPs: activators of the complete program of cholesterol and fatty acid synthesis in the liver. J Clin Invest *109*, 1125-1131.

Howe, J.R., Roth, S., Ringold, J.C., Summers, R.W., Jarvinen, H.J., Sistonen, P., Tomlinson, I.P., Houlston, R.S., Bevan, S., Mitros, F.A., *et al*. (1998). Mutations in the SMAD4/DPC4 gene in juvenile polyposis. Science *280*, 1086-1088.

Huang, W.C., Li, X., Liu, J., Lin, J., and Chung, L.W. (2012). Activation of androgen receptor, lipogenesis, and oxidative stress converged by SREBP-1 is responsible for regulating growth and progression of prostate cancer cells. Mol Cancer Res *10*, 133-142.

Ichikawa, M., Asai, T., Saito, T., Seo, S., Yamazaki, I., Yamagata, T., Mitani, K., Chiba, S., Ogawa, S., Kurokawa, M., *et al*. (2004). AML-1 is required for megakaryocytic maturation and lymphocytic differentiation, but not for maintenance of hematopoietic stem cells in adult hematopoiesis. Nat Med *10*, 299-304.

Inaba, H., Greaves, M., and Mullighan, C.G. (2013). Acute lymphoblastic leukaemia. Lancet *381*, 1943-1955.

Iwamaru, A., Szymanski, S., Iwado, E., Aoki, H., Yokoyama, T., Fokt, I., Hess, K., Conrad, C., Madden, T., Sawaya, R., *et al*. (2007). A novel inhibitor of the STAT3 pathway induces apoptosis in malignant glioma cells both in vitro and in vivo. Oncogene *26*, 2435-2444.

Iwasaki, H., and Akashi, K. (2007). Hematopoietic developmental pathways: on cellular basis. Oncogene *26*, 6687-6696.

J. Thomas, T.P.S., Dev K.Singh (2012). Cholesterol: Biosynthesis, Functional Diversity, Homeostatis and Regulation by Natural Products. In Biochemistry (New York).

Jacobsen, F.W., Stokke, T., and Jacobsen, S.E. (1995). Transforming growth factor-beta potently inhibits the viability-promoting activity of stem cell factor and other cytokines and induces apoptosis of primitive murine hematopoietic progenitor cells. Blood *86*, 2957-2966.

Javelaud, D., Mohammad, K.S., McKenna, C.R., Fournier, P., Luciani, F., Niewolna, M., Andre, J., Delmas, V., Larue, L., Guise, T.A., *et al*. (2007). Stable overexpression of Smad7 in human melanoma cells impairs bone metastasis. Cancer Res *67*, 2317-2324.

Jenkins, B.J., Grail, D., Nheu, T., Najdovska, M., Wang, B., Waring, P., Inglese, M., McLoughlin, R.M., Jones, S.A., Topley, N., *et al*. (2005). Hyperactivation of Stat3 in

gp130 mutant mice promotes gastric hyperproliferation and desensitizes TGF-beta signaling. Nat Med *11*, 845-852.

Jude, C.D., Climer, L., Xu, D., Artinger, E., Fisher, J.K., and Ernst, P. (2007). Unique and independent roles for MLL in adult hematopoietic stem cells and progenitors. Cell Stem Cell *1*, 324-337.

Kaartinen, V., Voncken, J.W., Shuler, C., Warburton, D., Bu, D., Heisterkamp, N., and Groffen, J. (1995). Abnormal lung development and cleft palate in mice lacking TGF-beta 3 indicates defects of epithelial-mesenchymal interaction. Nat Genet *11*, 415-421.

Kamisuki, S., Mao, Q., Abu-Elheiga, L., Gu, Z., Kugimiya, A., Kwon, Y., Shinohara, T., Kawazoe, Y., Sato, S., Asakura, K., *et al*. (2009). A small molecule that blocks fat synthesis by inhibiting the activation of SREBP. Chem Biol *16*, 882-892.

Kang, K., Robinson, G.W., and Hennighausen, L. (2013). Comprehensive meta-analysis of Signal Transducers and Activators of Transcription (STAT) genomic binding patterns discerns cell-specific cis-regulatory modules. BMC Genomics *14*, 4.

Kinlen, L. (1988). Evidence for an infective cause of childhood leukaemia: comparison of a Scottish new town with nuclear reprocessing sites in Britain. Lancet *2*, 1323-1327.

Kondo, M., Scherer, D.C., Miyamoto, T., King, A.G., Akashi, K., Sugamura, K., and Weissman, I.L. (2000). Cell-fate conversion of lymphoid-committed progenitors by instructive actions of cytokines. Nature *407*, 383-386.

Kornblau, S.M., Banker, D.E., Stirewalt, D., Shen, D., Lemker, E., Verstovsek, S., Estrov, Z., Faderl, S., Cortes, J., Beran, M., *et al*. (2007). Blockade of adaptive defensive changes in cholesterol uptake and synthesis in AML by the addition of pravastatin to idarubicin + high-dose Ara-C: a phase 1 study. Blood *109*, 2999-3006.

Koskela, H.L., Eldfors, S., Ellonen, P., van Adrichem, A.J., Kuusanmaki, H., Andersson, E.I., Lagstrom, S., Clemente, M.J., Olson, T., Jalkanen, S.E., *et al*. (2012). Somatic STAT3 mutations in large granular lymphocytic leukemia. N Engl J Med *366*, 1905-1913.

Kretzschmar, M. (2000). Transforming growth factor-beta and breast cancer: Transforming growth factor-beta/SMAD signaling defects and cancer. Breast Cancer Res *2*, 107-115.

Kulkarni, A.B., Huh, C.G., Becker, D., Geiser, A., Lyght, M., Flanders, K.C., Roberts, A.B., Sporn, M.B., Ward, J.M., and Karlsson, S. (1993). Transforming growth factor beta 1 null mutation in mice causes excessive inflammatory response and early death. Proc Natl Acad Sci U S A *90*, 770-774.

Kume, S., Haneda, M., Kanasaki, K., Sugimoto, T., Araki, S., Isshiki, K., Isono, M., Uzu, T., Guarente, L., Kashiwagi, A., *et al*. (2007). SIRT1 inhibits transforming growth factor beta-induced apoptosis in glomerular mesangial cells via Smad7 deacetylation. J Biol Chem *282*, 151-158.

Larochelle, A., Savona, M., Wiggins, M., Anderson, S., Ichwan, B., Keyvanfar, K., Morrison, S.J., and Dunbar, C.E. (2011). Human and rhesus macaque hematopoietic stem cells cannot be purified based only on SLAM family markers. Blood *117*, 1550-1554.

Larsson, J., Goumans, M.J., Sjostrand, L.J., van Rooijen, M.A., Ward, D., Leveen, P., Xu, X., ten Dijke, P., Mummery, C.L., and Karlsson, S. (2001). Abnormal angiogenesis but intact hematopoietic potential in TGF-beta type I receptor-deficient mice. Embo j *20*, 1663-1673.

Larsson, J., and Karlsson, S. (2005). The role of Smad signaling in hematopoiesis. Oncogene *24*, 5676-5692.

Lausten-Thomsen, U., Madsen, H.O., Vestergaard, T.R., Hjalgrim, H., Nersting, J., and Schmiegelow, K. (2011). Prevalence of t(12;21)[ETV6-RUNX1]-positive cells in healthy neonates. Blood *117*, 186-189.

Lawrence, H.J., Christensen, J., Fong, S., Hu, Y.L., Weissman, I., Sauvageau, G., Humphries, R.K., and Largman, C. (2005). Loss of expression of the Hoxa-9 homeobox gene impairs the proliferation and repopulating ability of hematopoietic stem cells. Blood *106*, 3988-3994.

Lebman, D.A., and Edmiston, J.S. (1999). The role of TGF-beta in growth, differentiation, and maturation of B lymphocytes. Microbes Infect *1*, 1297-1304.

Lebrun, J.-J. (2012). The dual role of TGF in human cancer: from tumor suppression to cancer metastasis. ISRN molecular biology *2012*.

Letterio, J.J., and Roberts, A.B. (1998). Regulation of immune responses by TGF-beta. Annu Rev Immunol *16*, 137-161.

Levy, D.E., and Lee, C.K. (2002). What does Stat3 do? J Clin Invest *109*, 1143-1148.

Li, H.Y., Appelbaum, F.R., Willman, C.L., Zager, R.A., and Banker, D.E. (2003). Cholesterol-modulating agents kill acute myeloid leukemia cells and sensitize them to therapeutics by blocking adaptive cholesterol responses. Blood *101*, 3628-3634.

Li, M., Jones, L., Gaillard, C., Binnewies, M., Ochoa, R., Garcia, E., Lam, V., Wei, G., Yang, W., Lobe, C., *et al*. (2013). Initially disadvantaged, TEL-AML1 cells expand and initiate leukemia in response to irradiation and cooperating mutations. Leukemia *27*, 1570-1573.

Li, X., Chen, Y.T., Hu, P., and Huang, W.C. (2014). Fatostatin displays high antitumor activity in prostate cancer by blocking SREBP-regulated metabolic pathways and androgen receptor signaling. Mol Cancer Ther *13*, 855-866.

Li, Y.S., Wasserman, R., Hayakawa, K., and Hardy, R.R. (1996). Identification of the earliest B lineage stage in mouse bone marrow. Immunity *5*, 527-535.

Lilljebjorn, H., Soneson, C., Andersson, A., Heldrup, J., Behrendtz, M., Kawamata, N., Ogawa, S., Koeffler, H.P., Mitelman, F., Johansson, B., *et al*. (2010). The correlation pattern of acquired copy number changes in 164 ETV6/RUNX1-positive childhood acute lymphoblastic leukemias. Hum Mol Genet *19*, 3150-3158.

Lin, H., and Grosschedl, R. (1995). Failure of B-cell differentiation in mice lacking the transcription factor EBF. Nature *376*, 263-267.

Linabery, A.M., and Ross, J.A. (2008). Trends in childhood cancer incidence in the U.S. (1992-2004). Cancer *112*, 416-432.

Linka, Y., Ginzel, S., Kruger, M., Novosel, A., Gombert, M., Kremmer, E., Harbott, J., Thiele, R., Borkhardt, A., and Landgraf, P. (2013). The impact of TEL-AML1 (ETV6-RUNX1) expression in precursor B cells and implications for leukaemia using three different genome-wide screening methods. Blood Cancer J *3*, e151.

Liu, Y., Elf, S.E., Miyata, Y., Sashida, G., Liu, Y., Huang, G., Di Giandomenico, S., Lee, J.M., Deblasio, A., Menendez, S., *et al*. (2009). p53 regulates hematopoietic stem cell quiescence. Cell Stem Cell *4*, 37-48.

Lopez, R.G., Carron, C., Oury, C., Gardellin, P., Bernard, O., and Ghysdael, J. (1999). TEL is a sequence-specific transcriptional repressor. J Biol Chem *274*, 30132-30138.

Luwor, R.B., Baradaran, B., Taylor, L.E., Iaria, J., Nheu, T.V., Amiry, N., Hovens, C.M., Wang, B., Kaye, A.H., and Zhu, H.J. (2013). Targeting Stat3 and Smad7 to restore TGF-beta cytostatic regulation of tumor cells in vitro and in vivo. Oncogene *32*, 2433-2441.

Lyons, R., Williams, O., Morrow, M., Sebire, N., Hubank, M., and Anderson, J. (2010). The RAC specific guanine nucleotide exchange factor Asef functions

downstream from TEL-AML1 to promote leukaemic transformation. Leuk Res *34*, 109-115.

Lyons, R.M., Keski-Oja, J., and Moses, H.L. (1988). Proteolytic activation of latent transforming growth factor-beta from fibroblast-conditioned medium. J Cell Biol *106*, 1659-1665.

Madden, E.A., Bishop, E.J., Fiskin, A.M., and Melnykovych, G. (1986). Possible role of cholesterol in the susceptibility of a human acute lymphoblastic leukemia cell line to dexamethasone. Cancer Res *46*, 617-622.

Maia, A.T., Ford, A.M., Jalali, G.R., Harrison, C.J., Taylor, G.M., Eden, O.B., and Greaves, M.F. (2001). Molecular tracking of leukemogenesis in a triplet pregnancy. Blood *98*, 478-482.

Mangolini, M., de Boer, J., Walf-Vorderwulbecke, V., Pieters, R., den Boer, M.L., and Williams, O. (2013). STAT3 mediates oncogenic addiction to TEL-AML1 in t(12;21) acute lymphoblastic leukemia. Blood *122*, 542-549.

Marculescu, R., Le, T., Simon, P., Jaeger, U., and Nadel, B. (2002). V(D)J-mediated translocations in lymphoid neoplasms: a functional assessment of genomic instability by cryptic sites. J Exp Med *195*, 85-98.

Maritano, D., Sugrue, M.L., Tininini, S., Dewilde, S., Strobl, B., Fu, X., Murray-Tait, V., Chiarle, R., and Poli, V. (2004). The STAT3 isoforms alpha and beta have unique and specific functions. Nat Immunol *5*, 401-409.

Massague, J. (1998). TGF-beta signal transduction. Annu Rev Biochem *67*, 753-791.

Massague, J. (2012). TGFbeta signalling in context. Nat Rev Mol Cell Biol *13*, 616-630.

Massague, J., and Chen, Y.G. (2000). Controlling TGF-beta signaling. Genes Dev *14*, 627-644.

Massague, J., Seoane, J., and Wotton, D. (2005). Smad transcription factors. Genes Dev *19*, 2783-2810.

Matsuoka, S., Ebihara, Y., Xu, M., Ishii, T., Sugiyama, D., Yoshino, H., Ueda, T., Manabe, A., Tanaka, R., Ikeda, Y., *et al*. (2001). CD34 expression on long-term repopulating hematopoietic stem cells changes during developmental stages. Blood *97*, 419-425.

McDermott, S.P., Eppert, K., Lechman, E.R., Doedens, M., and Dick, J.E. (2010). Comparison of human cord blood engraftment between immunocompromised mouse strains. Blood *116*, 193-200.

McMahon, K.A., Hiew, S.Y., Hadjur, S., Veiga-Fernandes, H., Menzel, U., Price, A.J., Kioussis, D., Williams, O., and Brady, H.J. (2007). Mll has a critical role in fetal and adult hematopoietic stem cell self-renewal. Cell Stem Cell *1*, 338-345.

Melchers, F. (2015). Checkpoints that control B cell development. J Clin Invest *125*, 2203-2210.

Metcalf, D. (2010). The colony-stimulating factors and cancer. Nat Rev Cancer *10*, 425-434.

Mikula, M., Proell, V., Fischer, A.N., and Mikulits, W. (2006). Activated hepatic stellate cells induce tumor progression of neoplastic hepatocytes in a TGF-beta dependent fashion. J Cell Physiol *209*, 560-567.

Millar, S.E. (2006). Smad7: licensed to kill beta-catenin. Dev Cell *11*, 274-276.

Mori, H., Colman, S.M., Xiao, Z., Ford, A.M., Healy, L.E., Donaldson, C., Hows, J.M., Navarrete, C., and Greaves, M. (2002). Chromosome translocations and covert leukemic clones are generated during normal fetal development. Proc Natl Acad Sci U S A *99*, 8242-8247.

Moroy, T., and Khandanpour, C. (2011). Growth factor independence 1 (Gfi1) as a regulator of lymphocyte development and activation. Semin Immunol *23*, 368-378.

Morrow, M., Horton, S., Kioussis, D., Brady, H.J., and Williams, O. (2004). TEL-AML1 promotes development of specific hematopoietic lineages consistent with preleukemic activity. Blood *103*, 3890-3896.

Morrow, M., Samanta, A., Kioussis, D., Brady, H.J., and Williams, O. (2007). TEL-AML1 preleukemic activity requires the DNA binding domain of AML1 and the dimerization and corepressor binding domains of TEL. Oncogene *26*, 4404-4414.

Mullighan, C.G. (2012). Molecular genetics of B-precursor acute lymphoblastic leukemia. J Clin Invest *122*, 3407-3415.

Mullighan, C.G., Goorha, S., Radtke, I., Miller, C.B., Coustan-Smith, E., Dalton, J.D., Girtman, K., Mathew, S., Ma, J., Pounds, S.B., *et al*. (2007). Genome-wide analysis of genetic alterations in acute lymphoblastic leukaemia. Nature *446*, 758-764.

Mullighan, C.G., Miller, C.B., Radtke, I., Phillips, L.A., Dalton, J., Ma, J., White, D., Hughes, T.P., Le Beau, M.M., Pui, C.H., *et al*. (2008a). BCR-ABL1 lymphoblastic leukaemia is characterized by the deletion of Ikaros. Nature *453*, 110-114.

Mullighan, C.G., Phillips, L.A., Su, X., Ma, J., Miller, C.B., Shurtleff, S.A., and Downing, J.R. (2008b). Genomic analysis of the clonal origins of relapsed acute lymphoblastic leukemia. Science *322*, 1377-1380.

Nakahata, S., Yamazaki, S., Nakauchi, H., and Morishita, K. (2010). Downregulation of ZEB1 and overexpression of Smad7 contribute to resistance to TGF-beta1-mediated growth suppression in adult T-cell leukemia/lymphoma. Oncogene *29*, 4157-4169.

Nakao, A., Afrakhte, M., Moren, A., Nakayama, T., Christian, J.L., Heuchel, R., Itoh, S., Kawabata, M., Heldin, N.E., Heldin, C.H., *et al*. (1997). Identification of Smad7, a TGFbeta-inducible antagonist of TGF-beta signalling. Nature *389*, 631-635.

Nerlov, C., Querfurth, E., Kulessa, H., and Graf, T. (2000). GATA-1 interacts with the myeloid PU.1 transcription factor and represses PU.1-dependent transcription. Blood *95*, 2543-2551.

Nicolas, F.J., and Hill, C.S. (2003). Attenuation of the TGF-beta-Smad signaling pathway in pancreatic tumor cells confers resistance to TGF-beta-induced growth arrest. Oncogene *22*, 3698-3711.

Niu, G., Wright, K.L., Ma, Y., Wright, G.M., Huang, M., Irby, R., Briggs, J., Karras, J., Cress, W.D., Pardoll, D., *et al*. (2005). Role of Stat3 in regulating p53 expression and function. Mol Cell Biol *25*, 7432-7440.

Notta, F., Doulatov, S., Laurenti, E., Poeppl, A., Jurisica, I., and Dick, J.E. (2011). Isolation of single human hematopoietic stem cells capable of long-term multilineage engraftment. Science *333*, 218-221.

Nunez, C., Nishimoto, N., Gartland, G.L., Billips, L.G., Burrows, P.D., Kubagawa, H., and Cooper, M.D. (1996). B cells are generated throughout life in humans. J Immunol *156*, 866-872.

Nutt, S.L., Heavey, B., Rolink, A.G., and Busslinger, M. (1999). Commitment to the B-lymphoid lineage depends on the transcription factor Pax5. Nature *401*, 556-562.

Nutt, S.L., Urbanek, P., Rolink, A., and Busslinger, M. (1997). Essential functions of Pax5 (BSAP) in pro-B cell development: difference between fetal and adult B lymphopoiesis and reduced V-to-DJ recombination at the IgH locus. Genes Dev *11*, 476-491.

Oida, T., and Weiner, H.L. (2010). Depletion of TGF-beta from fetal bovine serum. J Immunol Methods *362*, 195-198.

Okada, H., Watanabe, T., Niki, M., Takano, H., Chiba, N., Yanai, N., Tani, K., Hibino, H., Asano, S., Mucenski, M.L., *et al*. (1998). AML1(-/-) embryos do not

express certain hematopoiesis-related gene transcripts including those of the PU.1 gene. Oncogene *17*, 2287-2293.

Okuda, T., van Deursen, J., Hiebert, S.W., Grosveld, G., and Downing, J.R. (1996). AML1, the target of multiple chromosomal translocations in human leukemia, is essential for normal fetal liver hematopoiesis. Cell *84*, 321-330.

Orkin, S.H. (2000). Diversification of haematopoietic stem cells to specific lineages. Nat Rev Genet *1*, 57-64.

Orkin, S.H., and Zon, L.I. (2002). Hematopoiesis and stem cells: plasticity versus developmental heterogeneity. Nat Immunol *3*, 323-328.

Osato, M., Asou, N., Abdalla, E., Hoshino, K., Yamasaki, H., Okubo, T., Suzushima, H., Takatsuki, K., Kanno, T., Shigesada, K., *et al*. (1999). Biallelic and heterozygous point mutations in the runt domain of the AML1/PEBP2alphaB gene associated with myeloblastic leukemias. Blood *93*, 1817-1824.

Oshima, M., Oshima, H., and Taketo, M.M. (1996). TGF-beta receptor type II deficiency results in defects of yolk sac hematopoiesis and vasculogenesis. Dev Biol *179*, 297-302.

Panzer-Grumayer, E.R., Cazzaniga, G., van der Velden, V.H., del Giudice, L., Peham, M., Mann, G., Eckert, C., Schrauder, A., Germano, G., Harbott, J., *et al*. (2005). Immunogenotype changes prevail in relapses of young children with TEL-AML1-positive acute lymphoblastic leukemia and derive mainly from clonal selection. Clin Cancer Res *11*, 7720-7727.

Papaemmanuil, E., Rapado, I., Li, Y., Potter, N.E., Wedge, D.C., Tubio, J., and Alexandrov, L.B. (2014). RAG-mediated recombination is the predominant driver of oncogenic rearrangement in ETV6-RUNX1 acute lymphoblastic leukemia. *46*, 116-125.

Peschon, J.J., Morrissey, P.J., Grabstein, K.H., Ramsdell, F.J., Maraskovsky, E., Gliniak, B.C., Park, L.S., Ziegler, S.F., Williams, D.E., Ware, C.B., *et al*. (1994). Early lymphocyte expansion is severely impaired in interleukin 7 receptor-deficient mice. J Exp Med *180*, 1955-1960.

Petrie, K., Guidez, F., Howell, L., Healy, L., Waxman, S., Greaves, M., and Zelent, A. (2003). The histone deacetylase 9 gene encodes multiple protein isoforms. J Biol Chem *278*, 16059-16072.

Pieper, K., Grimbacher, B., and Eibel, H. (2013). B-cell biology and development. J Allergy Clin Immunol *131*, 959-971.

Poirel, H., Oury, C., Carron, C., Duprez, E., Laabi, Y., Tsapis, A., Romana, S.P., Mauchauffe, M., Le Coniat, M., Berger, R., *et al*. (1997). The TEL gene products: nuclear phosphoproteins with DNA binding properties. Oncogene *14*, 349-357.

Prieyl, J.A., and LeBien, T.W. (1996). Interleukin 7 independent development of human B cells. Proc Natl Acad Sci U S A *93*, 10348-10353.

Puel, A., Ziegler, S.F., Buckley, R.H., and Leonard, W.J. (1998). Defective IL7R expression in T(-)B(+)NK(+) severe combined immunodeficiency. Nat Genet *20*, 394-397.

Pui, C.H., Carroll, W.L., Meshinchi, S., and Arceci, R.J. (2011). Biology, risk stratification, and therapy of pediatric acute leukemias: an update. J Clin Oncol *29*, 551-565.

Pui, C.H., Robison, L.L., and Look, A.T. (2008). Acute lymphoblastic leukaemia. Lancet *371*, 1030-1043.

Pui, C.H., Schrappe, M., Ribeiro, R.C., and Niemeyer, C.M. (2004). Childhood and adolescent lymphoid and myeloid leukemia. Hematology Am Soc Hematol Educ Program, 118-145.

Rawson, R.B. (2003). The SREBP pathway--insights from Insigs and insects. Nat Rev Mol Cell Biol *4*, 631-640.

Reya, T., and Clevers, H. (2005). Wnt signalling in stem cells and cancer. Nature *434*, 843-850.

Reynaud, D., Demarco, I.A., Reddy, K.L., Schjerven, H., Bertolino, E., Chen, Z., Smale, S.T., Winandy, S., and Singh, H. (2008). Regulation of B cell fate commitment and immunoglobulin heavy-chain gene rearrangements by Ikaros. Nat Immunol *9*, 927-936.

Roberts, A.B., and Wakefield, L.M. (2003). The two faces of transforming growth factor beta in carcinogenesis. Proc Natl Acad Sci U S A *100*, 8621-8623.

Romana, S.P., Le Coniat, M., Poirel, H., Marynen, P., Bernard, O., and Berger, R. (1996). Deletion of the short arm of chromosome 12 is a secondary event in acute lymphoblastic leukemia with t(12;21). Leukemia *10*, 167-170.

Romana, S.P., Mauchauffe, M., Le Coniat, M., Chumakov, I., Le Paslier, D., Berger, R., and Bernard, O.A. (1995). The t(12;21) of acute lymphoblastic leukemia results in a tel-AML1 gene fusion. Blood *85*, 3662-3670.

Rompaey, L.V., Potter, M., Adams, C., and Grosveld, G. (2000). Tel induces a G1 arrest and suppresses Ras-induced transformation. Oncogene *19*, 5244-5250.

Rouce, R.H., Shaim, H., Sekine, T., Weber, G., Ballard, B., Ku, S., Barese, C., Murali, V., Wu, M.F., Liu, H., *et al*. (2015). The TGF-beta/SMAD pathway is an important mechanism for NK cell immune evasion in childhood B-acute lymphoblastic leukemia. Leukemia.

Roudaia, L., Cheney, M.D., Manuylova, E., Chen, W., Morrow, M., Park, S., Lee, C.T., Kaur, P., Williams, O., Bushweller, J.H., *et al*. (2009). CBFbeta is critical for AML1-ETO and TEL-AML1 activity. Blood *113*, 3070-3079.

Rumfelt, L.L., Zhou, Y., Rowley, B.M., Shinton, S.A., and Hardy, R.R. (2006). Lineage specification and plasticity in CD19- early B cell precursors. J Exp Med *203*, 675-687.

Sandel, P.C., and Monroe, J.G. (1999). Negative selection of immature B cells by receptor editing or deletion is determined by site of antigen encounter. Immunity *10*, 289-299.

Sanford, L.P., Ormsby, I., Gittenberger-de Groot, A.C., Sariola, H., Friedman, R., Boivin, G.P., Cardell, E.L., and Doetschman, T. (1997). TGFbeta2 knockout mice have multiple developmental defects that are non-overlapping with other TGFbeta knockout phenotypes. Development *124*, 2659-2670.

Scandura, J.M., Boccuni, P., Massague, J., and Nimer, S.D. (2004). Transforming growth factor beta-induced cell cycle arrest of human hematopoietic cells requires p57KIP2 up-regulation. Proc Natl Acad Sci U S A *101*, 15231-15236.

Schindler, J.W., Van Buren, D., Foudi, A., Krejci, O., Qin, J., Orkin, S.H., and Hock, H. (2009). TEL-AML1 corrupts hematopoietic stem cells to persist in the bone marrow and initiate leukemia. Cell Stem Cell *5*, 43-53.

Schroder, M., Kroeger, K.M., Volk, H.D., Eidne, K.A., and Grutz, G. (2004). Preassociation of nonactivated STAT3 molecules demonstrated in living cells using bioluminescence resonance energy transfer: a new model of STAT activation? J Leukoc Biol *75*, 792-797.

Sheen, C., Vincent, T., Barrett, D., Horwitz, E.M., Hulitt, J., Strong, E., Grupp, S.A., and Teachey, D.T. (2011). Statins are active in acute lymphoblastic leukaemia (ALL): a therapy that may treat ALL and prevent avascular necrosis. Br J Haematol *155*, 403-407.

Shimano, H. (2001). Sterol regulatory element-binding proteins (SREBPs): transcriptional regulators of lipid synthetic genes. Prog Lipid Res *40*, 439-452.

Shimano, H., Horton, J.D., Hammer, R.E., Shimomura, I., Brown, M.S., and Goldstein, J.L. (1996). Overproduction of cholesterol and fatty acids causes massive liver enlargement in transgenic mice expressing truncated SREBP-1a. J Clin Invest *98*, 1575-1584.

Shimano, H., Horton, J.D., Shimomura, I., Hammer, R.E., Brown, M.S., and Goldstein, J.L. (1997). Isoform 1c of sterol regulatory element binding protein is less active than isoform 1a in livers of transgenic mice and in cultured cells. J Clin Invest *99*, 846-854.

Shimomura, I., Shimano, H., Horton, J.D., Goldstein, J.L., and Brown, M.S. (1997). Differential expression of exons 1a and 1c in mRNAs for sterol regulatory element binding protein-1 in human and mouse organs and cultured cells. J Clin Invest *99*, 838-845.

Simonsson, M., Heldin, C.H., Ericsson, J., and Gronroos, E. (2005). The balance between acetylation and deacetylation controls Smad7 stability. J Biol Chem *280*, 21797-21803.

Sive, J.I., and Gottgens, B. (2014). Transcriptional network control of normal and leukaemic haematopoiesis. Exp Cell Res *329*, 255-264.

Slattery, M.L., Herrick, J., Curtin, K., Samowitz, W., Wolff, R.K., Caan, B.J., Duggan, D., Potter, J.D., and Peters, U. (2010). Increased risk of colon cancer associated with a genetic polymorphism of SMAD7. Cancer Res *70*, 1479-1485.

Smith, E.M., Gisler, R., and Sigvardsson, M. (2002). Cloning and characterization of a promoter flanking the early B cell factor (EBF) gene indicates roles for E-proteins and autoregulation in the control of EBF expression. J Immunol *169*, 261-270.

Snyder, M., Huang, X.Y., and Zhang, J.J. (2008). Identification of novel direct Stat3 target genes for control of growth and differentiation. J Biol Chem *283*, 3791-3798.

Soderberg, S.S., Karlsson, G., and Karlsson, S. (2009). Complex and context dependent regulation of hematopoiesis by TGF-beta superfamily signaling. Ann N Y Acad Sci *1176*, 55-69.

Somasundaram, R., Prasad, M.A., Ungerback, J., and Sigvardsson, M. (2015). Transcription factor networks in B-cell differentiation link development to acute lymphoid leukemia. Blood *126*, 144-152.

Stams, W.A., Beverloo, H.B., den Boer, M.L., de Menezes, R.X., Stigter, R.L., van Drunen, E., Ramakers-van-Woerden, N.L., Loonen, A.H., van Wering, E.R., Janka-Schaub, G.E., *et al*. (2006). Incidence of additional genetic changes in the TEL and AML1 genes in DCOG and COALL-treated t(12;21)-positive pediatric ALL, and their relation with drug sensitivity and clinical outcome. Leukemia *20*, 410-416.

Starr, R., Willson, T.A., Viney, E.M., Murray, L.J., Rayner, J.R., Jenkins, B.J., Gonda, T.J., Alexander, W.S., Metcalf, D., Nicola, N.A., *et al*. (1997). A family of cytokine-inducible inhibitors of signalling. Nature *387*, 917-921.

Stolfi, C., De Simone, V., Colantoni, A., Franze, E., Ribichini, E., Fantini, M.C., Caruso, R., Monteleone, I., Sica, G.S., Sileri, P., *et al*. (2014). A functional role for Smad7 in sustaining colon cancer cell growth and survival. Cell Death Dis *5*, e1073.

Stolfi, C., Marafini, I., De Simone, V., Pallone, F., and Monteleone, G. (2013). The dual role of Smad7 in the control of cancer growth and metastasis. Int J Mol Sci *14*, 23774-23790.

Swaminathan, S., Klemm, L., Park, E., Papaemmanuil, E., Ford, A., Kweon, S.M., Trageser, D., Hasselfeld, B., Henke, N., Mooster, J., *et al*. (2015). Mechanisms of clonal evolution in childhood acute lymphoblastic leukemia. Nat Immunol *16*, 766-774.

Tajima, F., Deguchi, T., Laver, J.H., Zeng, H., and Ogawa, M. (2001). Reciprocal expression of CD38 and CD34 by adult murine hematopoietic stem cells. Blood *97*, 2618-2624.

Till, J.E., and McCulloch, E.A. (1980). Hemopoietic stem cell differentiation. Biochim Biophys Acta *605*, 431-459.

Topka, S., Vijai, J., Walsh, M.F., Jacobs, L., Maria, A., Villano, D., Gaddam, P., Wu, G., McGee, R.B., Quinn, E., *et al*. (2015). Germline ETV6 Mutations Confer Susceptibility to Acute Lymphoblastic Leukemia and Thrombocytopenia. PLoS Genet *11*, e1005262.

Travis, M.A., and Sheppard, D. (2014). TGF-beta activation and function in immunity. Annu Rev Immunol *32*, 51-82.

Tsai, A.G., Lu, H., Raghavan, S.C., Muschen, M., Hsieh, C.L., and Lieber, M.R. (2008). Human chromosomal translocations at CpG sites and a theoretical basis for their lineage and stage specificity. Cell *135*, 1130-1142.

Tsapogas, P., Zandi, S., Ahsberg, J., Zetterblad, J., Welinder, E., Jonsson, J.I., Mansson, R., Qian, H., and Sigvardsson, M. (2011). IL-7 mediates Ebf-1-dependent lineage restriction in early lymphoid progenitors. Blood *118*, 1283-1290.

Tsuzuki, S., and Seto, M. (2013). TEL (ETV6)-AML1 (RUNX1) initiates self-renewing fetal pro-B cells in association with a transcriptional program shared with embryonic stem cells in mice. Stem Cells *31*, 236-247.

Tsuzuki, S., Seto, M., Greaves, M., and Enver, T. (2004). Modeling first-hit functions of the t(12;21) TEL-AML1 translocation in mice. Proc Natl Acad Sci U S A *101*, 8443-8448.

Uchida, H., Downing, J.R., Miyazaki, Y., Frank, R., Zhang, J., and Nimer, S.D. (1999). Three distinct domains in TEL-AML1 are required for transcriptional repression of the IL-3 promoter. Oncogene *18*, 1015-1022.

Uchida, H., Zhang, J., and Nimer, S.D. (1997). AML1A and AML1B can transactivate the human IL-3 promoter. J Immunol *158*, 2251-2258.

Vaidya, A., and Kale, V.P. (2015). TGF-beta signaling and its role in the regulation of hematopoietic stem cells. Syst Synth Biol *9*, 1-10.

van Delft, F.W., Horsley, S., Colman, S., Anderson, K., Bateman, C., Kempski, H., Zuna, J., Eckert, C., Saha, V., Kearney, L., *et al*. (2011). Clonal origins of relapse in ETV6-RUNX1 acute lymphoblastic leukemia. Blood *117*, 6247-6254.

van der Weide, K., de Jonge-Peeters, S., Huls, G., Fehrmann, R.S., Schuringa, J.J., Kuipers, F., de Vries, E.G., and Vellenga, E. (2012). Treatment with high-dose simvastatin inhibits geranylgeranylation in AML blast cells in a subset of AML patients. Exp Hematol *40*, 177-186.e176.

van der Weyden, L., Giotopoulos, G., Rust, A.G., Matheson, L.S., van Delft, F.W., Kong, J., Corcoran, A.E., Greaves, M.F., Mullighan, C.G., Huntly, B.J., *et al*. (2011). Modeling the evolution of ETV6-RUNX1-induced B-cell precursor acute lymphoblastic leukemia in mice. Blood *118*, 1041-1051.

Vilimanovich, U., Bosnjak, M., Bogdanovic, A., Markovic, I., Isakovic, A., Kravic-Stevovic, T., Mircic, A., Trajkovic, V., and Bumbasirevic, V. (2015). Statin-mediated inhibition of cholesterol synthesis induces cytoprotective autophagy in human leukemic cells. Eur J Pharmacol *765*, 415-428.

Vitols, S., Gahrton, G., Bjorkholm, M., and Peterson, C. (1985). Hypocholesterolaemia in malignancy due to elevated low-density-lipoprotein-receptor activity in tumour cells: evidence from studies in patients with leukaemia. Lancet *2*, 1150-1154.

Wake, M.S., and Watson, C.J. (2015). STAT3 the oncogene - still eluding therapy? Febs j *282*, 2600-2611.

Wang, L.C., Kuo, F., Fujiwara, Y., Gilliland, D.G., Golub, T.R., and Orkin, S.H. (1997). Yolk sac angiogenic defect and intra-embryonic apoptosis in mice lacking the Ets-related factor TEL. Embo j *16*, 4374-4383.

Wang, L.C., Swat, W., Fujiwara, Y., Davidson, L., Visvader, J., Kuo, F., Alt, F.W., Gilliland, D.G., Golub, T.R., and Orkin, S.H. (1998). The TEL/ETV6 gene is required specifically for hematopoiesis in the bone marrow. Genes Dev *12*, 2392-2402.

Wang, Q., Stacy, T., Binder, M., Marin-Padilla, M., Sharpe, A.H., and Speck, N.A. (1996). Disruption of the Cbfa2 gene causes necrosis and hemorrhaging in the central nervous system and blocks definitive hematopoiesis. Proc Natl Acad Sci U S A *93*, 3444-3449.

Whitman, M. (1998). Smads and early developmental signaling by the TGFbeta superfamily. Genes Dev *12*, 2445-2462.

Wiemels, J.L., Ford, A.M., Van Wering, E.R., Postma, A., and Greaves, M. (1999). Protracted and variable latency of acute lymphoblastic leukemia after TEL-AML1 gene fusion in utero. Blood *94*, 1057-1062.

Williams, K.J., Argus, J.P., Zhu, Y., Wilks, M.Q., Marbois, B.N., York, A.G., Kidani, Y., Pourzia, A.L., Akhavan, D., Lisiero, D.N., *et al*. (2013). An essential requirement for the SCAP/SREBP signaling axis to protect cancer cells from lipotoxicity. Cancer Res *73*, 2850-2862.

Wilson, A., Murphy, M.J., Oskarsson, T., Kaloulis, K., Bettess, M.D., Oser, G.M., Pasche, A.C., Knabenhans, C., Macdonald, H.R., and Trumpp, A. (2004). c-Myc controls the balance between hematopoietic stem cell self-renewal and differentiation. Genes Dev *18*, 2747-2763.

Wontakal, S.N., Guo, X., Smith, C., MacCarthy, T., Bresnick, E.H., Bergman, A., Snyder, M.P., Weissman, S.M., Zheng, D., and Skoultchi, A.I. (2012). A core

erythroid transcriptional network is repressed by a master regulator of myelo-lymphoid differentiation. Proc Natl Acad Sci U S A *109*, 3832-3837.

Woodward, M.J., de Boer, J., Heidorn, S., Hubank, M., Kioussis, D., Williams, O., and Brady, H.J. (2010). Tnfaip8 is an essential gene for the regulation of glucocorticoid-mediated apoptosis of thymocytes. Cell Death Differ *17*, 316-323.

Wrzesinski, S.H., Wan, Y.Y., and Flavell, R.A. (2007). Transforming growth factor-beta and the immune response: implications for anticancer therapy. Clin Cancer Res *13*, 5262-5270.

Yagi, H., Deguchi, K., Aono, A., Tani, Y., Kishimoto, T., and Komori, T. (1998). Growth disturbance in fetal liver hematopoiesis of Mll-mutant mice. Blood *92*, 108-117.

Yamamoto, R., Morita, Y., Ooehara, J., Hamanaka, S., Onodera, M., Rudolph, K.L., Ema, H., and Nakauchi, H. (2013). Clonal analysis unveils self-renewing lineage-restricted progenitors generated directly from hematopoietic stem cells. Cell *154*, 1112-1126.

Yan, X., Liao, H., Cheng, M., Shi, X., Lin, X., Feng, X.H., and Chen, Y.G. (2016). Smad7 Protein Interacts with Receptor-regulated Smads (R-Smads) to Inhibit Transforming Growth Factor-beta (TGF-beta)/Smad Signaling. J Biol Chem *291*, 382-392.

Yan, X., Liu, Z., and Chen, Y. (2009). Regulation of TGF-beta signaling by Smad7. Acta Biochim Biophys Sin (Shanghai) *41*, 263-272.

Yoo, J.Y., Huso, D.L., Nathans, D., and Desiderio, S. (2002). Specific ablation of Stat3beta distorts the pattern of Stat3-responsive gene expression and impairs recovery from endotoxic shock. Cell *108*, 331-344.

Yoshida, T., Ng, S.Y., Zuniga-Pflucker, J.C., and Georgopoulos, K. (2006). Early hematopoietic lineage restrictions directed by Ikaros. Nat Immunol *7*, 382-391.

Yu, H., and Jove, R. (2004). The STATs of cancer--new molecular targets come of age. Nat Rev Cancer *4*, 97-105.

Zelent, A., Greaves, M., and Enver, T. (2004). Role of the TEL-AML1 fusion gene in the molecular pathogenesis of childhood acute lymphoblastic leukaemia. Oncogene *23*, 4275-4283.

Zeng, H., Yucel, R., Kosan, C., Klein-Hitpass, L., and Moroy, T. (2004). Transcription factor Gfi1 regulates self-renewal and engraftment of hematopoietic stem cells. Embo j *23*, 4116-4125.

Zhai, Y., Gao, X., Wu, Q., Peng, L., Lin, J., Zuo, Z. (2008). Fluvastatin decreases cardiac fibrosis possibly through regulation of TGF-B1/SMAD7 expression in the spontaneously hypertensive rats. Eur J Pharmacol *587*, 196-203.

Zhang, J., and Li, L. (2005). BMP signaling and stem cell regulation. Dev Biol *284*, 1-11.

Zhang, M., and Swanson, P.C. (2008). V(D)J recombinase binding and cleavage of cryptic recombination signal sequences identified from lymphoid malignancies. J Biol Chem *283*, 6717-6727.

Zhang, M.Y., Churpek, J.E., Keel, S.B., Walsh, T., Lee, M.K., Loeb, K.R., Gulsuner, S., Pritchard, C.C., Sanchez-Bonilla, M., Delrow, J.J., *et al*. (2015). Germline ETV6 mutations in familial thrombocytopenia and hematologic malignancy. *47*, 180-185.

Zhang, S., Ekman, M., Thakur, N., Bu, S., Davoodpour, P., Grimsby, S., Tagami, S., Heldin, C.H., and Landstrom, M. (2006). TGFbeta1-induced activation of ATM and p53 mediates apoptosis in a Smad7-dependent manner. Cell Cycle *5*, 2787-2795.

Zhang, S., Fei, T., Zhang, L., Zhang, R., Chen, F., Ning, Y., Han, Y., Feng, X.H., Meng, A., and Chen, Y.G. (2007). Smad7 antagonizes transforming growth factor beta signaling in the nucleus by interfering with functional Smad-DNA complex formation. Mol Cell Biol *27*, 4488-4499.

Zhu, L., Chen, S., and Chen, Y. (2011). Unraveling the biological functions of Smad7 with mouse models. Cell Biosci *1*, 44.

Zhuang, Y., Soriano, P., and Weintraub, H. (1994). The helix-loop-helix gene E2A is required for B cell formation. Cell *79*, 875-884.

APPENDIX

Table 10 - 250 Down-regulated genes picked up by Strand NGS analysis following SMAD7 knockdown

Gene Symbol	Entrez Gene Name
AARS	alanyl-tRNA synthetase
AATK	apoptosis-associated tyrosine kinase
ABCB10	ATP-binding cassette, sub-family B (MDR/TAP), member 10
ACAT2	acetyl-CoA acetyltransferase 2
ADAM11	ADAM metallopeptidase domain 11
ADCY7	adenylate cyclase 7
ADGRB2	adhesion G protein-coupled receptor B2
ALOX5AP	arachidonate 5-lipoxygenase-activating protein
ANKRD63	ankyrin repeat domain 63
APPL1	adaptor protein, phosphotyrosine interaction, PH domain and leucine zipper containing 1
AQP3	aquaporin 3 (Gill blood group)
ARHGAP11A	Rho GTPase activating protein 11A
ARHGEF39	Rho guanine nucleotide exchange factor (GEF) 39
ARPP19	cAMP-regulated phosphoprotein, 19kDa
AS3MT	arsenite methyltransferase
ASAP2	ArfGAP with SH3 domain, ankyrin repeat and PH domain 2
ASNS	asparagine synthetase (glutamine-hydrolyzing)
ASPM	asp (abnormal spindle) homolog, microcephaly associated (Drosophila)
AUNIP	aurora kinase A and ninein interacting protein
AURKB	aurora kinase B
B4GALNT3	beta-1,4-N-acetyl-galactosaminyl transferase 3
BACE2	beta-site APP-cleaving enzyme 2
BRCA2	breast cancer 2, early onset

BRIP1	BRCA1 interacting protein C-terminal helicase 1
BUB1	BUB1 mitotic checkpoint serine/threonine kinase
C11orf96	chromosome 11 open reading frame 96
C18orf54	chromosome 18 open reading frame 54
C5orf22	chromosome 5 open reading frame 22
C6orf222	chromosome 6 open reading frame 222
C6orf223	chromosome 6 open reading frame 223
CA2	carbonic anhydrase II
CACNA1G	calcium channel, voltage-dependent, T type, alpha 1G subunit
CACNA2D4	calcium channel, voltage-dependent, alpha 2/delta subunit 4
CAMK4	calcium/calmodulin-dependent protein kinase IV
CASC4	cancer susceptibility candidate 4
CASC4P1	cancer susceptibility candidate 4 pseudogene 1
CASC5	cancer susceptibility candidate 5
CCDC117	coiled-coil domain containing 117
CCDC15	coiled-coil domain containing 15
CCDC74B	coiled-coil domain containing 74B
CCNB2	cyclin B2
CD109	CD109 molecule
CDC20	cell division cycle 20
CDC42EP4	CDC42 effector protein (Rho GTPase binding) 4
CDC42EP5	CDC42 effector protein (Rho GTPase binding) 5
CDC6	cell division cycle 6
CDCA2	cell division cycle associated 2
CDT1	chromatin licensing and DNA replication factor 1
CECR1	cat eye syndrome chromosome region, candidate 1
CENPA	centromere protein A
CENPH	centromere protein H
CENPK	centromere protein K
CENPU	centromere protein U
CEP128	centrosomal protein 128kDa
CEP55	centrosomal protein 55kDa
CIT	citron rho-interacting serine/threonine kinase
CKAP2L	cytoskeleton associated protein 2-like

CKS1BP7	CDC28 protein kinase regulatory subunit 1B pseudogene 7
CORO2A	coronin, actin binding protein, 2A
CPD	carboxypeptidase D
CPED1	cadherin-like and PC-esterase domain containing 1
CYS1	cystin 1
DARS2	aspartyl-tRNA synthetase 2, mitochondrial
DCK	deoxycytidine kinase
DENND2A	DENN/MADD domain containing 2A
DERL3	derlin 3
DHCR7	7-dehydrocholesterol reductase
DIAPH3	diaphanous-related formin 3
DLGAP5	discs, large (Drosophila) homolog-associated protein 5
DMC1	DNA meiotic recombinase 1
DNM1	dynamin 1
DPRXP4	divergent-paired related homeobox pseudogene 4
DSCC1	DNA replication and sister chromatid cohesion 1
E2F2	E2F transcription factor 2
E2F8	E2F transcription factor 8
ECT2	epithelial cell transforming 2
ELOVL2	ELOVL fatty acid elongase 2
ELOVL6	ELOVL fatty acid elongase 6
EME1	essential meiotic structure-specific endonuclease 1
EML5	echinoderm microtubule associated protein like 5
ENO2	enolase 2 (gamma, neuronal)
EPX	eosinophil peroxidase
ERI2	ERI1 exoribonuclease family member 2
ETV4	ets variant 4
FADS1	fatty acid desaturase 1
FADS2	fatty acid desaturase 2
FAM129A	family with sequence similarity 129, member A
FAM72A	family with sequence similarity 72, member A
FAM72B	family with sequence similarity 72, member B
FAM72C/FAM 72D	family with sequence similarity 72, member D

FBXO43	F-box protein 43
FDPS	farnesyl diphosphate synthase
FOLR2	folate receptor 2 (fetal)
FOXM1	forkhead box M1
GALNT12	polypeptide N-acetylgalactosaminyltransferase 12
GAREML	GRB2 associated, regulator of MAPK1-like
GAS2L3	growth arrest-specific 2 like 3
GCSAM	germinal center-associated, signaling and motility
GINS1	GINS complex subunit 1 (Psf1 homolog)
GJC1	gap junction protein, gamma 1, 45kDa
GNAZ	guanine nucleotide binding protein (G protein), alpha z polypeptide
GNL3LP1	guanine nucleotide binding protein-like 3 (nucleolar)-like pseudogene 1
GPC4	glypican 4
GPR161	G protein-coupled receptor 161
GSG2	germ cell associated 2 (haspin)
HINT2	histidine triad nucleotide binding protein 2
HJURP	Holliday junction recognition protein
HMGB2	high mobility group box 2
HMMR	hyaluronan-mediated motility receptor (RHAMM)
IGFBP2	insulin-like growth factor binding protein 2, 36kDa
IL21R	interleukin 21 receptor
IQGAP2	IQ motif containing GTPase activating protein 2
IRF4	interferon regulatory factor 4
ITGB3BP	integrin beta 3 binding protein (beta3-endonexin)
ITGB7	integrin, beta 7
JDP2	Jun dimerization protein 2
JPH1	junctophilin 1
JPH2	junctophilin 2
KBTBD13	kelch repeat and BTB (POZ) domain containing 13
KCNH2	potassium channel, voltage gated eag related subfamily H, member 2

KIAA0895	KIAA0895
KIAA1804	mixed lineage kinase 4
KIF11	kinesin family member 11
KIF14	kinesin family member 14
KIF15	kinesin family member 15
KIF18B	kinesin family member 18B
KIF21B	kinesin family member 21B
KIF2C	kinesin family member 2C
KLK1	kallikrein 1
LBR	lamin B receptor
LHX2	LIM homeobox 2
LINC01224	
LOC100507002	uncharacterized LOC100507002
LOC441179	uncharacterized LOC441179
LRP4	low density lipoprotein receptor-related protein 4
LSS	lanosterol synthase (2,3-oxidosqualene-lanosterol cyclase)
LTBP1	latent transforming growth factor beta binding protein 1
MAD2L1	MAD2 mitotic arrest deficient-like 1 (yeast)
MAGEL2	melanoma antigen family L2
MAP2K6	mitogen-activated protein kinase kinase 6
MASTL	microtubule associated serine/threonine kinase-like
MCM7	minichromosome maintenance complex component 7
MFI2	antigen p97 (melanoma associated) identified by monoclonal antibodies 133.2 and 96.5
mir-671	microRNA 671
MND1	meiotic nuclear divisions 1 homolog (S. cerevisiae)
MNS1	meiosis-specific nuclear structural 1
MRC2	mannose receptor, C type 2
MSANTD3-TMEFF1	MSANTD3-TMEFF1 readthrough
MSMO1	methylsterol monooxygenase 1
MTFR2	mitochondrial fission regulator 2
MYCN	v-myc avian myelocytomatosis viral oncogene neuroblastoma derived homolog

NCAPG2	non-SMC condensin II complex, subunit G2
NCAPH	non-SMC condensin I complex, subunit H
NDRG2	NDRG family member 2
NEIL3	nei endonuclease VIII-like 3 (E. coli)
NEK2	NIMA-related kinase 2
NGFR	nerve growth factor receptor
NLRP6	NLR family, pyrin domain containing 6
NNT-AS1	NNT antisense RNA 1
NRGN	neurogranin (protein kinase C substrate, RC3)
NTRK1	neurotrophic tyrosine kinase, receptor, type 1
NUF2	NUF2, NDC80 kinetochore complex component
NUSAP1	nucleolar and spindle associated protein 1
NXPH4	neurexophilin 4
OIP5	Opa interacting protein 5
OPN3	opsin 3
OTUD6B	OTU domain containing 6B
P2RX7	purinergic receptor P2X, ligand gated ion channel, 7
PALD1	phosphatase domain containing, paladin 1
PALLD	palladin, cytoskeletal associated protein
PBK	PDZ binding kinase
PCK1	phosphoenolpyruvate carboxykinase 1 (soluble)
PCK2	phosphoenolpyruvate carboxykinase 2 (mitochondrial)
PHGDH	phosphoglycerate dehydrogenase
PHLDB2	pleckstrin homology-like domain, family B, member 2
PKMYT1	protein kinase, membrane associated tyrosine/threonine 1
PLAUR	plasminogen activator, urokinase receptor
PLK1	polo-like kinase 1
PLS1	plastin 1
POLQ	polymerase (DNA directed), theta
PPP4R4	protein phosphatase 4, regulatory subunit 4
PRAME	preferentially expressed antigen in melanoma
PRF1	perforin 1 (pore forming protein)

PRIM1	primase, DNA, polypeptide 1 (49kDa)
PRKAR2B	protein kinase, cAMP-dependent, regulatory, type II, beta
PRR11	proline rich 11
PTGS1	prostaglandin-endoperoxide synthase 1 (prostaglandin G/H synthase and cyclooxygenase)
PTPN22	protein tyrosine phosphatase, non-receptor type 22 (lymphoid)
PTPN7	protein tyrosine phosphatase, non-receptor type 7
PTPRR	protein tyrosine phosphatase, receptor type, R
PYGL	phosphorylase, glycogen, liver
RAB3B	RAB3B, member RAS oncogene family
RAD51	RAD51 recombinase
RAD54L	RAD54-like (S. cerevisiae)
RASD2	RASD family, member 2
RASSF4	Ras association (RalGDS/AF-6) domain family member 4
RIMS3	regulating synaptic membrane exocytosis 3
RMI1	RecQ mediated genome instability 1
RMI2	RecQ mediated genome instability 2
RNF182	ring finger protein 182
RTKN2	rhotekin 2
SASS6	spindle assembly 6 homolog (C. elegans)
SEL1L3	sel-1 suppressor of lin-12-like 3 (C. elegans)
SESTD1	SEC14 and spectrin domains 1
SFN	stratifin
SIGLEC16	sialic acid binding Ig-like lectin 16 (gene/pseudogene)
SKA3	spindle and kinetochore associated complex subunit 3
SLC16A14	solute carrier family 16, member 14
SLC1A4	solute carrier family 1 (glutamate/neutral amino acid transporter) member 4
SLC26A2	solute carrier family 26 (anion exchanger), member 2
SLC30A3	solute carrier family 30 (zinc transporter), member 3
SLC4A11	solute carrier family 4, sodium borate transporter, member 11
SLC4A4	solute carrier family 4 (sodium bicarbonate cotransporter), member 4
SLC6A19	solute carrier family 6 (neutral amino acid transporter), member 19

	solute carrier family 7 (cationic amino acid transporter, y+ system)
SLC7A3	member 3
SMC1A	structural maintenance of chromosomes 1A
SMC2	structural maintenance of chromosomes 2
SNX24	sorting nexin 24
SOAT1	sterol O-acyltransferase 1
SPC24	SPC24, NDC80 kinetochore complex component
SPC25	SPC25, NDC80 kinetochore complex component
SPNS2	spinster homolog 2 (Drosophila)
SPTB	spectrin, beta, erythrocytic
SREBF1	sterol regulatory element binding transcription factor 1
SRPR	signal recognition particle receptor (docking protein)
SRSF12	serine/arginine-rich splicing factor 12
STARD4	StAR-related lipid transfer (START) domain containing 4
STIL	SCL/TAL1 interrupting locus
STON1	stonin 1
STON1-	
GTF2A1L	STON1-GTF2A1L readthrough
TICRR	TOPBP1-interacting checkpoint and replication regulator
	transmembrane protein with EGF-like and
TMEFF1	two follistatin-like domains 1
TMEM144	transmembrane protein 144
TMEM150C	transmembrane protein 150C
TMEM169	transmembrane protein 169
TMEM194A	transmembrane protein 194A
TMEM194B	transmembrane protein 194B
TNFRSF18	tumor necrosis factor receptor superfamily, member 18
TOP2A	topoisomerase (DNA) II alpha 170kDa
TPX2	TPX2, microtubule-associated
TRIM45	tripartite motif containing 45
TRNP1	TMF1-regulated nuclear protein 1
TSC22D3	TSC22 domain family, member 3
TSPAN4	tetraspanin 4
TTF2	transcription termination factor, RNA polymerase II

TTK	TTK protein kinase
TUBA4A	tubulin, alpha 4a
VASH2	vasohibin 2
VAT1L	vesicle amine transport 1-like
VPS4B	vacuolar protein sorting 4 homolog B (S. cerevisiae)

This table shows the list of 250 downregulated genes with 1.5 fold change or higher common to both shRNA upon *SMAD7* knockdown, identified by Strand NGS analysis of RNA-sequencing data.

Table 11- 56 upregulated genes picked up by Strand NGS analysis following SMAD7 knockdown

Gene Symbol	Entrez Gene Name
ARHGAP24	Rho GTPase activating protein 24
ARHGEF37	Rho guanine nucleotide exchange factor (GEF) 37
ARPC3P5	actin related protein 2/3 complex, subunit 3 pseudogene 5
BTG2	BTG family, member 2
BZRAP1-AS1	BZRAP1 antisense RNA 1
C19orf38	chromosome 19 open reading frame 38
CCND2	cyclin D2
CHIAP3	chitinase, acidic pseudogene 3
CTSA	cathepsin A
DUSP26	dual specificity phosphatase 26 (putative)
ECM2	extracellular matrix protein 2, female organ and adipocyte specific
FBXO39	F-box protein 39
FGF18	fibroblast growth factor 18
GBP4	guanylate binding protein 4
GTF2IRD2P1	GTF2I repeat domain containing 2 pseudogene 1
HIST1H2AC	histone cluster 1, H2ac
HIST1H2BD	histone cluster 1, H2bd
HIST1H2BJ	histone cluster 1, H2bj
HIST1H2BK	histone cluster 1, H2bk
HIST1H4H	histone cluster 1, H4h
HIST2H2BE	histone cluster 2, H2be
IGLC2	immunoglobulin lambda constant 2 (Kern-Oz- marker)
IGLV3-21	immunoglobulin lambda variable 3-21
ITM2A	integral membrane protein 2A
KCNJ2-AS1	KCNJ2 antisense RNA 1 (head to head)
LINC-ROR	long intergenic non-protein coding RNA, regulator of reprogramming
LINC00158	long intergenic non-protein coding RNA 158

LINC01021	long intergenic non-protein coding RNA 1021
LINC01033	
LOC100130705	uncharacterized LOC100130705
LOC101927501	uncharacterized LOC101927501
LOC101929448	uncharacterized LOC101929448
LOC115110	uncharacterized LOC115110
LOC285628	uncharacterized LOC285628
LRRC70	leucine rich repeat containing 70
MMRN1	multimerin 1
MXD4	MAX dimerization protein 4
NOL4	nucleolar protein 4
PAG1	phosphoprotein membrane anchor with glycosphingolipid microdomains 1
PBXIP1	pre-B-cell leukemia homeobox interacting protein 1
PDE1A	phosphodiesterase 1A, calmodulin-dependent
PLK2	polo-like kinase 2
PNPLA7	patatin-like phospholipase domain containing 7
PYHIN1	pyrin and HIN domain family, member 1
RGMB-AS1	RGMB antisense RNA 1
RPS6P12	ribosomal protein S6 pseudogene 12
SCAMP1-AS1	SCAMP1 antisense RNA 1
SERTAD1	SERTA domain containing 1
SH3BP5	SH3-domain binding protein 5 (BTK-associated)
SLC7A8	solute carrier family 7 (amino acid transporter light chain, L system), member 8
SNX18P26	sorting nexin 18 pseudogene 26
TLE4	transducin-like enhancer of split 4
TMEM150A	transmembrane protein 150A
TNFRSF14	tumor necrosis factor receptor superfamily, member 14
TRPM4	transient receptor potential cation channel, subfamily M, member 4
TWF1	twinfilin actin-binding protein 1
USP30-AS1	USP30 antisense RNA 1

This table shows the list of 56 upregulated genes with 1.5 fold change or higher common to both shRNA upon *SMAD7* knockdown, identified by Strand NGS analysis of RNA-sequencing data.